Identification of X-chromosomal genes that drive global X-dosage effects in mammals

Inaugural-Dissertation

to obtain the academic degree

Doctor rerum naturalium (Dr. rer. nat.)

submitted to the Department of Biology, Chemistry, Pharmacy

at the Freie Universität Berlin

by

Oriana Genolet Alberdi

Berlin, 2020

The present work was conducted from February 2015 to July 2020 at the Max Planck Institute for Molecular Genetics in Dr. Edda Schulz´s research group.

1st Reviewer: Dr. Edda Schulz

2nd Reviewer: Prof. Dr. Petra Knaus

Date of defense: 02.11.2020

Table of Contents

Acknowledgements

No man is an island, as the English poet John Donne writes, and so is this work a product of not one but many, all of whom I would like to give my deepest gratitude. This work would not have been conceivable without Dr. Edda Schulz, who gave me the opportunity to be part of a wonderful and extremely interesting project, and who mentored me throughout its duration. Thank you for the discussions, for supporting my ideas and helping them become realities, for your inputs and suggestions in the most critical times, and for being there whenever I needed help or advice.

I would like to give my deepest thanks to my amazing lab colleagues, who supported me both intellectually and emotionally in these past five years. Liat Ravid, who significantly increased my daily smiling rates, and whose feedback, help and advice are one of the pillars that this work rests on. Ilona Dunkel, a special thanks to you for your great kindness, your tireless patience and your constant support. Thank you for listening whenever I had something to say, and the valuable advice that kept me going in the times of hardship. Verena Mutzel, for always keeping up the smile and her contagious optimism, for all the discussions on X-chromosome inactivation and for all the constructive feedback during manuscript writing. Guido Pacini, the R wizard, for all his help concerning all things bioinformatics- and statistics-related, I could not have done it without you. Rutger Gjaltema, for his willingness to share knowledge whenever asked, which made a great impact in many experiments and lastly, Zeba Sultana, for helping me unravel the convoluted world of signaling cascades and for her very useful feedback during manuscript writing. A very special thanks to my excellent Master student Anna Monaco, who helped bring this work forward and whose experiments make a significant part of this thesis. Thank you for having always stayed positive and motivated yourself, and for having motivated me to be a good teacher by being a terrific student.

I would like to also thank the people who contributed the advice and knowledge that shaped this project, including Prof. Petra Knaus, Prof. Nils Blüthgen and Dr. Heiner Schrewe. Thank you for your great feedback and for your availability and willingness to meet every year to discuss my project. Michael Böttcher, whose invaluable advice on CRISPR screen design, execution and analysis proved to be vital for this work. Thank you for everything.

Many thanks also to the facilities at the Max Planck Institute for their wonderful service and guidance, specially Norbert Mages and Sven Klages from the sequencing facility, who were always willing to help in any way possible, Uta Marchfelder from the FACS facility, for her help and flexibility whenever it came to sorting outside standard working hours and Dr. David Meierhofer and Beata Lukaszewsa-McGreal from the Mass spectrometry facility, whose advice and help made the last section of this work possible.

Last but not least, I would like to thank my family and friends for their unlimited support and for filling these past years with happiness and unforgettable memories. Miguel Cabrera, my husband, for the laughter, advice and patience that endows me with strength during difficult moments and for helping me see things in perspective at times when I tend to focus on the negatives. My parents, Margarita Alberdi and Luis Carlos Genolet, and my brother, Manuel Genolet, who are my biggest fans. Thank you for celebrating my victories, even more than myself, thank you for always being there for me. Gracias totales!

1. Introduction

1.1. Early mammalian development: from fertilization to germ-layer formation

Embryogenesis is the process during early development that starts with the fertilization of the egg cell by a sperm cell and ends around the onset of organogenesis (Gilbert, 2000). In mammals, the fertilized egg (zygote) undergoes a series of cell divisions maintaining a constant embryonic cytoplasmic volume that give rise to a structure called the morula around the 8-16 cell stage (Fig. 1) (Barlow et al., 1972). This is followed by the appearance of small intercellular cavities that subsequently merge into a single blastocoel at approx. the 16-32 cell stage, leading to the formation of the blastula (Motosugi et al., 2005). Development continues through the differentiation of cells into two different cell types: trophoblast cells and the inner cell mass (ICM), generating thus what is known as the blastocyst (Fig. 1) (Nishioka et al., 2009; Rayon et al., 2014; Wicklow et al., 2014). Trophoblast cells make up the outer layer of the blastocyst and build extraembryonic tissues such as the placenta, while ICM cells differentiate further into primitive endoderm (hypoblast) or primitive ectoderm (epiblast) (Fig. 1) (Chazaud et al., 2006; Morris et al., 2010; Yamanaka et al., 2010). From these two, only the latter will give rise to the embryo proper.

Implantation, the stage at which the embryo adheres to the uterine wall, occurs around embryonic day 4.5-5 (E4.5-5), accompanied by a remodeling of the epiblast that involves the formation of a rosette of polarized cells and later on the establishment of an epithelium around a central lumen (proamniotic cavity) (Fig. 1) (Bedzhov and Zernicka-Goetz, 2014). Gastrulation begins through the formation of an anterior-posterior axis and the ingression of cells in the posterior region of the epiblast, building the so-called primitive streak. This is followed by the establishment of three primary germ layers that will form the organs and tissues of the adult organism: ectoderm, mesoderm and ectoderm (Kiecker et al., 2016; Tam et al., 1993). After gastrulation has taken place, it is followed by the process of organogenesis, which continues until birth. Here, the three germ layers will form the internal organs of the fetus: the endoderm will give rise to the epithelial parts of the lungs, liver, pancreas, the stomach, etc, whereas the mesoderm layer will generate tissues such as muscle, bone and cartilage. Lastly, the ectoderm will build, among others, the epidermis and the nervous system.

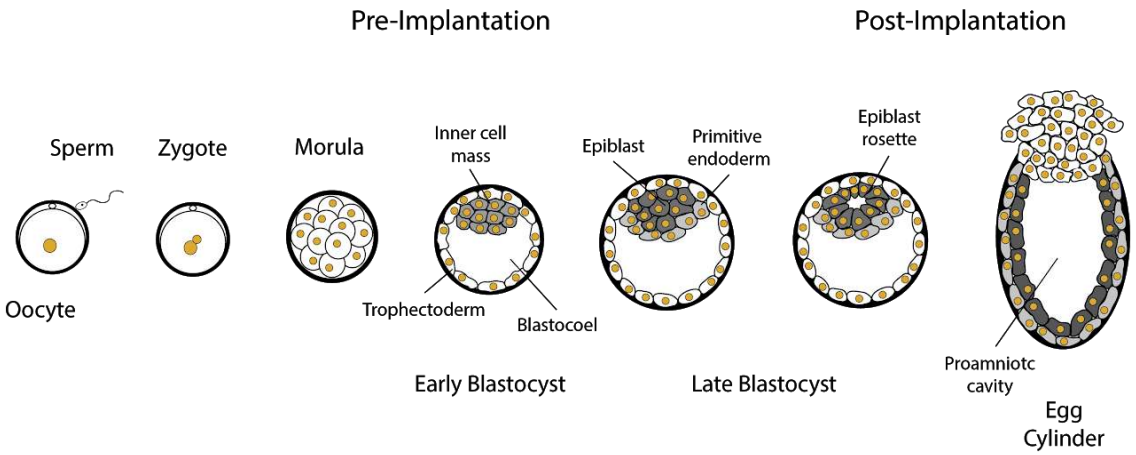

Figure 1: Early mammalian development. The fertilized zygote undergoes a series of cell divisions giving rise to the morula. This is followed by the appearance of the blastocoel and the first lineage decision forming inner cell mass (ICM) and trophectoderm cells. Later on, the ICM cells differentiate further into primitive endoderm cells and epiblast cells, the latter giving rise later on to the embryo proper. As development continues, epiblast cells become polarized forming a rosette structure around a lumen that will become the proamniotic cavity.

1.2. Pluripotency defined

The ability of a cell to differentiate into different cell types is defined as potency. The differentiation potential of a given cell, however, varies throughout developmental progression. So are zygotes as well as blastomere cells from the Morula stage capable of differentiating into all possible cell types, whereas cells from the ICM of the early preimplantation blastocyst, where the first lineage segregation has occurred, are able to differentiate into all three germ layers but not certain extraembryonic tissues (Fig. 2). While the first are defined as totipotent cells, the latter are coined as pluripotent (Mitalipov and Wolf, 2009). An even further restricted differentiation potential is displayed by multipotent and oligopotent cells, such as hematopoietic stem cells that give rise to many blood cell types, or lymphoid cells that form B and T cells, respectively.

Pluripotency could be first captured *in vitro* by Martin Evans and Matthew Kaufman in 1981 by dispersing cells from the ICM of the murine preimplantation blastocyst and passaging them through co-culture with mouse embryonic fibroblasts (feeder cells), which administered the necessary signals for self-renewal and pluripotency maintenance (Evans and Kaufman, 1981; Martin, 1981). This allowed for the generation of mouse embryonic stem cell lines (mESCs), which provided an excellent *in vitro* model for early mammalian development.

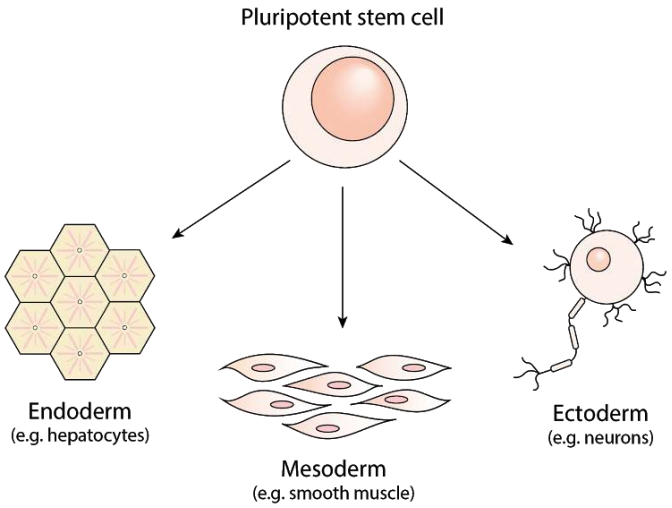

Figure 2: Pluripotency. Pluripotent cells are able to differentiate into all three germ layers: endoderm, mesoderm and ectoderm. These germ layers will give rise to the different tissues and organs of the adult organism. The endoderm will thus give rise to the epithelial parts of the lungs, liver, pancreas, the stomach, etc, whereas the mesoderm layer will generate tissues such as muscle, bone and cartilage. Lastly, the ectoderm will build, among others, the epidermis and the nervous system.

Key for the maintenance of the pluripotency state is the expression of a group of core transcription factors that restrict differentiation and at the same time sustain self-renewal capabilities: Oct4, Sox2 and Nanog (OSN) (Avilion et al., 2003; Boyer et al., 2005; Chambers et al., 2003, 2007; Loh et al., 2006; Masui et al., 2007; Mitsui et al., 2003; Nichols et al., 1998; Silva et al., 2009; Wang et al., 2012). They exert their functions by repressing lineage-specific genes and at the same time by activating genes that mediate the pluripotency state, including binding to their own promoters in a positive-feedback fashion (Boyer et al., 2005; Chen et al., 2008; Kim et al., 2008; Loh et al., 2006). Overexpression of a combination of these and/or other pluripotency-promoting factors in differentiated somatic cells of adult organisms allows for the generation of induced pluripotent cells lines (iPSCs), highlighting their essential role as the main drivers of the pluripotent state (Takahashi and Yamanaka, 2006).

1.2.1 The naive and primed pluripotent state

In order to further dissect the different early stages of the developmental continuum, the term naive and primed pluripotency were coined defining epiblast cells of the murine pre- or postimplantation epiblast, respectively (Nichols and Smith, 2009). Extensive characterization of both states, which was possible to a great extent through the derivation of naive and primed pluripotent stem cell lines *in vitro* (naive mESCs and epiblast stem cells (EpiSCs), respectively) (Brons et al., 2007; Tesar et al., 2007), led to the specification of their distinct functional and molecular signatures.

While both naive mESCs as well as primed EpiSCs are able to differentiate into all three germ layers *in vitro*, only the former is able to give rise to the germline (e.g. the cells that will later differentiate into oocytes and sperm cells) when injected back into early embryos (Huang et al. 2012). This ability to incorporate external pluripotent cells into normal development is a characteristic of early mammalian embryos, which readily accommodate alterations in cell numbers, resulting in chimeric animals. Primed pluripotent cells are thus more restricted in their differentiation potential compared to naive pluripotent stem cells and are conditioned for further differentiation, hence the name “primed” pluripotent.

Several molecular signatures additionally distinguish naive from primed pluripotent stem cells. A key trait of naive mESCs is for instance their increased expression of a certain set of transcription factors associated with naive pluripotency, including Prdm14, Klf4, Klf2, Esrrb, Tfcp2l1, Tbx3, Tcl1 and Gbx2 (Fig. 3) (Boroviak et al., 2015; Dunn et al., 2014; Ivanova et al., 2006; Kalkan et al., 2017; Martello et al., 2012, 2013; Niwa et al., 2009; Tai and Ying, 2013; Yamaji et al., 2013; Yeo et al., 2014; Ye et al., 2013). The overexpression of combinations of these markers can revert cells to the naive pluripotent state, inducing hallmarks of the naive states such as X chromosome reactivation (see below) (Bao et al., 2009; Guo et al., 2009). Primed pluripotent stem cells, on the other hand, express significantly lower levels of naive pluripotency factors together with increased expression of primed markers such as Fgf5, Otx2 and Zic2 (Acampora et al., 2013; Buecker et al., 2014; Kalkan et al., 2017; Klein et al., 2015; Kondoh, 2018; Marks et al., 2012; Matsuda et al., 2017).

Distinct epigenetic states (changes that do not involve alterations in the DNA sequence) have also been reported between naive and primed pluripotent stem cells. Significant differences have been observed, for example, in the degree of global CpG methylation, with naive cells being found in a genome-wide hypomethylated state (Fig. 3) (Ficz et al., 2013; Habibi et al., 2013; Leitch et al., 2013; von Meyenn et al., 2016; Smith et al., 2012). DNA methylation is a process in which a methyl group is added to a cytosine base in the DNA and it is usually associated with transcriptional repression, especially when located at gene promoters (Smith and Meissner, 2013). It is established by DNA methyltransferases (DNMTs), of which two kinds can be distinguished: the maintenance methyltransferase Dnmt1 and the *de novo* methyltransferases Dnmt3a and Dnmt3b (Hermann et al., 2004; Jeltsch, 2006; Okano et al., 1999; Smith and Meissner, 2013). These two *de novo* methyltransferases act together with Dnmt3l, which lacks methyltransferase activity but facilitates Dnmt3a/b chromatin targeting (Ooi et al., 2007). While maintenance DNA Methyltransferases are able to bind hemimethylated DNA (only one of the two complementary DNA strands is methylated), de novo methyltransferases recognize unmethylated DNA (Hermann et al., 2004; Jeltsch, 2006; Okano et al., 1999). In agreement with their global CpG hypomethylation state, Dnmt1 and/or Dnmt3a/b knockout naive mESCs can be propagated in culture, which is not the case for primed pluripotent cells (Chen et al., 2003; Jackson et al., 2004; Lei et al., 1996; Tsumura et al., 2006). The latter also express significantly higher levels of de novo methyltransferases Dnmt3a, Dnmt3b and Dnmt3l, which is accompanied by a meaningful rise in genome-wide CpG methylation levels (Fig. 3) (Habibi et al., 2013).

Lastly, female naive pluripotent cells possess two active X chromosomes (Fig. 3) (Rastan and Robertson, 1985), which become randomly silenced once they undergo the transition to the primed state. The process of silencing one of the two X chromosomes present in females is known as X chromosome inactivation and it represents the

manner how mammals compensate the double X chromosome dosage present in XX females vs the single dosage exhibited by XY males. The latter is achieved through the expression of the long non-coding RNA (lncRNA) Xist, which coats the inactive X chromosome and recruits epigenetic modifiers leading to heterochromatinization and gene silencing (see below for further details) (Galupa and Heard 2018). This point is of particular importance for this work, since its focus involves the identification of the genetic determinants underlying sex differences in mESCs that arise from a double X-dosage in female cells.

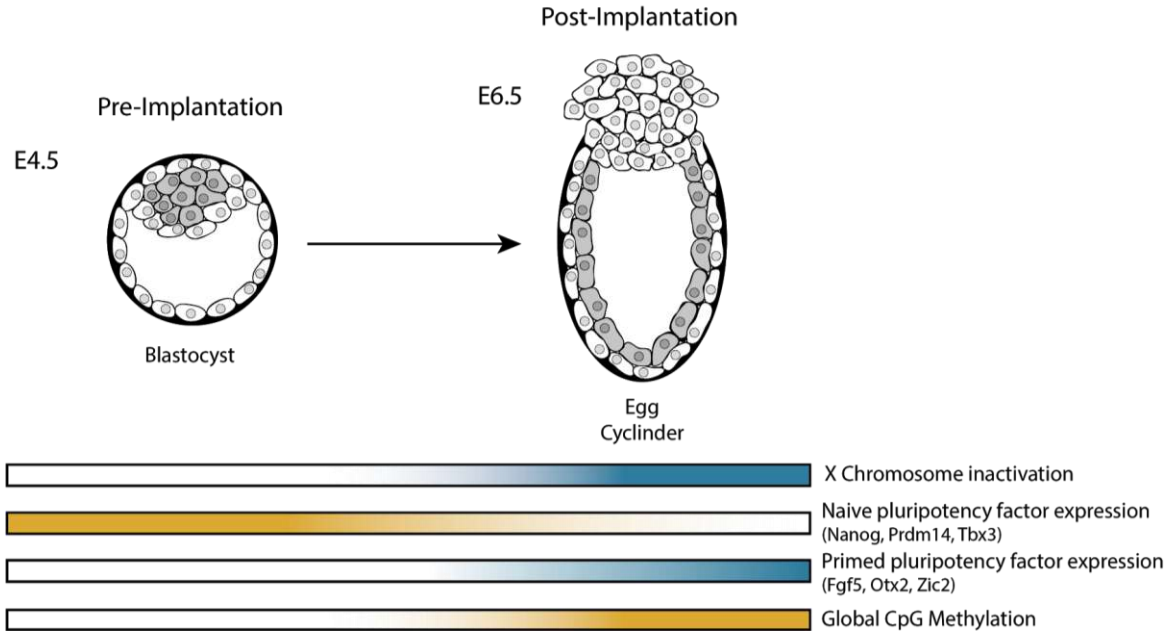

Figure 3: The naive and primed state of pluripotency. Epiblast cells of the pre-implantation mouse blastocyst express higher levels of naive pluripotency markers and display global CpG hypomethylation. On the other hand, epiblast cells of the post-implantation blastocyst have already undergone X chromosome inactivation, express primed pluripotency markers and display higher levels of global CpG methylation.

Pluripotent stem cells represent a valuable tool to study human development in vitro, since embryo manipulation for research purposes is restricted or forbidden in many countries. Human pluripotent stem cells (hPSCs) can also be derived from the early blastocyst, however, their characteristics resemble that of murine EpiSCs and are therefore thought to be found in a primed-like pluripotent state (Brons et al., 2007; Tesar et al., 2007; Thomson et al., 1998; Vallier et al., 2005; Ying and Smith, 2017). Nevertheless, culture conditions have recently been developed that seem to induce a shift of hPSCs towards a more naive state of pluripotency (Takashima et al., 2014; Theunissen et al., 2014). This highlights the importance of specific culture conditions in capturing the different stages of the pluripotency developmental continuum.

1.2.2 In vitro maintenance and signaling cues sustaining diverse pluripotency states

Extracellular cues are key for shaping cellular behaviors or inducing cell fates during developmental progression, taking many forms such as proteins, lipids, peptides or small molecules. They act by inhibiting or activating intracellular signal transduction pathways that transform these cues into cellular responses, such as differentiation, apoptosis, proliferation, migration, etc (Anon. 2010). Identifying and understanding the signaling molecules and pathways that are key for capturing the different stages of early development *in vitro* has proven a challenging task, however, many progress has been made in the last decades.

The maintenance of mouse embryonic stem cells in culture was first possible using serum-supplemented media together with feeder cells, which secreted factors that allowed for the propagation of these cells in the pluripotent state. Later on, the discovery of leukemia inhibitory factor (LIF), a molecule secreted by feeder cells,

permitted the maintenance of feeder-free mESCs (Smith and Hooper, 1987; Smith et al., 1988; Williams et al., 1988). Furthermore, the use of serum could be replaced through the addition of the bone morphogenetic protein 4 (BMP4) to the culture media (Ying et al., 2003), leading thus to the identification of molecules responsible for the maintenance of pluripotency (Ying and Smith, 2017).

LIF binds the gp130 receptor activating the pluripotency-inducing Jak/Stat3 and Akt signaling pathways, while also activating at the same time the differentiation-inducing mitogen activated protein kinase (MAPK) signaling pathway (Fig. 4) (Niwa et al., 1998, 2009). The SMAD pathway activating BMP4 molecule, on the other hand, induces the expression of Dusp9, a MAPK pathway inhibitor, balancing the signaling input towards pluripotency maintenance (Li et al., 2012). Additionally, BMP4-induced ID proteins are able to block the differentiation of mESCs into neural lineages (Fig. 4) (Ying et al. 2003).

Capturing the naive state of pluripotency *in vitro* has been possible through the inhibition of two signaling molecules: Mek (a main component of the differentiation-inducing MAPK signaling pathway) and the glycogen synthase-kinase 3 (Gsk3), hence the name 2i medium (Fig. 4) (Burdon et al., 1999; Sato et al., 2004; Wray et al., 2010; Ying et al., 2008). While Gsk3 inhibition is important for the maintenance of clonogenicity and viability in mESCs (Ying et al., 2008), the inhibition of the MAPK signaling pathway is essential to block mESC differentiation (Kunath et al., 2007; Stavridis et al., 2007).

Maintenance of mESCs *in vitro* is therefore usually accomplished using Serum and LIF (Serum/LIF) conditions or though the further addition of 2i inhibitors (2i/LIF), which keeps the cells in a more naive state of pluripotency by blocking the differentiation-inducing MAPK signaling pathway.

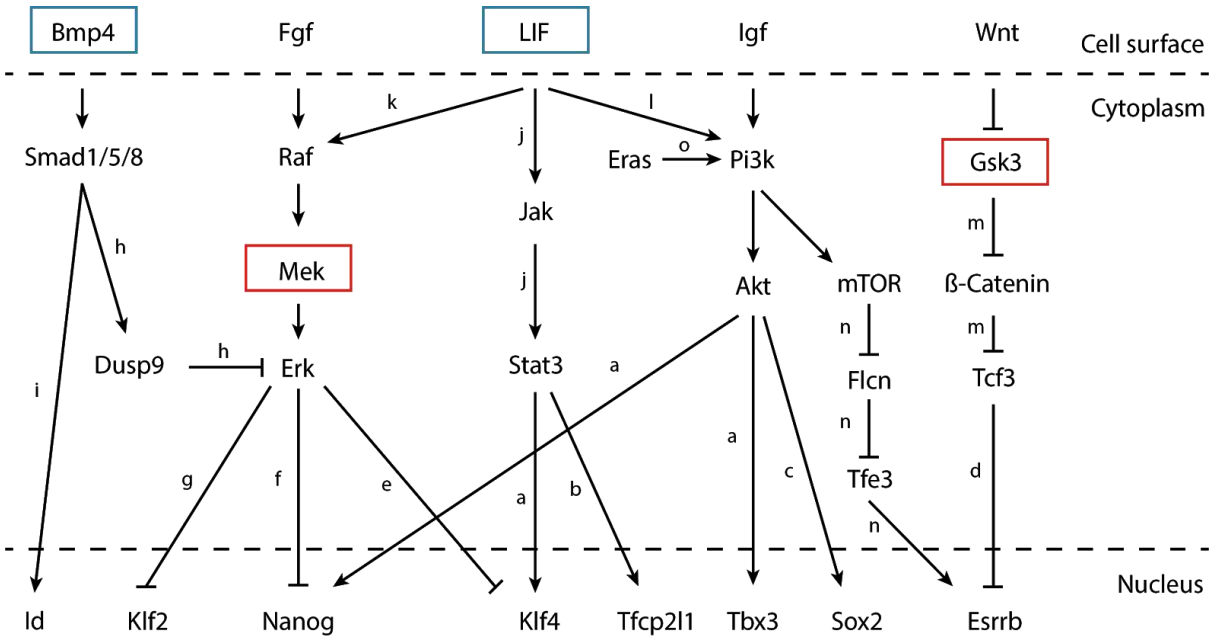

Figure 4: The mESC signaling network. Signaling pathways known to be involved in mediating the pluripotency state and their modulation of pluripotency factor expression. The addition of LIF and Bmp4 to the culture media promotes the naive pluripotency state (blue boxes), together with the inhibition of the Mek and Gsk3 kinases (red boxes). The shown interactions are based on the following literature: a. (Niwa et al., 2009), b. (Martello et al., 2013), c. (Fang et al., 2014; Jeong et al., 2010), d. (Martello et al., 2012), e. (Kim et al., 2012), f. (Kim et al., 2014b), g. (Yeo et al., 2014), h. (Li et al., 2012), i. (Ying et al., 2003), j. (Matsuda et al., 1999; Niwa et al., 1998), k. (Burdon et al., 1999; Fukada et al., 1996), l. (Paling et al., 2004), m. (Wray et al., 2011), n. (Betschinger et al., 2013), o. (Zhao et al., 2015) (Adapted from Schulz, 2017).

The MAPK pathway is activated through the binding of extracellular mitogens such as fibroblast growth factor (Fgf) to their membrane receptor, leading to the activation of a kinase cascade composed of Raf, Mek and Erk

(Fig. 4). Fgf4 is secreted, during early embryonic development, from the epiblast cells of early blastocysts to induce primitive endoderm differentiation in neighboring cells by activating the MAPK signaling pathway (cells in the developing embryo are in constant communication with adjacent cells through the secretion of signaling molecules, driving this way the process of embryogenesis). Interestingly, Fgf4-/- mutant mESCs fail to differentiate into both neural as well as mesodermal lineages (Kunath et al., 2007; Stavridis et al., 2007). This is also the case for homozygous mutant cells for the Erk2 kinase, the main Erk isoform in mESCs (Kunath et al., 2007).

Lastly, in contrast to naive mESCs, primed EpiSCs are maintained through the addition of the MAPK activator Fgf2 together with Activin to the culture medium (Brons et al., 2007; Tesar et al., 2007).

1.3. The MAPK signaling pathway

This next section focuses specifically on the MAPK signaling pathway, given that the first part of this work aims at identifying X-linked MAPK inhibitors that, when present in a double dosage in female cells, lead to sex differences in mESCs.

Four sub-families of MAPKs can mediate the mitogen-activated protein kinase (MAPK) signaling pathway: Erk1/2, Jnk, p38 and Erk5 (Johnson and Lapadat, 2002). While Jnk and p38 are usually activated by stress signals, the MAPK/Erk pathway controls many cellular responses such as proliferation, migration, apoptosis and differentiation (Johnson and Lapadat, 2002). It is therefore crucial for cell survival and its dysregulation has been linked to many diseases such as cancer (Roberts and Der, 2007).

1.3.1 Cascade components at a glance

Fgf ligands represent the main activators of the MAPK signaling pathway during early development. Vertebrates possess 22 types of Fgf ligands and five types of Fgf receptors; although in the early embryo, Fgf4 and Fgfr2 are predominantly expressed (Arman et al., 1998; Goldin and Papaioannou, 2003; Johnson and Williams, 1993; Lanner and Rossant, 2010; Ornitz and Itoh, 2001; Rappolee et al., 1994). Fgf receptors consist of an extracellular ligand-binding domain, a single transmembrane domain and an intracellular domain with tyrosine kinase activity. Ligand binding leads to dimerization and subsequent phosphorylation of its intracellular domain, recruiting a complex that binds to the phosphorylated residue comprising the fibroblast growth factor receptor substrate 2 (Frs2), the Src homology region 2 domain-containing phosphatase 2 (Shp2 or Ptpn11) and the growth factor receptor-bound protein 2 (Grb2) (Fig. 5) (Burgar et al., 2002; Gotoh, 2008; Kouhara et al., 1997; Lin et al., 1997; Lowenstein et al., 1992; Ong et al., 2000; Sarabipour and Hristova, 2016; Schlessinger et al., 2000; Yan et al., 2002). This leads to the activation of the Ras GTPase by the nucleotide exchange factor son of sevenless (SOS) through the exchange of GDP for GTP (Margarit et al., 2003; Rajalingam et al., 2007; Simon and Schreiber, 1995). Active Ras then starts the sequential phosphorylation of the kinases Raf, Mek and lastly Erk (Fig. 5).

The Raf kinase phosphorylates the two isoforms of Mek (Mek1 and Mek2) at serine 217 and 221 residues (in mouse Mek1/2), which lie within the activation loop. Curiously, while Mek1 seems to be indispensable for developmental progression ($Mek1^{-/-}$ knockout mice die around E10.5), $Mek2^{-/-}$ mice are viable (Bélanger et al., 2003; Bissonauth et al., 2006). Meks (mitogen activated protein kinase kinase) phosphorylate residues tyrosine 205/185 and threonine 203/183 of both mouse Erk isoforms, Erk1 and Erk2 (Roskoski, 2012). Also in this case, one isoform plays a more essential role during development, since $Erk2^{-/-}$ mice die after implantation, whereas $Erk1^{-/-}$ mice are phenotypically normal (Hatano et al., 2003; Nekrasova et al., 2005; Saba-El-Leil et al., 2003).

Erk targets comprise both nuclear as well as cytoplasmic proteins with diverse function, including kinases, transcription factors and RNA-binding proteins. Nuclear targets, such as the ETS family transcription factor ETS Like-1 protein (Elk-1), can be activated by Erk following its nuclear translocation through Mek-mediated

phosphorylation. C-terminal Elk1 phosphorylation increases its affinity to the serum response factor (SRF), building a dimer that can bind to serum response elements (SRE) and Elk1 binding sites, leading to transcriptional activation of target genes such as Egr1 and c-Fos (Marais et al., 1993; Whitmarsh et al., 1995). The latter, for example, plays an important role in proper progression of differentiation and proliferation (Eferl and Wagner, 2003).

Among several other MAPK target genes are found negative feedback regulators such as dual specificity phosphatases (Dusp) and Sprouty proteins (Spry), which allow for the modulation of signaling responses (see below).

1.3.2 Negative feedback regulation of the MAPK signaling pathway

The MAPK signaling pathway is controlled by several negative-feedback mechanisms that regulate its magnitude, duration and location within the cell to ensure homeostasis (Fig. 5). For once, Erk has been shown to phosphorylate numerous MAPK pathway components such as Fgf receptors, SOS, Frs2, Raf and Mek, leading to their inhibition by preventing association with other pathway components in most cases (Fig. 5) (Brummer et al., 2003; Eblen et al., 2004; Kamioka et al., 2010; Lake et al., 2016; Lax et al., 2002; Ritt et al., 2010; Wu et al., 2003; Zakrzewska et al., 2013).

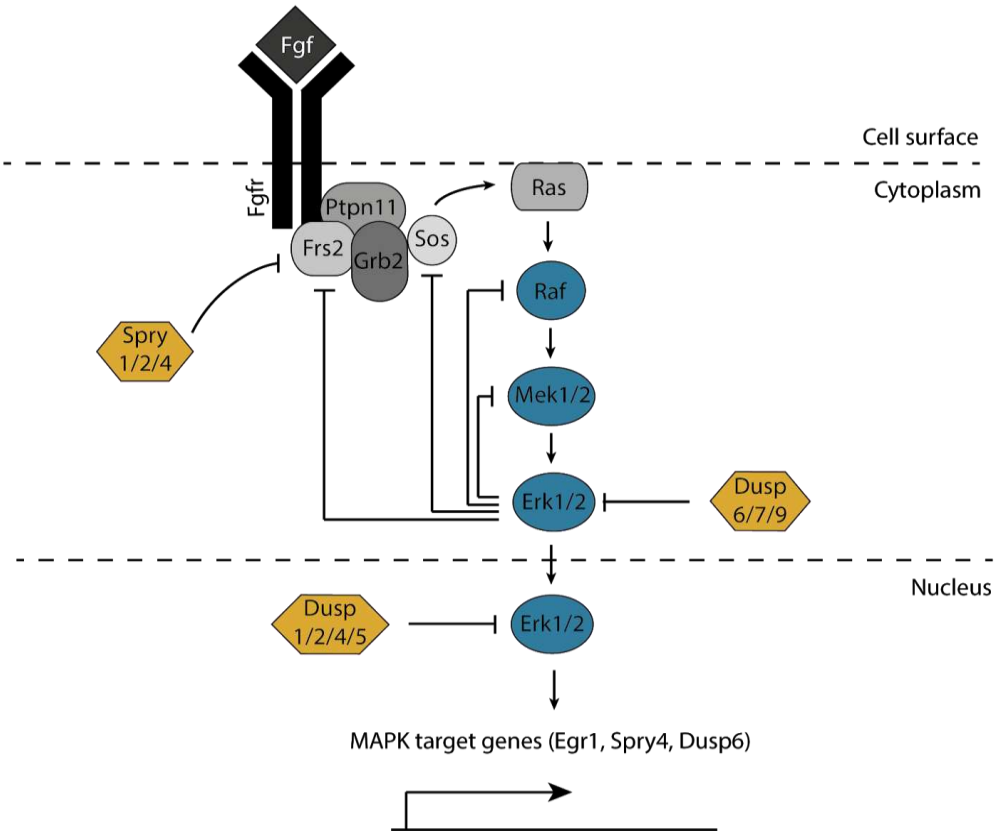

Figure 5: The MAPK signaling pathway and its negative feedback regulation. Briefly, the fibroblast growth factor (Fgf) binds the Fgf receptor (Fgfr), leading to its phosphorylation and subsequent activation. This induces the formation of a complex consisting of the FgfR Substrate 2 (Frs2), the growth factor receptor-bound protein 2 (Grb2) and Src homology region 2 domain-containing phosphatase 2 (Shp2 or Ptpn11). This leads to the activation of the Ras GTPase, triggering the kinase cascade of Raf, Mek and Erk. Activated Erk translocates to the nucleus to activate MAPK target genes and feedback regulators (dual specificity phosphatases (Dusps) and Sprouty proteins). Negative feedback regulation has been reported from Erk to Mek1/2, Raf, Sos and Frs2, among others. Additionally, Sprys mediate pathway inhibition upstream of Erk and Dusps are able to dephosphorylate and inactivate Erk both in nuclear as well as cytoplasmic compartments (Adapted from Lake et al., 2016).

Furthermore, several MAPK target genes represent known feedback regulators, such as dual specificity phosphatases (Dusp) and Sprouty proteins. The mechanism of action of the latter still needs further elucidation, however, studies have reported an inhibitory effect of Spry1 and Spry2 on binding of Grb2 to Frs2 (Fig. 5) (Hanafusa et al., 2002). Additionally, Sprouty proteins could mediate their inhibiting action by binding to Raf-1 (Sasaki et al., 2003; Yusoff et al., 2002). Nevertheless, further insights need to be gained to properly elucidate the inhibitory effect of Sprouty proteins on the MAPK pathway.

Dusps, on the other hand, are able to dephosphorylate and inactivate both the threonine and tyrosine residues necessary for the activation Erk1/2 proteins (Fig. 5). They consists of an N-terminal docking domain, which mediates substrate recognition, and a C-terminal catalytic domain (Dickinson and Keyse, 2006; Owens and Keyse, 2007). A subgroup of the Dusps are the dual-specificity MAPK phosphatases (MPKs) that can be divided into three groups (Caunt and Keyse, 2013). The first group is represented by nuclear proteins that are able to dephosphorylate Erk1/2 but also JNK and p38 (which are part of other MAPK signaling pathways): Dusp1, Dusp2, Dusp4 and Dusp5 (the latter only inactivates Erk1/2). The second group comprises cytoplasmic located Erk-specific phosphatases: Dusp6, Dusp7 and Dusp9 (Figure 5). Lastly, the third group contains the JNK/p38 specific phosphatases Dusp8, Dusp10 and Dusp16. Due to their distribution in particular cellular compartments, Dusps are able to regulate Erk specifically in either the cytoplasm or the nucleus, leading to localized signaling modulation (Kidger et al., 2017).

Additionally, Dusps have been shown to mediate cross talk between different signaling pathways. Induction of Dusp9 expression through Bmp4-mediated Smad1/4 and 5 activation has been shown to inhibit Erk and thus differentiation of mESCs (Li et al., 2012; Ramesh et al., 2008). On the other hand, transforming growth factor-β (TGFß) has also been shown to induce Dusp4 expression through Smad3 activation, leading to Erk dephosphorylation and promoting apoptosis by blocking the Erk-dependent degradation of BIM (Bcl-2-interacting mediator of cell death) (Li et al., 2012; Ramesh et al., 2008).

1.3.3 The role of the MAPK pathway during early development

During early development, the activation of the MAPK pathway mediated by Fgf4 is necessary for the formation of primitive endoderm lineages from the ICM of the pre-implantation blastocyst (Fig. 6). Fgf4 is expressed in an autocrine fashion under the control of Oct4 and Sox2 in Nanog-high epiblast cells (Yuan et al., 1995), whereas primitive endoderm cells, on the other hand, express low levels of Nanog and high levels of the Fgf4 receptor Fgfr2 and the primitive endoderm (PE) marker Gata6 (Chazaud et al., 2006; Guo et al., 2010; Plusa et al., 2008).

The key role of the MAPK pathway in the formation of the PE in the preimplantation epiblast is further confirmed in blastocysts treated with Mek inhibitors or devoid of MAPK components such as Grb2, Fgf4 and Fgfr2, which display an expanded pluripotent epiblast and show peri-implantation lethality (Arman et al., 1998; Chazaud et al., 2006; Cheng et al., 1998; Feldman et al., 1995; Kang et al., 2013; Yamanaka et al., 2010). The fact that the pluripotent epiblast is still present in these blastocysts further supports the notion that pluripotency can be maintained in the complete absence of MAPK signaling, while being key for the further development and differentiation of the early blastocyst. This is also shown in mESCs with homozygous Fgf4 or Erk2 mutations, which lack the ability to differentiate towards neural or mesodermal lineages (Kunath et al., 2007; Stavridis et al., 2007).

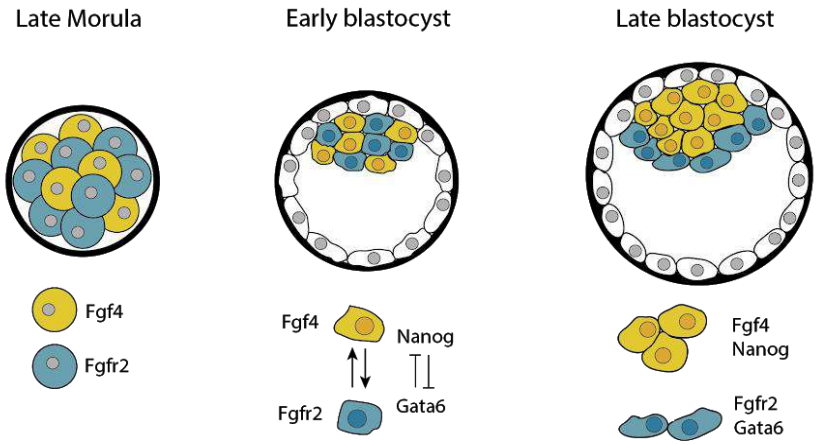

Figure 6: Role of MAPK signaling in lineage decisions during early embryonic development. Around the late morula/early blastocyst stage, cells start expressing either Fgf4 or Fgfr2 in a salt and pepper pattern. Fgf4 secreting epiblast cells express high levels of Nanog whereas Fgfr2 expressing cells also express the primitive endoderm markers Gata6. Nanog and Gata6 expression is mutually exclusive. Activation of the MAPK pathway mediated by Fgf4 is therefore necessary for the formation of primitive endoderm lineages from the ICM of the pre-implantation blastocyst (Adapted from Lanner and Rossant 2010).

In summary, MAPK signaling is indispensable for the differentiation of primitive endoderm lineages from the pluripotent ICM as well as neural and mesodermal lineages from pluripotent mESCs, representing a pivotal differentiation-inducing pathway. Its activation is a key step for the transition from the naive to the primed pluripotency state, which is additionally accompanied by a series of epigenetic changes, such as the process of X-chromosome inactivation (XCI) in female mammals. The next section will focus on outlining this dosage compensation mechanism in detail, as the main focus of this work involves the identification of the genes underlying sex differences in mESCs that arise from a double X-dosage in female cells. These differences are present also during differentiation, which encompasses the process of XCI.

1.4. Dosage compensation of sex chromosomes and X-chromosome inactivation in mammals

The process of sex determination in organisms with sexual reproduction is, in many species, based on genetic differences such as heteromorphic sex chromosomes (e.g. X and Y or Z and W sex chromosomes). Males may represent the heterogametic species displaying an XY genotype whereas female are homogametic XX, such as in mammals (male heterogamety). Alternatively, in other species such as birds, females have acquired the heterogametic ZW genotype (female heterogamety) (Mank, 2013).

During evolution, sex chromosomes arise from a pair of autosomal chromosomes that seize to recombine (proto sex chromosomes), leading to extensive gene loss and to the accumulation of repetitive DNA in the sex-limited Y and W chromosomes (Disteche, 2012; Vicoso and Bachtrog, 2009). In humans, it is estimated that only 3% of the genes located in the proto Y-chromosome have been retained in the Y chromosome, whereas 98% of the genes found on the proto X chromosome are still present in the X chromosome (Disteche, 2016). This extreme imbalance in gene dosage poses a natural form of aneuploidy, which becomes neutralized through the process of dosage compensation.

1.4.1 Dosage compensation mechanisms

Dosage compensation of sex chromosomes varies between different species and has been extensively studied in *D. melanogaster, C. elegans and M. musculus* (Disteche, 2016). In *D. melanogaster,* dosage compensation is accomplished through the upregulation of X-linked genes in males by the male-specific lethal (MSL) complex to

achieve the double X-chromosomal dosage present in females (Fig. 7) (Kuroda et al., 2016). In *C. elegans*, on the other hand, the dosage compensation complex (DCC) binds to both X chromosomes in hermaphrodite worms, resulting in a two-fold repression of gene expression (Albritton and Ercan, 2018).

In mammals, dosage compensation is achieved through the process of X chromosome inactivation (XCI), which starts with the upregulation of the lncRNA Xist from one of the two X chromosomes (Fig. 7, see below) (Lyon, 1961). Here, one of the two X chromosomes present in females undergoes heterochromatinization, leading to the transcriptional silencing of most of its genes and to the formation of the Barr body in the cell nucleus (Barr and Bertram, 1949; Dixon-McDougall and Brown, 2016; Robert Finestra and Gribnau, 2017).

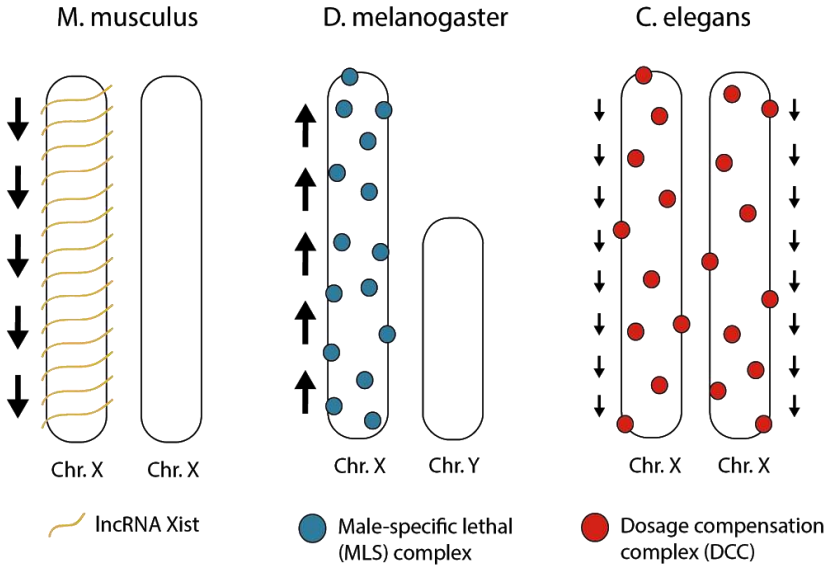

Figure 7: Mechanisms of X-dosage compensation in mammals (*M. musculus*), flies (*D. melanogaster*) and worms (*C. elegans*). In mammals, one of the two X-chromosomes becomes inactivated through the spreading and coating of the lncRNA Xist, which leads to heterochromatinization and silencing of most X-linked genes. In flies, on the other hand, the male-specific lethal (MSL) complex increases X-chromosomal dosage in males by acetylating and opening its chromatin. Lastly, the dosage compensation complex (DCC) downregulates gene expression in both X-chromosomes leading to a two-fold repression in hermaphrodite worms.

There are two forms of X-chromosome inactivation: imprinted and random (Okamoto et al., 2011). Marsupials, for instance, undergo imprinted XCI exclusively by silencing the paternal X chromosome in all somatic cells (Grant et al., 2012). Placental mammals, on the other hand, display random X chromosome inactivation in all somatic tissues (Deng et al., 2014; Moreira de Mello et al., 2010; Okamoto et al., 2011; Petropoulos et al., 2016).

Curiously, both imprinted as well as random XCI are observed in mice, the most well studied model organism for XCI. Imprinted dosage compensation occurs around the four-to-eight-cell stage of the preimplantation blastocyst, leading to the inactivation of the paternally inherited X chromosome (Xp) (Fig. 8) (Borensztein et al., 2017a; Mak et al., 2004; Okamoto et al., 2004). Around embryonic day E3.5, the naive pluripotent epiblast cells of the preimplantation blastocyst that give rise to the embryo proper will start to reactivate their X chromosome, whereas trophectoderm and primitive endoderm cells, that give rise to extraembryonic lineages, retain their imprinted Xp status (Mak et al. 2004; Okamoto et al. 2004; Takagi 2003; Borensztein et al. 2017; Cheng et al. 2019; Mohammed et al. 2017). The process of random XCI starts around E5.5 so that primed epiblast cells from the postimplantation blastocyst at E6.5 (and later on all somatic cells) already express either maternal or paternal X-linked genes (Fig. 8) (Mohammed et al. 2017; Cheng et al. 2019).

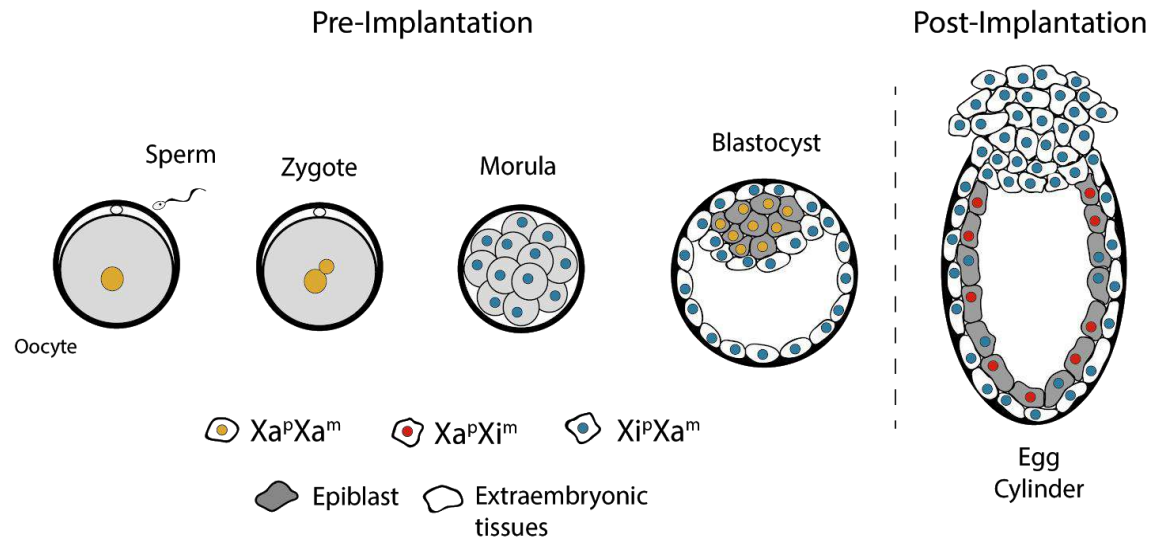

Figure 8: Forms of X chromosome inactivation in early mouse development. Imprinted XCI occurs in mice around the four- to eight- cell stage, where only the paternal X chromosome becomes inactivated ($Xi^{P}Xa^{m}$). Around E3.5, cells of the inner cell mass that will become embryo-forming epiblast cells start reactivating their X chromosome ($Xa^{P}Xa^{m}$), whereas cells giving rise to extra-embryonic tissues retain their imprinted Xp status. Finally, random X chromosome inactivation is observed in epiblast cells of the post-implantation egg cylinder ($Xi^{P}Xa^{m}$ and $Xa^{P}Xi^{m}$).

1.4.2 XCI in placental mammals is mediated by the lncRNA Xist

X-chromosome inactivation is mediated by long non-coding RNA molecules (lncRNAs) encoded on the X chromosome that act *in cis:* Rsx (RNA-on-the-silent X) in marsupials and Xist (X inactive specific transcript) in placental mammals (Borsani et al., 1991; Brockdorff et al., 1991, 1992; Brown, 1991; Brown et al., 1992; Clemson et al., 1996; Gendrel and Heard, 2014; Grant et al., 2012).

Xist upregulation from one of the two X-chromosomes (monoallelic) present in females marks the start of X chromosome inactivation (XCI), which takes place during the transition from the naive to the primed pluripotent state. This is followed by the coating of the X chromosome *in cis* by this lncRNA, which then recruits epigenetic regulators that lead to chromosome silencing. Xist is pivotal for the X chromosome choice involved in the process of random XCI, as the mutation of just one copy of Xist in females leads to non-random XCI, with all cells inactivating only the wildtype X chromosome (Marahrens et al., 1997; Penny et al., 1996).

Female-specific monoallelic upregulation of Xist is ensured by several factors, many of which are located close to the Xist locus in a region called the X inactivation center (Xic) (Fig. 9). A model has been proposed in which a double dosage of a trans-acting activator (tXA) is required for Xist upregulation from one of the X chromosomes present in female cells, and that a negative feedback loop involving the silencing of this activator from the inactive X chromosome could ensure monoallelic Xist upregulation (Jonkers et al. 2009; Barakat et al. 2011; Augui et al. 2011; Mutzel et al. 2019). Additionally, Xist silencing in the active X chromosome could be positively reinforced by a cis-acting repressor (cXR) (Mutzel et al. 2019).

One candidate for the trans-acting activator of Xist is the E3 ubiquitin protein ligase Rnf12, which targets the pluripotency factor Rex1 for degradation, a known naive pluripotency factor and strong Xist repressor (Barakat et al., 2011; Gontan et al., 2012, 2018; Jonkers et al., 2009). Other lncRNAs located in the Xic have additionally been proposed to act as Xist activators: Jpx and Ftx, however, only Jpx could exert a function *in trans* and it additionally appears to escape X-chromosome inactivation (Fig. 9) (Barakat et al., 2014; Carmona et al., 2018;

Sun et al., 2013; Tian et al., 2010; Chureau et al., 2011; Hosoi et al., 2018; Barakat et al., 2014; Carmona et al., 2018; Furlan et al., 2018; Tian et al., 2010).

The most well characterized cis-acting repressor (cXR), on the other hand, is the lncRNA Tsix, whose locus overlaps Xist and is transcribed antisense to the latter (Figure 9). It is essential for proper dosage compensation in females, as heterozygous mutants with a deletion of the Tsix promoter and enhancer regions have skewed XCI towards the mutated X chromosome (Lee, 2005; Lee and Lu, 1999; Lee et al., 1999). Xist repression by Tsix seems to be transcription-dependent, leading to chromatin changes along the Xist promoter that ultimately downregulate Xist expression (Navarro et al., 2005, 2006, 2009; Ohhata et al., 2008; Sado et al., 2005; Shibata et al., 2008; Sun et al., 2006).

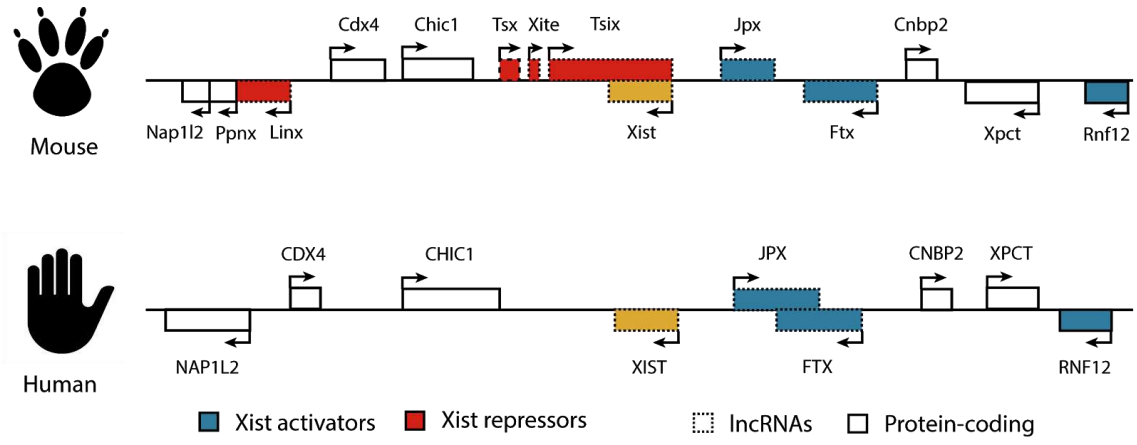

Figure 9: Regulation of Xist by the X inactivation center (Xic). The Xic harbors a series of lncRNAs and protein-coding genes, some of which have been shown to affect Xist expression and the process of X chromosome inactivation. The lncRNAs Jpx and Ftx, together with the trans-acting Rnf12 protein are found among the Xist activators. Tsix represses Xist expression and is itself positively regulated by Tsx and Xite, whereas Linx has been shown to repress Xist expression through long-range mechanisms.

The process of X-chromosome inactivation is tightly coupled to the onset of differentiation and the transition from the naive to the primed pluripotent state, which comprises the downregulation of various pluripotency markers. It has been shown that several pluripotency factors bind Xist, Tsix and their regulatory sequences and regulators (Rnf12, Jpx) (Chen et al., 2008; Donohoe et al., 2009; Navarro et al., 2008, 2010). An over early upregulation of Xist due to either knockdown of the pluripotency factor Oct4 or knockout of the Tsix repressor leads to a higher proportion of cells expressing this lncRNA in a biallelic form (Donohoe et al., 2009; Lee, 2005). This could be in accordance with a proposed model in which the proportion of biallelically Xist-expressing cells depends on the precise timing of Xist upregulation, with fast Xist upregulation generating a higher proportion of bialellic cells, and trans-acting activator (tXA) silencing, with slow silencing also promoting a higher fraction of biallelic cells (Mutzel et al. 2019).

Furthermore, effective chromosome silencing can only be achieved through Xist upregulation during early differentiation, pointing to an impossibility of XCI induction in differentiated cells (Wutz and Jaenisch, 2000). Initiation and termination of XCI is thus tightly coupled to developmental progression to ensure its successful completion.

Monoallelic Xist upregulation in females during differentiation sets the onset of XCI and represents a tightly regulated process, ensured by many cis- and trans-acting factors. This is followed by the coating of the X chromosome by Xist *in cis* and the recruitment of epigenetic regulators that will ultimately lead to chromosome silencing. How this happens is the subject of the next section.

1.4.3 The silencing of an X chromosome

Ectopic expression of an inducible Xist cDNA from an autosomal chromosome leads to gene silencing in cis, albeit to a lower degree than in female cells, demonstrating that Xist alone is capable of mediating chromosome inactivation (Chow et al., 2007; Tang et al., 2010; Wutz and Jaenisch, 2000). The latter is accompanied by a series of epigenetic changes that ensure the formation of heterochromatin on the inactive X, ultimately leading to gene silencing and X dosage compensation. These include histone deacetylation by the deacetylase HDAC3, followed by the Polycomb repressive complex 1 (PRC1) mediated H2AK119 ubiquitination, which in turns recruits PRC2 leading to H3K27me3 accumulation (Fig. 10) (Brockdorff, 2017; Chaumeil et al., 2006; Disteche and Berletch, 2015; Żylicz et al., 2019). Maintenance of the X inactivation state is then ensured through the replacement of histone H2A by macrohistone H2A and through the deposition of CpG DNA Methylation by the Dnmt3b methyltransferase (Costanzi and Pehrson, 1998; Gendrel et al., 2012).

Xist interacts with several proteins that mediate the heterochromatization and subsequent inactivation of a single X chromosome. Several of these proteins have been identified in mouse through Xist pull-down approaches (Chu et al., 2015; McHugh et al., 2015; Minajigi et al., 2015). Among the most important mediators of Xist silencing were found Spen, a known transcriptional repressor, whose dysregulation leads to significant defects in X-linked gene silencing, hnRNPK, Rbm15, hnRNPU and CIZ1 (Fig. 10) (Chu et al., 2015; Dossin et al., 2020; McHugh et al., 2015; Moindrot et al., 2015; Monfort et al., 2015; Nesterova et al., 2019; Shi et al., 2001; Nesterova et al., 2019; Patil et al., 2016; Hasegawa et al., 2010; Ridings-Figueroa et al., 2017; Sunwoo et al., 2017). They seem to bind Xist through several of its identified domains, including the A-, B- and C-repeats, leading to transcriptional silencing, histone deacetylation and the recruitment of polycomb repressive complex 1 and 2 (Fig. 10) (Bousard et al., 2018; Chu et al., 2015; Colognori et al., 2019; Pintacuda et al., 2017; Wutz et al., 2002).

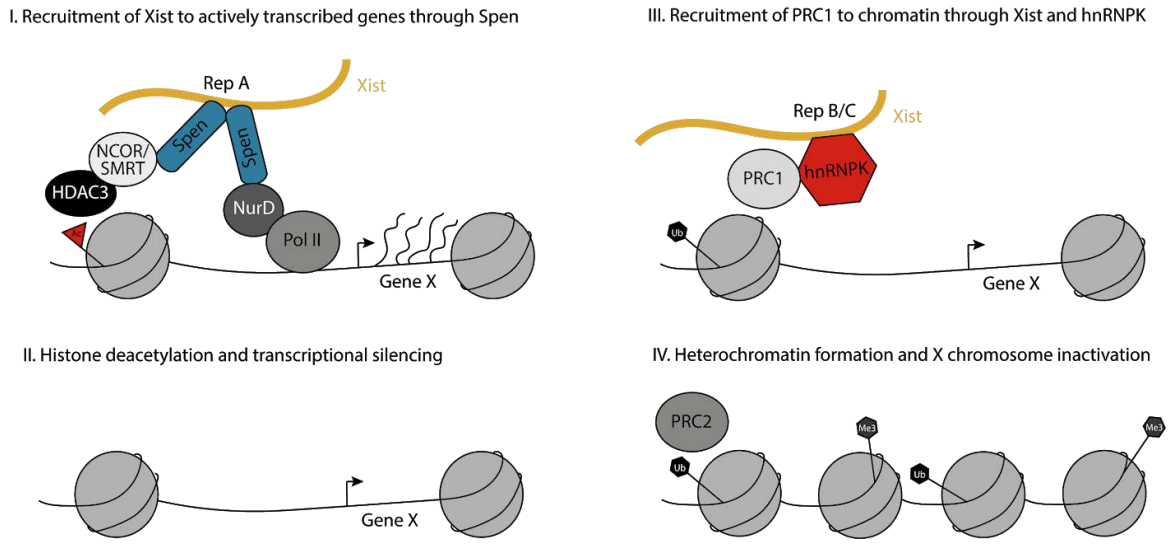

Figure 10: Molecular mechanisms behind the process of X-chromosome inactivation in mice. Xist recruits Spen to actively transcribed genes through the interaction of Spen with NurD and Pol II. This is turn leads to the deacetylation of gene regulatory elements through the interaction of Spen with the NCOR/SMRT complex and HDAC3, inducing gene silencing. Xist subsequently recruits Polycomb group proteins to chromatin through its interaction with hnRNPK, leading to the ubiquitination of histones. This in turns mediates the recruitment of PRC2, which induces heterochromatin formation and X chromosome inactivation.

Interestingly, some X-linked genes escape the process of XCI and remain expressed from both X-chromosomes; these are termed as “escapee” genes. It has been shown that approx. 15% of X-linked genes escape XCI in humans, whereas this number is reduced to 3% in the mouse (Berletch et al., 2010; Carrel and Willard, 2005; Yang et al., 2010).

In conclusion, X-chromosome inactivation is a precisely orchestrated process that starts with the upregulation of the lncRNA Xist from one the two X-Chromosomes present in females during a very specific developmental window at the transition from the naive to the primed pluripotent state. The timing and manner of Xist upregulation is tightly regulated by several activators and repressors present in the vicinity of Xist in the X inactivation center (Xic), together with various pluripotency factors. Silencing of one X chromosome is subsequently mediated through Xist coating and several Xist interacting proteins that recruit epigenetic modifiers, leading to heterochromatinization and the formation of the Barr body in female cells.

1.5. Sex differences in mammals due to variations in X-chromosomal dosage

X dosage compensation takes place during the transition from the naive to the primed pluripotent state in female mammals. Therefore, in the preimplantation blastocyst, before this process has taken place, females express X-linked genes at around two-fold higher levels, which leads to substantial sex differences between male and female blastocysts.

Dosage imbalance is largely neutralized in somatic cells after XCI has taken place. However, sex differences may still arise from increased expression of a subset of escapee genes, which could cause female individuals to be either more or less prone to the acquirement of certain disease phenotypes, such as various cancer types (Ratnu et al., 2017; Schurz et al., 2019; Snell and Turner, 2018).

The next sections will focus on the sex differences observed in early embryonic development and in mESCs, which represent an excellent *in vitro* model for these early stages of developmental progression, as they possess two active X chromosomes, which become inactive in the process of differentiation. Clarifying the phenotypic differences arising from variations in X-chromosomal dosages in early mammalian development is essential for this work, as its main focus lies in the identification of X-chromosomal genes that underlie them.

1.5.1 Sex differences during early embryonic development

It has been reported that in many species, including mice, rats, cows and humans, female embryos develop slower compared to males (Fig. 11) (Alfarawati et al., 2011; Avery et al., 1989, 1991; Luna et al., 2007; Ménézo et al., 1999; Ray et al., 1995; Scott and Holson, 1977; Seller and Perkins-Cole, 1987; Tsunoda et al., 1985; Yadav et al., 1993; Zwingman et al., 1993). Since these differences manifest at developmental stages where fetal hormones are not yet produced, they have been attributed to variations in sex-chromosomal dosages.

Both an increase in cell number and weight (Scott and Holson, 1977) as well as more advanced stages of development (Seller and Perkins-Cole, 1987; Tsunoda et al., 1985) (e.g. higher number of somites or faster blastocoel formation in male embryos at a certain developmental time-point) have been reported in male blastocysts. It is therefore difficult to distinguish whether these differences are caused by increased proliferation rates in male embryos or genes that affect developmental progression and differentiation, or both. In this context, the Y-linked gene SRY has been shown to have mitogenic properties and it is expressed from very early on during development in human and mouse (Fiddler et al., 1995; Zwingman et al., 1993). However, the contribution of the Sry gene to the observed sex differences has been ruled out in mice in a study where the weight of male embryos with a *Sry* deletion was compared to the one of female embryos at E10.5, showing still significant differences (Burgoyne et al., 1995). The authors additionally concluded that the sex differences observed in early blastocysts at this embryonic stage could be attributed to a combinatorial effect of the Y-chromosome during the preimplantation period and X-chromosomal dosage (XX vs. X) at later embryonic stages around E9.5 (Burgoyne et al., 1995).

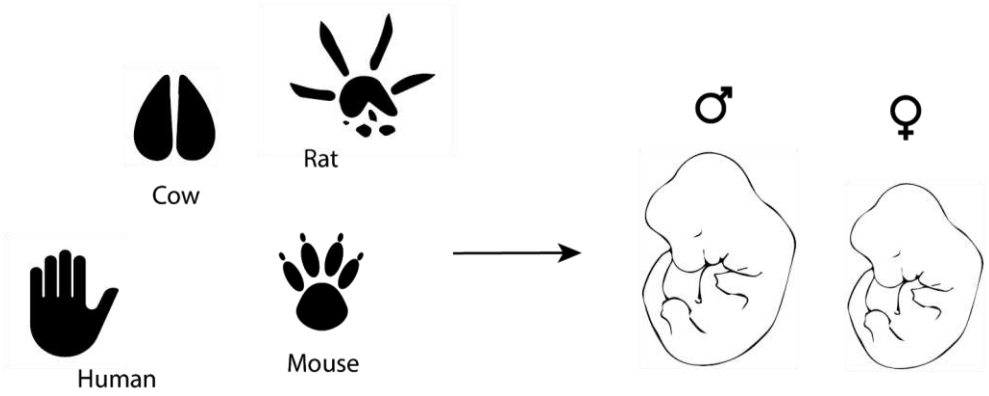

Figure 11: Sex differences during early development. Female embryos of many mammalian species develop slower compared to their male counterparts at early stages of development. Since no fetal hormones are secreted during this time, it has been proposed that the observed sex differences are due to variations in sex chromosome dosage.

Other evidence of X-chromosomal dosage effects was reported in a study that compared the weights of XY, XX, XmO and XpO embryos also at 10.5 dpc, the latter two exhibiting X chromosomes derived either paternally (XpO) or maternally (XmO) (Thornhill and Burgoyne, 1993). Curiously, while XpO developed at a similar rate compared to XX blastocysts, XmO developed at much faster rates comparable to XY embryos. It was therefore proposed that a paternally inherited X chromosome slows the development of XX embryos, which could be attributed to differential expression of certain genes between the two X chromosomes due to genomic imprinting. This phenomenon, where genes are expressed in a parent-of-origin-specific manner, is due to the presence of epigenetic marks such as DNA methylation or histone modification in imprinted genes that are inherited from sperm and oocyte cells (Ferguson-Smith 2011).

1.5.2 Sex differences in murine mouse embryonic stem cells

Female mESCs possess two active X-chromosomes and undergo the process of XCI once induced to differentiate. Interestingly, it has recently been reported that both female mESCs as well as iPSCs (induced pluripotent stem cells) are found in a more naive state of pluripotency compared to their male counterparts (Fig. 12) (Schulz et al. 2014; Song et al. 2019). It was shown that these differences arise due to varying X-chromosomal dosage, as the XO subclones of female mESCs behave similar to male cells.

Female mESCs display lower levels of the differentiation-inducing MAPK signaling pathway, which is reflected in their lower expression levels of MAPK target genes (Fig. 12). Curiously, phosphorylation levels of MAPK pathway components such as Erk and Mek are higher in XX wildtype cells, which is due to a reduced negative feedback activity of the pathway caused by the lower expression levels of feedback regulators (Fritsche-Guenther et al., 2011; Sturm et al., 2010).

Higher expression of naive pluripotency markers such as Nanog, Prdm14 and Tcl1 in Serum/LIF culture conditions is another marked sex difference between female and male mESCs, even though expression of core pluripotency factors such as Oct4 and Sox2 remains largely unchanged (Fig. 12) (Schulz et al., 2014). When induced to differentiate via LIF withdrawal or EpiSC differentiation protocols, female mESCs fail to efficiently downregulate pluripotency factors compared to male cells, where significantly lower levels are observed from day 1 of differentiation (Fig. 12). This situation reminisces of the sex differences reported in in vivo blastocysts, where male embryos are faster to reach more advanced stages of development (Burgoyne et al., 1995; Mittwoch, 1993; Thornhill and Burgoyne, 1993).

Additionally, male mESCs exhibit global CpG methylation levels close to ~60%, compared to the approx. 30% observed in female mESCs, which resemble the 20-30% CpG methylation levels observed in naive pluripotent stem cells cultured under 2i conditions (Schulz et al., 2014; Zvetkova et al., 2005).

Inhibition of MAPK signaling leads to a strong shift towards the naive pluripotency state, accompanied by an increase in pluripotency factor expression and global DNA hypomethylation (Ficz et al., 2013; Habibi et al., 2013; Hackett et al., 2013; Leitch et al., 2013; Milagre et al., 2017; Ooi et al., 2010; Pasque et al., 2018; Schulz et al., 2014; Silva et al., 2009; Zvetkova et al., 2005). It was therefore hypothesized that one or more X-encoded MAPK inhibitors present in a double dosage in female mESCs might be responsible for the observed female-specific pluripotency phenotype. This could pose a biological checkpoint to guarantee that only the cells in which successful XCI has taken place contribute to the adult organism. However, when this study was initiated, the identity of the genes mediating the observed sex differences in mESCs remained unknown.

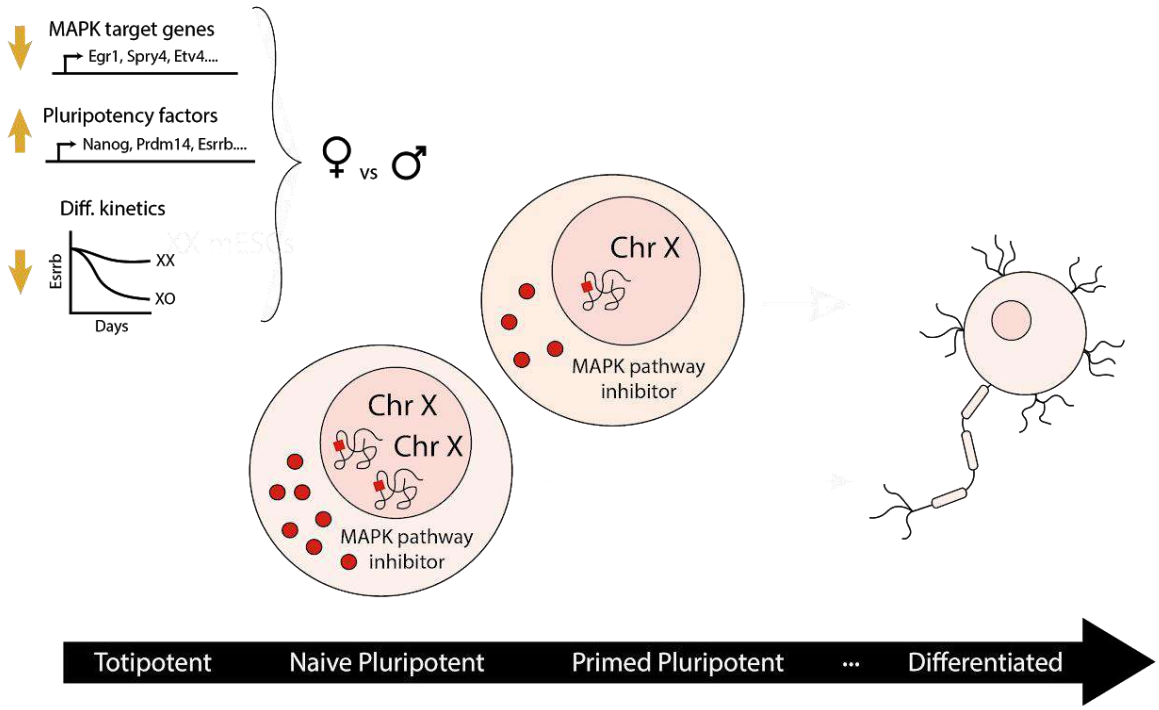

Figure 12: Sex differences in mouse embryonic stem cells. Female mESCs are found in a more naive state of pluripotency, as they display lower levels of the differentiation-inducing MAPK signaling pathway, while at the same time expressing higher levels of naive pluripotency factors and exhibiting slower differentiation kinetics compared to their male counterparts (yellow arrows). These effects might be mediated through an X-encoded MAPK inhibitor (red), which would be present in a double dosage in female mESCs. This might ensure the developmental progression of cells that have successfully undergone X chromosome inactivation, and have thus reduced the levels of the putative MAPK inhibitor and subsequently of pluripotency factor expression.

1.5.3 Genes mediating the sex differences observed in mESCs

Genes responsible for mediating sex differences in mESCs caused by X-chromosomal dosage effects should be located on the X chromosome and their expression should be at least two-fold higher in female mESCs. Additionally, a heterozygous mutation of such a gene in female mESCs should lead to a male-like phenotype. In this context, the heterozygous deletion of the Erk-specific phosphatase Dusp9 in female mESCs has been shown to lead to global CpG methylation levels similar to those observed in males (Choi et al., 2017). However, other studies have shown that these female mutants do not display significant reductions in pluripotency factor expression or faster differentiation kinetics (Song et al., 2019). Therefore, Dusp9 seems to mainly account for one aspect of the reported sex differences when expressed from just one allele in female cells.

Dusp9 overexpression in male mESCs, on the other hand, has been shown to lead to a decrease in global CpG methylation while at the same time increasing pluripotency factor expression (Choi et al., 2017). Strikingly, these cells also displayed higher levels of Erk phosphorylation, which is counterintuitive considering that overexpression of an Erk phosphatase should in fact decrease pErk levels (Li et al., 2012).

The aforementioned results suggest that Dusp9 might act together with other genes to mediate the female pluripotency phenotype, which, until now, remain elusive.

Candidate genes such as Zic3, known to positively regulate Nanog expression and the pluripotent state (Declercq et al., 2013; Lim et al., 2007, 2010), and Tfe3, which has been shown to block differentiation and increase Esrrb levels (Betschinger et al., 2013), have also been studied in mESCs. It was shown that their heterozygous mutation in female mESCs does not lead to a significant reduction in pluripotency factor expression or differentiation kinetics (Song et al., 2019). Furthermore, other X-linked genes such as Nr0b1 and Zfx have been reported to induce a differentiation blockage; however, their contribution to the female pluripotency phenotype has not been characterized so far (Galan-Caridad et al., 2007; Khalfallah et al., 2009; Zhang et al., 2014).

Overall, the question as to which genes underlie the sex differences observed in mESCs and iPSCs still remains open in the stem cell field. Since the X chromosome harbors approx. 1000 genes, it seems very challenging to assess their involvement in the previously mentioned phenotypes in an unbiased and effective manner. With the advent of new and promising technologies such as CRISPR pooled screens, it now appears that we can start looking for answers.

2. Aims of study

Female mouse embryonic stem cells (mESCs) are found in a more naive state of pluripotency compared to their male counterparts, as they display lower levels of MAPK signaling and higher expression of pluripotency factors. Additionally, these cells fail to down-regulate pluripotency factors during differentiation as effectively as male cells or their XO subclones. The genes mediating these observed sex differences remain, however, largely unknown.

Aim 1: Identification of X-linked genes that drive sex differences in mouse embryonic stem cells (mESCs)

In this work, I aimed at identifying the X-linked genes underlying the sex differences observed in mESCs in an unbiased and high-throughput manner through a series of complementary pooled CRISPR Knockout screens. In a first primary screen, I made use of a fluorescent MAPK-sensitive reporter in order to identify inhibitors of the MAPK signaling pathway by generating an sgRNA library targeting the majority of X-linked genes. I then performed a series of secondary screens targeting several top hits from the primary screen that made use of reporters that assessed pluripotency factor expression in the undifferentiated state and during differentiation, together with phosphorylation of MAPK pathway components. This way, I generated a list of candidate X-linked genes involved in the modulation of several of the observed sex differences.

Aim 2: Validation of top hits from the generated screens in male and female mESCs

After identifying candidate genes that could mediate the observed gender differences in mESCs, I validated the top ranking genes from the previously conducted pooled CRISPR knockout screens. For this, I implemented the CRISPRa Suntag system in order to overexpress these genes in male cells, which should lead to a shift towards a more naive state of pluripotency. Additionally, I generated heterozygous mutants in female mESCs by using the CRISPR/Cas9 technology. I subsequently assessed whether female mESCs with a single dosage of the genes of interest exhibited a male-like phenotype, including higher MAPK signaling leves, lower expression of pluripotency factors, faster differentiation kinetics and an increase in global CpG methylation.

3. Materials

3.1. Antibodies

Table 1. Antibodies used in this study

Epitope	Supplier	Number	Dilution
Primary antibodies			
Phospho-MEK1/2 (Ser221) (166F8)	Cell Signaling	2338	1:2000
Mek1/2 (L38C12)	Cell Signaling	4694	1:1000
Phospho-p44/42 MAPK (Erk1/2) (Thr202/Tyr204) (197G2)	Cell Signaling	4377	1:1000
p44/42 MAP Kinase (L34F12)	Cell Signaling	4696	1:2000
KLHL13 Monoclonal Antibody (8D1)	Thermo Fisher	MA5-15658	1:1000
Dusp9 Antibody	Kind gift from Keyse lab (Dickinson et al. 2002)	-	1:10000
GFP	Sigma-Aldrich	11814460001	1:1000
B-Tubulin	Cell Signaling	2146	1:1000
Secondary antibodies			
IR Dye800W Goat anti-Rabbit IgG	Li cor	P/N 926-32211	1:15000
IR Dye680W Goat anti-Mouse IgG	Li cor	P/N 926-68070	1:15000
Antibodies for pMek intracellular staining			
Phospho-MEK1/2 (Ser221) (166F8)	Cell Signaling	2338	1:100
Alexa Fluor 647 Goat anti-Rabbit	Thermo Fisher Scientific	A-21244	1:400

3.2. Plasmids

A unique identifier of the plasmids used in this study is given in brackets in column 1 as an SP (Schulz Plasmid) number.

Table 2. Plasmids used in this study.

Vector	Function	Source	Promoter	Bacterial resistance	Mammalian resistance

302 reporter (SP35)	Amplification of the SRE/Elk-sensitive promoter	Kind gift from Morkel and Brummer lab	SRE/Elk	Ampicillin	-
pCAGG-L/eGFP (SP9)	Amplification of PolyA sequence	O. Masui	Chicken-B-Actin	Ampicillin	-
lentiGuide-puro (SP32)	sgRNA Library cloning, cloning of sgRNAs targeting Mek and Erk locus	Addgene 52963, (Sanjana et al., 2014)	U6 (sgRNA)	Ampicillin	Puromycin
lenti MS2-P65-HSF1-Hygro (SP63)	SRE-Elk reporter cloning	Addgene 61426, (Konermann et al., 2015)	-	Ampicillin	Hygromycin
pUC19 (SP194)	Cloning of repair template for Nanog and Esrrb reporter generation	Thermo Fisher Scientific SD0061	Lac	Ampicillin	-
PX330 (SP301)	sgRNA cloning for Nanog and Esrrb reporter generation	Addgene 42230, (Cong et al., 2013)	CBh (Cas9), U6 (sgRNA)	Ampicillin	-
pLP1	Lentiviral packaging	Thermo Fisher Scientific	-	Ampicillin	-
pLP2	Lentiviral packaging	Thermo Fisher Scientific	-	Ampicillin	-
VSVG	Lentiviral packaging	Thermo Fisher Scientific	-	Ampicillin	-
PX458 (SP177)	sgRNA cloning for Dusp9 mutant generation	Addgene 48138, (Ran et al., 2013)	CBh (Cas9), U6 (sgRNA)	Ampicillin	-
pU6-sgRNA-EF1Alpha-puro-T2A-BFP (SP65)	CRISPRa sgRNA cloning	Addgene 60955, (Gilbert et al., 2014)	EF1a (Puro), U6 (sgRNA)	Ampicillin	Puromycin
pLenti-PGK-GFP-Blast (SP51)	Cloning of constructs for Klhl13 Immunoprecipitation experiments	Addgene 19069, (Campeau et al., 2009)	PGK	Ampicillin	Blasticidin
pCAG-Cre (SP44)	Cre recombinase expression	Addgene 13775, (Matsuda and Cepko, 2007)	CAG	Ampicillin	-
lentiCas9-Blast (SP54)	Cas9 expression	Addgene 52962, (Sanjana et al., 2014)	EFS	Ampicillin	Blasticidin
pSuper-Puro (SP10)	SRE/Elk reporter cloning	-	H1	Ampicillin	Puromycin

3.3. Primers

All primers were purchased from Sigma-Aldrich and sequences are listed in the 5´to 3´orientation.

Table 3. qPCR primer pairs used in this study

Target gene	Primer Name	Forward	Reverse	Source
Nanog	ES025/ES026	AGGATGAAGTGCAAGCGGTG	TGCTGAGCCCTTCTGAATCAG	Navarro et al, 2008
Esrrb	ES193/ES194	CTGCAGCTGGTGCGCAGGTA	CCTGGAGCTTCTGCACCGCC	Schulz et al., 2014
Prdm14	ES191/ES192	ACAGGCCATACCAGTGCGTGT	GTGGCTGTCGTGGGCAGCAT	Designed by E. G. Schulz
Arpo	Arpo_F/Arpo_R	TCCAGAGGCACCATTGAAATT	TCGCTGGCTCCCACCTT	Designed by E. G. Schulz
Rrm2	Rrm2_F/Rrm2_R	CCGAGCTGGAAAGTAAAGCG	ATGGGAAAGACAACGAAGCG	Schulz et al., 2014
Egr1	ES431/ES432	GTGTCGAATCTGCATGCGTAA	ATCACTCCTGGCAAACTTCCT	Li et al, 2012
Spry4	ES489/ES490	GACCCACTCGGGTTCGGGGA	GGGGGCTCCATGAGGCTGGA	Schulz et al., 2014

Table 4. PCR primer pairs used in this study

Target	Primer Name	Forward	Reverse
SRE-Elk promoter	OG109/OG110	TGGTTAATTAGCTAGGGGATCCC AGGATGTCCATATTAG	CTCCACTGCCTGTACACACATTGA TCCTAGCAGAAGCAC
PolyA sequence	OG19/OG20	GCTAGGATCAATGTGTGACGGTG GCTAATAAAGGAAATTTATTT	GGGAACAAAAGCTGGGTCGACGA TCTTCATAAGAGAAGAGG
Nanog_WT	OG152/OG155	TGAACGCATCTGGAAGCCTT	GTATGCCACCTTTGGTCCCA
Nanog_mCherry	g6_2f/mCherry_ seq_rev	TGTTTAAGGTCGGGCTGT	TACATGAACTGAGGGGAC
Nanog_Puro	OG166/OG167	GCAGAAGAAGACCATGGGCT	ACATGGTGGCTCACAACCAT
Nanog_Puro2	OG162/OG163	GTCACCGAGCTGCAAGAACT	GAGGCCTTCCATCTGTTGCT
Esrrb_WT	OG156/OG159	CTCTGACTCAGCCCTGCATC	CACTAAGCACTGCCCATCCA
Esrrb_mCherry	g7_2f/mCherry_ seq_rev	AGGAAAATGGGGGACAGA	TACATGAACTGAGGGGAC
Esrrb_Puro	OG164/OG165	GCGCCTACAACGTCAACATC	ACATGGCCAGGAAGCAAGAA
Esrrb_Puro2	OG162/OG163	GTCACCGAGCTGCAAGAACT	GAGGCCTTCCATCTGTTGCT
Klhl13_WT	OG138/OG140	CAGGGAGGCTGAGTTGACTT	CAGTGGCTCCCAAACTCCAA

Klhl13_Deletion	OG138/OG144	CAGGGAGGCTGAGTTGACTT	CTTTCTGAGGACTTCCAAATCCT
Dusp9	OG197/OG198	CAGGACAGGGGTTGACTTCC	CGTTCTCCGCTTCAGCCTTA
Dusp9 (NGS)	OG202/OG210	AATGATACGGCGACCACCGAGATCTACACTCTTTCCCTACACGACGCTCTTCCGATCT(Sample Barcode)GCCTTGCCTCTCTCCACAGCA	CAAGCAGAAGACGGCATACGAGAT(Illumina Barcode)GTGACTGGAGTTCAGACGTGTGCTC TTCCGATCTCAGCTCCTGACGCAGCCACA
Dusp9 (Gibson cloning)	OG200/OG201	CACCGTGGGCTTGTACTCGGTCATGGTAAGCAGGACAGGGGTTGACTTCC	TCCTCTTCCTCATCTCCGGGCCTTTCGACCCGTTCTCCGCTTCAGCCTTA
sgRNA library (Cloning)	OG113/OG114	TAACTTGAAAGTATTTCGATTTCTTGGCTTTATATATCTTGTGGAAAGGACGAAACACCG	ACTTTTTCAAGTTGATAACGGACTAGCCTTATTTTAACTTGCTATTTCTAGCTCTAAAAC
sgRNA library (Amplification)	OG115/OG116	AATGGACTATCATATGCTTACCGTAACTTGAAAGTATTTCG	CTTTAGTTTGTATGTCTGTTGCTATTATGTCTACTATTCTTTCC
sgRNA library (NGS)	OG125/OG126	AATGATACGGCGACCACCGAGATCTACACTCTTTCCCTACACGACGCTCTTCCGATCTTCTTGTGGAAAGGACGAAACACCG	CAAGCAGAAGACGGCATACGAGAT(Illumina barcode)GTGACTGGAGTTCAGACGTGTGCTCTTCCGATCTTCTACTATTCTTTCCCCTGCACTGT
Karyotyping (NGS)	OG218/OG219	AATGATACGGCGACCACCGAGATCTACACTCTTTCCCTACACGACGCTCTTCCGATCT	CAAGCAGAAGACGGCATACGAGAT(Illumina Barcode)GTGACTGGAGTTCAGACGTGTGCTCTTC CGATC

3.4. gRNAs

gRNAs were ordered from Sigma-Aldrich with a desalting purity grade and sequences are listed in the 5´to 3´orientation. gRNAs for the generation of Klhl13 deletion mutants were ordered from IDT (Alt-R® CRISPR-Cas9 crRNA)

Table 5. gRNAs used in this study

Target gene	**Sequence**	**Function**	**Source**
Mek1 (Map2k1)	CGTTAACCGCCGAGCCATCG	Mek1 knockout	crispr.mit.edu
Mek1 (Map2k1)	GGCGGTTAACGGGACCAGCT	Mek1 knockout	crispr.mit.edu
Mek1 (Map2k1)	ATGGGCGTCGGCTTCTTCTT	Mek1 knockout	crispr.mit.edu
Erk2 (Mapk1)	CGCGGGCAGGTGTTCGACGT	Erk2 knockout	crispr.mit.edu

Erk2 (Mapk1)	CGCCTTCTCCGATGTACGAG	Erk2 knockout	crispr.mit.edu
Erk2 (Mapk1)	TACGAGAGGTTGGTGTAGCG	Erk2 knockout	crispr.mit.edu
Nanog	CGTAAGTCTCATATTTCACC	mCherry tagging	crispr.mit.edu
Nanog	GACTCCACCAGGTGAAATAT	mCherry tagging	crispr.mit.edu
Esrrb	TGTGCTGGGCCATCACACCT	mCherry tagging	crispr.mit.edu
Esrrb	TGCTGGAGGCCAAGGTGTGA	mCherry tagging	crispr.mit.edu
Klhl13	TACTGAGTGTCAACTATCAC	Deletion mutant generation	crispr.mit.edu
Klhl13	TGTACTAGTTCATAGTAACT	Deletion mutant generation	crispr.mit.edu
Klhl13	TGGAACTAGGTAGACTAGGC	Deletion mutant generation	crispr.mit.edu
Klhl13	ACACTCTGGAGACAGGGCGT	Deletion mutant generation	crispr.mit.edu
Dusp9	CGACCATGGAGAGTCTGAGT	Deletion mutant generation	crispr.mit.edu
Klhl13	GAGGGGAGCGTGTGGGCGG	CRISPRa (Overexpression)	CRISPR library designer (CLD) (Heigwer et al. 2016)
Klhl13	CACATGGCTTCTAGTGTCC	CRISPRa (Overexpression)	CRISPR library designer (CLD) (Heigwer et al. 2016)
Dusp9	CCCAGGCGGGACAGGGTCA	CRISPRa (Overexpression)	Horlbeck *et al.* 2016
Dusp9	GGAGAGCCAACCAGGGCTA	CRISPRa (Overexpression)	Horlbeck *et al.* 2016
Non-targeting	GCGCGCGGATCAAATCAGC	CRISPRa control	Horlbeck *et al.* 2016
Non-targeting	TCGGACCGGTAACGCCTGT	CRISPRa control	Horlbeck *et al.* 2016

3.5. Oligos

Oligos were ordered from Sigma-Aldrich with a desalting purity grade or with HPLC purity grade if the sequence was larger than 40bp. Sequences are listed in the 5´to 3´orientation.

Table 6. Oligos used in this study

Name	Sequence	Function
OG41_MCS_SRE/Elk_F	TCCCCTACCCGGTAGAGGTACCAAAC CATGGAAAGGGCCCAGCTAGGATCA ATGTG	Cloning of pSuper-puro-MCS-PolyA
OG42_MCS_SRE/Elk_R	CACATTGATCCTAGCTGGGCCCTTTC CATGGTTTGGTACCTCTACCGGGTAG GGGA	Cloning of pSuper-puro-MCS-PolyA
NIaIII adapter top	GATCGGAAGAGCGAGAACAA	Karyotyping protocol
NIaIII adapter bottom	GTGACTGGAGTTCAGACGTGTGCTCT TCCGATCCATG	Karyotyping protocol
PstI adapter top	ACACTCTTTCCCTACACGACGCTCTTC CGATCT(Barcode)TGCA	Karyotyping protocol
PstI adapter bottom	(Barcode)AGATCGGAAGAGCGTCGT GTAGGGAAAGAGTGT	Karyotyping protocol

4. Methods

4.1. Molecular cloning

Molecular cloning can be used to insert target DNA sequences into vectors (circular DNA molecules). The generated plasmid can then be transformed into bacterial cells and amplified through specific replication sequences present in bacterial vectors.

This work implemented two different molecular cloning strategies: restriction enzyme cloning and recombination cloning systems, described in detail in section 4.1.1 and 4.1.2, respectively (see Table 7, Cloning method for each plasmid generated in this study). After generation of the target plasmid through either of these methods, it was transformed into bacterial cells. For this, chemically competent cells were immersed for 45 sec into a 42°C water bath (heat-shock transformation) and subsequently plated on Ampicillin plates (0.1 mg/ml, Sigma). Colonies were picked the following day and mini plasmid preparations were carried out using the Peqgold Plasmid Miniprep Kit and following the manufacturer´s instructions. Positive colonies were verified (see Table 7, Strategy for verification) and a colony containing the desired plasmid without DNA sequence mutations was inoculated into 100 ml of LB with Ampicillin (0.1 mg/ml, Sigma) and cultured overnight at 37°C and 200 rpm. A plasmid midi-prep was carried out the next day using the NucleoBond Xtra Midi Plus kit (Macherey-Nagel) and following the manufacturer's instructions (see Table 7 for a list of plasmids generated in this study).

Table 7. Plasmids generated in this study. In column one (Plasmid), a unique identifier of the plasmids generated in this study is given in brackets as an SP (Schulz Plasmid) number. Additionally, the name of the person that generated it is written in brackets.

Plasmid	Source of insert	Original plasmid and restriction enzymes used	Cloning method	Strategy for verification
pSuper-puro-MCS-PolyA (SP27) (by O. Genolet)	(1) MCS oligo sequences (OG41/OG42) (2) The PolyA sequence of the pCAGG-L/eGFP plasmid was amplified using the CloneAmp HiFi PCR Premix, primers with homology overhangs (OG19/OG20), and a Tm of 53°C.	pSuper-puro digested with EcoRI/KpnI (NEB)	In-Fusion HD cloning kit (Takara Bio)	Restriction digest using KpnI and SalI, followed by sanger sequencing of positive clones
pSuper-puro-SRE/Elk-GFP-PEST-PolyA (SP25) (by O. Genolet)	SRE/Elk-sensitive promoter and GFP-PEST were digested from the 302 reporter plasmid using KpnI and ApaI	KpnI/ApaI (NEB) digested pSuper-puro-MCS-PolyA	Restriction cloning	Restriction digest using KpnI and ApaI, followed by sanger sequencing of positive clones
pLenti-SRE/Elk-GFP-PEST-Hygro (SP300) (by O. Genolet)	SRE/Elk-sensitive promoter and GFP-PEST were amplified from the 302 reporter plasmid by using the Phusion High-Fidelity DNA Polymerase (NEB), primers with homology overhangs	lenti-MS2-P65-HSF1-Hygro, digested with NheI and BsrGI (NEB)	In-Fusion HD cloning kit (Takara Bio)	The presence of the SRE-Elk-GFP amplicon was examined via restriction digest with BamHI and BsrGI (NEB). Correct sequence of positive colonies was verified via sanger sequencing

	(OG109/OG110), and a Tm of 62°C			
pUC19-Nanog-mCherry-puro (by J. Schmiedel)	Gene blocks (IDT) of upstream/downstream homology arms and PCR amplicons of the mCherry and the puromycin sequence	pUC19 linearized with XbaI (NEB)	NEBuilder® HiFi DNA Assembly Cloning Kit (NEB)	PCR and restriction digest, followed by sanger sequencing of positive clones
pUC19-Esrrb-mCherry-puro (by J. Schmiedel)	Gene blocks (IDT) of upstream/downstream homology arms and PCR amplicons of the mCherry and the puromycin sequence	pUC19 linearized with XbaI (NEB)	NEBuilder® HiFi DNA Assembly Cloning Kit (NEB)	PCR and restriction digest, followed by sanger sequencing of positive clones
lentiGuide-Mek1_KO (by O. Genolet)	sgRNA oligo sequence (equimolar mix of three different sgRNAs targeting Mek1)	lentiGuide-puro linearized with BsmBI (NEB)	Restriction cloning	Restriction digest, followed by sanger sequencing of positive clones
lentiGuide-Erk2_KO (by O. Genolet)	sgRNA oligo sequence (equimolar mix of three different sgRNAs targeting Erk2)	lentiGuide-puro linearized with BsmBI (NEB)	Restriction cloning	Restriction digest, followed by sanger sequencing of positive clones
PX330-Nanog_sgRNA1 (by J. Schmiedel)	sgRNA oligo sequence	PX330 linearized with BbsI (NEB)	Restriction cloning	Restriction digest, followed by sanger sequencing of positive clones
PX330-Nanog_sgRNA2 (by J. Schmiedel)	sgRNA oligo sequence	PX330 linearized with BbsI (NEB)	Restriction cloning	Restriction digest, followed by sanger sequencing of positive clones
PX330-Esrrb_sgRNA1 (by J. Schmiedel)	sgRNA oligo sequence	PX330 linearized with BbsI (NEB)	Restriction cloning	Restriction digest, followed by sanger sequencing of positive clones
PX330-Esrrb_sgRNA2 (by J. Schmiedel)	sgRNA oligo sequence	PX330 linearized with BbsI (NEB)	Restriction cloning	Restriction digest, followed by sanger sequencing of positive clones
PX458-Dusp9_sgRNA1 (by O. Genolet)	sgRNA oligo sequence	PX458 linearized with BbsI (NEB)	Restriction cloning	Restriction digest, followed by sanger sequencing of positive clones
pU6-Klhl13.1-EF1Alpha-puro-T2A-BFP (by A. Monaco)	sgRNA oligo sequence	pU6-sgRNA-EF1*α*-puro-T2A-BFP digested with BlpI and BstXI (NEB)	Restriction cloning	Restriction digest, followed by sanger sequencing of positive clones
pU6-Klhl13.2-EF1Alpha-puro-T2A-BFP (by A. Monaco)	sgRNA oligo sequence	pU6-sgRNA-EF1*α*-puro-T2A-BFP digested with BlpI and BstXI (NEB)	Restriction cloning	Restriction digest, followed by sanger sequencing of positive clones
pU6-Dusp9.1-EF1Alpha-puro-T2A-BFP (by A. Monaco)	sgRNA oligo sequence	pU6-sgRNA-EF1*α*-puro-T2A-BFP digested	Restriction cloning	Restriction digest, followed by sanger sequencing of positive clones

		with BlpI and BstXI (NEB)		
pU6-Dusp9.2-EF1Alpha-puro-T2A-BFP (by A. Monaco)	sgRNA oligo sequence	pU6-sgRNA-EF1*a*-puro-T2A-BFP digested with BlpI and BstXI (NEB)	Restriction cloning	Restriction digest, followed by sanger sequencing of positive clones
pU6-NTC.1-EF1Alpha-puro-T2A-BFP (by A. Monaco)	sgRNA oligo sequence	pU6-sgRNA-EF1*a*-puro-T2A-BFP digested with BlpI and BstXI (NEB)	Restriction cloning	Restriction digest, followed by sanger sequencing of positive clones
pU6-NTC.2-EF1Alpha-puro-T2A-BFP (by A. Monaco)	sgRNA oligo sequence	pU6-sgRNA-EF1*a*-puro-T2A-BFP digested with BlpI and BstXI (NEB)	Restriction cloning	Restriction digest, followed by sanger sequencing of positive clones
pLenti-PGK-Degron-GFP-Blast (SP234)	Gene amplification by Genscript	pLenti-PGK-GFP-Blast	Cloned by Genscript	-
pLenti-PGK-Degron-GFP-Klhl13-Blast (SP235)	Gene amplification by Genscript	pLenti-PGK-GFP-Blast	Cloned by Genscript	-
pLenti-PGK-GFP-Blast (SP233)	Gene amplification by Genscript	pLenti-PGK-GFP-Blast	Cloned by Genscript	-
pLenti-PGK-GFP-Kelch (SP238)	Gene amplification by Genscript	pLenti-PGK-GFP-Blast	Cloned by Genscript	-

4.1.1 Restriction enzyme cloning

This method was used for the cloning of sgRNAs into target vectors. sgRNAs targeting the Mek1 (Map2k1), Erk2 (Mapk1), Nanog, Esrrb, Klhl13 and Dusp9 locus were designed using the CRISPR-Cas9 online tool http://crispr.mit.edu:8079/. Off-target scores based on *in silico* quality and off-target predictions (Hsu et al., 2013) were compared among the candidate sgRNAs and only the top-scoring sgRNAs were selected.

CRISPRa sgRNA sequences (see Table 5) targeting the Dusp9 gene were taken from previously published libraries (Horlbeck et al., 2016), whereas sgRNAs targeting the mESC-specific Klhl13 isoform (ENSMUST00000115313.7) were designed using the CRISPR library designer (CLD) from the Boutros lab (Heigwer et al. 2016).

Knockout sgRNAs targeting the start of the Mek1 and Erk2 locus were cloned into the lentiGuide-puro plasmid (Shalem et al. 2014; Sanjana et al. 2014). This plasmid is used for lentiviral delivery of sgRNAs, allowing for stable expression of the the sgRNA of interest in a target cell population after puromycin selection. The cell line of use should already stably express the Cas9 endonuclease enzyme. The three sgRNAs targeting each locus were mixed in an equimolar ratio before cloning into the lentiGuide-puro vector.

Plasmids PX330 and PX458 were used for cloning of sgRNAs implemented for genome editing (Nanog, Esrrb, Klhl13 and Dusp9). Both plasmids co-express the wildtype Cas9 nuclease together with the sgRNA of interest under the Pol III U6 promoter, the PX458 additionally expresses the GFP fluorescent protein. These plasmids

allow for transient expression of the Cas9 nuclease in the cells of interest, leading to double strand breaks in the target DNA.

The plasmid pU6-sgRNA-EF1*α*-puro-T2A-BFP was used to clone sgRNAs for gene overexpression (CRISPRa). This plasmid is used for endogenous target gene overexpression in cells that stably express a mutated version of the Cas9 endonuclease, termed as dead Cas9 (dCas9), capable of binding but not cutting the target DNA. Additionally, the dCas9-binding handle sequence of the sgRNA has been optimized in this plasmid for improved dCas9 binding, which yields higher overexpression efficiencies (see section 4.2.7 for additional information on the CRISPR/Cas9 system and sgRNA structure) (Chen et al., 2013). The pU6-sgRNA-EF1*α*-puro-T2A-BFP is a lentiviral plasmid, which allows for stable expression of the sgRNA of interest.

For sgRNA cloning (gRNA sequences are found in Table 5) into the PX330/PX458, lentiGuide-puro or pU6-sgRNA-EF1*α*-puro-T2A-BFP plasmids, two complementary oligos containing the guide sequence and BbsI (PX330/PX458), BsmBI (lentiGuide-puro) or BlpI/BstXI (pU6-sgRNA-EF1*α*-puro-T2A-BFP) homologous overhangs (Fig. 13) were annealed and cloned into the BbsI, BsmBI or BlpI/BstXI (NEB) digested target plasmid by using 0.5 µl of the T4 DNA ligase enzyme (NEB) in 10 µl total reaction volume (cloned plasmids are found in Table 7). For the ligation reaction, 50 ng of the digested and gel-purified (using the NucleoSpin Gel and PCR Clean-up, Macherey-Nagel) plasmid were implemented, together with 1 µl of 1:200 diluted and previously annealed oligo sequences. The mixture was first incubated for 10 min at RT and subsequently heat-inactivated at 65°C for 10 min.

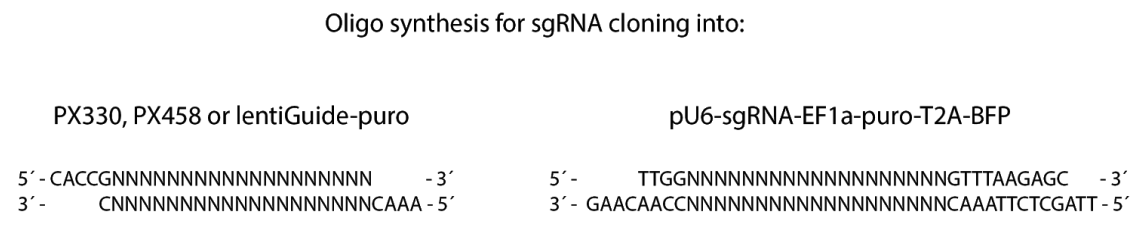

Figure 13: Schematic representation of oligo synthesis for sgRNA cloning into PX330/PX458, lentiGuide-puro or pU6-sgRNA-EF1a-puro-T2A-BFP. For cloning sgRNAs into the PX330/PX458, lentiGuide-puro or pU6-sgRNA-EF1a-puro-T2A-BFP vector, complementary oligos need to be designed containing the target sgRNA flanked by sequences complementary to the ends generated by the BbsI, BsmBI and BlpI/BstXI restriction enzymes, respectively.

Additionally, restriction cloning was used for the generation of the pSuper-puro-SRE/Elk-GFP-PEST-PolyA plasmid. For this, the SRE/Elk-sensitive promoter and GFP-PEST sequence was digested from the 302 reporter plasmid using KpnI and ApaI and cloned into the KpnI/ApaI digested pSuper-puro-MCS-PolyA (the pSuper-puro-MCS-PolyA plasmid was generated using recombination cloning, see below for details) by using 1 µl of the T4 DNA ligase enzyme (NEB) in 20µl total reaction volume (cloned plasmids are found in Table 7). For the ligation reaction, 50 ng of the digested and gel-purified plasmid were implemented, together with 45 ng of the digested and gel-purified insert (SRE/Elk-GFP-PEST). Incubation of the ligation reaction was performed as described previously for sgRNA cloning.

4.1.2 Recombination cloning

Recombination cloning systems offer the advantage that DNA sequences can be cloned into linearized plasmids without further treatment of the insert (such as restriction digestion) and with a specific direction using complementary sequences to the target vector. This method was implemented in this work for the cloning of the SRE-Elk reporter plasmid pLenti-SRE/Elk-GFP-PEST-Hygro (SRE/Elk promoter sequence is found in Supp. Table S5) together with the pSuper-puro-MCS-PolyA (by using the In-Fusion cloning kit from Takara Bio following the manufacturer's instructions), and the Nanog/Esrrb repair templates pUC19-Nanog-mCherry-puro and

pUC19-Esrrb-mCherry-puro (by using the NEBuilder® HiFi DNA Assembly Cloning Kit (NEB)) (Plasmids and cloning strategy found in Table 7).

For cloning of the Nanog/Esrrb repair templates, homology arms were ordered as gene blocks (gBlocks, IDT) containing 20bp long overlapping sequences, and the mCherry and Puromycin sequence were amplified from existing plasmids (Fig. 14). A reaction was carried out using the NEBuilder® HiFi DNA Assembly Cloning Kit (NEB) with 0.05 pmol of each of the 4 DNA fragments and 10 µl of the NEBuilder master mix. Samples were incubated for 60 min at 50°C, diluted 1:4 by adding 60 µl of ddH_2O and placed on ice. A total of 2 µl of the reaction was transformed into OneShot Top10 chemically competent cells (Thermo Fisher Scientific).

Figure 14: Schematic representation of repair template for C-terminal tagging of the Nanog and Esrrb locus. Repair templates consisted of a P2A self-cleaving peptide followed by the mCherry coding sequence and a puromycin-resistance cassette, flanked by ~400bp homology regions to the Nanog/Esrrb locus (Esrrb-HA-Upstream: chr12:86,518,604-86,519,062, Esrrb-HA-Downstream: chr12:86,519,066-86,519,521, Nanog-HA-Upstream: chr6:122,713,142-122,713,552, Nanog-HA-Downstream: chr6:122,713,556-122,714,007 (GRCm38/mm10 Assembly)).

4.2. Cell culture

4.2.1 Cell culture conditions

All mESC lines were grown without feeder cells on gelatin-coated flasks (Millipore, 0.1%) in serum-containing ES cell medium (DMEM (Sigma), 15% FBS (PanBiotech), 0.1 mM ß-Mercaptoethanol (Sigma), 1000 U/ml leukemia inhibitory factor (LIF, Merck)). mESCs were passaged every second day at a density of $4*10^4$ cells/cm^2 and medium was changed daily.

Hek293T cells were cultured in DMEM supplemented with 10% FBS and passaged every 2 to 3 days.

4.2.2 Differentiation of mouse embryonic stem cells

The differentiation of cells in this work was achieved through LIF withdrawal either from +LIF/Serum conditions, or from 2i/LIF conditions. For the latter, cells were first adapted to 2i+LIF medium (ES cell medium (see above) with addition of 3 µM Gsk3 inhibitor CT-99021 (Axon Medchem) and 1 µM MEK inhibitor PD0325901 (Axon Medchem)) for at least five passages before undergoing differentiation.

Cells were differentiated via LIF withdrawal in DMEM supplemented with 10% FBS and 0.1 mM ß-Mercaptoethanol at a density of $2*10^2$ cells/cm^2 in fibronectin-coated dishes (10 µg/ml, Merck).

4.2.3 Cell lines

A detailed list of all cell lines used in this study is given below. The parental 1.8 XX mESC line, which carries a homozygous insertion of 7xMS2 repeats in Xist exon 7, was a gift from the Gribnau lab (Schulz et al., 2014).

The female TX1072 mESC line was derived from a cross of a TX/TX $R26^{rtTA/rtTA}$ female (Savarese et al. 2006) with a Mus musculus castaneus male. This cell line carries a doxycycline inducible promoter in front of the Xist gene in one of its two X-chromosomes (Schulz et al. 2014).

E14-STN male cells expressing the CRISPRa SunTag system were a kind gift from the Navarro lab.

Low-passage Hek293T cells, which were used for lentivirus generation, were a kind gift from the Yaspo lab.

Table 8. Cell lines used in this study. A unique cell line identifier is given in column 3 as an SC number (Schulz cells).

Cell line	Clone	Cell line number	Clone number thesis	Method of generation	Parental cell line	Plasmid for genomic integration	Selection	Genotype verification
1.8 XX	A3	SC01	1	Sub-cloning	1.8 XX	-	-	FISH for X-chromosomal status
1.8 XX	C9	SC01	2	Sub-cloning	1.8 XX	-	-	FISH for X-chromosomal status
1.8 XO	F1	SC12	1	Sub-cloning	1.8 XX	-	-	FISH for X-chromosomal status
1.8 XO	F12	SC12	2	Sub-cloning	1.8 XX	-	-	FISH for X-chromosomal status
1.8 XO	D1	SC12	3	Sub-cloning	1.8 XX	-	-	FISH for X-chromosomal status
1.8 XX K13-HET	H6.2	SC29	1	Genome editing	1.8 XX	-	-	Genotyping PCR, Klhl13 RNA FISH, Immunoblotting
1.8 XX K13-HET	B1	SC29	2	Genome editing	1.8 XX	-	-	Genotyping PCR, Klhl13 RNA FISH, Immunoblotting
1.8 XX K13-HOM	D1	SC30	1	Genome editing	1.8 XX	-	-	Genotyping PCR, Klhl13 RNA FISH, Immunoblotting
1.8 XX K13-HOM	C6	SC30	2	Genome editing	1.8 XX	-	-	Genotyping PCR, Klhl13 RNA FISH, Immunoblotting
1.8 XX D9-HET	D4B1	SC31	1	Genome editing	1.8 XX	-	-	Sanger sequencing, NGS, Immunoblotting
1.8 XX D9-HET	C6B9	SC31	2	Genome editing	1.8 XX	-	-	Sanger sequencing, NGS, Immunoblotting
1.8 XX D9-HOM	F10	SC32	1	Genome editing	1.8 XX	-	-	Sanger Sequencing, Immunoblotting
1.8 XX D9-HOM	H4	SC32	2	Genome editing	1.8 XX	-	-	Sanger Sequencing, Immunoblotting
1.8 XX D9K13-HET	A8D5	SC33	1	Genome editing	1.8 XX	-	-	Sanger sequencing, NGS, Genotyping PCR (for K13 del), Immunoblotting

1.8 XX D9K13-HET	C2E2	SC33	2	Genome editing	1.8 XX	-	-	Sanger sequencing, NGS, Genotyping PCR (for K13 del), Immunoblotting
E14-STN	Clonal origin	SC40	-	Piggybac transposition	-	-	-	-
TX1072 SRE-Elk	Clone 2	SC59	-	Random integration	TX1072	pSuper-Puro-SRE/Elk-GFP-PEST	Puromycin (1ng/µl)	Flow cytometry
1.8 XX SRE-Elk	Clone 3	SC26	-	Lentiviral transduction	1.8 XX	pLenti-SRE/Elk-GFP-PEST-Hygro	Hygromycin (250 µg/ml)	Flow cytometry
1.8 XX Nanog-mCherry	D9	SC27	-	Genome editing	1.8 XX	pUC19-Nanog-mCherry-puro	Puromycin (1ng/µl)	Genotyping PCR, flow cytometry
1.8 XX Esrrb-mCherry	H7	SC28	-	Genome editing	1.8 XX	pUC19-Esrrb-mCherry-puro	Puromycin (1ng/µl)	Genotyping PCR, flow cytometry
E14-STN-NT.1	Non-clonal	SC49	-	Lentiviral transduction	E14-STN	pU6-NTC.1-EF1Alpha-puro-T2A-BFP	Puromycin (1ng/µl)	Immunoblotting
E14-STN-NT.2	Non-clonal	SC49	-	Lentiviral transduction	E14-STN	pU6-NTC.2-EF1Alpha-puro-T2A-BFP	Puromycin (1ng/µl)	Immunoblotting
E14-STN-Dusp9.1	Non-clonal	SC50	-	Lentiviral transduction	E14-STN	pU6-Dusp9.1-EF1Alpha-puro-T2A-BFP	Puromycin (1ng/µl)	Immunoblotting
E14-STN-Dusp9.2	Non-clonal	SC50	-	Lentiviral transduction	E14-STN	pU6-Dusp9.2-EF1Alpha-puro-T2A-BFP	Puromycin (1ng/µl)	Immunoblotting
E14-STN-Klhl13.1	Non-clonal	SC51	-	Lentiviral transduction	E14-STN	pU6-Klhl13.1-EF1Alpha-puro-T2A-BFP	Puromycin (1ng/µl)	Immunoblotting
E14-STN-Klhl13.2	Non-clonal	SC51	-	Lentiviral transduction	E14-STN	pU6-Klhl13.2-EF1Alpha-puro-T2A-BFP	Puromycin (1ng/µl)	Immunoblotting
1.8 XX K13-HOM D-GFP	Non-clonal	SC54	-	Lentiviral transduction	1.8 XX K13-HOM Clone 2	pLenti-PGK-Degron-GFP-Blast	Blasticidin (5 ng/µl)	Immunoblotting

1.8 XX K13-HOM D-GFP-Klhl13	Non-clonal	SC55	-	Lentiviral transduction	1.8 XX K13-HOM Clone 2	pLenti-PGK-Degron-GFP-Klhl13-Blast	Blasticidin (5 ng/µl)	Immunoblotting
1.8 XX K13-HOM GFP	Non-clonal	SC52	-	Lentiviral transduction	1.8 XX K13-HOM Clone 2	pLenti-PGK-GFP-Blast	Blasticidin (5 ng/µl)	Immunoblotting
1.8 XX K13-HOM GFP-Kelch	Non-clonal	SC53	-	Lentiviral transduction	1.8 XX K13-HOM Clone 2	pLenti-PGK-GFP-Kelch-Blast	Blasticidin (5 ng/µl)	Immunoblotting

4.2.4 Sub-cloning

For the generation of clonal cell lines, 10 cells/cm^2 were plated into 10 cm plates and grown for 9 days, after which clones were transferred to one well of a 96-well plate and expanded. Medium was changed every 2-3 days. 1.8 XO subclones can be generated through sub-cloning of female cells because 5-10% of all XX mESC lines have lost one of their X-chromosomes due to X-chromosomal instability.

4.2.5 Lentiviral transduction

The use of lentiviral vectors permits stable expression of a gene of interest by inserting the desired transgene into the host's DNA. Once this happens, the gene of interest is propagated along with the host cell and is not lost through cell division. Virus generation is carried out in mammalian cells such as Hek293T through their transfection with a specific set of plasmids: pLP1, pLP2 and VSVG. These packaging vectors represent a third generation packaging system with increased safety measures, as the main viral genes are encoded in three different plasmids instead of two (Dull et al., 1998). The pLP1 vector carries the gag and pol genes, the first codes for the viral capsid components and the second for the reverse transcriptase and integrase. pLP2, on the other hand, carries the rev gene, whose protein binds to the Rev Response Element (RRE) within unspliced and partially spliced transcripts, facilitating this way nuclear export. Lastly, the VSVG vector carries the genes that code for envelope proteins.

The transgene sequence of interest must be flanked by long terminal repeats (LTRs), which will mediate the insertion of the DNA sequence into the host genome. These are found in lentiviral vector backbones used for the cloning of the desired expression construct.

In this work, DNA constructs were first packaged into lentiviral particles for the generation of cell lines expressing the transgene of interest. For this, 1*10^6 Hek293T cells were seeded into one well of a 6-well plate and transfected the next day with the lentiviral packaging vectors: 1.2 µg pLP1, 0.6 µg pLP2 and 0.4 µg VSVG (Thermo Fisher Scientific), together with 2 µg of the desired construct using lipofectamine 2000 (Thermo Fisher Scientific).

Hek293T supernatant containing the viral particles was harvested after 48 h. 0.2*10^6 mESCs were seeded per 12-well and transduced the next day with 500 µl of viral supernatant and 8 ng/µl polybrene (Sigma). Antibiotic selection was started two days after transduction and kept for at least 3 passages.

4.2.6 Random integration

Generation of genetically modified cell lines can be achieved through the delivery of transgenes into the cell using standard transfection reagents such as lipofectamine, leading to the random integration of the transgene in the host's genome in a very low percentage of cells, where double-stranded DNA breaks have sporadically occurred and have been subsequently repaired (Smirnov et al. 2020).

Random integration was used in this work for the generation of the TX1072 SRE-Elk cell line (see Table 8). Here, $1*10^6$ cells were seeded in a 6-well plate and transfected the next day with 2.5 µg of the NotI linearized pSuper-puro-SRE/Elk-GFP-PEST-PolyA plasmid and 10 µl Lipofectamine 2000 (Thermo Fisher Scientific) following manufacturer's instructions. The next day, 90% and 10% of cells were passaged into two separate 10 cm culture dishes and puromycin selection (1 ng/µl, Sigma) was started the day after. Individual clones were picked after 8 days of selection and GFP fluorescence was measured via flow cytometry.

4.2.7 Genome editing

Genome editing is achieved by relying on the cells ability to repair double strand breaks (DSBs) by using a set of mechanisms such as homology directed repair (HDR (Carroll, 2017)) or non-homologous end-joining (NHEJ), which allows the cell to avoid cell death by DNA damage. During HDR, a cell is able to repair DSBs in the DNA using a homologous DNA sequence on the sister chromatid, whereas during NHEJ, the break ends are directly ligated together without the use of an homologous template, which often leads to deletions in the original DNA sequence. Genome editing was a highly inefficient process, as it relied on spontaneous DSBs that occurred in a very small subset of cells, requiring the screening of hundreds of clones, until the emergence of tailored nucleases, which increased the rate DSBs in specific target DNA sequences. The first generation of engineered nucleases included zinc-finger nucleases (ZNFs) and transcription activator-like effector nucleases (TALENs), however, the time needed for the generation of one enzyme targeting a specific genomic region was still considerable, ranging from several weeks to months (Carroll, 2017). The advent of the CRISPR/Cas9 technology has significantly reduced the time needed for the generation of genome edits, as the targeting of the Cas9 endonuclease to a specific genomic region is mediated through an RNA oligo.

CRISPR (clustered regularly interspaced short palindromic repeats) is a microbial adaptive immune system that is based on nucleases guided by RNA molecules to cleave a specific sequence of DNA (Horvath and Barrangou, 2010). The type II CRISPR system derived from *Streptococcus pyogenes* consists of three main components: a Cas9 nuclease enzyme, a crRNA (CRISPR RNA) which contains the complementary region to the target DNA (protospacer) and the tracrRNA (trans-activating CRISPR RNA), which mediates both maturation of the crRNA and binds the Cas9 nuclease (also known as the scaffold) (Cong et al., 2013; Makarova et al., 2011). The latter two have been recently fused to generate single guide RNAs (sgRNAs) that bind both the target DNA sequence and the Cas9 (Jinek et al., 2012). One requirement of the Cas9 endonuclease from *Streptococcus pyogenes* (spCas9) is that the target DNA must be preceded by a 5´NGG protospacer adjacent motif (PAM) sequence, slightly restricting the number of target sequences in the genome.

Once the Cas9 endonuclease cleaves the genome, the resulting double strand break (DSB) will be amended by the cell using the two main pathways for DNA damage repair mentioned previously: NHEJ or HDR. The first is generally exploited to generate gene knockouts, whereas the latter is used together with repair templates to insert DNA sequences into a genomic target site (Cho et al., 2013; Ran et al., 2013). For this, the Cas9-induced DSB should be not more than 10 bp away from the site of modification and repair template homology arms should range from 30 to 1000 bp depending on the size of the desired insert (Singh et al., 2015). Colony screening can be facilitated through the incorporation of a resistance cassette, which can be flanked by loxP sites for subsequent removal.

4.2.7.1 1.8-Nanog-mCherry and 1.8-Esrrb-mCherry reporter cell lines

1.8-Nanog-mCherry and 1.8-Esrrb-mCherry reporter lines were generated by tagging the C-Terminus of the Nanog/Esrrb locus with the fluorescent protein mCherry using CRISPR-Cas9 mediated homologous recombination (HR). For the generation of the cell lines, a repair template was generated that included the mCherry sequence preceded by a P2A self-cleaving peptide together with a puromycin resistance cassette flanked by loxP sites (Fig. 15). Cells were transfected with the respective repair templates together with two sgRNAs targeting the C-terminus of either the Nanog or the Esrrb locus (see Table 5) and subsequently selected for target sequence insertion. In order to make both reporter cell lines puromycin-sensitive again, the resistance cassette was excised through transient transfection with Cre recombinase. This is of great importance since the lentiviral sgRNA-expressing constructs used during the generated pooled CRISPR screens (see below, section 4.4) include a puromycin resistance cassette for the selection of cells where a stable sgRNA genomic integration has occurred. Lastly, clones were screened for correct mCherry insertion and fluorescence.

For the generation of the Nanog- and Esrrb-mCherry reporter cell lines, $1*10^6$ female 1.8 mESCs were seeded into a 6 cm dish and transfected the following day with 4 µg of the repair template (pUC19-Nanog-mCherry-puro or pUC19-Esrrb-mCherry-puro plasmids, Table 7) and 1.5 µg of each of the sgRNAs plasmids co-expressing the Cas9 endonuclease (PX330-Nanog-sgRNA1/2 and PX330-Esrrb-sgRNA1/2, Table 7) using 16.5 µl of lipofectamine 3000 and 22 µl of P3000 reagent (Thermo Fisher Scientific) according to manufacturer's recommendations. Puromycin selection (1 ng/µl, Sigma) was started two days after transfection and was kept for 3 days.

The loxP flanked puromycin selection cassette was subsequently excised through transient expression of the CRE recombinase enzyme. To this end, $1*10^5$ cells were nucleofected with 0.8 µg of the CRE recombinase expression plasmid pCAG-Cre (see Table 2) by using the Amaxa 4D-Nucleofector together with the P3 Primary Cell 4D-Nucleofector Kit S and DN100 program (LONZA). Cells were subsequently seeded for clone picking at a density of 10 cells/cm^2 into 10 cm plates and grown for 9 days, after which clones were transferred to one well of a 96-well plate and expanded.

Finally, expanded clones were tested via puromycin treatment as well as genotyped for loss of the puromycin cassette by PCR, and additionally for the proper insertion of the mCherry tag into the C-terminus of the Nanog or Esrrb locus (Fig. 15). All PCRs were carried out by using the Hotstart Taq Polymerase (Qiagen), a Tm of 56°C and 30 cycles (Primer sequences are listed in Table 4).

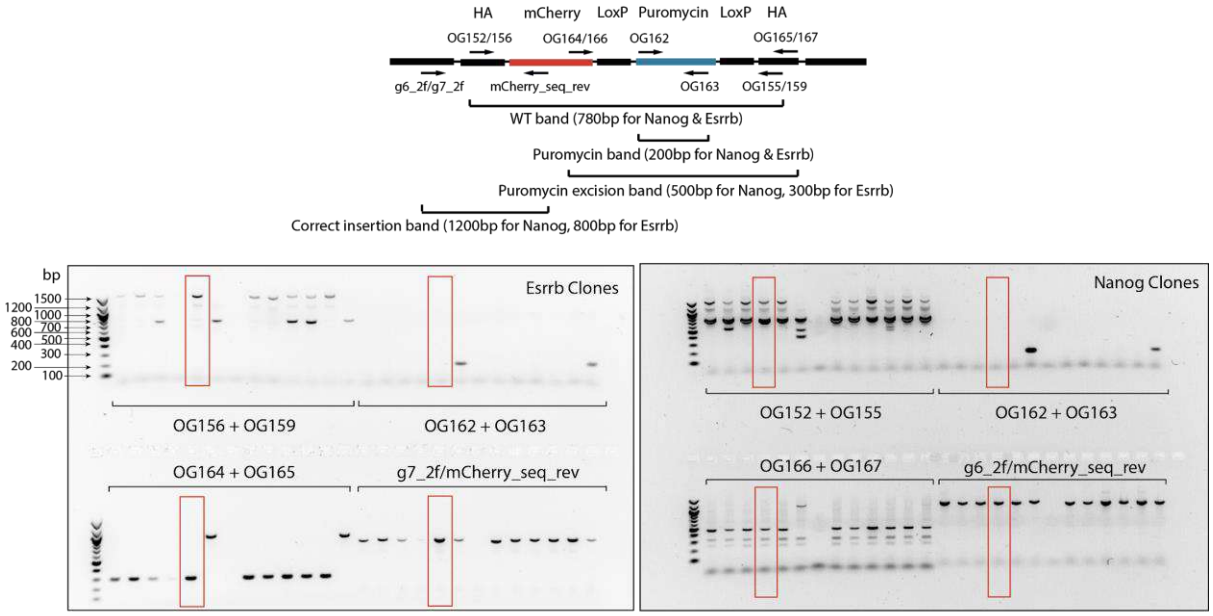

Figure 15. Genotyping of Nanog and Esrrb reporter clones. Genotyping strategy (above, primer binding is shown as arrows and PCR products with respective lengths are shown below) and **g**enotyping results (below) using the indicated primer pairs. The clone for each cell line used in the secondary screens is highlighted in red.

4.2.7.2 Dusp9 and Klhl13 mutant cell lines

A gene knockout can be achieved in a given cell line through the generation of a gene deletion or a frameshift mutation. In both cases, the Cas9 endonuclease should be transiently delivered to the cell population together with the gRNA(s) of interest, which will induce double strand breaks in the start of the coding sequence (frameshift mutants) or around the promoter or whole gene locus (deletion mutants).

The Cas9 endonuclease and gRNAs of interest can be delivered into the cell type of interest through different methods, depending on the experiment´s goal and design. Lentiviral systems can be useful for cells that are difficult to transfect, or when a single genome integration is aspired, such as in pooled CRISPR screens (see below). On the other hand, if transient Cas9 and gRNA delivery is sufficient and/or desired, such as for the generation of knockout cell lines, researchers can make of plasmids expressing the Cas9 and gRNA or Cas9-gRNA ribonucleoprotein complexes (RNP) (DeWitt et al., 2017; Zuris et al., 2015). The latter is especially advantageous when trying to minimize off-target effects due to the shorter half-life of the Cas9 protein compared to plasmid delivery.

In order to generate Klhl13 mutant mESCs, 4 guide RNAs were designed to target a 4.5 kb region around the *Klhl13* (K13) promoter with the Alt-R® CRISPR-Cas9 System (IDT), which contains all necessary reagents for the delivery of Cas9-gRNA ribonucleoprotein complexes (RNP) into target cells, together with the mutant Alt-R HiFi Cas9 nuclease exhibiting significantly reduced off-target effects. Here, 4 different crRNAs (Table 5, 2 guides binding upstream of the Klhl13 promoter and 2 downstream) and the Cas9 binding trcrRNA were mixed in equimolar concentrations and the 4 crRNAs and tracrRNA duplexes were subsequently pooled together. 2.1 µl PBS, 1.2 µl of the tra+cr duplex (100 µM Stock), 1.7 µl Cas9 (61 µM Stock) and 1 µl electroporation enhancer were pipetted together and incubated for 20 min. 10^5 cells were nucleofected with the mixture using the CP106 program of the Amaxa 4D-Nucleofector (Lonza) and plated on gelatin-coated 48-well plates. After 48 h, cells were seeded at a density of 10 cells/cm^2 into 10 cm plates. Individual clones were picked, expanded and genotyped for the presence of the promoter deletion.

The genotyping strategy to identify heterozygous (HET) and homozygous (HOM) clones is shown below in Fig. 16. Primers OG138 and OG140 (Primer sequences are listed in Table 4) were used for the PCR amplification of the wildtype allele. For this, the HotStart Taq Polymerase (Qiagen) was used with an annealing temperature of 51°C and 35 cycles. For the PCR amplification of alleles harboring a promoter deletion, the Phusion HiFi Polymerase (NEB) was implemented with an annealing temperature of 63°C, 35 cycles and primers OG138 and OG144.

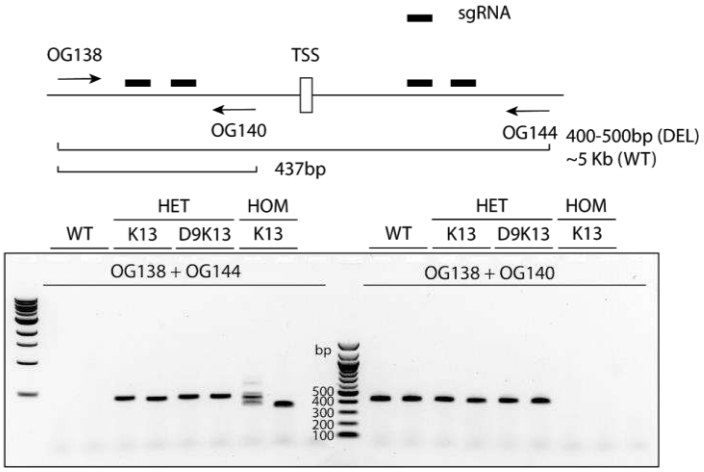

Figure 16. PCR genotyping of Klhl13 mutant cell lines. Thick bars indicate gRNA binding sites and arrows indicate primer-binding positions. PCR products are shown below.

For the generation of Dusp9 (D9) mutants, an sgRNA targeting the start of the coding region was designed (Table 5) and cloned into the PX458 (PX458-Dusp9_sgRNA1, Table 7), with the goal of generating frameshift-mutant cell lines. Here, $2*10^6$ WT and K13HET (Clone 1) cells were nucleofected as described above with 5 µg of the PX458-Dusp9_sgRNA1 plasmid and subsequently plated on gelatin-coated 6 cm plates. The PX458 plasmid is used for the co-expression of an sgRNA of interest together with the Cas9 nuclease, which is coupled to the green fluorescent protein (GFP) by a T2A self-cleaving peptide, allowing the assessment of Cas9 expression levels with single-cell resolution. One day after transfection, high GFP+ cells that were successfully transfected with the PX458 plasmid and expressed significant levels of the Cas9 endonuclease were single-cell sorted in a 96-well plate and expanded. Clones were screened for homozygous or heterozygous frameshift deletions via Immunoblotting and Sanger-sequencing (Fig. 17A-B, see below).

Heterozygous deletion of several selected clones was further confirmed via NGS (Fig. 17C). For this, a region surrounding the Dusp9 deletion was amplified using the Phusion HiFi Polymerase (NEB) with a total of 30 cycles and an annealing temperature of 65°C (Primer sequences in Table 4, OG197/OG198). A second PCR using again the Phusion HiFi Polymerase (NEB) with a total of 14 cycles and an annealing temperature of 65°C was performed in order to attach the illumina adaptors and barcodes (Table 4, OG202/OG210). A dual barcoding strategy was employed, where Illumina barcodes were included in the reverse and custom sample barcodes in the forward primers. Samples containing the same Illumina barcode but different custom sample barcodes were pooled in an equimolar fashion and sequenced on the Illumina Miseq platform PE150. Samples were aligned using Bowtie2 (Langmead and Salzberg, 2012) and an index containing sample barcodes and possible deletion sequences based on previously generated Sanger sequencing data, gaining approximately 4000 reads per sample.

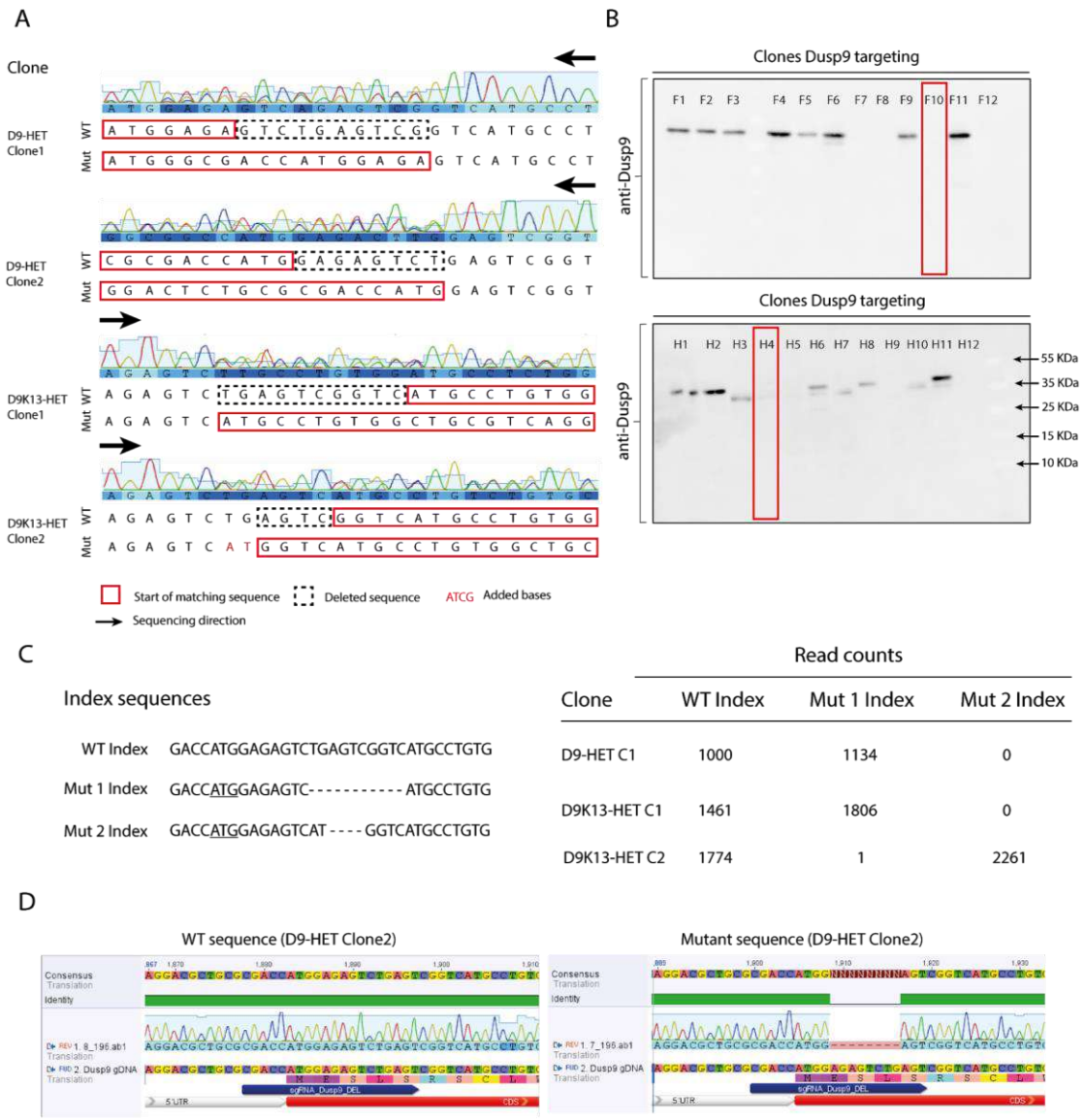

Figure 17. Generation of Dusp9 homozygous and heterozygous mutants. (A) Sanger sequencing results of D9-HET and D9K13-HET clones. **(B)** Screening for D9-HOM clones with an XX wildtype background via Immunoblotting. Clones used in this study are highlighted in red (F10/D9-HOM Clone 1 and H4/D9-HOM Clone 2). **(C)** NGS sequencing results from the D9-HET/D9K13-HET clones. The index used for the alignment if shown in the left and the number of counts aligning to each index for each clone is shown in a table in the right. **(D)** Sanger sequencing results of the cloning of an amplicon generated from D9-HET Clone 2 gDNA spanning the target deletion. Seven bacterial clones were sequenced: 5/7 showed the 8bp deletion and 2/7 the wildtype sequence.

The presence of a mutant and wildtype allele in a second Dusp9 heterozygous clone (D9-HET Clone 2) was confirmed through the cloning of the PCR amplicon surrounding the start of the Dusp9 coding sequence into a mammalian expression plasmid and subsequent Sanger-sequencing of single transformed bacterial clones (Fig. 17D). This was due to the fact that it was not possible to generate two D9-HET clones in a first attempt, so a second one was implemented after the previously described round of NGS for the mutant clones. For this, primers OG197 and OG198 spanning the Dusp9 deletion were attached to complementary sequences of the pSuper-Puro plasmid for Gibson cloning (Primers OG200/OG201, sequences are listed in Table 4). The pSuper-puro was digested with NheI and PstI and a Gibson reaction was carried out to insert the PCR amplicon generated

using the OG200/OG201 primers from the gDNA of D9-HET Clone 2. After transformation, colonies were picked and seven positive colonies were Sanger sequenced.

4.3. Karyotyping

The use of cell lines with a normal karyotype is of particular importance since chromosome trisomies or monosomies can affect gene expression and therefore lead to confounding results. Traditional karyotyping methods involve the harvesting of cells during metaphase, their staining with DAPI or FISH probes for chromosome painting and their microscopic analysis (chromosome counting). However, they are time intensive and hard to upscale to numerous cell lines. Furthermore, the identification of small chromosomal duplications or deletions using this method is quite challenging. In this study, cell lines were karyotyped via double digest genotyping-by-sequencing (ddGBS), a reduced representation genotyping method. This allows for the karyotyping of dozens of cell lines simultaneously, reducing at the same time the hands-on time significantly to 2-3 days.

In this protocol, the gDNA of each cell line is digested using two different restriction enzymes (RE), NIaIII and PstI, after which oligonucleotide adapters are ligated complementary to the generated overhangs (Fig. 18, NIaIII overhangs in red, PstI overhangs in blue). This is followed by the amplification of gDNA using sequencing primers complementary to the ligated NIaIII and PstI adapters (Fig. 18, OG218 and OG219), and subsequent next generation sequencing of the sample. A great advantage of this method is that the sequencing of gDNA using restriction enzymes together with their specific adapters allows the achievement of a higher coverage than if the whole genome was sequenced at random.

The protocol was performed as described in the Palmers lab website, which was adapted from previously published protocols (Elshire et al., 2011). The forward and reverse strands of a barcode adapter and common adapter were diluted and annealed (Fig. 18), after which they were pipetted into each well of a 96-well PCR plate together with 1 µg of gDNA from each sample and dried overnight (Oligo sequences are listed in Table 6). The following day samples were digested with 20 µl of a NIaIII and PstI enzyme mix (NEB) in NEB Cutsmart Buffer at 37°C for 2 h.

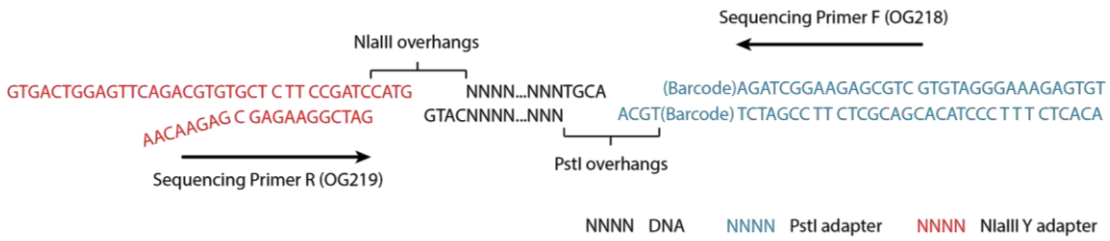

Figure 18. Schematic representation of the karyotyping protocol. PstI adapters (blue) and NIaIII adapters (red) are first annealed and then pipetted together with the sample DNA into each well of a 96-well. The DNA is dried overnight, subsequently digested with the NIaIII and PstI restriction enzymes and then ligated. Samples are cleaned, quantified, pooled in an equimolar fashion and size selected using gel electrophoresis. Lastly, ligated DNA is amplified with Illumina sequencing primers (OG218/OG219) and sequenced on the Illumina platform.

After the digest, a 30 µl mix consisting of 1.6 µl of T4 DNA Ligase (NEB), 5µl 10X T4 DNA Ligase Buffer (NEB) and 23.4µl ddH_2O was added to each well and placed on a thermocycler (16°C 60 min followed by 80°C 30min for enzyme inactivation). By doing this, barcode and common adapters with ends complementary to those generated by the two restriction enzymes were ligated to the genomic DNA.

Samples were cleaned with CleanNGS beads (CleanNA) to remove the restriction and digestion mix using 90 µl of beads for each well and following manufacturer's instructions. Samples were eluted in 25 µl ddH_2O and DNA was quantified using a dsDNA HS Qubit assay (Thermofisher). Samples were pooled in an equimolar fashion,

size-selected (300-450bp) by loading 400 ng of each pooled sample on an agarose gel, followed by a cleaning step using the Nucleospin Gel and PCR Cleanup kit (Macherey-Nagel). Samples were subsequently PCR-amplified using the Phusion HF polymerase (NEB) and an annealing temperature of 68°C over 15 amplification cycles (primers OG218/OG219, Table 4). Resulting amplicons were cleaned with CleanNGS beads in a 1:1.2 ratio (sample:beads) to eliminate primer dimers and sequenced with 2x75bp on the Miseq platform (12 pM loading concentration), yielding from $0.2*10^6$ to $1*10^6$ fragments per sample.

Data processing and statistical analysis was performed on the public Galaxy server usegalaxy.eu. For this, fastq files were uploaded and demultiplexed using the "Je-demultiplex" tool (Girardot et al., 2016). Reads were mapped to the mm10 mouse reference genome (GRCm38) using “Map with BWA” (Li and Durbin, 2009, 2010). Read counts for each chromosome were calculated with “multiBamSummary” (Ramírez et al., 2016) and normalized to a previously karyotyped XX control cell line (using dapi stained metaphase spreads and chromosome painting).

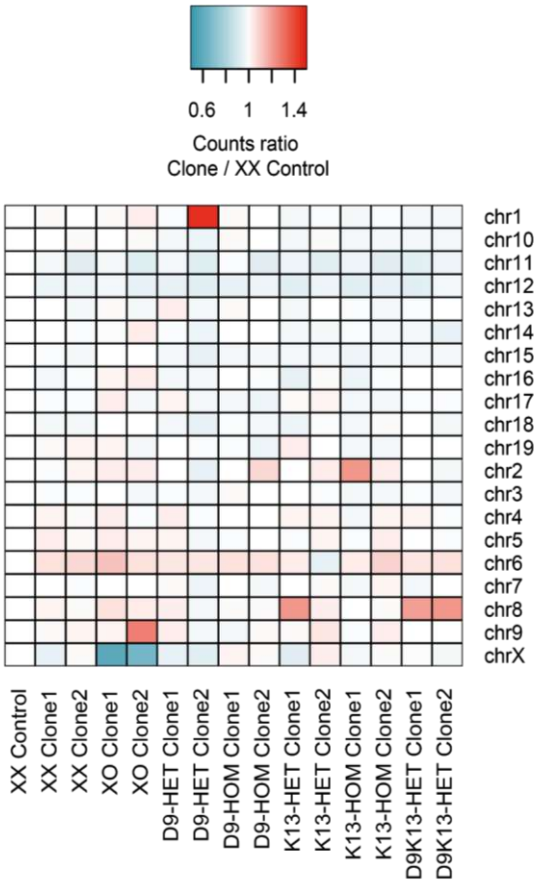

Figure 19. Karyotyping of mutant cell lines used in this study by double digest genotyping by sequencing (ddGBS). Counts mapping to each chromosome were normalized to an XX clone that had previously been karyotyped via metaphase spreads.

From the two clones used from each genotype in this study (XX, XO, K13-HET, K13-HOM, D9-HET, D9-HOM and D9K13-HET), at least one displayed a normal karyotype, with only one clone exhibiting a trisomy of chromosome 1 (D9-HET Clone 2) (Fig. 19).

4.4. CRISPR Knockout screens

Pooled CRISPR screens are a powerful tool for the identification of genes underlying a specific phenotype in an unbiased and high-throughput manner. The implementation of such a screening strategy requires the execution

of certain key steps that lead to the identification of the genes mediating the phenotype of interest, starting with the design and cloning of an sgRNA library targeting a vast number genes into a lentiviral plasmid (section 4.4.1). Such plasmids usually express a resistance marker for future selection of cells with stably integrated sgRNAs. Next, the cloned sgRNA library will be packed into lentiviral particles that will be used for the transduction of the cell line of interest with a low multiplicity of infection (MOI) (section 4.4.2), which will guarantee that each cell becomes transduced with maximally one viral particle (section 4.4.3 and 4.4.4). In this work, cells transduced with the sgRNA library had been previously transduced with lentivirus carrying the Cas9 endonuclease and subsequently selected, in order to ensure stable Cas9 expression in all cells (section 4.4.3 and 4.4.4). Another option implemented in CRISPR screens is the use of a lentiviral plasmid that co-expressess the sgRNA library together with the Cas9 nuclease, however, this leads to a lower viral yield (Sanjana et al. 2014).

Cells that were transduced with the lentiviral sgRNA library will be selected and expanded for several passages, after which a population of interest will be enriched (phenotypic enrichment, section 4.4.3 and 4.4.4). This works implemented fluorescent readouts in all of the generated pooled screens for the selection of specific cell populations with either high or low readout activity through fluorescence activated cell sorting (FACS) (section 4.4.3 and section 4.4.4). Cell pellets from the enriched populations (sorted cells) together with input controls (unsorted cells) can be frozen after phenotypic enrichment, which is then followed by gDNA isolation and amplification of the sgRNA cassettes (a region surrounding the genomically integrated sgRNA) present in each sample (section 4.4.6). Identification of the amplified sgRNAs from each sample can be achieved through next generation sequencing (NGS) (section 4.4.6), which is then followed by data analysis in order to quantify the abundance of the sgRNAs present in a given sample. By comparing sgRNA abundances in the sorted vs unsorted populations, genes can be identified that either promote or inhibit the phenotype of interest (section 4.4.7).

Pivotal for the implementation of pooled CRISPR screens is the maintenance of the sgRNA library representation or coverage, which is defined as the average number of cells or molecules per sgRNA present in a sample. This will ensure that all sgRNAs are detected in the final data analysis step, which is important for statistical testing. Coverage should thus be maintained at all screening steps, which include library cloning, lentiviral transduction, cell splitting, phenotypic enrichment, sequencing library preparation as well as next generation sequencing (NGS). In the pooled CRISPR screens carried out in this work, a coverage of X300 was maintained throughout all steps.

4.4.1 Design and cloning of sgRNA libraries

One of the first steps in a pooled CRISPR screen is the design of the sgRNA library. This includes the decisions of which genes will be targeted during the screening procedure (genome wide or a certain subset of genes), the number of sgRNAs per gene and the sgRNA binding sites within the gene locus, which will depend on the perturbation system of choice. In a knockout CRISPR screen, such as the ones conducted in this work, the sgRNAs will be targeted to the early exons of the genes with the aim to generate frameshift mutations (Shalem et al. 2014). Alternatively, sgRNAs can be targeted upstream or downstream of the transcriptional start site (TSS) in CRISPR interference (CRISPRi) or CRISPR activation (CRISPRa) screens that induce either gene knockdown or overexpression, respectively (Gilbert et al. 2014).

sgRNA sequences targeting the desired genes together with non-targeting controls can be extracted from previously published genome-wide libraries for sgRNA library design *in silico*. This is followed by library synthesis on a microarray and subsequent library amplification using primers that include complementary sequences to the lentiviral plasmid of choice for recombination cloning. Both amplification and cloning are carried out with the pooled sgRNA library oligos, requiring the maintenance of library coverage at these steps. The lentiviral plasmid for library cloning contains a Pol III promoter together with the sgRNA scaffold for Cas9 binding.

For the GeCKOx library used in this study, a list of protein-coding and miRNA genes on the X chromosome was obtained from the NCBI Reference Sequence (Refseq) track on the UCSC genome browser (Pruitt et al. 2005; Pruitt et al. 2014). sgRNA sequences for the targeted X-linked genes, together with the sequences for positive screen controls (MAPK regulators) and non-targeting control sgRNAs were extracted from the genome-wide GeCKO library (Shalem et al., 2014). For the GeCKOxs library, the 50 most enriched and depleted X-linked genes and the 10 most enriched and depleted MAPK regulators from the primary screen were identified using HitSelect (Diaz et al., 2015). The 3 top-scoring sgRNAs for each gene were incorporated in the GeCKOxs library together with 10 non-targeting sgRNA controls. Additionally, several pluripotency regulators were added as positive controls.

The GeCKOx and GeCKOxs sgRNA libraries were cloned into the lentiGuide-puro sgRNA expression plasmid (Table 2). The vector was digested with BsmBI (NEB) overnight at 37°C and gel-purified. sgRNA sequences were synthesized by CustomArray flanked with OligoL (TGGAAAGGACGAAACACCG) and OligoR (GTTTTAGAGCTAGAAATAGCAAGTTAAAATAAGGC) sequences. For the amplification of the library, 8 or 5 (GeCKOx/GeCKOxs) PCR reactions (Primer sequences are listed in Table 4, OG113/OG114) with 5ng from the synthesized oligo pool were carried out using the Phusion Hotstart Flex DNA Polymerase (NEB), with a total of 14 cycles and an annealing temperature of 63°C in the first 3 cycles and 72°C in the following 11 cycles. The amplicons were subsequently gel-purified.

Amplified sgRNAs were ligated into the vector though Gibson assembly (NEB). Two 20 µl Gibson reactions were carried out using 7 ng of the gel-purified insert and 100 ng of the vector. The reactions were pooled, EtOH-precipitated to remove excess salts that might impair bacterial transformation and resuspended in 12.5 µl H_2O. 9 µl of the eluted DNA were transformed into 20 µl of electrocompetent cells (MegaX DH10B, Thermo Fisher Scientific) according to the manufacturer's protocol using the ECM 399 electroporator (BTX). After a short incubation period (1 h, 37°C 250rpm) in 1 ml SOC medium, 9 ml of LB medium with Ampicillin (0.1 mg/ml, Sigma) were added to the mixture and dilutions were plated in Agar plates (1:100, 1:1000 and 1:10000) to determine the coverage of the sgRNA libraries (600x for the GeCKOx and 2500x for the GeCKOxs). 500 ml of LB media with Ampicillin were inoculated with the rest of the mixture and incubated overnight for subsequent plasmid purification using the NucleoBond Xtra Maxi Plus kit (Macherey-Nagel) following the manufacturer's instructions. To assess library composition and sgRNA representation via deep-sequencing, a PCR reaction was carried out to add illumina adaptors by using the Phusion High Fidelity DNA Polymerase (NEB), with an annealing temperature of 60°C and 14 cycles (OG125/OG126, Table 4). The PCR amplicon was gel-purified by using the Nucleospin Gel and PCR Clean-up kit (Macherey-Nagel) following the manufacturer's instructions. Libraries were sequenced paired-end 50 bp on the HiSeq 2500 Platform yielding approximately 25 Mio. Fragments for the GeCKOx (20 pM loading concentration) and $1.3*10^6$ fragments for the GeCKOxs library (22 pM loading concentration).

sgRNA counts from the cloned GeCKOx and GeCKOxs libraries were obtained by using MaGeck_count (from the MAGeCK CRISPR screen analysis tools (Li et al., 2014, 2015b)) on the public Galaxy server usegalaxy.eu (Afgan et al., 2016) and analyzed in RStudio 3.5.3 (see section 4.4.7 for details).

4.4.2 Generation of a lentiviral-packaged sgRNA library for mESC transduction

To generate virus carrying sgRNAs of the GeCKOx/GeCKOxs libraries, HEK293T cells were seeded into 12/8 10 cm plates and transfected the next day at 90% confluence. Each plate was transfected with 6.3 µg of pPL1, 3.1 µg of pLP2 and 2.1 µg of VSVG vectors (Thermo Fisher Scientific, Table 2) together with 10.5 µg of the GeCKOx/GeCKOxs library plasmids in 1 ml of Opti-MEM (Life technologies). 60 µl Lipofectamine 2000 Reagent (Thermo Fisher Scientific) were diluted in 1 ml Opti-MEM. Both mixtures were incubated separately for 5 min and then combined followed by a 20 min incubation, after which they were added dropwise to the HEK293T cells. Medium was changed 6 h after transfection. Transfected HEK293T cells were cultured for 48 h at 37°C, afterwards the medium was collected and centrifuged at 1800 x g for 15 min at 4°C. Viral supernatant was further

concentrated 10-fold using the lenti-X^{TM} Concentrator (Takara Bio) following the manufacturer's instructions and subsequently stored at -80°C.

To assess the viral titer, 5 serial 10-fold dilutions of the viral stock were applied to each well of a 6-well mESC plate (MOCK plus 10^{-2} to 10^{-6}) for transduction with 8 ng/µl polybrene (Merck). Two replicates were generated for each well. Selection with puromycin (1 ng/µl, Sigma) was started two days after transduction and colonies were counted after 8 days. The number of colonies multiplied with the dilution factor yields the transducing units per ml (TU/ml), which ranged from 0.5-1.5*10^6 TU/ml.

The amount of viral supernatant given to each mESC flask in order to achieve a multiplicity of infection (MOI) of 0.3 (meaning 0.3 viral particles per cell) was calculated as follows:

(Total number of cells per well) x (Desired MOI) = Total transducing units needed (TU)

(Total TU needed) / (TU/ml reported from dilution) = Total ml of lentiviral particles to add to each well

4.4.3 Primary screen on X-chromosomal genes for MAPK regulators

For the SRE-Elk screen, female 1.8-SRE-Elk mESCs (Table 8) were passaged twice before transduction with viral supernatant carrying the lentiCas9 plasmid (Table 2). Blasticidin selection (5 ng/µl, Roth) was started two days after transduction and kept for 4 passages, after which 6*10^6 cells were transduced with the sgRNA library (MOI=0.3). Puromycin selection (1 ng/µl, Sigma) was started 48 h after transduction and kept until harvesting at day 7 after transduction. The 25% of cells with the highest reporter activity were sorted. From these cells, 6-8*10^6 cells were snap-frozen and 6*10^6 were cultured for two additional days and subsequently sorted for GFP fluorescence (top 25%). Around 8*10^6 unsorted cells were snap-frozen on day 7 and day 9 after transduction.

4.4.4 Secondary screens for modulators of pluripotency factor expression, differentiation kinetics and phosphorylation of MAPK pathway components

For the secondary screens, 2*10^6 female 1.8 XX Nanog-mCherry, 1.8 XX Esrrb-mCherry (Table 8) or 1.8 XX mESCs were transduced with the lentiCas9 plasmid as described above and subsequently with the GeCKOxs library.
1.8 XX mESCs were stained for pMek on day 7 after transduction and the 25% of cells with the lowest pMek signal were sorted. 1.8-Esrrb-mCherry mESCs were passaged for differentiation (LIF withdrawal) on day 5 and differentiated for 3 days, after which cells were harvested and the 10% cells with the lowest mCherry fluorescence were sorted. 1.8-Nanog-mCherry mESCs were harvested on day 7 and the 25% cells with the lowest mCherry fluorescence were sorted. From these cells, around 2*10^6 were cultured for two additional days and subsequently sorted for mCherry fluorescence (bottom 25%). Approximately 1*10^6 sorted and unsorted cells were snap-frozen for subsequent library preparation from all the secondary screens in order to maintain good library representation.

4.4.5 pMek intracellular staining

For the intracellular pMek staining, cells were washed with PBS and dissociated to single cells with a 5 min trypsin (Life technologies) incubation. Trypsinization was stopped through addition of medium with serum. Cells were disaggregated and pelleted, washed with PBS and immediately fixed with 1.5% PFA (1 ml/1*10^6 cells). The cell mixture was incubated for 10 min at room temperature and subsequently centrifuged for 5min at 500 x g.

Cells were resuspended in ice-cold MeOH, incubated for 10 min on ice (0.5 ml/1*10^6 cells) and centrifuged for 5 min at 500 x g. Cells were washed once with staining buffer (PBS + 1% BSA, 2 ml/1*10^6 cells) and blocked for 10 min in staining buffer. Cells were subsequently incubated with the pMek-specific antibody (Cell Signaling, #2338,1:100, antibodies are listed in Table 1) for 30 min at room temperature (100 µl/1*10^6 cells), then washed twice with staining buffer. Cells were then incubated with an anti-rabbit-Alexa647 antibody (Thermo Fisher

Scientific,1:400, Table 1) for 15 min at room temperature (100 µl/1*10^6 cells) and washed twice with staining buffer before FACS sorting using the BD FACSAria™ II.

4.4.6 Preparation of sequencing libraries

For the SRE-Elk screen, genomic DNA was isolated from the frozen cell pellets using the DNeasy Blood and Tissue kit (Qiagen) following the manufacturer's instructions. For the secondary screens, genomic DNA from frozen cell pellets was isolated via Phenol/Chloroform extraction due to higher gDNA yields. Briefly, cell pellets were thawed and resuspended in 250 µl of Lysis buffer (1% SDS (Thermo Fisher Scientific), 0.2 M NaCl and 5 mM DTT (Roth) in TE Buffer) and incubated overnight at 65°C. 200 µg of RNAse A (Thermo Fisher Scientific) were added to the sample and incubated at 37°C for 1 h. 100 µg of Proteinase K (Sigma) were subsequently added followed by a 1 h incubation at 50°C. Phenol/Chloroform/Isoamyl alcohol (Roth) was added to each sample in a 1:1 ratio, the mixture was vortexed at room temperature for 1 min and subsequently centrifuged at 16000 x g for 10 min at room temperature. The aqueous phase was transferred to a new tube and 1 ml 100% EtOH, 90 µl 5 M NaCl and 1 µl Pellet Paint (Merck) was added to each sample, after which samples were mixed and incubated at -80°C for 1 h. DNA was pelleted through centrifugation for 16000 x g for 15 min at 4°C, pellets were then washed twice with 70% EtOH, air-dried and resuspended in 50 µl H_2O.

The PCR amplification of the sgRNA cassette was performed in two PCR steps as described previously with minor modifications (Shalem et al., 2014). The first PCR reaction is necessary for an effective amplification of sgRNA sequences from gDNA, while the second PCR allows for the addition of sequencing primers and sample barcodes to the resulting amplicons.

In order to ensure proper library coverage (300x), each sample was amplified in 6/2 PCR reactions (2 µg DNA/reaction) in the primary/secondary screens using the ReadyMix Kapa polymerase (Roche) with a total of 20 cycles and an annealing temperature of 55°C (Primer sequences in Table 4, OG115/OG116).

Successful amplification was verified on a 1% agarose gel and a second nested PCR was performed to attach sequencing adaptors and sample barcodes using 2.5 µl of the sample from the first PCR with a total of 11 cycles and an annealing temperature of 55°C (OG125/OG126, Table 4).

Resulting amplicons were loaded on a 1% agarose gel and purified using the Nucleospin Gel and PCR clean-up kit (Macherey-Nagel). Libraries from the primary screen were sequenced 2x50bp on the HiSeq 2500 Platform (18 pM loading concentration) yielding approximately 4x10^6 fragments per sample. Secondary screens were sequenced 2x75bp (Pluripotency and differentiation screens) on the Nextseq 500 (2.2 pM loading concentration) or 2x50 (pMek screen) on the HiSeq 2500 Platform (20 pM loading concentration).

4.4.7 Data analysis

Data processing and statistical analysis was performed on the public Galaxy server usegalaxy.eu (Afgan et al., 2016) with the MAGeCK CRISPR screen analysis tools (Li et al., 2014, 2015b). To this end, fastq files for read1 were uploaded to the Galaxy server. Alignment and read counting was performed with MAGeCK_count. Duplicated sgRNAs (sgRNAs that targeted more than one gene present in the library and were therefore not unique) were excluded, leaving 6508 unique sgRNA sequences. Statistical analysis was performed with MAGeCK_test for the primary screen (SRE-Elk) and the three secondary screens (Pluripotency, Differentiation and pMek). Additionally, MAGeCK_mle was implemented for statistical analysis of the two performed pMek screens (Harvesting at RT vs. 4°C) for the generation of Fig. 34D (see section 5.2.4).

Normalized counts and gene hit summary files were downloaded and analyzed in RStudio 3.5.3 using the stringr, tidyr , data.table, dplyr and gplots packages. For easier interpretation of the results, common names were used instead of official gene symbols for a subset of genes in all figures (Erk2 for Mapk1, Mek1 for Map2k1, Fthl17e for Fthl17, Fthl17f for Gm5635 and H2al1m for 1700012L04Rik). The 50 most enriched and depleted genes for

the generation of the GeCKOxs sgRNA library from the primary screen were extracted using HitSelect (Diaz et al., 2015).

4.5. DNA methylation profiling

Global CpG methylation levels were measured using the luminometric methylation assay (LUMA), which makes use of the different sensitivities of the HpaII and MspI restriction enzymes to CpG methyl groups. Both enzymes target the same CCGG sequence, but while MspI cuts both unmethylated and methylated DNA, HpaII is methylation-sensitive (Fig. 20). The amount of DNA cut by either MspI or HpaII is then normalized to the amount of overhangs generated by EcoRI, which should be the same in both samples.

This differential sensitivity towards CpG methylation combined with a bioluminometric polymerase extension assay allows for quantification of methylated DNA in a given sample. After an enzymatic digest, generated overhangs are used as primers in a pyrosequencing reaction (Fig. 20). Here, each dNTP addition leads to the release of inorganic phosphate (PPi), which is converted to ATP by the ATP-Sulfurylase. The latter is then used by the luciferase enzyme to convert luciferin to oxyluciferin, emitting a light signal proportional to the amount of dNTP incorporated in the sample.

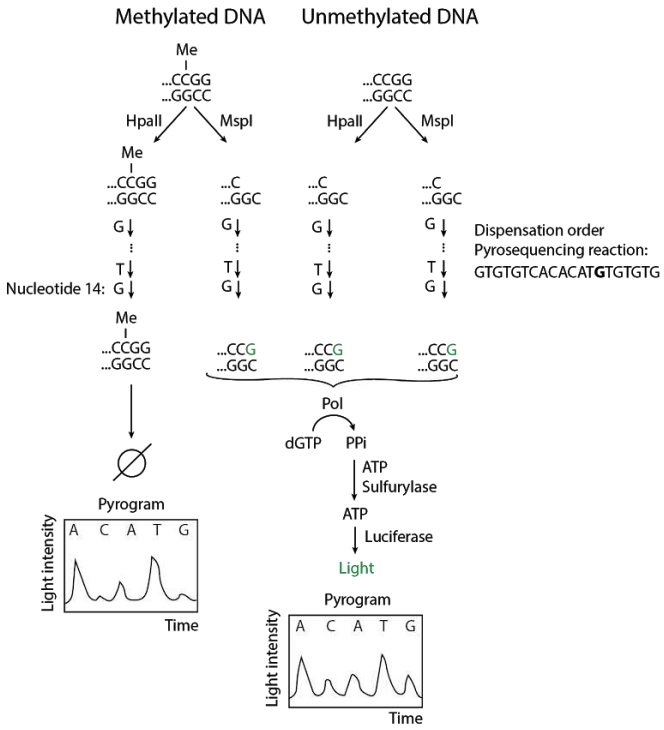

Figure 20. The luminometric methylation assay (LUMA). This assay makes use of the different sensitivities of the HpaII and MspI restriction enzymes to CpG methyl groups. Both enzymes target the same CCGG sequence, but while MspI cuts both unmethylated and methylated DNA, HpaII is methylation-sensitive. After an enzymatic digest, generated overhangs are used as primers in a pyrosequencing reaction. Here, each dNTP addition leads to the release of inorganic phosphate (PPi), which is converted to ATP by the ATP-Sulfurylase. The latter is then used by the luciferase enzyme to convert luciferin to oxyluciferin, emitting a light signal proportional to the amount of dNTP incorporated in the sample.

The luminometric methylation assay was performed as described previously (Pilsner et al., 2010). For this, genomic DNA was isolated using the DNeasy Blood and Tissue Kit (Qiagen) and 500 ng of DNA were digested either with HpaII/EcoRI (NEB) (Tube A) or MspI/EcoRI (NEB) (Tube B) in Tango Buffer (Thermo Fisher Scientific) in a total of 20 µl for 4 h at 37°C. 15 µl of Pyrosequencing Annealing Buffer (Qiagen) were mixed with 15 µl of

each sample and overhangs were quantified by Pyrosequencing using the following dispensation order GTGTGTCACACATGTGTGTG (nucleotides were pipetted in a two-fold dilution) in the PyroMark Q24 (Qiagen). The peak height from dispensation 13 (T) corresponds to the EcoRI digestion and the peak height from dispensation 14(G) corresponds to the HpaII or the MspI digestion. For each sample, the HpaII/EcoRI ratio for tube A and the MspI/EcoRI ratio for tube B were calculated. The fraction of methylated DNA is then defined as 1-((HpaII/EcoRI) / (MspI/EcoRI)).

4.6. Flow Cytometry

Flow cytometry allows for the measurement of multiple physical characteristics of single cells (Adan et al., 2017). Here, cell populations are passed through a fluidics stream in a flow chamber to allow single cells to move through a laser beam. Cell properties such as size and internal complexity are measured through light scattering of the laser light. Forward scattered light (FSC) is proportional to cell surface area, while side scattered light (SSC) is proportional to cell granularity. This allows for the differentiation of various cell populations within one sample or the separation of live cell populations from cell debris.

Flow cytometry also enables the measurement of fluorescence intensities, allowing the assessment of cell populations labeled with a fluorophore or expressing fluorescent proteins. Here, electrons of a fluorescent compound are excited with a laser emitting light energy of a specific wavelength (Absorption spectrum), rising to a higher energy level. Decay of the electron to its ground state leads to photon emission (Emission spectrum), or what is termed fluorescence. Different laser and filter combinations can be applied to assess fluorescence of several compounds simultaneously in a given cell.

In this work, the green fluorescent protein (GFP, excitation max. 488 nm and emission max 509 nm) and the mCherry protein (excitation max 587 nm and emission max. 610 nm) were implemented as fluorescent reporters in the primary (section 4.4.3) and two secondary (section 4.4.4) CRISPR Knockout screens. Additionally, an intracellular staining strategy was used in a third secondary screen (section 4.4.4 and 4.4.5) using a secondary Alexa Fluor 647 conjugated antibody (excitation max 651 nm, emission max 667 nm).

For the experiments described in this work, cells were resuspended in Sorting buffer (1% FCS and 1mM EDTA, section 4.4.3 and 4.4.4 (Primary screen together with pluripotency and differentiation secondary screens)) or Staining Buffer (PBS + 1% BSA, section 4.4.5, pMek screen) before flow cytometry and cells were sorted using the BD FACSAria^{TM} II. The sideward and forward scatter areas were used for live cell gating, whereas the height and width of the sideward and forward scatters were used for doublet discrimination. Analysis of FCS files was carried out using the FlowJo V10 Software (BD Biosciences). FCS files of the gated single cell populations were visualized using RStudio and the Flowcore package.

4.7. Immunoblotting

Immunoblotting is used to detect and quantify target protein levels. Here, samples are subjected to gel electrophoresis in order to separate proteins by molecular weight, after which they are transferred onto a membrane (either PVDF or Nitrocellulose) through electrophoresis. This is followed by blocking of the membrane to prevent nonspecific binding of antibodies and subsequent incubation with a primary antibody of choice that will detect the target protein. Proteins are made visible through secondary antibodies that bind the primary antibodies, which are conjugated either to a reporter enzyme such as the horseradish peroxidase (HRP) or near-infrared dye labelled secondary antibodies (the latter were implemented in this study, see below).

Lysates were prepared from ~ $2*10^6$ cells by washing with ice-cold PBS, directly adding Bioplex Cell Lysis Buffer (Biorad) supplemented with the provided inhibitors and shaking plates at 4°C at 300 rpm for 30 min, after which the lysates were transferred to 1.5 ml eppendorf tubes and centrifuged at 4°C and 4500 x g for 20 min, in order

to remove unlysed cells and cellular debris. The soluble Protein fraction was transferred to a clean tube and quantified using the Pierce BCA kit (Thermo Fisher Scientific). The principle of protein quantification via BCA is the presence of bicinchoninic acid and copper (II) sulfate added in the solution added to each sample for quantification. Peptide bonds in proteins reduce Cu2+ to Cu+ in a manner proportional to the amount of protein present in the sample. Subsequently, two molecules of bicinchoninic acid chelate with the Cu+, forming a purple colored complex that absorbs light at a wavelength of 562 nm.

For signaling proteins, 25 µg protein was applied per lane. For Dusp9 10 µg and for Klhl13 40 µg were loaded per lane. Proteins were separated by molecular weight via SDS-polyacrylamide gel electrophoresis and transferred to nitrocellulose membranes (GE Healthcare) using the Trans-Blot Turbo semi-dry transfer system (Bio-rad). Membranes were blocked for 1 h with Odyssey Blocking Buffer/PBS (1:1) (Li-COR) at room temperature, followed by an incubation with primary antibody (in Odyssey Blocking Buffer/PBST (1:1)) overnight at 4°C.

Signals were detected using near-infrared dye labelled secondary antibodies added in a 1 h incubation step at room temperature (in Odyssey Blocking Buffer/PBST (1:1), allowing for linear quantification of target epitopes. This offers an advantage over luminescence-based detection systems, which depend on the enzyme kinetics of the horseradish peroxidase (HRP) and do not allow this type of quantification. Membranes were scanned using Li-COR Odyssey and band intensities were quantified using the Image Studio Lite Ver 5.2 by calculating median intensities of the band area and subtracting the adjacent top/bottom background. Antibodies are listed in Table 1.

4.8. RNA extraction, reverse transcription, qPCR

Quantitative polymerase chain reaction (qPCR) allows the monitoring of specific DNA amplicons during the PCR reaction by making use of DNA-binding fluorescent dyes, such as SYBR Green, which binds specifically to double-stranded DNA (dsDNA). An increase in the amount of DNA produced during the PCR reaction will therefore lead to a quantifiable increase in the fluorescent intensity measured each cycle, as the dye will only fluoresce when bound to dsDNA.

For gene expression profiling, ~ $2*10^6$ cells were washed with ice-cold PBS and lysed by directly adding 500 µl of Trizol (Invitrogen). RNA was isolated using the Direct-Zol RNA Miniprep Kit (Zymo Research) following the manufacturer's instructions. For quantitative PCR (qPCR), 1 µg RNA was reverse transcribed using Superscript III Reverse Transcriptase (Invitrogen) with random hexamer primers (Thermo Fisher Scientific) and RNA expression levels were quantified in the QuantStudio™ 7 Flex Real-Time PCR machine (Thermo Fisher Scientific) using 2xSybRGreen Master Mix (Applied Biosystems), normalizing to Rrm2 and Arpo. Primer sequences are listed in Table 3.

4.9. RNA FISH

RNA fluorescence in situ hybridization (FISH) relies on the use of fluorescent probes that bind to a target RNA allowing for its accurate detection and localization using wide-field fluorescence microscopy. Several probes can be used for RNA FISH, such as fluorescently labelled DNA oligonucleotides and plasmids or bacterial artificial chromosomes (BACs), all containing sequences complementary to the target RNA. Whereas fluorescently labelled oligonucleotides can be purchased from several companies for immediate use, plasmids and BAC probes need to be labelled with fluorescent dyes prior to RNA FISH in order to detect transcribed RNA in fixed cells. This can be done through Nick-translation, where the DNA to be processed is treated with DNAse in order to induce single stranded "nicks". The DNA Polymerase I subsequently removes nucleotides in the "nick" through 5'-3' exonuclease activity, and replaces these by adding fluorescently labelled nucleotides.

This work made use of two BAC probes spanning genomic regions of the X-linked genes HuweI (RP24-157H12) and Klhl13 (RP23-36505). BACs were purified using the NucleoBond BAC kit (Macherey-Nagel) and fluorescently labelled by nick-translation (Abbot) using dUTP-Atto550 (Jena Bioscience) for the HuweI probe and Green dUTP (Enzo) for the Klhl13 probe.

RNA FISH was performed based on previous protocols (Chaumeil et al., 2008). Here, cells were singled out using Accutase (Invitrogen) and placed onto #1.5 (1mm) coverslips for 10 min. Coverslips had been previously coated using 0.01% Poly-L-Lysine diluted in H_2O followed by a 10 min incubation at room temperature. Cells were fixed with 3% paraformaldehyde in PBS for 10 min at room temperature and permeabilized for 5 min on ice in PBS containing 0.5%Triton X-100 and 2 mM Vanadyl-ribonucleoside complex (New England Biolabs). Coverslips were stored in -20°C in 70% EtOH until further use.

Before incubation with the target probes, the fixed cells were dehydrated through an ethanol series (80, 95 and 100%) and subsequently air-dried. Per coverslip, 60 ng labelled probe was ethanol precipitated with Cot1 repeats (in order to suppress repetitive sequences in the BAC DNA that could hamper the visualization of specific signals), resuspended in formamide, denatured (10 min 75°C) and competed for 1 h at 37°C. Probes were then co-hybridized in hybridization buffer overnight (50% Formamide, 20% Dextran Sulfate, 2X SSC, 1 µg/µl BSA and 10 mM Vanadyl-ribonucleoside (ribonuclease inhibitor)). To reduce background, three 7 min washes were carried out at 42°C in 50% Formamide/2XSSC (pH 7.2) followed by three 5 min washes in 2X SSC at room temperature. Nuclei were stained with 0.2 mg/ml DAPI and mounted using Vectashield mounting medium for fluorescence (Vector Laboratories). Images were acquired using a widefield Z1 Observer (Zeiss) equipped with a 100-x objective and the filter set 38 and 43 (Zeiss). Image analysis was carried out using the Zen lite 2012 software (Zeiss).

4.10. RNA-seq

RNA-seq uses next generation sequencing (NGS) to quantify the relative amount of RNA transcripts found in a given sample. Two different RNA-seq methods were used in this work.

In the first method, libraries were generated using the Tru-Seq Stranded Total RNA library preparation kit (Illumina) with 1 µg starting material and amplified with 15 Cycles of PCR. This was carried out by the Sequencing Core Facility at the Max Planck Institute for Molecular Genetics (MPIMG). Libraries were sequenced 2x50bp on one HiSeq 2500 lane (22 pM loading concentration), which generated ~40 Mio. fragments per sample. The reads were mapped with the STAR aligner allowing for maximally 2 mismatches to the mm10 mouse reference genome (GRCm38) and quantified using the ENSEMBL gene annotation (Dobin et al., 2013). Read mapping was carried out by Dr. Edda Schulz. Normalized counts (rpkm) were obtained using the EdgeR package in RStudio (Robinson et al., 2010).

In a second method the QuantSeq 3‘ mRNA-Seq Library Prep Kit (FWD) for Illumina (Lexogen) was used with 800 ng starting material. Here, transcripts are sequenced from the 3´-end, generating just one fragment per transcript. Unique molecular identifiers (UMIs) are additionally tagged to individual transcripts, which permits the identification of PCR duplicates, eliminating amplification biases. Quantseq library preparation was carried out by Ilona Dunkel.

Samples were sequenced with 1x75bp on the NextSeq 500 Platform (2 pM loading concentration). The count matrix was generated with the FWD-UMI Mouse (GRCm38) Lexogen QuantSeq 2.6.1 pipeline from the BlueBee NGS data analysis platform (https://www.bluebee.com/). Differential expression analysis was carried out using the EdgeR package in RStudio, together with normalization of gene expression values (cpm) (Robinson et al., 2010).

4.11. Immunoprecipitation

Immunoprecipitation is a technique where a protein is enriched using an antibody that binds specifically to one (monoclonal antibody) or several of its epitopes (polyclonal antibody). The antibody is usually bound to beads (such as agarose or magnetic beads) and can be detached from them through either denaturation or enzymatic digest, allowing for the elution of the protein of interest. This work made use of a GFP tag coupled to a protein of interest in order to pull-down its interaction partners.

The GFP Immunoprecipitation protocol implemented in this study was performed as described previously with minor modifications (Hubner et al., 2010). Cells were treated with 15 µM of the proteasome inhibitor MG132 for 3 h prior to harvesting. This was done in order to stabilize Klhl13 protein targets, which would otherwise be subjected to proteasomal degradation. Cells were singled out using trypsin, pelleted and resuspended in 1 ml of Lysis Buffer containing 150 mM NaCl, 50 mM Tris, pH 7.5, 5% glycerol, 1% IGEPAL-CA-630, 1 mM $MgCl_2$, 200 U benzonase (Merck), and EDTA-free complete protease inhibitor cocktail (Roche). Cells were incubated on ice for 30 min to allow cell lysis. Lysates were centrifuged at 4000 x g and 4°C for 15 min to remove cell debris and the supernatant was incubated with 50 µl magnetic beads coupled to monoclonal mouse anti-GFP antibody (Miltenyi Biotec) for 20 min on ice. Magnetic columns were equilibrated by washing first with 250 µl of 100% EtOH followed by two washes with the same volume of lysis buffer. After the 20 min incubation, the lysates were applied to the column followed by three washes with 800 µl of ice-cold wash buffer I (150 mM NaCl, 50 mM Tris, pH 7.5, 5% glycerol, and 0.05% IGEPAL-CA-630) and two washes with 500 µl of wash buffer II (150 mM NaCl, 50 mM Tris, pH 7.5, and 5% glycerol). Column-bound proteins were subsequently pre-digested with 25 µl 2 M urea in 50 mM Tris, pH 7.5, 1 mM DTT, and 150 ng trypsin (Roche) for 30 min at room temperature. Proteins were eluted by adding two times 50 µl elution buffer (2 M urea in 50 mM Tris, pH 7.5, and 5 mM chloroacetamide). Samples were further digested overnight at room temperature, since the trypsin treatment implemented during the elution step is not sufficient for the generation of tryptic peptides for downstream Mass spectrometry analysis. The tryptic digest was subsequently stopped by adding formic acid to a final concentration of 2%.

4.12. Mass spectrometry

Quantitative proteomics of cell samples can be achieved through two different methods: the first one being stable isotope labelling by amino acids in cell culture (SILAC) and the second one label free quantification (Wong and Cagney, 2010). A major disadvantage of the first is, however, is the need to culture cells in a specific medium, which can drastically differ from the original. High costs are something to be further considered.

Label-free protein quantification bases on the premise that identical peptides across different LC-MS/MS experiments can be compared directly. Samples are therefore normalized relative to the mean of all protein abundance ratios, offering the major advantage that no extra steps are required for sample preparation.

4.12.1 Sample Preparation for proteomics with Label-Free Quantification (LFQ)

Proteomics sample preparation was done according to a published protocol with minor modifications (Kulak et al., 2014). Approximately $2*10^7$ cells were lysed under denaturing conditions in a buffer containing 3 M guanidinium chloride (GdmCl), 5 mM tris(2-carboxyethyl)phosphine, 20 mM chloroacetamide and 50 mM Tris-HCl pH 8.5. Lysates were denatured at 95°C for 10 min shaking at 1000 rpm in a thermal shaker and sonicated in a water bath for 10 min. A small aliquot of cell lysate was used for the bicinchoninic acid (BCA) assay to quantify the protein concentration. 50 µg protein of each lysate was diluted with a dilution buffer containing 10% acetonitrile and 25 mM Tris-HCl, pH 8.0, to reach a 1 M GdmCl concentration. Then, proteins were digested with LysC (Roche, Basel, Switzerland; enzyme to protein ratio 1:50, MS-grade) shaking at 700 rpm at 37°C for 2 h. The digestion mixture was diluted again with the same dilution buffer to reach 0.5 M GdmCl, followed by a tryptic

digestion (Roche, enzyme to protein ratio 1:50, MS-grade) and incubation at 37°C overnight in a thermal shaker at 700 rpm.

4.12.2 LC-MS/MS Instrument Settings for Shotgun Proteome Profiling

Shotgun Proteome Profiling was carried out by the Mass spectrometry facility of the Max Planck Institute for Molecular Genetics (MPIMG), according to their established protocol.

4.12.3 Data analysis

Raw MS data were processed with MaxQuant software (v1.6.0.1) and searched against the mouse proteome database UniProtKB with 22,286 entries, released in December 2018. Parameters of MaxQuant database searching were a false discovery rate (FDR) of 0.01 for proteins and peptides, a minimum peptide length of seven amino acids, a first search mass tolerance for peptides of 20 ppm and a main search tolerance of 4.5 ppm, and using the function “match between runs”. A maximum of two missed cleavages was allowed for the tryptic digest. Cysteine carbamidomethylation was set as fixed modification, while N-terminal acetylation and methionine oxidation were set as variable modifications. Contaminants, as well as proteins identified by site modification and proteins derived from the reversed part of the decoy database, were strictly excluded from further analysis.

The calculation of significantly differentially expressed proteins for both the proteomics (K13 HOM vs XX wildtype) as well as the IP datasets (GFP-Kelch/D-GFP-Klhl13 vs GFP/D-GFP) was done with Perseus (v1.6.1.3). LFQ intensities, originating from at least two different peptides per protein group were transformed by $\log_2$. Only groups with valid values in at least one group were used, missing values were replaced by values from the normal distribution. Statistical analysis for differential expression was done by a two-sample t-test with Benjamini-Hochberg (BH, FDR of 0.05) correction for multiple testing.

For the identification of Klhl13 interaction partners, cut-offs were set from the data displayed in the volcano plots using a previously published method (Keilhauer et al., 2015). Briefly, a graphical formula as a smooth combination of the following parameters was implemented:

$-\log_{10}(p) \geq c / |x| - x_o$

x: enrichment factor of a protein

p: p-value of the t-test, calculated from replicates

x_o: fixed minimum enrichment

c: curvature parameter

We optimized parameters c and xo such as to have 10% FDR (left-sided outliers) while maximizing the number of right-sided outliers. In the case of the GFP-Kelch IP, c = 0.32 and x_o = 0.02. For the GFP-Klhl13 IP, c = 0.28 and x_o = 0.04. Proteins without an associated gene name were filtered out in further analyses.

5. Results

5.1. Pooled CRISPR knockout screen reveals several putative MAPK inhibitors as candidate genes underlying the female pluripotency phenotype

MAPK pathway inhibition leads to an enhanced naive pluripotent state in mouse embryonic stem cells (mESCs) by increasing pluripotency factor expression and blocking differentiation (Kunath et al., 2007; Silva et al., 2009). Since this pathway seems to regulate many of the traits that underlie the female pluripotency phenotype (Schulz et al., 2014; Song et al., 2019), we hypothesized that one or several X-chromosomal MAPK inhibitors could be responsible for the observed sex differences.

Since the X chromosome harbors approx. 1000 genes, we decided to implement a pooled screen in order to screen most of the candidate genes in a high-throughput and unbiased manner. Screens are usually performed in two possible formats: arrayed and pooled. In the first, a single perturbation is carried out in the multiple cells present in one well of a multi-well plate. Disadvantages of this method include the requirement of specialized microscopic equipment for monitoring of perturbation outcomes together with high costs, which limit screening library size.

In pooled screens, a library is applied *en masse* to a population of cells so that a single gene will be perturbed in each cell. This is followed by the selection of a population of interest based on a biological readout (e.g. sorted cells or treated cells), which depends on the question addressed in the research project. Possible readouts include gene reporter activity, protein expression assessed via fluorescent tagging, cell activity (proliferation, migration, etc) or drug resistance.

During a pooled CRISPR screen, a population of cells is transduced with lentiviral particles carrying an sgRNA library targeting the genes of interest (sgRNA library) in a way that each cell is transduced with only one sgRNA. After the phenotypic enrichment of a cell population with the phenotype of interest, which usually includes drug selection or fluorescent activated cell sorting (FACS), genes are identified by amplifying the sgRNAs present in both enriched and control cell populations (e.g. treated vs. untreated or sorted vs. unsorted) followed by next generation sequencing (NGS) and comparison of their relative abundances. Screen hits are finally determined by assessing statistical enrichment or depletion of several sgRNAs per gene in the target population (e.g treated or sorted). A great advantage of pooled screens is that they allow the screening of a large number of genes in an unbiased and cost-effective manner, whereas a small disadvantage is the limitation of available screening readouts.

Several steps need to be established before carrying out a pooled CRISPR screen. First, the perturbation system (e.g. gene knockout, knockdown or overexpression) should be selected and its efficiency tested in the cell line of interest (section 5.1.1). This is followed by the generation of an sgRNA library targeting the subset of genes to be screened, including also positive and negative controls (section 5.1.2). Next, a readout should be chosen to answer the research question addressed, which in this work is the identification of X-linked MAPK inhibitors. A MAPK-sensitive fluorescent reporter should be therefore generated in the cell line of interest and its functionality tested (section 5.1.3). The results of these steps will be shown in the following sections.

5.1.1 Assaying for Cas9 knockout efficiency in female mESCs

So far, possible technologies to assess loss of function (LoF) phenotypes include shRNA, CRISPR interference (CRISPRi) and CRISPR knockout screens, however, the latter has proven the most efficient (Evers et al., 2016). Additionally, sgRNA libraries for CRISPR knockout screens tend to be usually smaller compared to CRISPRi libraries, since for the latter sgRNA activity is less predictable and therefore more sgRNAs targeting each gene

(and its various isoforms) are needed. For these reasons, a knockout perturbation system was chosen over CRISPRi. We next sought out to test Cas9 knockout efficiency in female mESCs.

To test for knockout efficiency using the Cas9 endonuclease, 1.8 female mESCs stably expressing the Cas9 endonuclease, which had been previously transduced with the lentiCas9 construct and subsequently blasticidin selected, were transduced with lentivirus carrying sgRNAs targeting the coding region of the MAPK pathway components *Mek* or *Erk* and selected for stable guide integration using puromycin. The lentiGuide-Mek1_KO and lentiGuide-Erk2_KO sgRNA plasmids implemented for this experiment were generated using an equimolar mix of three different sgRNAs that were cloned into the lentiGuide-puro plasmid (see Table 2 and Table 7). Mek and Erk protein levels were subsequently assessed via Immunoblotting. We observed an approx. 70% reduction of total Mek levels and 50% reduction of total Erk levels (Fig. 21). In theory, very efficient sgRNAs should generate a mixed population of cells carrying frameshift mutations that would include 11% wildtype cells, 44% heterozygous mutant cells and another 44% of homozygous mutant cells. This means that, theoretically, these sgRNAs should lead to a reduction of protein levels of approx. 66%, which is similar to those observed in the Mek mutants. The slightly lower reduction of Erk levels could be due to the fact that the sgRNAs implemented for this locus were not as efficient.

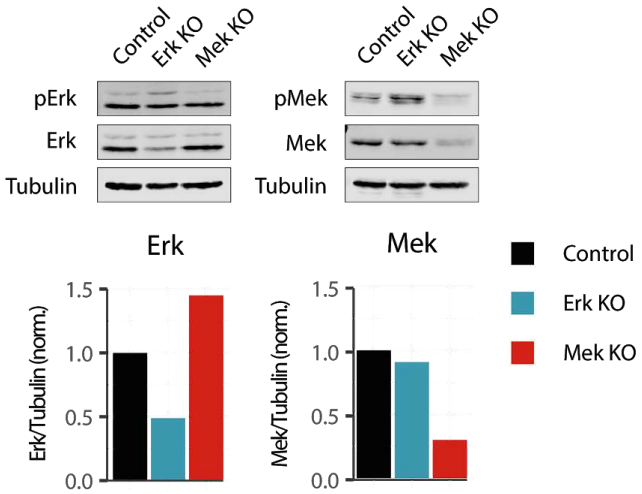

Figure 21. Assaying for Cas9 knockout efficiency in female mESCs. Erk and Mek protein levels quantified via Immunoblotting from female mESCs stably expressing the Cas9 nuclease and sgRNAs targeting the coding sequences of the *Mek* (red) or *Erk* locus (blue), or no sgRNA (control, black). Only one replicate was performed.

In summary, an effective reduction of protein levels could be reached through the employment of the Cas9 endonuclease together with sgRNAs targeting the *Mek* or *Erk* coding sequences. CRISPR knockout screens using the Cas9 nuclease represent therefore a suitable loss of function technology for implementation in female mESCs.

5.1.2 Generation of an sgRNA knockout library targeting X-chromosomal genes

As a first step to screen for X-chromosomal genes that modulate the MAPK pathway in female mESCs, an sgRNA knockout library was generated to target the genes present on the X Chromosome. For this, sgRNA sequences were extracted from the previously published GeCKO library (Shalem et al. 2014). From 1067 X-chromosomal genes, 961 were present in the GeCKO library with approx. 6 sgRNAs targeting each gene (Fig. 22A). Additionally, 237 positive control genes known to have an effect on the MAPK pathway were included from the Gene Ontology (GO) terms “Erk1 and Erk2 Cascade” (GO 0070371), “Regulation of Erk1 and Erk2 Cascade” (GO 0070372), “Negative regulation of Erk1 and Erk2 Cascade” (GO 0070373) and “Positive regulation of Erk1 and Erk2 Cascade” (GO 0070374). MAPK regulators Grb2, Fgfr2, Dusp5, Dusp7, and Dusp2 were added as additional controls, since

they were not found in the gene ontology annotations and represent important pathway components or negative regulators. Lastly, 100 non-targeting control sgRNAs were included in the GeCKOx library (Fig. 22A). These represent negative controls, which should not have an effect on the MAPK signaling pathway and should theoretically be neither enriched nor depleted after phenotypic enrichment.

The GeCKOx oligo library was cloned and proper sgRNA representation was assessed via next generation sequencing (NGS) (Fig. 22B). Alignment of the sgRNA library using MaGeck_count (Li et al., 2014, 2015b) on the galaxy server usegalaxy.eu (Afgan et al., 2016) excluded sgRNAs that targeted more than one gene present in the library and were therefore duplicated, leaving 6508 unique sgRNA sequences. Out of these, only one sgRNA had no detectable counts after read alignment: sgRNA_6894_mmu-mir-3620. All sgRNAs were present in comparable abundance with a 4-fold difference between the 10th and 90th percentile, which is considered an ideal distribution width (Imkeller et al. 2020) (Fig. 22B).

A

sgRNA Class	# Genes	# sgRNAs
X-linked genes	961	5566
Erk1 & Erk2 Cascade (GO0070371)	12	72
Regulation of Erk1 & Erk2 Cascade (GO0070372)	22	132
Negative regulation of Erk1 & Erk2 Cascade (GO0070373)	49	294
Positive regulation of Erk1 & Erk2 Cascade (GO0070374)	154	924
Additional MAPK regulators	5	30
Non-targeting controls (NTC)	NA	100
Total		7118

B

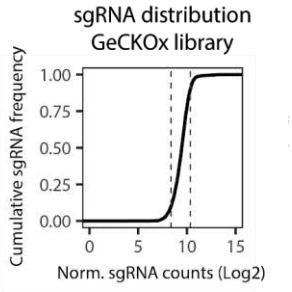

Figure 22. Generation of an sgRNA library targeting the X chromosome. (A) Composition of the GeCKOx sgRNA library targeting 961 X-linked genes and 242 genes involved in the regulation of the MAPK signaling pathway, with approx. 6 sgRNAs per gene. Additionally, 100 non-targeting controls (NTCs) were added. **(B)** Cumulative sgRNA frequency in the cloned GeCKOx sgRNA library. Dashed lines indicate the 10th and 90th percentiles.

To sum up, an sgRNA library targeting 961 X-linked genes and 242 known MAPK regulators as positive controls could be successfully generated. 100 non-targeting sgRNAs were additionally included in the library as negative controls.

5.1.3 Generation of a MAPK sensitive reporter in female mESCs

A MAPK sensitive fluorescent reporter was generated in order to monitor MAPK pathway activity on a single cell level, where the expression of an unstable green fluorescent protein (GFP-Pest) is driven by a MAPK sensitive promoter with binding sites for MAPK downstream components (Serum response factor (SRF) and Elk1, see Supp. Table S5 for sequence). The ETS like-1 protein (Elk1) is activated through Erk phosphorylation after nuclear translocation and forms an heterodimer with the SRF to activate MAPK target genes (Gille et al., 1995).

In order to test the functionality of the reporter and its sensitivity to X-chromosomal dosage, it was randomly integrated in the genome of the TX1072 female cell line, in which the expression of the lncRNA Xist can be monoallelically induced through the addition of doxycycline (Fig. 23A) (Schulz et al. 2014). This is turn causes the progressive silencing of X-linked genes over several days from one of the two X-Chromosomes present in the cell line. The aforementioned decrease in X-chromosomal dosage should then lead to a subsequent increase of MAPK signaling levels possibly due to silencing of putative X-linked MAPK inhibitors (Schulz et al. 2014). Indeed, after addition of doxycycline during four consecutive days, a slight increase in GFP fluorescence was observed (Fig. 23B).

We additionally tested whether the SRE-Elk reporter would be sensitive to external perturbations of the MAPK pathway. For this, we randomly integrated the SRE-Elk reporter into the genome of 1.8 XX cells using lentivirus and assessed reporter functionality via treatment with a Mek inhibitor, which showed the expected decrease in GFP fluorescence (Fig. 23C).

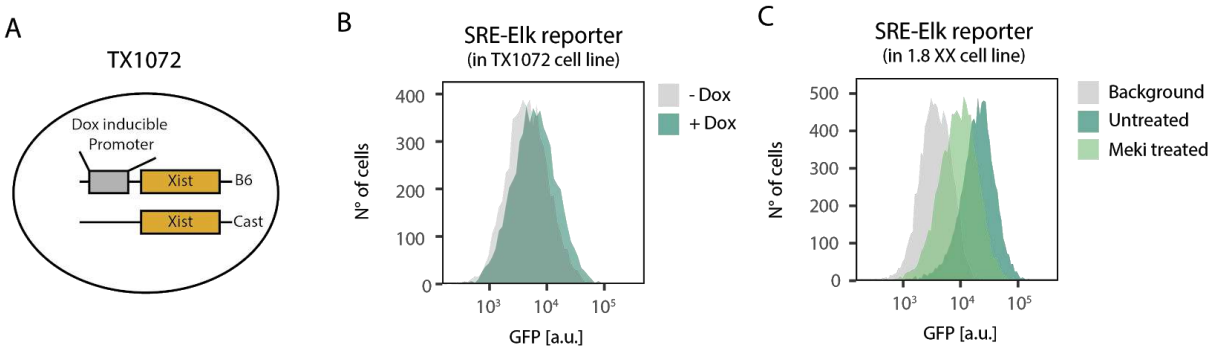

Figure 23. Generation of a MAPK-sensitive fluorescent reporter for a pooled CRISPR knockout screen. (A) Schematic representation of the TX1072 cell line, where expression of the lncRNA Xist from the B6 allele can be induced via doxycycline treatment **(B)** Measurement of GFP fluorescence via flow cytometry in TX1072 female cells carrying a stably integrated MAPK-sensitive reporter treated for 4 days with 1µg/ml doxycycline (Green, +Dox) together with a non-treated control (Grey, -Dox). **(C)** Measurement of GFP fluorescence via flow cytometry in 1.8 female mESCs carrying a stably integrated MAPK-sensitive reporter (1.8 SRE-Elk cells) treated for 48h with 1µM of the Mek inhibitor U0126 (Meki treated) or with DMSO (Untreated). The parental cell line without reporter integration is shown in grey.

In conclusion, the SRE-Elk MAPK reporter appears to be slightly sensitive to X-chromosomal dosage. Additionally, a robust decrease in GFP fluorescence could be observed when cells carrying the randomly integrated reporter were treated with a Mek inhibitor, pointing to a strong reporter response towards external perturbations of the MAPK pathway. Thus, the SRE-Elk reporter seems to represent a suitable readout to assess MAPK pathway activity on a single cell level.

5.1.4 Pooled CRISPR knockout screen workflow

During the screen, 1.8 XX mESCs carrying a randomly integrated SRE-Elk reporter (1.8 SRE-Elk cells) were transduced with lentivirus carrying the Cas9 endonuclease and subsequently selected with blasticidin for stable expression in all cells. After selection and expansion for several passages, cells were transduced with the GeCKOx sgRNA library with a multiplicity of infection (MOI) of 0.3, ensuring this way the transduction of each cell with maximally one viral particle (Fig. 24). Cells were puromycin selected two days after transduction and expanded for 5 additional days, followed by FACS-sorting of cells with high reporter activity. An additional sorting step of the previously sorted population was carried out after two days in culture in order to further enrich for cells with increased MAPK pathway activity (Fig. 24). Three independent replicates were performed. The genomically integrated sgRNAs in the unsorted and double-sorted cell fractions were finally amplified and their sequences determined via NGS. This way, the comparison of sgRNAs present in the double-sorted population compared to the sorted population allowed for the identification of enriched or depleted sgRNAs. Furthermore, statistical testing using MaGeck enabled us to establish significant scoring genes, where consistent effects where observed in several sgRNAs targeting a certain gene.

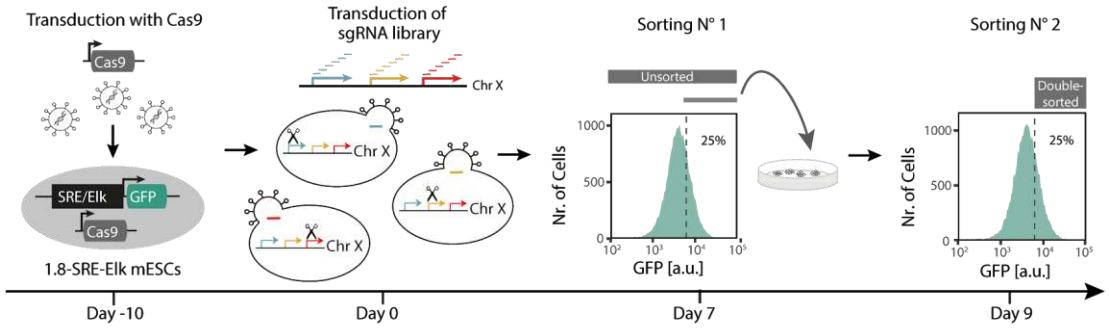

Figure 24. Pooled CRISPR Knockout screen for the identification of X-linked modulators of the MAPK signaling pathway. Workflow of the SRE-Elk screen: 1.8 SRE-Elk mESCs carrying a stably integrated MAPK reporter, where GFP expression is driven by an SRE-Elk promoter (with binding site for downstream components of the MAPK pathway), were transduced with a construct expressing the Cas9 endonuclease. After selection for several passages, cells were transduced with the GeCKOx sgRNA library targeting the majority of X-chromosomal genes and further selected for sgRNA integration. A GFP-high population was sorted via flow cytometry after seven days of expansion, cultured for two additional days and subsequently sorted again (double-sorted population). Genomically integrated sgRNAs were amplified from the unsorted and double sorted population and abundance was quantified via deep-sequencing. The screen was performed in three independent replicates.

5.1.5 Results of the pooled CRISPR knockout screen for the identification of X-linked MAPK pathway inhibitors

In order to assess the quality of the generated screen data, we first compared the correlation of all the analyzed samples, observing that sorted and double-sorted fractions were highly correlated in all the replicates (Fig. 25A). Additionally, sgRNAs were present in comparable abundance in all samples, meaning that a good library coverage was maintained throughout all steps of the screen, and non-targeting controls were neither enriched nor depleted, as expected (Fig. 25B-C).

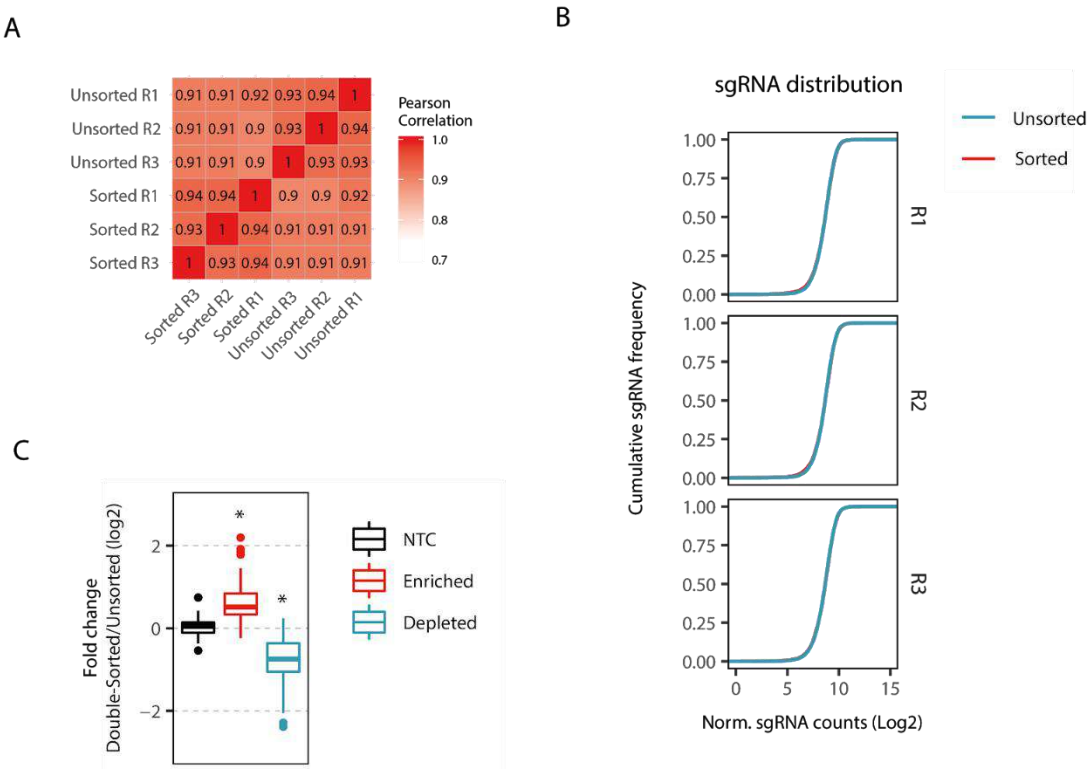

Figure 25. Quality controls for the pooled CRISPR Knockout screen for the identification of X-linked modulators of the MAPK signaling pathway. (A) Pearson correlation coefficients between the unsorted and the double-sorted fractions of the three replicates in the SRE-Elk screen. **(B)** sgRNA distributions in the unsorted and double-sorted fractions of all three replicates. **(C)** Mean fold change of the double-sorted vs the unsorted fractions of the 100 Non-targeting controls and the individual sgRNAs targeting significantly enriched and depleted genes (FDR < 0.05, MAGeCK), * p < 0.05, Wilcoxon rank-sum test.

We next assessed the enrichment/depletion in the screen results of known MAPK regulators included in the library, to determine whether it correlated to their GO annotations or known function from the literature. Here, central MAPK pathway components such as Erk2, Grb2, Frs2, Mek1 and Ptpn11 were highly and significantly depleted in the double-sorted fraction, as expected, confirming the validity of the generated screen (Fig. 26). The Mek1 kinase showed lower depletion compared to other main components such as Grb2 and Erk2, possibly due to genetic compensation by its isoform Mek2, which is also highly expressed in mESCs (El-Brolosy and Stainier, 2017).

The known pathway inhibitor Csk was the strongest enriched gene in the target population (Okada, 2012) (Fig. 26). Csk inhibits Src family kinases, which activate the MAPK signaling pathway through Raf phosphorylation (Pearson et al., 2001). Curiously, the tumor suppressor gene Fbxw7, annotated in the GO database as a MAPK activator, was found among the strongly enriched hits. Our results are however in accordance to studies that have shown an increase in MAPK signaling upon Fbxw7 knockdown in melanoma cancer cell lines, also in agreement with its role as tumor suppressor (Cheng et al., 2013). Lastly, Flcn, a known negative regulator of MAPK signaling (Baba et al., 2008; Cash et al., 2011), was the last of the three MAPK regulators that scored among the significantly enriched genes (Fig. 26).

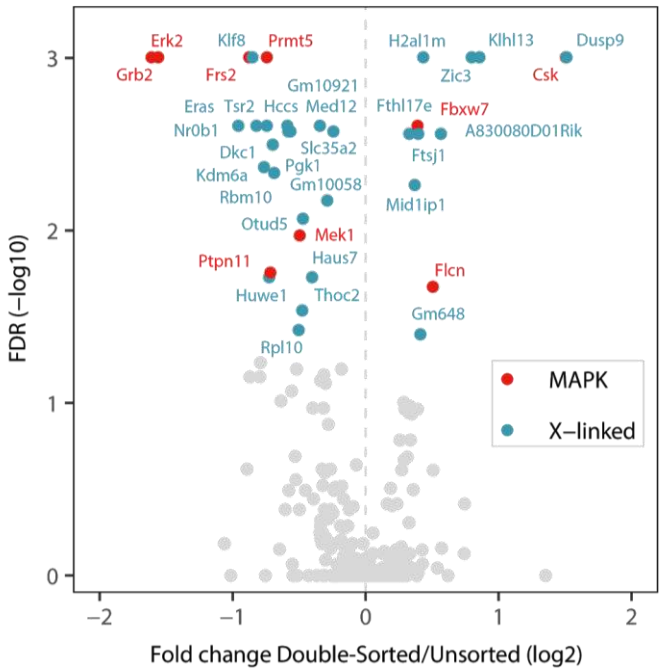

Figure 26. Identification of X-linked modulators of the MAPK signaling pathway in female mESCs via a pooled CRISPR knockout screen. Volcano plot displaying significantly enriched and depleted (FDR > 0.05, MAGeCK) X-linked genes (blue) and known MAPK regulators as positive controls (red).

Among the X-linked genes, 9 were significantly enriched in our primary screen: Dusp9, Klhl13, Zic3, H2al1m, Fthl17e, A830080D01Rik, Ftsj1, Mid1ip1 and Gm648 (Fig. 26). Dusp9 is a known Erk phosphatase and MAPK inhibitor (Caunt and Keyse, 2013, Li et al., 2012), and Zic3 a known pluripotency factor (Declercq et al., 2013; Lim et al., 2007, 2010). The remaining genes, on the other hand, have not yet been linked to the modulation of naive pluripotency in mESCs.

Interestingly, a larger number consisting of 18 X-linked genes scored significantly in the screen as putative MAPK activators: Klf8, Eras, Nr0b1, Tsr2, Hccs, Gm10921, Med12, Dkc1, Slc35a2, Pgk1, Kdm6a, Rbm10, Gm10058, Otud5, Haus7, Huwel, Thoc2 and Rpl10 (Fig. 26). It has been shown that siRNA-mediated knockdown of Klf8 mRNA leads to lower levels of phosphorylated Erk in colorectal cancer cells, pointing to a possible role as MAPK activator (Shi et al., 2015). Eras, on the other hand, is a known activator of the Akt signaling pathway and a strong driver of mouse embryonic stem cell proliferation (Takahashi et al., 2003).

In order to rule out the possibility that gene enrichment/depletion might be due to faster or slower proliferation of targeted cells between the two sampling time points (day 7 and day 9), we compared the sgRNA frequency in the cloned sgRNA library to the unsorted cell fraction from day 7 (Fig. 27). We found that six from the 18 identified putative X-linked MAPK activators led to faster proliferation in mESCs: Eras, Tsr2, Gm10921, Gm10058, Haus7 and Rpl10. More importantly, none of the identified X-linked MAPK inhibitors negatively affected proliferation, which would lead to the enrichment of their sgRNAs between day 7 and day 9 of the screen, eventually leading to false positive hits. Lastly, sgRNAs targeting several essential ribosomal genes were strongly depleted after expansion (Rps4x, Rpl10, Las1l, Rpl36a, Rpl39, etc), confirming the knockout efficiency of the Cas9 nuclease during the screen.

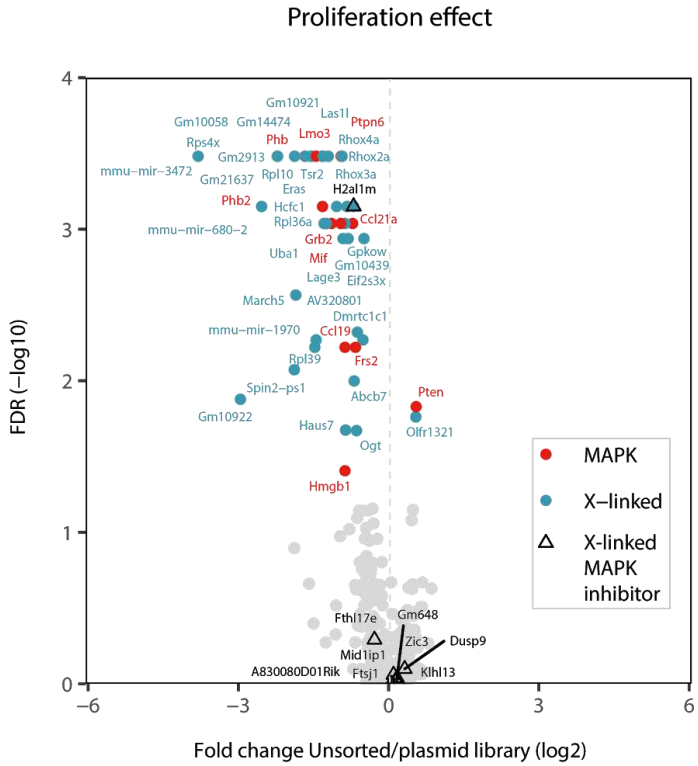

Figure 27. Proliferation effect of the pooled CRISPR Knockout screen for the identification of X-linked modulators of the MAPK signaling pathway. Volcano plot displaying significantly enriched and depleted (FDR > 0.05, MAGeC) X-linked genes (blue) and known MAPK regulators as positive controls (red) in the unsorted fraction vs the cloned plasmid library.

In summary, we have identified several putative MAPK inhibitors among hundreds of X-linked genes through the implementation of a pooled CRISPR knockout screen. These genes are strong putative candidates underlying the sex differences observed in mESCs.

5.2. Secondary screens reveal X-linked candidate genes additionally involved in the regulation of pluripotency factor expression, differentiation kinetics and Mek phosphorylation

After identifying several putative X-linked MAPK inhibitors in the previous primary screen, we set out to investigate which of these genes also had an effect in the other sex differences observed between female and male mESCs, namely pluripotency factor expression, differentiation kinetics and Mek phosphorylation. We carried out for this purpose a series of complementary screens using different fluorescent readout systems for each of the assessed phenotypes, which would allow us the identification of candidate genes in an unbiased manner.

5.2.1 Generation of an sgRNA library targeting the most enriched and depleted genes from the primary screen

First, the GeCKOxs (GeCKOx small) sgRNA library was designed targeting the 50 most enriched and depleted X-linked genes, together with the 10 most enriched and depleted MAPK controls from the primary screen (Fig. 28A). For this, the 3 most effective sgRNAs based on their previous scoring were selected. Additionally, 10 non-targeting sgRNAs together with sgRNAs targeting 10 known pluripotency regulators (Sox2, Tbx3, Tcf3, Fgf2, Stat3, Esrrb, Tfcp2l1, Klf2, Nanog and Oct4) were included from literature searches as further controls (Fig. 28A). The GeCKOxs library was cloned and sgRNA representation was assessed via NGS, which revealed that all sgRNAs were present and in comparable abundance with a 2.1-fold difference between the 10th and 90th percentile (Imkeller et al. 2020) (Fig. 28B).

The generation of a small GeCKOx library (GeCKOxs) targeting 100 X-linked putative MAPK regulators together with 20 known MAPK and 10 pluripotency regulators as positive controls was therefore successful. Additionally, 10 sgRNAs were included as negative controls.

A

sgRNA class	# Genes	# sgRNAs
50 Top enriched X-linked genes	50	150
50 Top depleted X-linked genes	50	150
10 Top enriched MAPK regulators	10	30
10 Top depleted MAPK regulators	10	30
Pluripotency regulators	10	30
Non-targeting controls	NA	10
Total		400

B

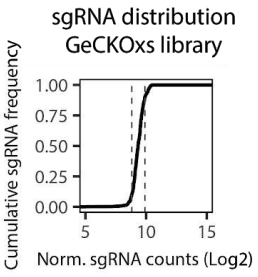

Figure 28. Generation of the GeCKOxs library for the secondary CRISPR knockout screens. (A) Composition of the GeCKOxs sgRNA library targeting the 50 most enriched and depleted genes, together with the 10 most enriched and depleted MAPK controls from the primary screen with 3 sgRNAs per gene. sgRNAs targeting 10 pluripotency regulators and 10 non-targeting controls (NTCs) were added additionally. **(B)** sgRNA distribution in the cloned GeCKOxs sgRNA library. Dashed lines represent the 10th and 90th percentiles.

5.2.2 Secondary CRISPR knockout screen for the identification of genes that modulate pluripotency factor expression in female mESCs

We generated a first secondary screen in order to determine which of the previous putative X-linked MAPK inhibitors would additionally modulate pluripotency factor levels in female mESCs. In order to monitor

pluripotency factor expression on a single-cell level, the *Nanog* locus was C-terminally tagged with mCherry (Fig. 29A). The later was chosen due to significantly higher expression levels in undifferentiated cells with two X chromosomes compared to their XO subclones (2-4 fold higher levels in XX vs XO) (Schulz et al., 2014). This C-terminal tagging strategy was also used to tag the Esrrb locus for a second secondary screen (see below in section 5.2.3). In order to keep the functionality of the endogenous protein, which could be hampered due to steric hindrances caused by the relatively large mCherry protein, a P2A cleaving peptide was incorporated between the C-terminus of the locus and the fluorescent tag (Fig. 29A). The repair template to tag Nanog with mCherry (pUC19-Nanog-mCherry-puro, Table 7) consisted of the P2A self-cleaving peptide followed by the mCherry coding sequence and a loxP-flanked puromycin-resistance cassette, flanked by ~400bp homology regions to the Nanog locus. This plasmid, together with the sgRNA-plasmids targeting the C-terminus of the Nanog locus, were cloned by Jörn Schmiedel. 1.8 XX cells were transiently transfected with the Cas9 endonuclease, sgRNAs targeting the C-terminus of the *Nanog* locus and the aforementioned repair template. Successfully tagged cells were selected based on their puromycin resistance and mCherry fluorescence, after which the puromycin selection cassette was excised via transient CRE recombinase expression. This was due to the fact that the GeCKOxs sgRNA library expresses a puromycin resistance cassette that is used for the selection of cells with stably integrated sgRNAs. Finally, 1.8 Nanog-mCherry clones were genotyped for targeted C-terminal tagging of the *Nanog* locus (see section 4.2.7.1, Fig. 15).

Reporter functionality was assessed by monitoring mCherry levels during differentiation. We observed a significant downregulation of fluorescence intensities around day 3, hinting that the generated reporters indeed mirrored pluripotency factor expression (Fig. 29B).

During the screen, cells carrying the Nanog reporter and stably expressing the Cas9 endonuclease were transduced with the GeCKOxs library and subsequently selected with puromycin. The cells with lower mCherry fluorescence were enriched on day 7 after transduction in two consecutive sorts similarly to the primary screen sorting workflow (sorted vs. double-sorted cells) (Fig. 29C). This sorting strategy was implemented due to our aim at identifying Nanog activators, that when knocked out would lead to lower pluripotency factor expression. Two replicates were carried out for this screen.

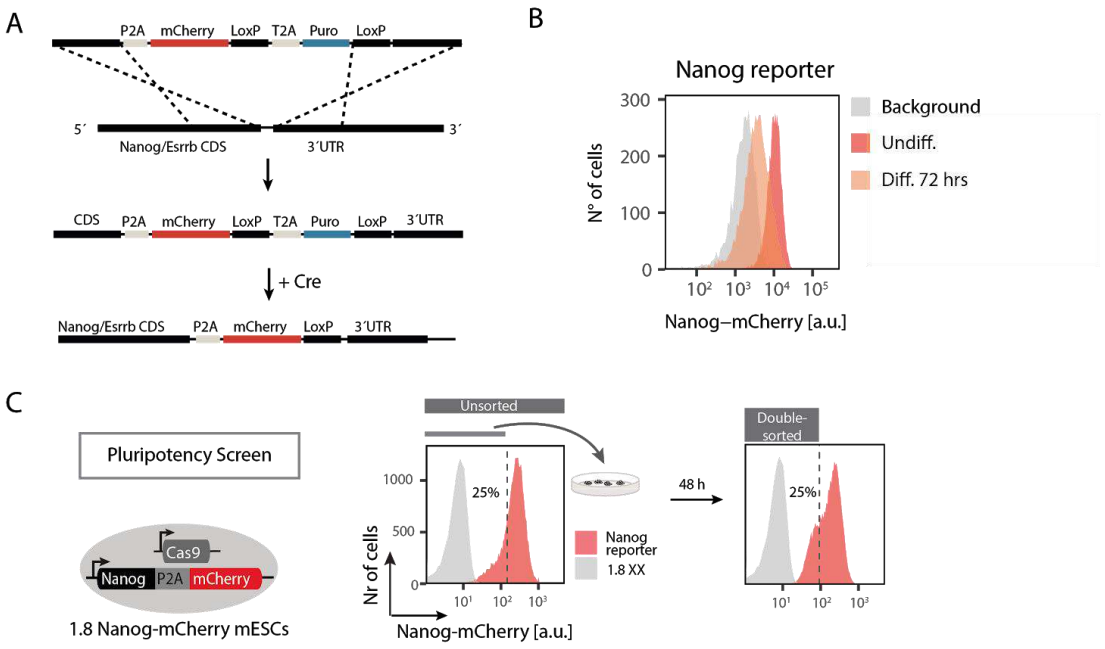

Figure 29. Secondary CRISPR knockout screen for the identification of genes modulating pluripotency factor expression in female mESCs. **(A)** Schematic representation of the generated Nanog and Esrrb fluorescent reporters. Briefly, the Nanog/Esrrb locus was C-terminally

tagged with mCherry via CRISPR/Cas9 mediated homologous recombination, where both proteins are linked to mCherry through a P2A self-cleaving peptide. The puromycin cassette was subsequently excised through transient CRE expression. **(B)** Flow cytometry measurement of mCherry levels in 1.8 Nanog-mCherry cells before and after 3 days of differentiation. **(C)** Workflow of the generated pluripotency screen for the identification of genes modulating pluripotency factor expression. 1.8 female wildtype mESCs or cells carrying mCherry-tagged Nanog locus that stably expressed the Cas9 endonuclease were transduced with the GeCKOxs sgRNA library, subsequently selected, and expanded. mCherry low cells were sorted via flow cytometry on day 7 after transduction, cultured for two days and sorted again. The screen was performed in two replicates.

Good library representation was maintained throughout all steps of the screens, what could be observed in the sgRNA cumulative distributions before and after sorting (Fig. 30A). Furthermore, non-targeting controls were neither enriched nor depleted (Fig. 30B).

MAPK regulators Ptpn2, Frs2, Erk2 and Grb2 were found among the most depleted genes in the pluripotency screen (Fig. 30C). Curiously, Ptpn2, a known negative regulator of the MAPK signaling pathway, scored as an anti-pluripotency factor (Mattila et al., 2005; van Vliet et al., 2005). Studies have shown, however, that this gene has an inhibitory effect on the Jak/STAT signaling pathway (Yamamoto et al., 2002), which is one of the main drivers of pluripotency in mouse embryonic stem cells (Niwa et al., 1998). Csk was again strongly enriched among the pluripotency-promoting factors, further confirming its role as a MAPK inhibitor (Fig. 30C). Additionally, Fbxw7 was also significantly enriched in the pluripotency screen, in accordance with the primary screen where it scored among the MAPK pathway inhibitors (Fig. 26).

Among the known pluripotency regulators included as controls in the GeCKOxs library, Tfcp2l1 together with Klf4 were enriched in the pluripotency screen, as expected (Fig. 30C). Nanog itself was also enriched (3.1 fold), albeit non-significantly (FDR=0.67). This could be due to the positive effect of Nanog on mESC proliferation and viability, which leads to a strong depletion of sgRNAs targeting this gene upon cell expansion and therefore highly variable sgRNA count number (Fig. 30D).

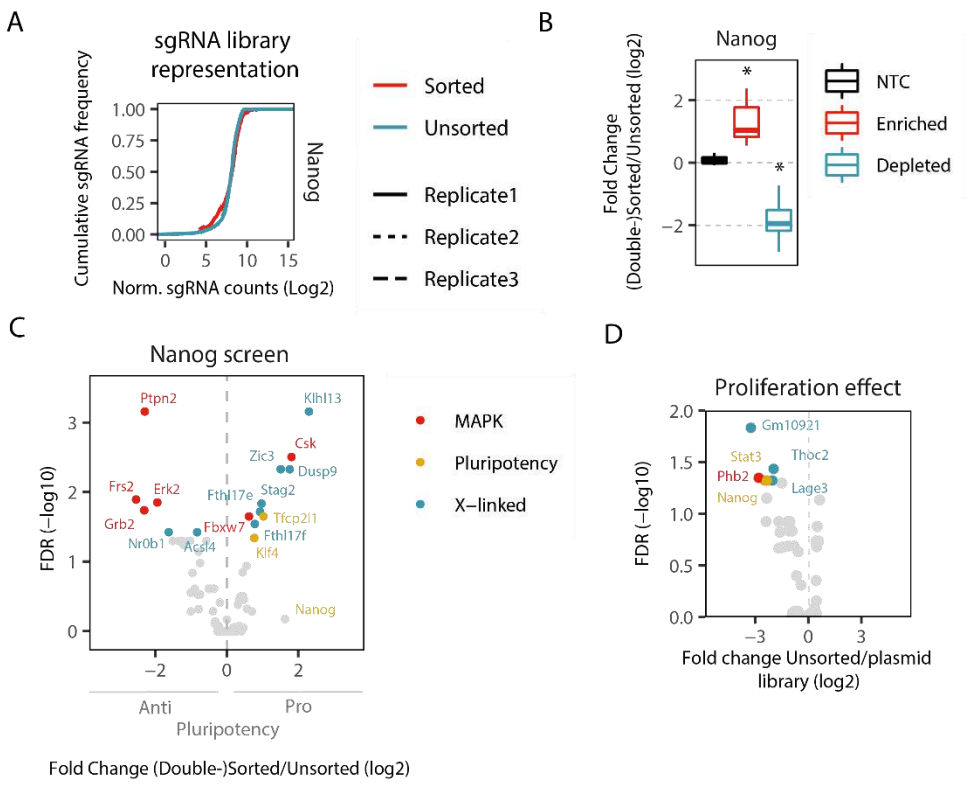

Figure 30. Identification of X-linked candidate genes from the primary screen that additionally modulate pluripotency factor expression in female mESCs via a secondary pooled CRISPR knockout screen. (A) sgRNA distribution of the sorted and unsorted fractions in all replicates of the pluripotency screen. **(B)** Mean fold change of the sorted vs the unsorted fractions of the 10 Non-targeting controls and the individual sgRNAs targeting significantly enriched and depleted genes in the pluripotency screen (FDR < 0.05, MAGeCK), * p < 0.05, Wilcoxon rank-

sum test. **(C)** Volcano plot displaying the most enriched and depleted (FDR < 0.05, MaGeCK) X-linked (blue), MAPK controls (red) and pluripotency controls (yellow) in the pluripotency screen. **(D)** Volcano plot displaying significantly enriched and depleted (FDR < 0.05, MAGeC) X-linked genes (blue), known MAPK regulators (red) and pluripotency factors (yellow) as positive controls in the unsorted fraction vs the cloned plasmid library in the pluripotency screen.

Two X-linked genes were found in the depleted fraction of the pluripotency screen: Nr0b1 and Ascl4 (Fig. 30C). Curiously, Nr0b1 has been linked to the maintenance of the pluripotency state in several studies, where its knockdown led to upregulation of differentiation specific markers (Khalfallah et al., 2009; Zhang et al., 2014). Interestingly, no significant change was documented regarding Nanog expression, with one report intriguingly showing an increase in pluripotency factors Tbx3 and Klf4 in Nr0b1 knockout ES cells (Fujii et al., 2015). Since all of these studies were carried out in male mESCs, it would be interesting to assess if the increase in Nanog upon Nr0b1 depletion observed in our results is a female specific phenotype.

A total of 6 X-linked genes were significantly enriched in the pluripotency screen: Klhl13, Zic3, Dusp9, Stag2, Fthl17e and Fthl17f (Fig. 30C). Interestingly, Klhl13 was the top hit in the pluripotency screen, pointing to the fact that this gene could play a bigger role in the modulation of pluripotency factor expression in female mESCs compared to the previous top X-linked hit Dusp9.

In summary, the pluripotency screen recovered several known MAPK and pluripotency regulator controls in the expected fractions, pointing to the validity of the screening approach. Among the X-linked genes, Klhl13 scored as the strongest positive regulator of pluripotency factor expression, posing as a novel and strong candidate underlying the sex differences observed in mESCs.

5.2.3 Secondary CRISPR knockout screen for the identification of genes that modulate differentiation kinetics in female mESCs

Female mESCs downregulate pluripotency factors significantly slower during differentiation compared to male cells (Schulz et al. 2014). In order to screen for X-linked modulators of differentiation kinetics in female mESCs among the candidates identified in the primary screen, the C-terminus of the locus coding for the pluripotency factor *Esrrb* was tagged with mCherry using the same strategy described above for the generation of the Nanog mCherry reporter (see section 5.2.2, Fig. 29A), which allowed us to assess pluripotency factor expression during differentiation on a single cell level. Esrrb was chosen as a reporter for this particular screen since it is downregulated significantly faster in male compared to female mESCs during differentiation (~6 fold lower in XO vs XX at day 3 of differentiation via LIF withdrawal) (Schulz et al., 2014).

Reporter functionality was assessed again by monitoring mCherry levels during differentiation, observing much like for the Nanog reporter, a significant downregulation of fluorescent intensity around day 3, which confirmed the functionality of the reporter in mirroring pluripotency factor levels during differentiation (Fig. 31A).

During the differentiation screen, cells stably expressing the Cas9 nuclease and the GeCKOxs library were expanded until day five and differentiated via LIF withdrawal from Serum/LIF conditions for three days, after which the low mCherry fluorescent cells were FACS sorted (Fig. 31B). Here, our goal was to determine which genes led to faster differentiation kinetics, and therefore lower Esrrb levels at day 3 of differentiation, upon knockout. Since a transient phenotype was analyzed in this screen, only a single sorting step was possible. Three replicates were generated.

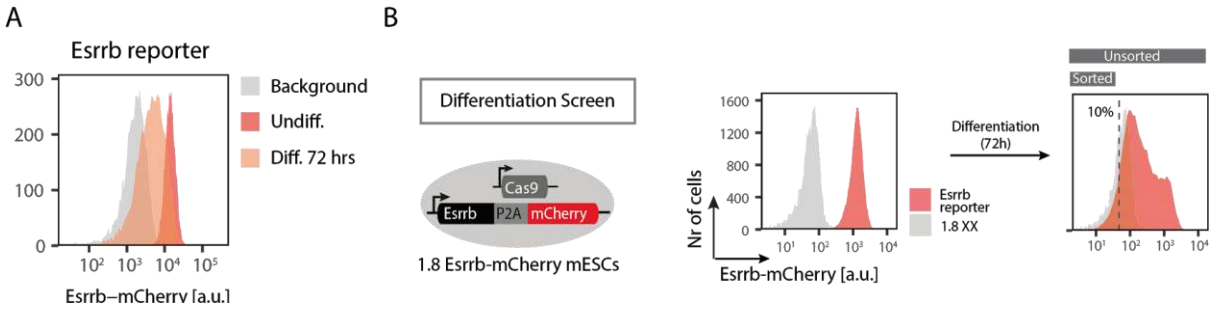

Figure 31. Secondary CRISPR knockout screen for the identification of genes modulating differentiation kinetics in female mESCs. (A) Flow cytometry measurement of mCherry levels in 1.8 Esrrb-mCherry cells before and after 3 days of differentiation. **(B)** Workflow of the generated differentiation screen for the identification of genes modulating differentiation kinetics. 1.8 female wildtype mESCs or cells carrying mCherry-tagged Esrrb locus that stably expressed the Cas9 endonuclease were transduced with the GeCKOxs sgRNA library and subsequently selected and expanded. Cells were differentiated on day 5 after transduction for 3 days and then the 10% of cells with the lowest mCherry fluorescence were FACS sorted. The screen was performed in three replicates.

Here again, good library representation was maintained throughout all steps of the screens and non-targeting controls were neither enriched nor depleted (Fig. 32A-B).

MAPK regulators Erk2, Flcn, Frs2, Grb2, Ptpn11 and Ptpn2 were found among the most depleted genes in the pluripotency screen (Fig. 32C). Surprisingly, Flcn, a gene that was found among the MAPK inhibitors in the primary screen, was identified in the differentiation screen as a strong pro-differentiation factor (Fig. 32C). This is however in accordance with previous reports that describe its central role in early differentiation (Betschinger et al., 2013). The mechanism through which a putative MAPK inhibitor might induce differentiation is nevertheless worthy of further investigation. Csk scored as an anti-differentiation factor, which is in accordance with its role as a MAPK inhibitor (Fig. 32C).

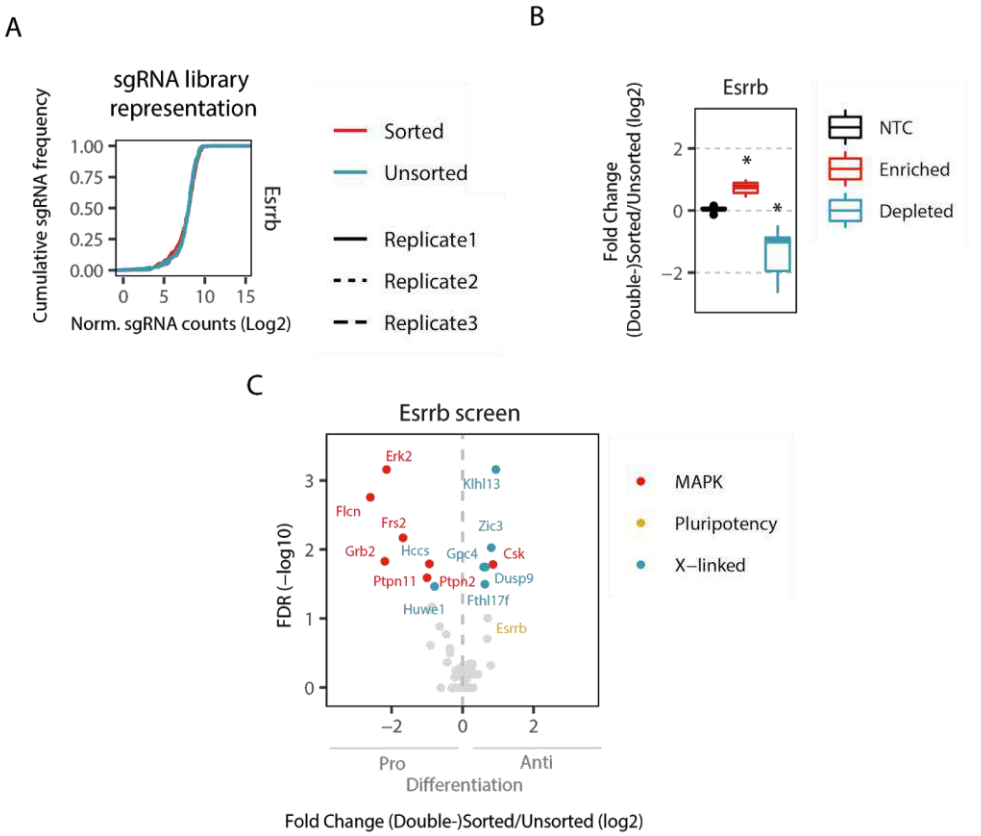

Figure 32. Identification of X-linked candidate genes from the primary screen that additionally modulate differentiation kinetics in female mESCs via a secondary pooled CRISPR knockout screen. (A) sgRNA distribution of the sorted and unsorted fractions in all replicates of the differentiation screen. **(B)** Mean fold change of the sorted vs the unsorted fractions of the 10 Non-targeting controls and the individual sgRNAs targeting significantly enriched and depleted genes in the differentiation screen (FDR < 0.05, MAGeCK), * p < 0.05, Wilcoxon rank-sum test. **(C)** Volcano plot displaying the most enriched and depleted (FDR < 0.05, MaGeCK) X-linked (blue), MAPK controls (red) and pluripotency controls (yellow) in the differentiation screen.

Surprisingly, none of the pluripotency regulators were significantly enriched in the differentiation screen. Esrrb itself was enriched (1.6 fold), albeit non-significantly (FDR=0.2) (Fig. 32C).

Two X-linked genes were found in the depleted fraction of the differentiation screen: Hccs and Huwe1 (Fig. 32C). In contrast, five X-linked genes including Klhl13, Zic3, Gpc4, Dusp9 and Fthl17f were found to be enriched (Fig. 32C). Similar to the pluripotency screen, both Klhl13 and Zic3 scored higher than Dusp9 in the differentiation screen, meaning that both genes could have a stronger effect on differentiation kinetics of female mESCs.

In conclusion, several known MAPK activators were depleted in the differentiation screen, which is expected given the fact that the MAPK pathway is necessary for lineage commitment and differentiation. Concerning the screened X-linked genes, Klhl13 scored again as the top candidate modulating differentiation kinetics in female mESCs, followed by Zic3.

5.2.4 Secondary CRISPR knockout screen for the identification of genes that modulate phosphorylation of MAPK components in female mESCs

Female mESCs display higher levels of Mek phosphorylation compared to their male counterparts, even though they express lower levels of MAPK targets. Increased pMek levels, however, are due to a reduced negative feedback activity of the pathway caused by the lower expression levels of feedback regulators (Fritsche-Guenther et al., 2011; Sturm et al., 2010).

In order to find out whether the X-linked genes targeted in the GeCKOxs library had an effect on the phosphorylation of MAPK pathway components, we implemented an intracellular staining as a reporter strategy by using a pMek-specific primary antibody and a secondary Alexa647-coupled antibody to determine the genes that lead to lower pMek levels, reflecting the XO pluripotency phenotype. Functionality of the pMek readout was assessed through the staining of XX, XO and XO cells treated with a Mek inhibitor (Fig. 33A). The highest pMek levels were observed as expected in the XO Meki treated cells due to inhibition of negative feedback regulation. Differences were also observed between the XO and XX cells, the latter exhibiting higher fluorescence intensities and mirroring thus the changes previously observed via Immunoblotting (Fig. 33A).

During the pMek screen, cells stably expressing the Cas9 endonuclease and the GeCKOxs library were harvested on day 7 after sgRNA library transduction, stained and the low pMek population enriched. This way, we expected to find genes that, when knocked out, would lead to a decrease in Mek phosphorylation, mirroring thus the XO phenotype. A single sorting step was possible also during this screen due to the fixation of cells as a requirement for the intracellular staining (Fig. 33B). Three replicates were carried out.

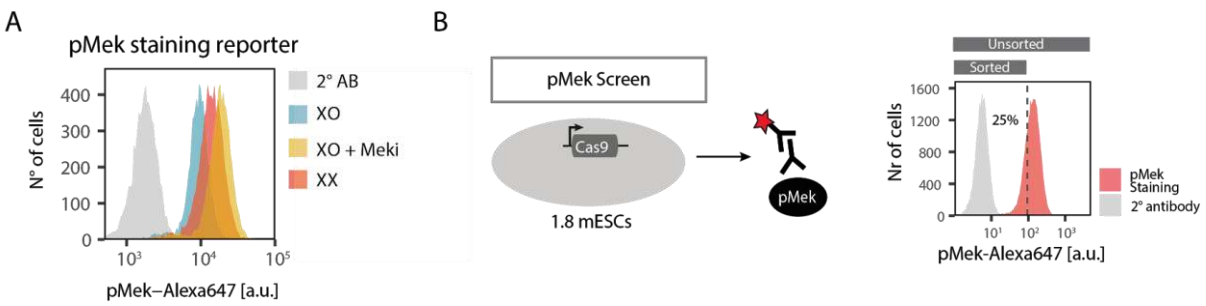

Figure 33. Secondary CRISPR knockout screen for the identification of genes modulating Mek phosphorylation in female mESCs. (A) Intracellular pMek staining of 1.8 XX (red), XO (blue) and XO cells treated with the Mek inhibitor (Meki, yellow) PD0325901 for 48h. **(B)** Workflow of the pMek screen for the identification of genes modulating Mek phosphorylation. 1.8 female wildtype mESCs that stably expressed the Cas9 endonuclease were transduced with the GeCKOxs sgRNA library, subsequently selected, and expanded. Cells were stained with an anti-pMek antibody coupled to an Alexa647 fluorophore on day 7 after transduction and the 25% of cells with the lowest signal were sorted. The screen was performed in three replicates.

Good library representation was maintained throughout all steps of the screens (Fig. 34A). Non-targeting controls, however, were slightly but significantly depleted (Fig. 34B).

Erk2 and Ptpn2 were significantly depleted in the pMek screen (Fig. 34C). These two genes were also depleted in the pluripotency, differentiation and SRE-Elk screen. Erk2 is a strong feedback regulator of the MAPK signaling pathway, which acts upstream of Raf by phosphorylating inhibitory sites (Fritsche-Guenther et al., 2011; Sturm et al., 2010). This could therefore be a reason why Erk2 is found consistently depleted in all screens. No MAPK regulators were enriched in the pMek screen.

Pluripotency regulators Stat3, Esrrb and Tfcp2l1 were found enriched in the pMek screen (Fig. 34C). Numerous studies have shown an effect of the MAPK signaling pathway on pluripotency factor expression and stability (Dhaliwal et al., 2018; Kim et al., 2014b; Silva et al., 2009; Yeo et al., 2014), interestingly, the opposite effect has also been observed for a few pluripotency factors, albeit not for Esrrb or Tfcp2l1 (Azami et al., 2018; Grabole et al., 2013; Mzoughi et al., 2017). We speculate that this phenomenon could be in part due to crosstalk between the Jak/STAT and MAPK signaling pathways (Cacalano et al., 2001), or to transcriptional regulation of MAPK feedback regulators or pathway components by pluripotency factors (Azami et al., 2018; Grabole et al., 2013).

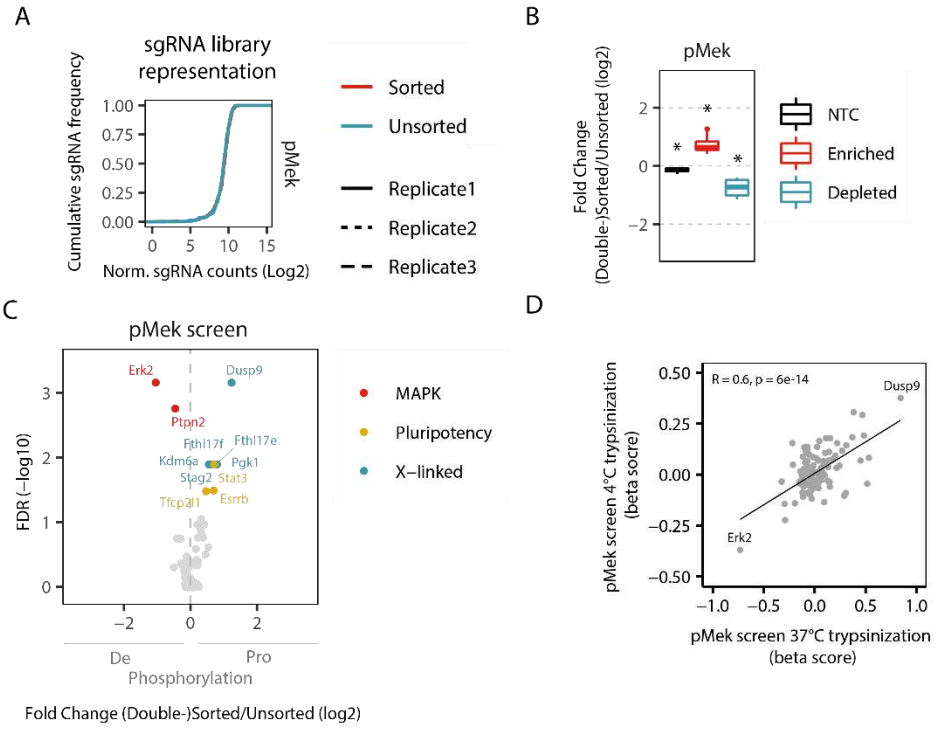

Figure 34. Identification of X-linked candidate genes from the primary screen that additionally modulate Mek phosphorylation in female mESCs via a secondary pooled CRISPR knockout screen. (A) sgRNA distribution of the sorted and unsorted fractions in all replicates of the differentiation screen. **(B)** Mean fold change of the sorted vs the unsorted fractions of the 10 Non-targeting controls and the individual sgRNAs targeting significantly enriched and depleted genes in the differentiation screen (FDR < 0.05, MAGeCK), * p < 0.05, Wilcoxon rank-sum test. **(C)** Volcano plot displaying the most enriched and depleted (FDR < 0.05, MaGeCK) X-linked (blue), MAPK controls (red) and pluripotency controls (yellow) in the differentiation screen. **(D)** Comparison of beta scores generated by using the MaGeCK_mle tool between the secondary pMek screen and one replicate of a pMek screen where trypsinization and fixation was performed at 4°C. The Pearson correlation coefficient (R) and p-value (p) are indicated. Each dot represents a gene.

The trypsinization of cells during harvesting for immunoblotting or intracellular staining has been shown to alter phospho-protein levels. Since the pMek screen was carried out using traditional trypsinization conditions (5 min incubation at 37°C), we assessed whether a more controlled trypsinization and fixation on ice at 4°C previous to the intracellular pMek staining would drastically change the results obtained during this secondary screen. An additional screen was therefore performed similarly to the previously described pMek screen except for the cell harvesting steps and the first steps of the intracellular staining, which were all carried out at 4°C on ice. Only one replicate was generated. We observed that both Dusp9 as well as Erk2 scored similarly under the two different trypsinization conditions, furthermore, a positive correlation of 0.6 was determined between the two screens, confirming the generated results (Fig. 34D).

Dusp9 was the strongest enriched X-linked gene in the pMek screen, followed by Pgk1, Fthl17e, Fthl17f, Kdm6a and Stag2 (Fig. 34C). Knockout of Kdm6a and Pgk1 was found to lead to higher phosphorylation levels as observed in XX cells, even though they were identified as MAPK activators in the primary screen.

Overall, Dusp9 was the only candidate gene that scored significantly in all four generated screens (including the primary SRE-Elk screen) (Fig. 35A). Additionally, from the X-linked MAPK inhibitors identified in the primary screen, Klhl13, Zic3, two genes of the Fthl17 cluster (Fthl17e and Fthl17f) and Stag2 were enriched in at least two screens (Fig. 35A). Surprisingly, Klhl13 was the strongest hit in both the pluripotency as well as the differentiation screen and Zic3 was the second strongest hit in the differentiation screen, indicating that these genes could have a more pronounced effect on the modulation of pluripotency factor expression and differentiation kinetics (Fig. 35A-B).

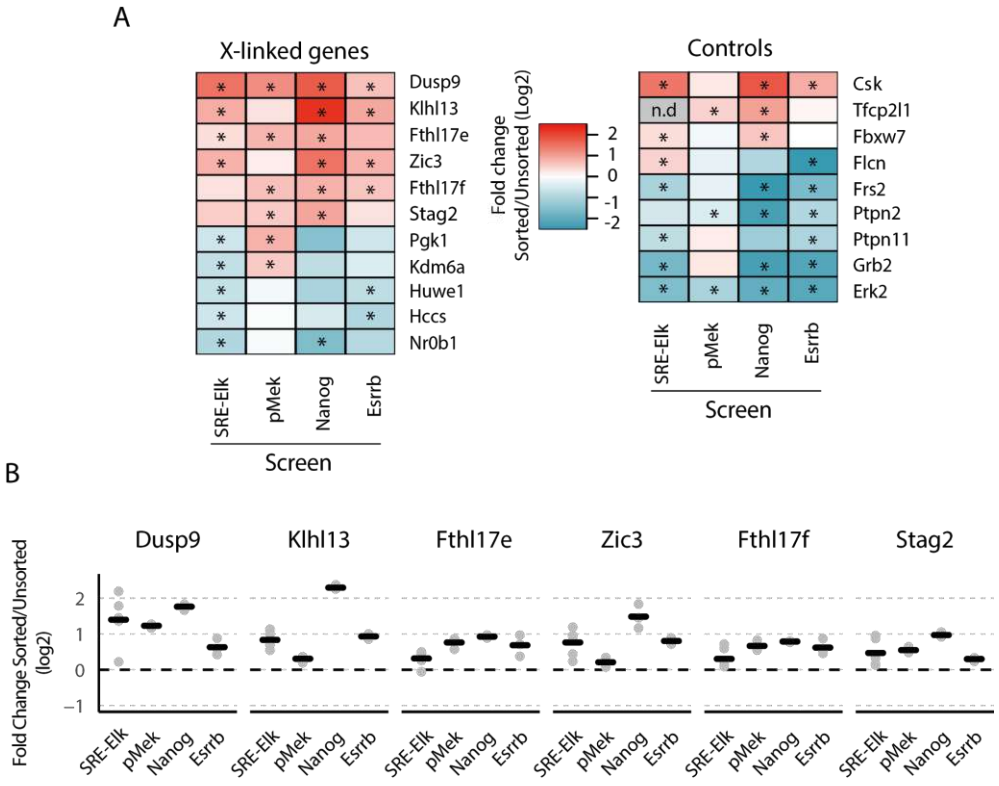

Figure 35. Identification of candidate genes mediating sex differences in mESCs via pooled CRISPR screens (A) Heatmap showing the enrichment in both the primary (SRE-Elk) and secondary CRISPR screens (pMek, Nanog, Esrrb) of significantly enriched or depleted genes in at least two screens. *FDR < 0.05 (MAGeCK), n.d non-determined. **(B)** Enrichment of individual sgRNAs targeting putative candidate genes mediating the female pluripotency phenotype in the primary and secondary screens.

5.2.5 Expression levels of candidate hits in XX and XO mESCs

A prerequisite for a candidate gene to mediate the sex differences observed in mESCs is that it should be expressed in a double dosage in female cells. In order to corroborate this, we analyzed RNA-seq data from the 1.8 XX cell line used in the screen and a generated XO subclone (Harvesting of cell material and library preparation was done by Zeba Sultana and Ilona Dunkel, whereas read mapping was carried out by Edda G. Schulz). Even though female cells expressed X-linked genes with an expected 2-fold difference (Fig. 36A), Zic3 and Stag2 were expressed at similar levels between XX and XO cells (Fig. 36B). Dusp9 and Klhl13 were expressed at 4.2- and 3.2-fold higher levels in female cells, whereas genes belonging to the Fthl17 cluster, which is maternally imprinted and therefore only expressed in females (Kobayashi et al., 2010), were essentially not expressed in the XO subclone (where the remaining X is probably maternally inherited).

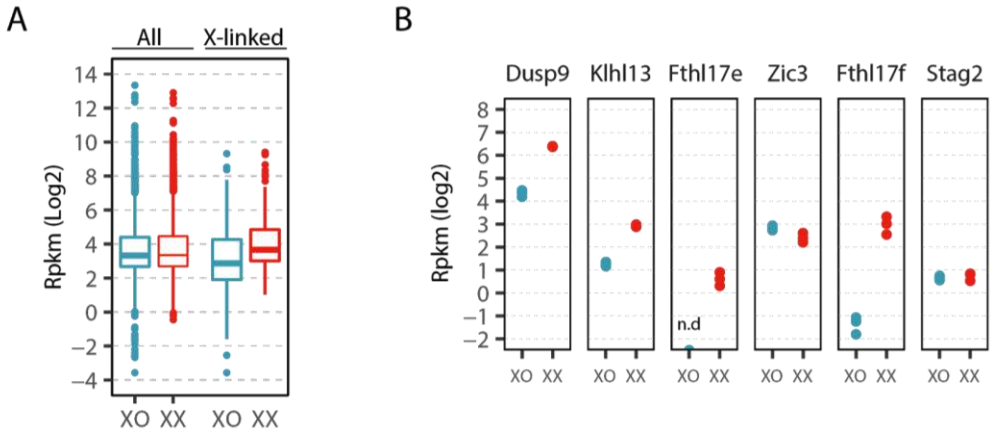

Figure 36. Expression levels of candidate hits in 1.8 XX and XO mESCs (A) Boxplot showing expression levels of all genes and only X-linked genes in 1.8 XX and 1.8 XO mESCs. **(B)** Expression level of X-linked genes enriched in at least two of the generated screens in 1.8 XX and XO mESCs assessed by RNA-seq, n.d. non-determined.

We have therefore determined four genes that could mediate the female pluripotency phenotype through the implementation of a series of pooled CRISPR screens: Dusp9, Klhl13, Fthl17e and Fthl17f. Dusp9, like previously mentioned, is an Erk phosphatase and known MAPK inhibitor (Caunt and Keyse, 2013). Previous publications have studied the role of Dusp9 in mediating sex differences in DNA methylation in mESCs (Choi et al., 2017), however, some have reported no changes in pluripotency factor expression and differentiation kinetics in heterozygous female mutants (Song et al., 2019). A further and deeper assessment of the role of Dusp9 in mediating the female pluripotency phenotype is therefore necessary. The remaining genes, on the other hand, have not been linked to the modulation of pluripotency in female mESCs and represent novel putative candidates. Klhl13 is a substrate adaptor protein for the E3 ubiquitin-protein ligase complex (Sumara et al., 2007), whereas the Fthl17 genes represent ferritin-like proteins with unknown functions that are partially nuclear and lack ferroxidase activity (Ruzzenenti et al., 2015).

In conclusion, we have identified several candidates that could mediate sex differences in mESCs. From these, we have decided to validate Dusp9 and Klhl13 as the top two scoring genes across all of the generated screens. Our screen results suggest that Dusp9 could have a stronger effect on the MAPK signaling pathway, as it represents the top X-linked hit in the SRE-Elk and pMek screens. Klhl13, on the other hand, could have a stronger effect on pluripotency factor expression and differentiation kinetics, being the strongest enriched gene in both the pluripotency as well as the differentiation screen. In order for a gene to underlie the sex differences observed in mESCs, its overexpression in male cells should lead to a female-like pluripotency phenotype, while the opposite should happen through their heterozygous deletion in female mESCs.

5.3. Klhl13 and Dusp9 overexpression in male mESCs leads to a shift towards the naive pluripotency state and slower differentiation kinetics in male mESCs

The ability of the Cas9 protein to bind specific DNA loci guided by an RNA molecule has been exploited for the modulation of gene expression levels. A mutated and nuclease-deficient Cas9 (dCas9) can be coupled to activator domains in order to increase gene expression, a technique termed as CRISPRa (activation).

Improved systems for CRISPR activation have been developed which allow for stronger overexpression efficiencies, among these we find the CRISPRa SuperNova tagging system (SunTag, Fig. 37A) (Heurtier et al., 2019; Tanenbaum et al., 2014). This system is based on antibody-antigen interactions to obtain an amplification of the activation signal. Here, a doxycycline-inducible dCas9 is fused with ten repeats of an epitope of the yeast GCN4 protein, while a second tet promoter drives the expression of a single-chain variable fragment (scFv) anti-GCN4 antibody fused with four repeats of the VP16 transcriptional activation domain, termed VP64. Under doxycycline treatment, the GCN4 epitope will be bound by multiple copies of the VP64 coupled anti-GCN4 antibody, leading to stronger transcriptional activation.

The advantages of the use of CRISPR activation systems are numerous. First, once the cell line expressing the SunTag system is established in the lab, the process of sgRNA design and cloning together with the cell line generation is fairly rapid. Moreover, it gives the possibility to overexpress a gene in its endogenous form within more physiological levels, as opposed to cDNA overexpression systems where expression levels can be significantly higher.

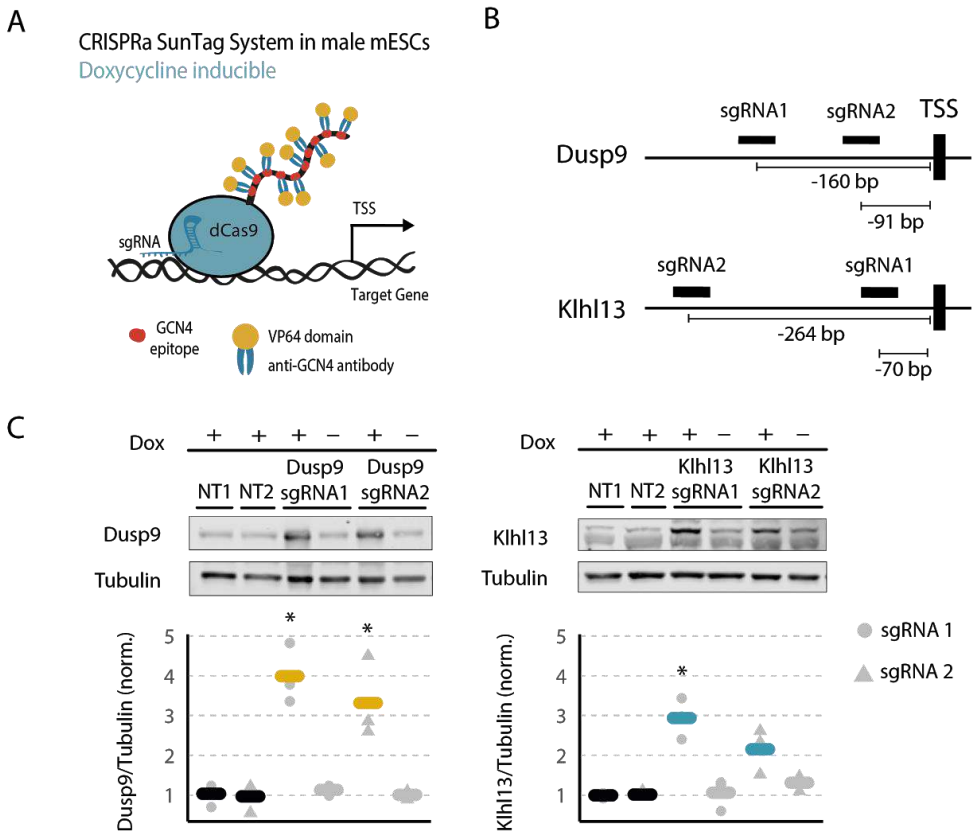

Figure 37. Dusp9 and Klhl13 overexpression in male mESCs using the CRISPRa SunTag system. (A) Schematic representation of the SunTag CRISPR system used for gene activation in male mESCs. **(B)** Position of the sgRNA sequences used to over-express Dusp9 and Klhl13. SgRNAs for Dusp9 were targeted -91 (chrX:73,639,328-73,639,346, GRCm38/mm10 Assembly) and -160bp (chrX: 73,639,259-73,639,277) bp, whereas for Klhl13 they were targeted -264 (chrX:23,365,328-23,365,347) and -70bp (chrX:23,365,134-23,365,152) bp upstream of the

transcriptional start site (TSS). **(C)** For overexpression of endogenous Dusp9 (yellow) or Klhl13 (blue), male E14 mESCs stably expressing the doxycycline-inducible SunTag System were transduced with one of two different sgRNAs tageting either the Dusp9 or Klhl13 promoter regions, or one of two non-targeting control sgRNAs (NTs). mESCs were treated for 3 days with 1 µg/ml of doxycycline before cell harvesting. Dusp9 (left) and Klhl13 (right) protein levels were quantified via Immunoblotting. Immunoblot signals were normalized to Tubulin and to the mean of the signals from cells transduced with the two NT control sgRNAs. Dots and triangles represent the two different sgRNAs and thick bars display the mean of three biological replicates. * $p < 0.05$ in a two-tailed paired Student´s T-test comparing the Dusp9/Klhl13 over-expressing samples and the mean of the two NT controls.

In order to over-express Dusp9 and Klhl13 in male mESCs, we made use of an E14 cell line carrying the components of the aforementioned CRISPRa SunTag system (E14-STN) (Heurtier et al., 2019; Tanenbaum et al., 2014) (Fig. 37A). The experimental part of the section 5.3 was performed by the master student Anna A. Monaco, who was supervised by O. Genolet.

E14-STN cells were transduced with one of two distinct sgRNAs targeting the promoter of either Dusp9 or Klhl13 (Fig. 37B). Two cell lines stably expressing different non-targeting sgRNAs (NTCs) were additionally used as controls. For Dusp9, overexpression levels of 4 and 3.3-fold were reached, which were quantified via Immunoblotting, whereas for Klhl13 they were 2.9- and 2.1-fold higher compared to the NTCs (Fig. 37C). We next assessed the phenotypes affected by sex differences in mESCs: MAPK pathway levels, pluripotency factor expression, differentiation kinetics and finally global CpG methylation. Results for all phenotypes are summarized in the end of the section in Fig. 40.

5.3.1 Overexpression of Dusp9 and to a lesser extent Klhl13 reduces levels of MAPK signaling activity in male mESCs

Female mESCs express lower levels of MAPK target genes compared to male cells (Schulz et al. 2014). If indeed Dusp9 and Klhl13 represent modulators of sex differences in mESCs, we would expect a reduction of MAPK targets upon overexpression of either of these genes in male mESCs. In order to test this, we first measured expression levels of two well-known MAPK target genes via qPCR: Egr1 and Spry4 (Casci et al., 1999; Hodge et al., 1998). Here, both genes were strongly downregulated upon Dusp9 overexpression (5.5/2.7-fold for Egr1/Spry4) to levels comparable to those of XX cells, which express approx. 2 to 10-fold lower levels of these two target genes (Fig. 38A). When overexpressing Klhl13, the reduction in expression levels observed for MAPK targets was much smaller (1.4/1.3-fold for Egr1/Spry4) and only significant for one of the Klhl13-targeting sgRNAs with respect to Spry4 levels (Fig. 38A).

We next assessed pMek and pErk levels in Dusp9/Klhl13 overexpressing cells via Immunoblotting, observing striking differences for both upon Dusp9 overexpression (22-fold increase in pMek and 12-fold decrease in pErk levels) (Fig. 38B). No differences were observed for Klhl13 overexpression, what is also in accordance with the generated pMek screen (Fig. 34C). Curiously, a previous study reported an increase in pErk upon Dusp9 overexpression. Since we observe striking differences in pErk levels depending on the cell harvesting technique used for subsequent Immunoblotting, we hypothesize that these discrepancies might be due to the requirement of trypsinization when analysing feeder-dependent cell lines (Choi et al., 2017). Indeed, when Dusp9 overexpressing cells are subjected to trypsinization previous to cell lysis, we observe a striking increase in pErk levels compared to cells that were lysed through direct addition of cell lysis buffer to the culture plate (Fig. 38C).

In summary, we confirm the role of Dusp9 as an Erk phosphatase and strong MAPK inhibitor affecting both target genes as well as phosphorylation levels of pathway intermediates. Klhl13, on the other hand, seems to slightly affect MAPK target genes but no differences could be observed in pMek/pErk levels, in accordance to a previously performed screen.

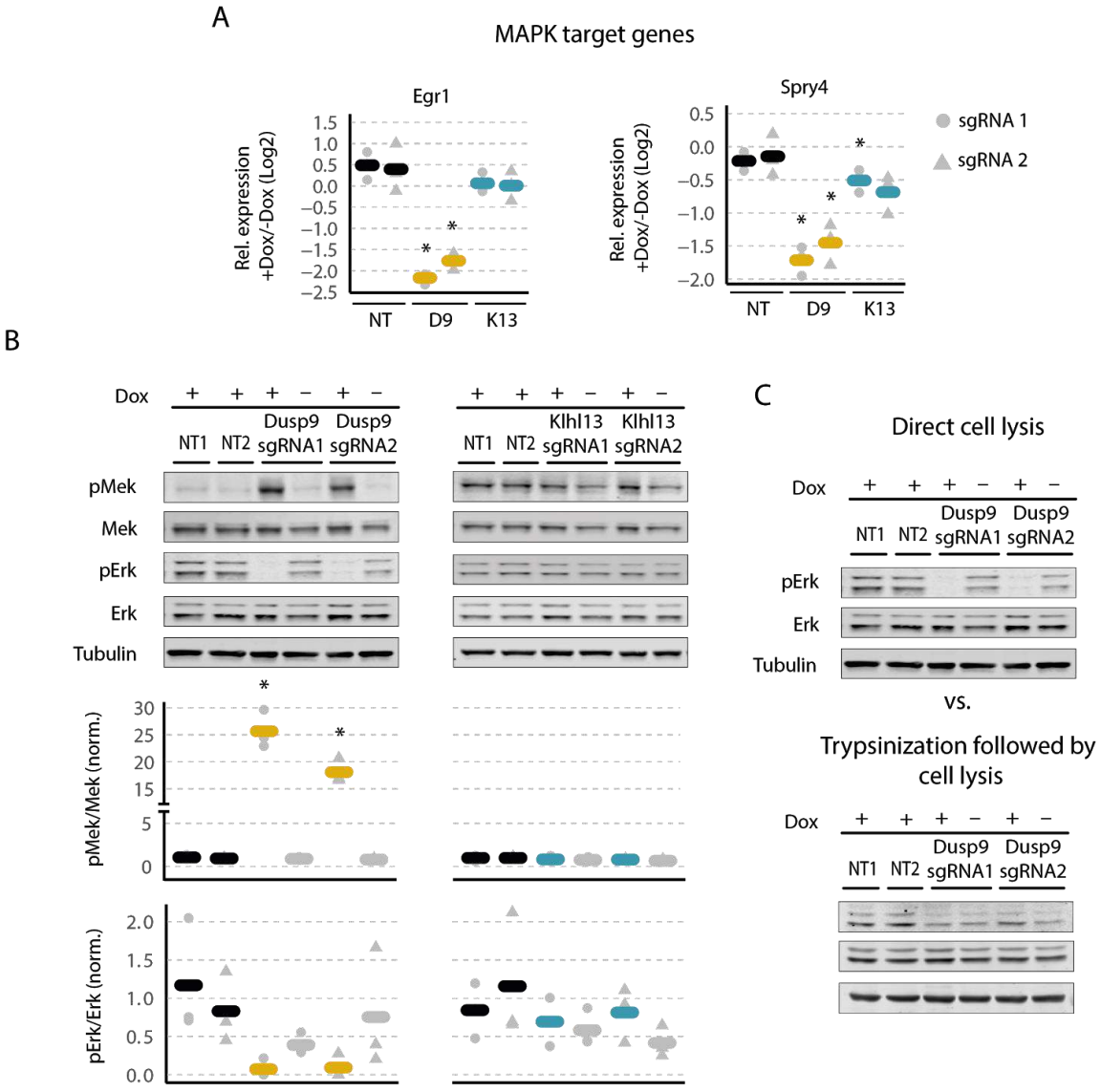

Figure 38. Overexpression of Dusp9 and to a lesser extent Klhl13 leads to inhibition of the MAPK signaling pathway in male mESCs. (A-B) For overexpression of endogenous Dusp9 (yellow) or Klhl13 (blue), male E14 mESCs stably expressing the doxycycline-inducible SunTag System were transduced with one of two different sgRNAs tageting either the Dusp9 or Klhl13 promoter regions, or one of two non-targeting control sgRNAs (NTs). mESCs were treated for 3 days with 1 µg/ml of doxycycline before cell harvesting. MAPK target gene expression was assessed via qPCR (A) and Mek and Erk phosphorylation levels were again quantified via immunoblotting (B). Immunoblot signals were normalized to total Mek/Erk levels and to the mean of the signals from cells transduced with the two NT control sgRNAs. qPCR values were normalized to two housekeeping genes and to their respective non-treated controls (-Dox). Dots and triangles represent the two different sgRNAs and thick bars display the mean of three biological replicates. * $p < 0.05$ in a two-tailed paired Student´s T-test comparing the Dusp9/Klhl13 over-expressing samples and the mean of the two NT controls. **(C)** Immunoblotting of pErk levels in male mESCs overexpressing Dusp9 protein harvested either through direct cell lysis (top) or trypsinization followed by cell pelleting and subsequent cell lysis (bottom).

5.3.2 Overexpression of Dusp9 and to a lesser extent Klhl13 increases expression of pluripotency factors and blocks differentiation in male mESCs

Female mESCs express higher levels of pluripotency factors and display slower differentiation kinetics compared to male cells, being found thus in a more naive state of pluripotency (Schulz et al. 2014). If indeed a double dosage of Dusp9 or Klhl13 leads to a shift towards the naive state of pluripotency in female mESCs, we would expect an increase in pluripotency factor levels upon overexpression of either of these genes in male mESCs. Additionally, these cells would display slower differentiation kinetics or fail to downregulate pluripotency factors altogether during differentiation.

We therefore assessed the expression of pluripotency factors Nanog and Prdm14 before, and additionally of Esrrb during differentiation via qPCR. We observed a significant increase of Nanog (1.7-1.5-fold) and Prdm14 (3-2.3-fold) levels in Dusp9 overexpressing cells in the undifferentiated state (Fig. 39A). These differences are comparable to those observed between XO and XX cells, the later expressing 2-4 fold higher levels of the two target genes (Choi et al., 2017; Schulz et al., 2014; Song et al., 2019). Cells overexpressing Klhl13, on the other hand, showed a slight increase in Prdm14 expression (1.6-fold) only in the cell line achieving higher Klhl13 overexpression levels (Fig. 39A). These differences were also observed during differentiation via LIF withdrawal from Serum/LIF conditions, where down-regulation of pluripotency factors across the measured timepoints was stalled in both Dusp9 overexpressing cell lines. A significant delay in developmental progression was, however, also observed in cells that overexpressed Klhl13 to higher levels (Fig. 39B). Overall, it seems that cells expressing higher levels of Dusp9 are found in a more naive state of pluripotency, whereas in the case of Klhl13 over-expressing cells, only a small shift towards the naive state could be detected.

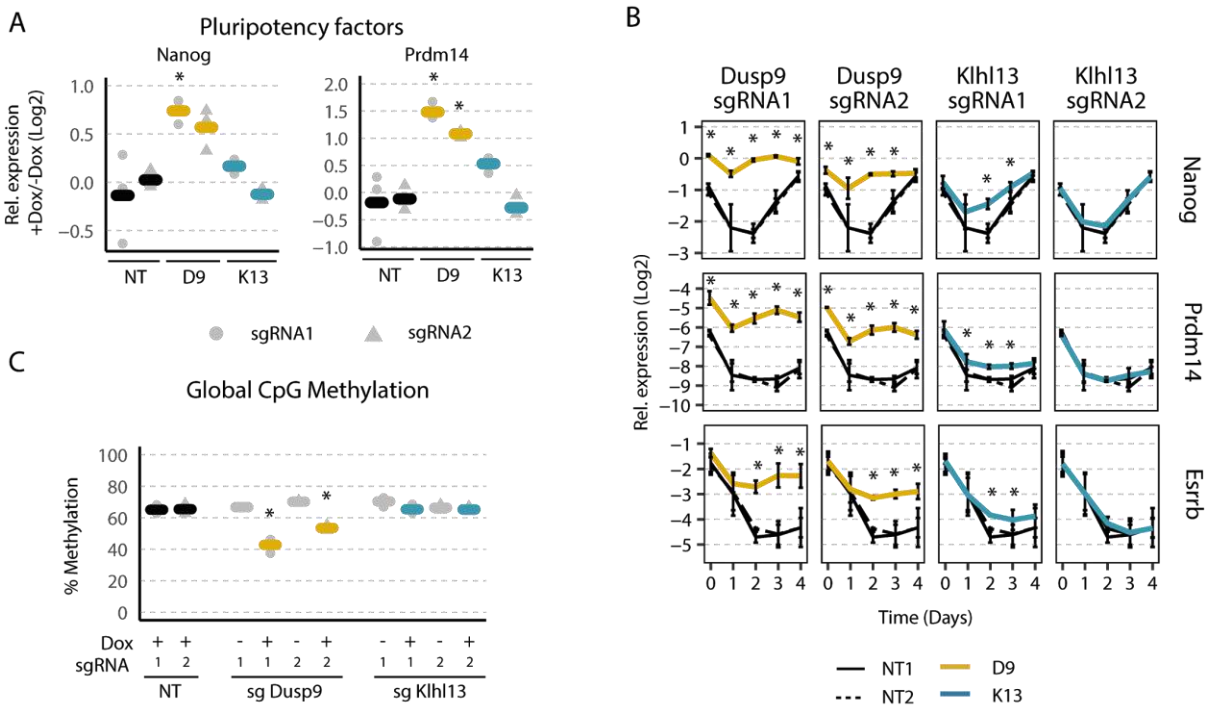

Figure 39. Overexpression of Dusp9 and to a lesser extent Klhl13 leads to a shift towards the naive pluripotency state and slower differentiation kinetics in male mESCs. (A-C) For overexpression of endogenous Dusp9 (yellow) or Klhl13 (blue), male E14 mESCs stably expressing the doxycycline-inducible SunTag System were transduced with one of two different sgRNAs tageting either the Dusp9 or Klhl13 promoter regions, or one of two non-targeting control sgRNAs (NTs). (A) mESCs were treated for 3 days with 1 µg/ml of doxycycline before cell harvesting and pluripotency target gene expression was assessed via qPCR. Values were normalized to two housekeeping genes and to their respective non-treated controls (-Dox). Dots and triangles represent the two different sgRNAs and thick bars display the mean of three biological replicates. (B) E14 SunTag mESCs were treated with 1 µg/ml doxycycline 24h previous to differentiation via LIF withdrawal from Serum/LIF conditions for Dusp9 or Klhl13 overexpression. Pluripotency factor expression was assessed during 4 days of differentiation via qPCR at different timepoints as indicated. Mean and standard deviation across three biological replicates is shown. (C) E14 SunTag mESCs were treated with 1 µg/ml doxycycline for three passages and global CpG methylation was assessed via pyrosequencing-based luminometric DNA methylation assay (LUMA). Dots and triangles represent the two different sgRNAs and thick bars display the mean of three biological replicates. * $p < 0.05$ in a two-tailed paired Student´s T-test comparing the Dusp9/Klhl13 over-expressing samples and the mean of the two NT controls.

Lastly, we monitored global CpG DNA methylation levels in cells overexpressing either Dusp9 or Klhl13. Here, cells were treated with doxycycline for 3 passages, since a decrease in CpG methylation levels upon Dusp9 overexpression has been shown to be caused by passive demethylation mechanisms (Choi et al., 2017). We observed a decrease in global CpG methylation from 60% in the NTCs to 53-42% in Dusp9 overexpressing cells, confirming previous studies (Choi et al., 2017) (Fig. 39C). These cell lines, however, did not seem to reach the

levels detected in female cells (20-30%, (Choi et al., 2017; Habibi et al., 2013; Zvetkova et al., 2005)), which could be due to other X-linked genes being necessary to attain the full methylation phenotype. Additionally, Dusp9 overexpression over more passages might lead to even lower global DNA methylation levels. Klhl13 overexpression, on the other hand, did not seem to have an effect on the assessed phenotype.

Phenotype	Dusp9 OE sgRNA1/ NT	Dusp9 OE sgRNA2/ NT	Klhl13 OE sgRNA1/ NT	Klhl13 OE sgRNA2/ NT	XX / XO (XY)
Gene overexpression levels	4 fold ↑	3.3 fold ↑	2.9 fold ↑	2.1 fold ↑	4.2/3.2 fold (Dusp9/Klhl13) ↑
MAPK target expression (Egr1/Spry4)	6.3/2.9 fold ↓	4.7/2.4 fold ↓	1.3/1.3 fold ↓	1.4/1.4 fold ↓	2 to 10 fold ↓
pMek levels	25 fold ↑	18 fold ↑	0.8 fold ↑	0.8 fold ↑	4 to 8 fold* ↑
pErk levels	13.7 fold ↓	10.7 fold ↓	1.4 fold ↓	1.2 fold ↓	2 fold* ↑
Pluripotency factor expression (Nanog/Prdm14)	1.7 /3.7 fold ↑	1.5/2.3 fold ↑	1.1/1.5 fold ↑	0.9/0.9 fold ↑	2 to 4 fold* ↑
Global CpG Methylation	42%	53%	65%	65%	30%/65%

Figure 40. Table summarizing the effects of Dusp9 and Klhl13 overexpression in E14-STN male mESCs. Gene overexpression levels, MAPK target gene expression, pMek and pErk levels, pluripotency factor expression and global CpG methylation levels in E14-STN cell lines overexpressing either Dusp9 or Klhl13 by using one of two different sgRNAs (sgRNA1/2) targeting the TSS of each gene and the Sun-Tag CRISPRa system, compared to two non-targeting controls (NT). Additionally, differences observed between XX and XO (or XY cells) are given as reference. Arrows indicate whether levels are higher or lower than the reference (NTs for Dusp9/Klhl13 overexpression or XO/XY cells for XX wildtype cells). * values taken from Schulz et al., 2014.

In summary, we observe a strong shift for cells overexpressing Dusp9 and a milder one for cells overexpressing Klhl13 towards a female-like pluripotency state (Fig. 40). The fact that smaller differences are observed in the case of Klhl13 could be attributed to the fact that lower overexpression levels were reached in these cells. This is of great importance in the performed experiments, which seem strongly dose dependent. Furthermore, unlike Dusp9, Klhl13 mediates its function as part of a complex, which might lead to its stoichiometric imbalance upon overexpression of only one of its members, leading to less pronounced overexpression phenotypes. The fact that small but significant effects are nevertheless observed upon Klhl13 overexpression with the stronger sgRNA (that leads to Klhl13 levels similar albeit slightly lower than the ones observed in female cells) implies that the later might also be a mediator of the sex differences observed in mESCs. The degree to which Dusp9 or Klhl13 mediate the female-associated naive pluripotency phenotype can be studied in a complementary fashion through the generation of heterozygous mutants in female mESCs. We thus went on to elucidate whether female mutants with two X chromosomes, but just one copy of the Dusp9/Klhl13 allele, would indeed display a male-like pluripotency phenotype.

5.4. Heterozygous deletion of Klhl13 and Dusp9 in female mESCs qualitatively recapitulates the male pluripotency phenotype

If both Klhl13 and Dusp9 are indeed mediators of the sex differences observed between female and male mESCs, their heterozygous deletion in female cells should lead to a male-like pluripotency phenotype. In order to test this hypothesis, we generated both heterozygous (HET) and homozygous (HOM) Dusp9 (D9) and Klhl13 (K13) mutants, together with double heterozygous mutants (D9K13) to assess for additive effects of the two genes. The generation of homozygous mutants might allow the detection of stronger gene-mediated effects on the mESC pluripotency phenotype. D9 mutants were generated by targeting an sgRNA to the start of the coding sequence for the generation of frameshift mutations (Fig. 41A). A first strategy where the protomer of the single Dusp9 isoform would be deleted by targeting the Cas9 endonuclease to regions upstream and downstream of the latter was unsuccessful in this work. Due to the fact that frameshift deletions are difficult to verify via PCR genotyping, a region surrounding the start of the Dusp9 coding sequence was amplified and Sanger-sequenced for detection of HET clones (see section 4.2.7.2, Fig. 17A). D9-HOM clones, on the other hand, were identified via Immunoblotting (Fig. 17B). Heterozygous deletions were additionally confirmed via NGS for the D9-HET Clone 1 and both D9K13-HET clones (Fig. 17C, Fig. 41B), whereas for the D9-HET Clone 2 the presence of a mutant and

wildtype allele was confirmed through the cloning of the PCR amplicon surrounding the start of the coding sequence into a mammalian expression plasmid and subsequent Sanger-sequencing of single bacterial clones (Fig. 17D, Fig. 41B). The latter was due to the fact that it was not possible to generate two D9-HET clones in a first attempt, so a second one was implemented.

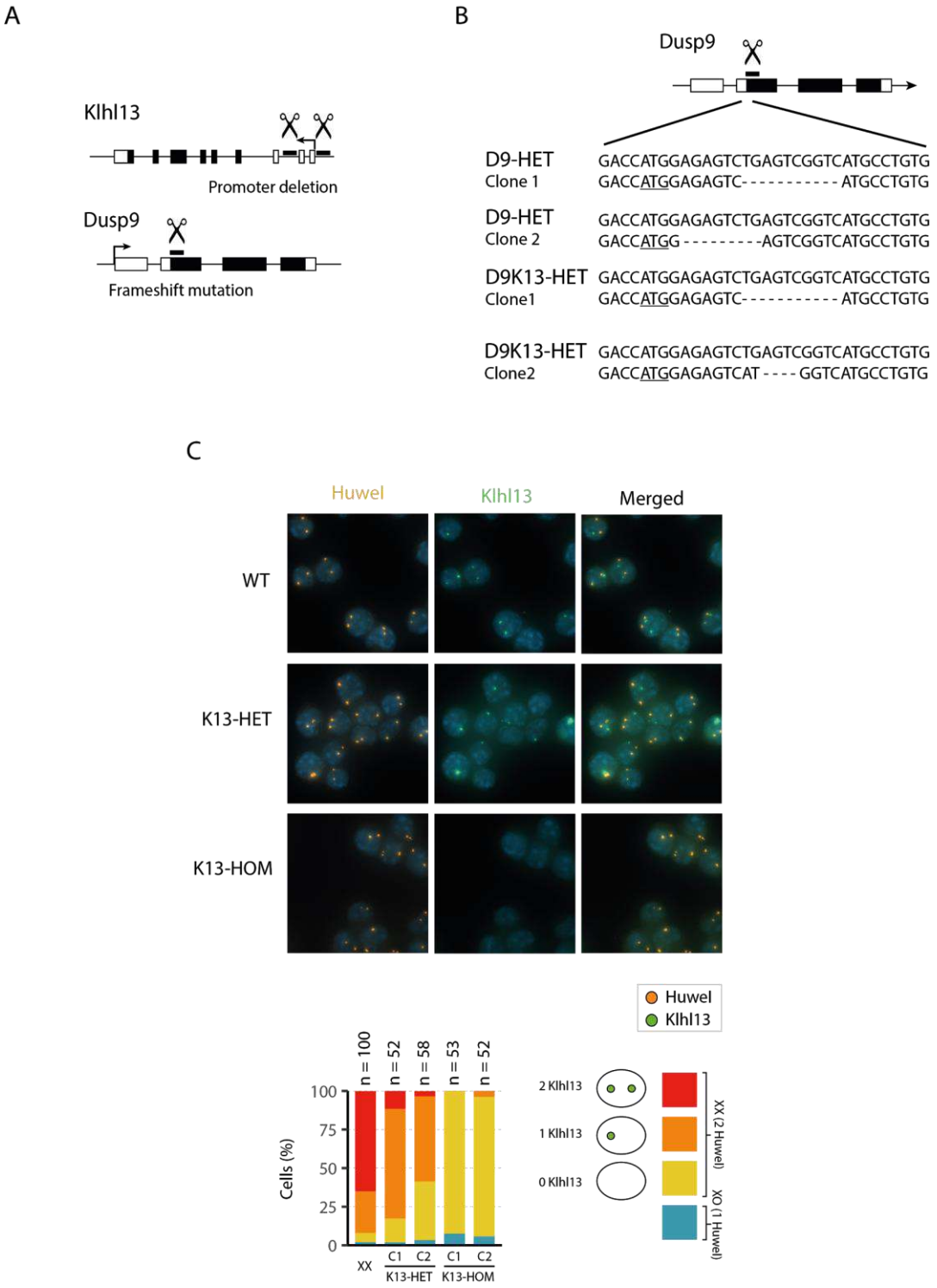

Figure 41. Generation of Dusp9 and Klhl13 mutant cell lines in female mESCs. (A) Strategy for the generation of Klhl13 and Dusp9 mutant cell lines. A region around 4.5 kb spanning the Klhl13 promoter and TSS was excised via CRISPR/Cas9, whereas for Dusp9, frameshift mutants were generated by targeting the start of the CDS. **(B)** Sequence of Dusp9 frameshift mutants. Start codon is underlined. **(C)** RNA fluorescence

in situ hybridization (FISH) of XX wildtype cell lines together with Klhl13 heterozygous and homozygous mutants. Probes for Klhl13 were used (green) together with an X-linked control gene (orange). A bar graph shows the fraction of cells with a specific pattern.

Heterozygous (HET) and homozygous (HOM) Klhl13 (K13) mutants were generated by deleting a 4.5 kb region around its promoter using CRISPR/Cas9 and mutants were identified via genotyping PCR (Fig. 41A, Fig. 16, see section 4.2.7.2). Loss of Klhl13 transcription in the respective mutants was additionally confirmed by nascent RNA FISH (Fig. 41C). All phenotypes were analyzed using two clones from each genotype except for differentiation kinetics, and all clones were karyotyped via double digest genotyping-by-sequencing (Elshire et al., 2011) (see section 4.3, Fig. 19).

Klhl13 and Dusp9 protein levels in all mutant cell lines were assessed via Immunoblotting. Here, Klhl13 levels were reduced ~2.7-fold in HET mutants compared to XX cells, whereas protein levels in the HOM mutants were not detected (Fig. 42). Dusp9 levels were ~1.8-fold lower in the HET mutant cell lines compared to XX cells, not reaching, however, the ~3.5-fold reduction observed in XO cells, pointing to additional regulatory mechanisms from other X-linked genes. In the HOM mutants, on the other hand, Dusp9 protein levels were not detected (Fig. 42).

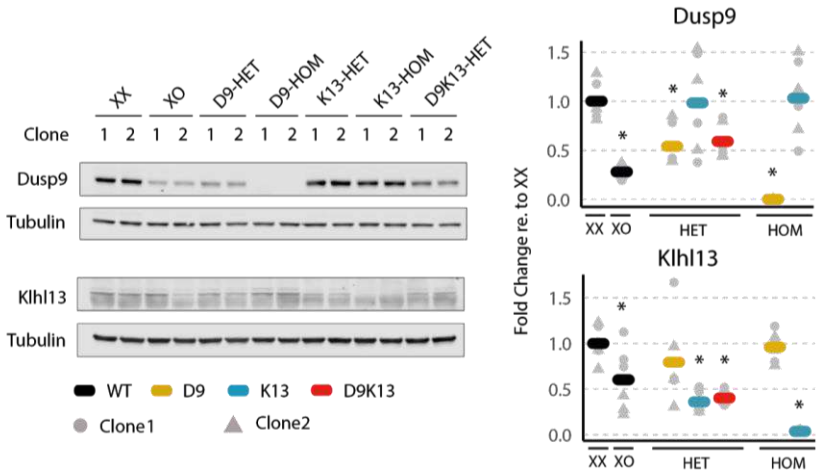

Figure 42. Generation of Dusp9 and Klhl13 mutant cell lines in female mESCs. Immunoblot quantification of Dusp9 (top) and Klhl13 (bottom) protein levels in Dusp9 (yellow) and Klhl13 (blue) heterozygous (HET) and homozygous (HOM) mutant cell lines together with Dusp9/Klhl13 double heterozygous mutants (red) compared with the parental XX and XO cells lines (black). Two clones were compared for each cell line and are depicted as grey circles (clone 1) or triangles (clone 2). The mean of the two clones and three biological replicates is shown as a thick line. Protein levels were normalized to ß-Tubulin and to the mean of the XX controls. * $p < 0.05$ from a two-tailed paired Student's t-test comparing each mutant/XO cell line vs. the XX controls.

5.4.1 Dusp9 and Klhl13 repress MAPK target gene expression in female mESCs, whereas Dusp9 additionally affects Mek phosphorylation levels

If Dusp9 and Klhl13 are indeed mediators of the female pluripotency phenotype in mESCs, their heterozygous deletion in female cells should lead to higher levels of the MAPK signaling pathway, including higher levels of MAPK target genes and lower levels of Mek phosphorylation.

We first assessed MAPK signaling levels in the generated mutants by quantifying Eg1 and Spry4 expression via qPCR. Here, levels were significantly increased in all mutant cell lines compared to the parental cell line albeit to different degrees (Fig. 43A). The strongest increase was observed in the D9-HOM mutants followed by D9K13-HET mutants, where MAPK target expression levels were 6.5/3.4-fold (Egr1/Spry4) higher compared to female wildtype cells. Levels of MAPK target genes Egr1 and Spry4 in D9K13-HET mutants therefore almost reached the ones observed in XO cells, which displayed 10.2/2.7 higher levels of Egr1 and Spry4, respectively, compared to

XX wildtype cells. Both D9 and K13 HET mutants showed significant upregulation of MAPK target genes, albeit to a lower extent compared to their respective HOM mutants (Fig. 43A).

To get a more global picture of signaling pathway levels that modulate the pluripotency state in mESCs, RNA-seq data was generated from all the previously assessed mutants and an extra XO clone (Clone 3). This data was then used to assess global expression of Mek, Gsk3 and Akt targets (Schulz et al., 2014; Watanabe et al., 2006; Wray et al., 2011). Library generation for this experiment was carried out by Ilona Dunkel.

Gsk3 signaling is associated to differentiation of mESCs and is blocked in 2i culture conditions (Sato et al., 2004; Wray et al., 2011; Ying et al., 2008), whereas Akt signaling is a strong pro-pluripotency pathway known to be upregulated in female mESCs (Watanabe et al. 2006; Schulz et al. 2014). Surprisingly, the strongest upregulation of Mek targets was observed this time in the K13-HOM mutants (Fig. 43B). This suggests that a greater number of Mek targets is upregulated to higher levels in K13-HOM mutants compared to D9-HOM mutants. D9K13-HET mutants showed the highest upregulation of Mek and Gsk3 targets among HET mutants, together with the strongest downregulation of Akt targets (Fig. 43B). Additionally, a higher upregulation of Mek and Gsk3 target genes could be observed for K13-HET mutants compared to D9-HET mutants. However, for all three signaling pathways, the effects detected in the D9K13 mutants could accounts for ~50% of the differences observed between XX and XO cells, suggesting the involvement of other genes in mediating the observed sex differences between female and male mESCs.

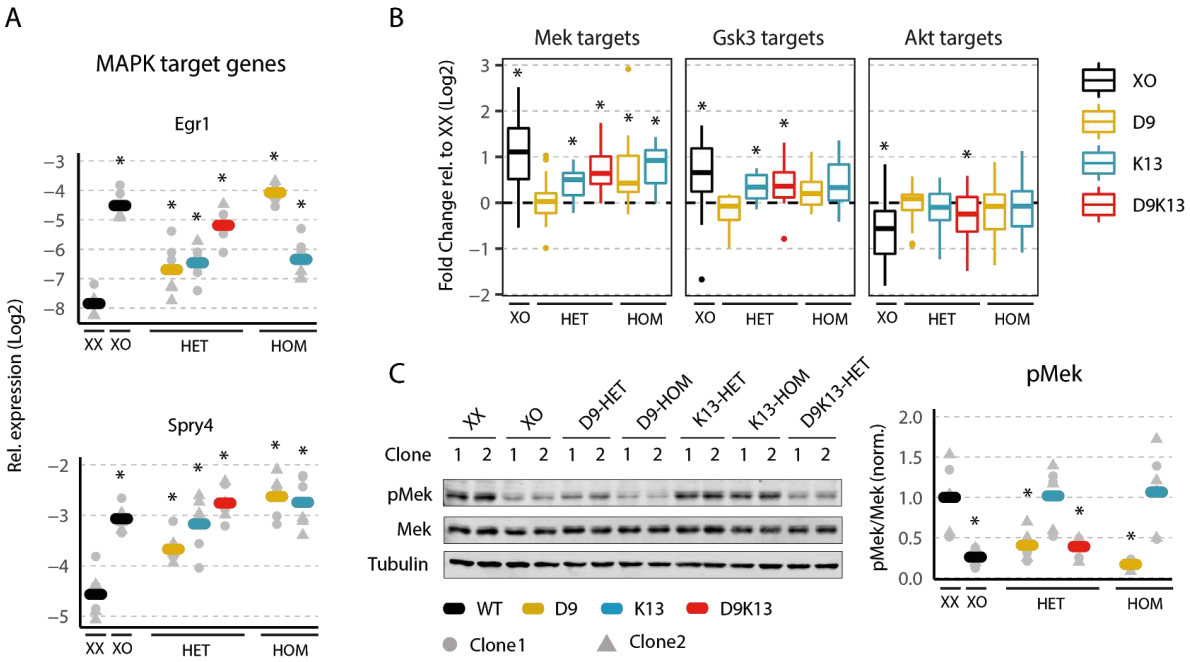

Figure 43. Dusp9 and Klhl13 inhibit the MAPK signaling pathway in female mESCs. (A) qPCR quantification of MAPK target genes Egr1 (top) and Spry4 (bottom) levels in Dusp9 (yellow) and Klhl13 (blue) heterozygous (HET) and homozygous (HOM) mutant cell lines together with Dusp9/Klhl13 double heterozygous mutants (red) compared with the parental XX and XO cells lines (black). Two clones were compared for each cell line and are depicted as grey circles (clone 1) or triangles (clone 2). The mean of two clones and three biological replicates is shown as a thick line. **(B)** Boxplots showing the expression of Mek (left), Gsk3 (middle) and Akt (right) target genes assessed via RNA-seq in cell lines with the indicated genotype. Boxes indicate the 25th and 75th percentiles and the central lines represent the median. **(C)** Immunoblot quantification of pMek protein levels in Dusp9 (yellow) and Klhl13 (blue) heterozygous (HET) and homozygous (HOM) mutant cell lines together with Dusp9/Klhl13 double heterozygous mutants (red) compared with the parental XX and XO cells lines (black). Two clones were compared for each cell line and are depicted as grey circles (clone 1) or triangles (clone 2). The mean of the two clones and three biological replicates is shown as a thick line. Protein levels were normalized to total Mek protein levels and to the mean of the XX controls. * $p < 0.05$ from a two-tailed paired Student's t-test (or Wilcoxon rank-sum test for (B)) comparing each mutant/XO cell line vs. the XX controls.

We next assessed Mek phosphorylation levels, where the strongest downregulation was observed in the D9-HOM mutants (7.5-fold reduction compared to XX wildtype cells) (Fig. 43C). D9-HET and D9K13-HET mutants

exhibited a 2.6-fold reduction compared to wildtype XX cells, approaching the 4.3-fold reduction observed in XO cells (Fig. 43C). K13 mutants, however, showed similar Mek phosphorylation levels compared to XX cells, in accordance with the previous screen results (see section 5.2.4) and Klhl13 overexpression experiments in male cells (see section 5.3.1).

In summary, it appears that Dusp9 has a stronger effect on Mek phosphorylation, whereas Klhl13 deletion mutants, on the other hand, exhibit higher levels of MAPK target genes, which is in contrast to results obtained from overexpression experiments (even though only two MAPK target genes were assessed in the latter). This is in accordance to the role of Dusp9 as an Erk phosphatase and MAPK inhibitor. The mechanism by which Klhl13 exerts an effect on MAPK target genes without affecting Mek phosphorylation, however, requires further study.

5.4.2 Klhl13, and to a lesser extent Dusp9, induce higher levels of pluripotency factor expression and lead to slower differentiation kinetics in female mESCs

If a double dosage of Dusp9 or Klhl13 in female mESCs leads to a shift towards the naive pluripotency state, their heterozygous female mutants should display a decrease in pluripotency factor expression, faster differentiation kinetics, and higher levels of CpG methylation. We first assessed pluripotency factor expression via qPCR, where the strongest downregulation of Nanog and Prdm14 compared to female wildtype cells was observed in the K13-HOM mutants (1.5-1.8-fold reduction compared to XX cells), followed by the D9K13-HET mutants (1.5-1.4-fold reduction compared to the parental cell line) (Fig. 44A). These changes in pluripotency factor expression could account for approx. half of the differences observed between XX and XO cells (2-2.4-fold lower levels than XX cells). D9K13-HET mutants displayed slightly lower Nanog levels compared to the single HET mutants, even though this was not the case for Prdm14 (Fig. 44A).

Differentiation kinetics were assessed next by measuring pluripotency factor expression via qPCR at different timepoints during differentiation. For this, all cell lines were first adapted to 2i/LIF conditions for at least five passages before undergoing differentiation via LIF withdrawal. Since adaptation of mESCs to 2i/LIF increases pluripotency factor levels significantly, we argued that a stronger downregulation of these markers would be observed during differentiation by starting from these conditions, potentially leading to stronger differences in pluripotency factor expression between female wildtype cells and the generated mutants.

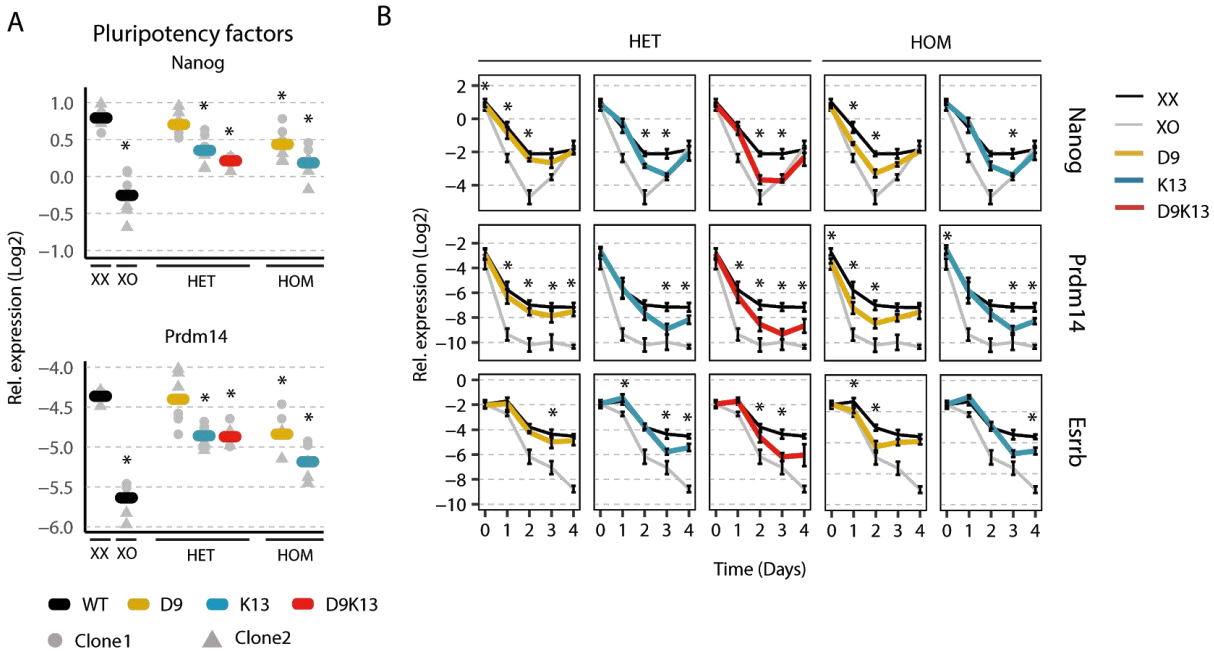

Figure 44. Mutation of Klhl13 and to a lesser extent Dusp9 in female mESCs leads to a significant decrease in pluripotency factor expression and faster differentiation kinetics. (A) qPCR quantification of Nanog (top) and Prdm14 (bottom) pluripotency factor levels in Dusp9 (yellow) and Klhl13 (blue) heterozygous (HET) and homozygous (HOM) mutant cell lines together with Dusp9/Klhl13 double heterozygous mutants (red) compared with the parental XX and XO cells lines (black). Two clones were compared for each cell line and are depicted as grey circles (clone 1) or triangles (clone 2). The mean of two clones and three biological replicates is shown as a thick line. **(B)** qPCR quantification of pluripotency factor expression during differentiation via 2i/LIF withdrawal in Dusp9 (yellow) and Klhl13 (blue) heterozygous (HET) and homozygous (HOM) mutant cell lines together with Dusp9/Klhl13 double heterozygous mutants (red) compared with the parental XX and XO cells lines (black). One clone was assessed for each mutant cell line and the mean and SD from three biological replicates is shown. * $p < 0.05$ from a two-tailed paired Student's t-test comparing each mutant/XO cell line vs. the XX controls.

During the four-day differentiation time course, the D9-HET mutant showed only a very small reduction in Nanog, Prdm14 and Esrrb levels compared to the parental cell line (Fig. 44B). K13-HET cells, on the other hand, downregulated all three factors with faster dynamics. Interestingly, the D9K13-HET mutant showed faster differentiation kinetics than both HET mutants and exhibited pluripotency factor expression levels closely resembling those of XO cells during differentiation (Fig. 44B).

Overall, Klhl13 mutants showed stronger effects on pluripotency factor expression and differentiation dynamics compared to Dusp9 mutants. Klhl13 poses thus a strong and novel modulator of the female pluripotency phenotype.

5.4.3 Mutation of Klhl13 and Dusp9 in female mESCs leads to a significant increase in global CpG methylation levels

Female mESCs display lower levels of global CpG methylation compared to their male counterparts, reflecting a more naive state of pluripotency. We therefore next assessed global CpG methylation levels in all mutant cell lines by implementing the LUMA assay (see section 4.5). Here, both single HET cell lines showed an increase of ~10% of global CpG methylation compared to female wildtype cells, whereas double HET mutants and HOM mutants showed increases of ~15% (Fig. 45A). Since XX wildtype cells exhibit values of approx. 30% global CpG methylation, compared to the approx. 60% displayed by XO cells, double heterozygous mutants could again account for around half of the differences observed between male and female mESCs. Similar patterns were observed concerning the expression of DNA methyltransferase enzymes, where the highest expression of Dnmt3b and Dnmt3I was observed in the K13-HOM mutants (2.1/2.6-fold for Dnmt3b/Dnmt3I in K13-HOM vs 3.7/2.2 in XO), followed closely by D9-HOM mutants (1.7/2.2-fold) and then D9K13-HET cells (1.5/1.5-fold) (Fig. 45B). Expression changes of both of these genes were even lower in single HET mutants. No significant increases were observed regarding Dnmt3a expression in any of the generated mutant cell lines (Fig. 45B). Our results are in contrast with other studies were female D9-HET mutant mESCs almost fully recapitulate CpG methylation levels observed in male cells (Choi et al., 2017; Song et al., 2019).

In conclusion, we observe that Dusp9 and Klhl13 affect DNA methylation levels in mESCs to a similar extent, and that D9K13-HET mutants recapitulate approx. half of the sex differences observed in mESCs regarding this specific phenotype.

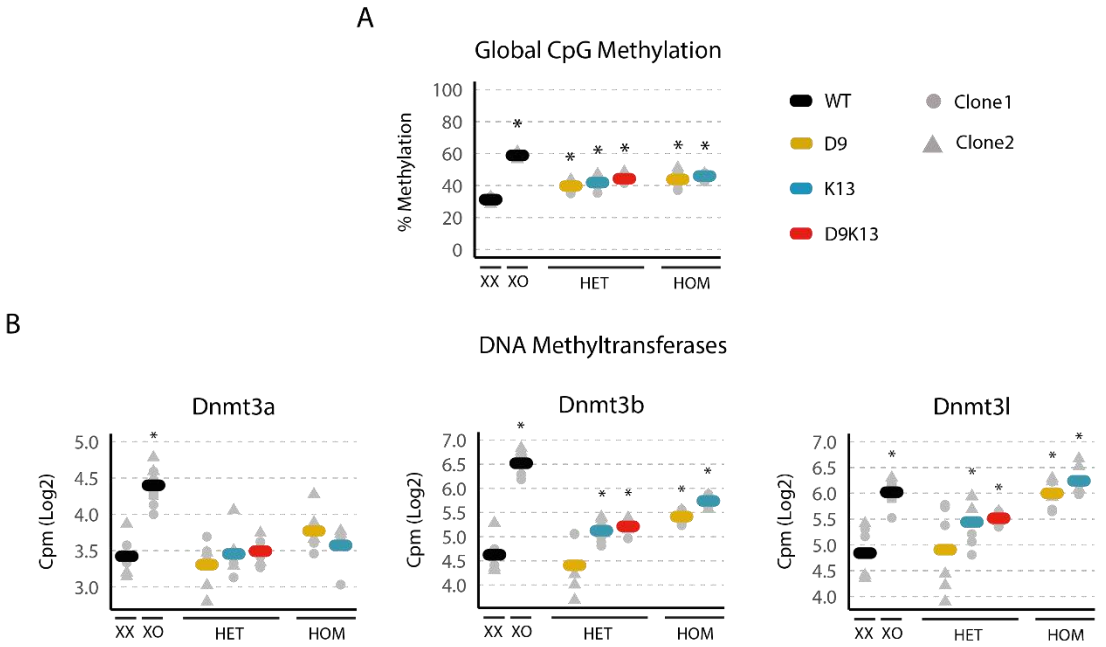

Figure 45. Heterozygous mutation of Dusp9 and Klhl13 induces an increase in global CpG methylation levels in female mESCs. (A-B) Dusp9 (yellow) and Klhl13 (blue) heterozygous (HET) and homozygous (HOM) mutant cell lines together with Dusp9/Klhl13 double heterozygous mutants (red) compared with the parental XX and XO cells lines (black). Two clones were compared for each cell line and are depicted as grey circles (clone 1), triangles (clone 2) or squares (clone 3). The mean of the two (A) or three (B) clones (for the XO clones only) and three biological replicates is shown as a thick line. (A) Global CpG methylation levels assessed via pyrosequencing-based luminometric DNA methylation assay (LUMA). (B) DNA Methyltransferase expression levels assessed via RNA-seq. * $p < 0.05$ from a two-tailed paired Student's t-test comparing each mutant/XO cell line vs. the XX wildtype controls.

5.4.4 Klhl13 contributes more strongly to the X-dosage induced global transcriptome changes compared to Dusp9

In order to see to which degree the generated mutants could recapitulate the XO phenotype at a global transcriptome level, we carried out a differential expression analysis (DEA) between XO/HET mutant cell lines and XX wildtype cells using EdgeR from RNA-seq data of all the generated mutants. Differentially expressed genes (DEGs) were defined as being significantly (p-value < 0.05) up- (Log2 Fold Change > 0.5) or downregulated (Log2 Fold Change < -0.5) between XO or HET mutants cell lines and XX wildtype cells. We then analyzed how many of the DEGs found in XO cells overlapped with the DEGs found in the HET mutant cell lines. Here, we observed again a smaller overlap of 148 genes between the D9-HET cell line and XO cells, compared to the 201 genes commonly differentially expressed between K13-HET and XO cells (Fig. 46A). The strongest overlap of 265 genes, however, was detected with the D9K13-HET cell line (Fig. 46A). A more similar transcriptome profile between D9K13-HET and XO cells was also confirmed when performing principal component analysis (PCA), followed by K13-HET cells and lastly by D9-HET mutants (Fig. 46B). This data suggest a stronger contribution of Klhl13 to the X-dosage induced transcriptome changes compared to Dusp9.

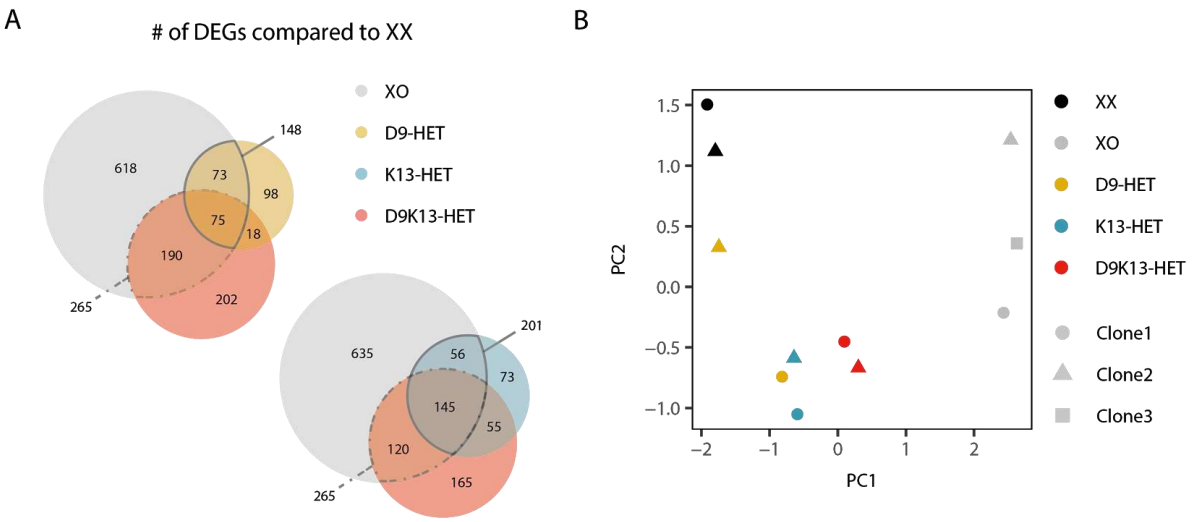

Figure 46. Global transcriptome profiling in Klhl13 and Dusp9 mutant cell lines. (A) Differentially expressed genes (DEGs) in XO (grey), K13-HET (blue), D9-HET (yellow) and D9K13-HET (red) cells compared to the parental XX cell line were identified via RNA sequencing. (log_2(fold-change) > 0.5 or log_2(fold-change) < -0.5, p-value < 0.05). Overlap between these genes is shown in the Venn diagrams. **(B)** Principal component analysis (PCA) of the 100 most variable genes between XX (black), XO (grey), D9-HET (yellow), K13-HET (blue) and D9K13-HET (red) cell lines. The average of three replicates is shown.

In summary, the effects observed in the D9K13-HET mutants regarding MAPK target gene expression, pluripotency factor expression, differentiation kinetics and global transcriptome profile suggest that multiple genes underlie the sex differences observed in mESCs. This is due to the fact that these mutants can qualitatively, albeit not quantitatively, recapitulate the XO pluripotency phenotype. Dusp9 seems to be responsible for the effects observed regarding Mek phosphorylation, whereas both genes seem to contribute to the reduction in MAPK target gene expression observed in female cells. Effects regarding pluripotency factor expression and differentiation kinetics seem to be, on the other hand, more strongly mediated by Klhl13. We have thus validated two essential genes underlying the female pluripotency phenotype, identifying hereby a key novel player: Klhl13.

Dusp9 seems to mediate the phenotypes associated with sex differences in mESCs through the inhibition of the MAPK signaling pathway by dephosphorylating one of its main cascade components: Erk. We were able to clarify the debated role of Dusp9 as an Erk phosphatase (see section 5.3.1), and to show that the previous hypothesis of Dusp9 acting downstream of Erk might be due to the effect of trypsinization before protein harvesting (Choi et al. 2017). We next set to investigate the mechanism by which Klhl13 mediates the observed differences in female mESCs, which, until now, remains elusive.

5.5. Identification of Klhl13 target proteins

Klhl13 is an adaptor protein for the Cullin-3-based E3 ubiquitin-protein ligase complex (Dhanoa et al. 2013; Pintard et al. 2004). It consists of a Cul3-binding BTB domain and five Kelch repeats that interact with specific substrates, leading to their ubiquitination by the E3 ubiquitin-protein ligase complex and subsequent proteasomal degradation (Dhanoa et al., 2013; Pintard et al., 2004). We reasoned that Klhl13 might mediate its function by reducing the protein abundance of factors leading to higher levels of MAPK signaling, lower levels of pluripotency factor expression and faster differentiation kinetics (Fig. 47A). In order to find Klhl13 target proteins, we first set out to find its interaction partners via IP-MS. We subsequently determined which of these candidate proteins were upregulated in K13-HOM cells compared to wildtype XX cells (Fig. 47B).

Identification of Klhl13 interaction partners was carried out by tagging either full-length Klhl13 (ENSMUST00000115313.7) or the substrate-binding Kelch domain (AA290 to AA585, extracted from the SMART

database (http://smart.embl-heidelberg.de/)) with the green fluorescent protein (GFP, Hein et al., 201), which was used for protein immunoprecipitation using a GFP-specific antibody (Fig. 47B). The GFP-Kelch construct was used in order to identify direct substrates of Klhl13 and not those that bind indirectly through Cul3 or other adaptor proteins present in the complex such as Klhl9. We nevertheless hoped to find Klhl13 substrates also by pulling-down full-length Klhl13, together with Cul3 and other complex components, and we reasoned that interaction partners found in both pull-downs would represent strong Klhl13 candidate substrates.

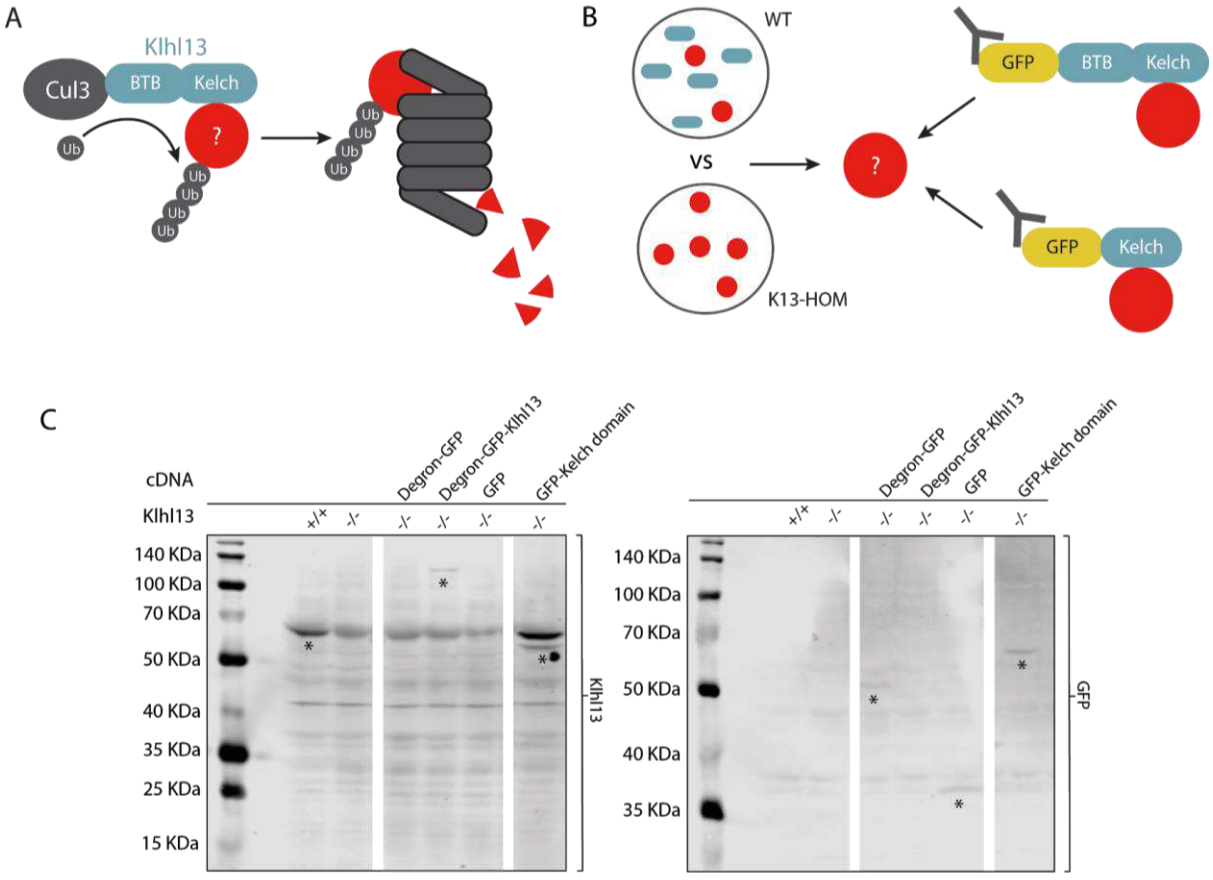

Figure 47. Strategy for the identification of Klhl13 target proteins that mediate its pluripotency-inducing phenotype. (A) Schematic representation of the putative mode of action behind the Klhl13-mediated female pluripotency phenotype. Klhl13 binds differentiation-inducing proteins via its Kelch domain and sends them for proteasomal degradation through the recruitment of the Cul3 E3 ubiquitin ligase complex. **(B)** Experimental strategy for the identification of Klhl13 target proteins. Comparison of the proteomes of XX wildtype cells and a K13-HOM mutant cell line allowed the determination of upregulated proteins in the later. Additional pull-down of Klhl13 and the Klhl13 Kelch domain interacting partners and subsequent IP-MS helped to determine Klhl13 binding partners. All three datasets were integrated for the identification of target proteins. **(C)** Immunoblotting of protein lysates from female K13-HOM cell lines expressing constructs for the identification of Klhl13 interacting proteins and an XX wildtype control. Membranes were incubated with an anti-Klhl13 antibody (left) and and anti-GFP antibody (right). *bands with the expected size.

The GFP-Klhl13 construct was additionally coupled to a degron domain consisting of a mutated cytosolic prolyl isomerase FKBP12^{F36V}, which was however not used in the reported experiments (Nabet et al., 2018). Plasmids for gene overexpression were cloned by Genscript and delivered as ready-to-use Midi preparations (pLenti-PGK-Degron-GFP-Blast, pLenti-PGK-Degron-GFP-Klhl13-Blast, pLenti-PGK-GFP-Blast, and pLenti-PGK-GFP-Kelch, Table 7).

These constructs were subsequently overexpressed in K13-HOM cells, which are depleted of endogenous Klhl13 protein (Fig. 47C). Cells were cultured for 3 h with a proteasomal inhibitor before harvesting for IP-MS in order to stabilize transient interactions. A total of 218 proteins for GFP-Klhl13 and 197 proteins for GFP-Kelch domain

were enriched after immunoprecipitation relative to the GFP only controls, with an overlap of 110 proteins enriched in both datasets (Fig. 48A-B, Fig. 48D). Six known Klhl13 interactors were significantly enriched in the GFP-Klhl13 IP (Fig. 48B). Three of them, Klhl22, Klhl21 and Klhl9, are proteins that interact with Klhl13 through Cul3, which was also among the significantly scoring interaction partners (Sowa et al., 2009). The other two known Klhl13 binding proteins found in the BioGRID database, Nudcd3 and Hsp90aa1, were also significantly enriched in the GFP-Kelch domain pull-down (Fig. 48A).

If Klhl13 indeed leads to the proteasomal degradation of its interaction partners, our protein of interest should be upregulated in cells depleted of Klhl13. We therefore carried out a proteomics profiling with label-free quantification (LFQ) of the two K13-HOM cell lines and compared it to wildtype female cells to determine differentially expressed proteins (Fig. 48C). Among the 110 proteins enriched in both IP-MS experiments, five were upregulated in K13-HOM cells from a total of 299 proteins: Scml2, Peg10, Alg13, Larp1, Cct3 (Fig. 48D). From these candidate proteins, the X-linked Alg13, which encodes a cytosolic and catalytic subunit recruited by Alg14 to the ER membrane for N-linked glycosylation of proteins (Gao et al., 2005), was found depleted in the pluripotency and differentiation screens (Enrichment = 0.39/0.52 and FDR = 0.05/0.07, respectively), pointing to a possible role as a differentiation-inducing factor (Fig. 48E). Scml2, another candidate gene, is a member of the Polycomb group proteins involved in transcriptional regulation, mediating the deposition of repressive histone marks H2AK119ub and H3K27me3 (Bonasio et al., 2014; Hasegawa et al., 2015; Maezawa et al., 2018), it is also encoded on the X chromosome., and it was strongly upregulated in K13-HOM cells (~8-fold). Peg10, on the other hand, represents a MAPK target gene and known oncogene, and was also found strongly upregulated in K13-HOM cells (~4-fold) (Xie et al. 2018). Lastly, Larp1 represents a transcriptional regulator and Cct3 is a member of the chaperonin containing TCP1 complex (CCT) (Philippe et al. 2018; Walkley et al. 1996; Tcherkezian et al. 2014).

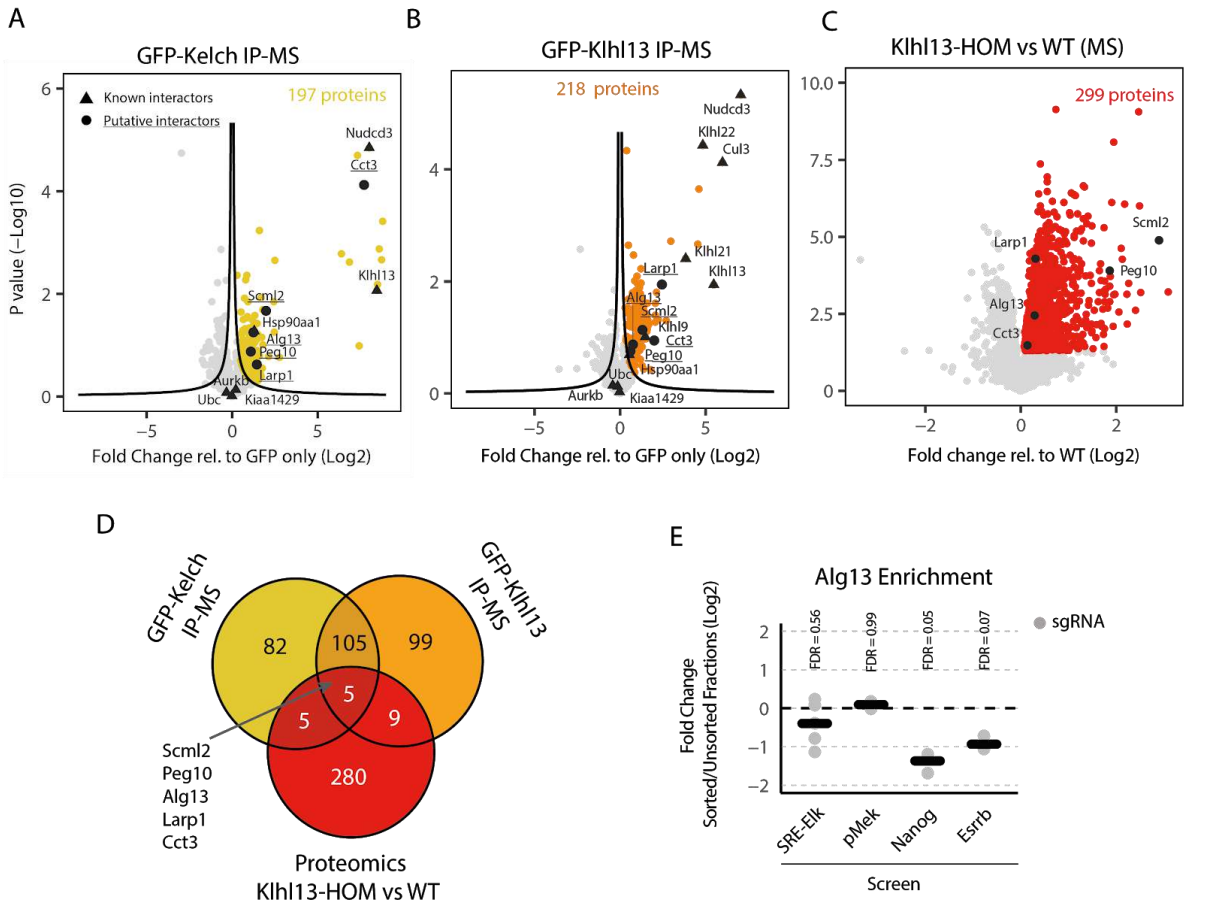

Figure 48. Identification of Klhl13 target proteins that mediate its pluripotency-inducing phenotype.. (A-B) Volcano plots showing the results of the GFP-Kelch (A) and GFP-Klhl13 pull-down (B). The fold change across three biological replicates relative to the GFP-only control

is shown against the p-value calculated via a two-sample Student's T-test with Benjamini-Hochberg correction for multiple testing. Black lines indicate the significance threshold that was chosen such that FDR<0.1, assuming that all depleted proteins (left-sided outliers) were false-positive. Triangles show known Klhl13 interaction partners (BioGRID database). **(C)** Volcano plot depicting differentially expressed proteins in the K13-HOM cell line compared to wildtype XX cells. The fold change across three biological replicates is shown against the p-value calculated via a two-sample Student's T-test with Benjamini-Hochberg correction for multiple testing. Upregulated proteins ($p < 0.05$) are highlighted in red. Black circles (A-C) represent the putative target proteins that were identified in all three datasets. **(D)** Venn diagram showing the putative Klhl13 target genes identified in all three datasets (A-C). **(E)** Results from all the four generated screens for Alg13. Grey dots indicate the enrichment of individual sgRNAs and thick black lines represent the mean. The false discovery rate for Alg13 in all the screens is also shown.

In conclusion, we have identified several putative Klhl13 target genes: Alg13, Scml2, Peg10, Larp1 and Cct3. Alg13, the most promising putative target protein, could represent a differentiation-inducing factor, leading at the same time to lower pluripotency factor levels. The role of the other identified targets in the context of sex differences in mESCs still requires further study.

6. Discussion

Female mESCs are found in a more naive state of pluripotency compared to their male counterparts and XO subclones. They display lower levels of MAPK signaling, higher expression of pluripotency factors and lower levels of global CpG methylation. Additionally, these cells downregulate pluripotency factors with significantly slower kinetics during differentiation.

We hypothesized that these sex differences could be due to the presence of one or several X-linked genes present in a double dosage in female mESCs that inhibit the MAPK signaling pathway and thus lead to a more naive pluripotency phenotype, and whose identity has remained unknown until now.

From a physiological perspective, the slower differentiation kinetics observed in female mESCs might ensure proper progression of the XCI process, which starts early during differentiation and takes several days to complete. This phenomenon might additionally pose a biological checkpoint in which only the cells that have successfully inactivated one of their X chromosomes can successfully downregulate their pluripotency factors, continue through their developmental progression and thus contribute to the developed organism.

In order to identify X-linked genes mediating the aforementioned sex differences in an unbiased manner, we made use of a series of complementary pooled CRISPR knockout screens. Since we hypothesized that these genes might act by inhibiting the MAPK pathway, we first carried out a primary screen that implemented a fluorescent MAPK-sensitive reporter and an sgRNA library that targeted the majority of X-linked genes.

Secondary screens were subsequently performed in order to determine, among the top scoring genes from the primary screen, which genes additionally had an effect on pluripotency factor expression, differentiation kinetics and phosphorylation of the MAPK component Mek. These genes should, moreover, be expressed at least at two-fold higher levels in female mESCs. This way, four X-linked candidate genes were identified: Dusp9, Klhl13, Fthl17e and Fthl17f.

The role of the two strongest hits found in the performed screens, Dusp9 and Klhl13, in mediating the sex differences observed in mESCs was confirmed by overexpressing these genes in male cells, which led to a shift towards a more naive state of pluripotency. Additionally, heterozygous and homozygous mutants were generated in female mESCs, which shifted these cells towards a more primed pluripotent state. Phenotypes such as pluripotency factor expression, differentiation kinetics, MAPK target gene expression, Mek phosphorylation levels and global CpG methylation were assessed in all generated cell lines. While Klhl13 seems to mediate stronger effects regarding pluripotency factor expression and differentiation kinetics, Dusp9 alone strongly modulates phosphorylation levels of MAPK pathway components. Curiously, both genes seem to affect expression of MAPK target genes.

Through Klhl13 Immunoprecipitation experiments together with proteomics profiling of the K13-HOM (homozygous) mutants compared to wildtype female mESCs, it was possible to determine putative Klhl13 target proteins that both interacted with Klhl13 and were upregulated in K13-HOM mutants. Five putative candidates were identified: Alg13, Scml2, Peg10, Larp1 and Cct3. The X-linked UDP-N-Acetylglucosaminyltransferase Subunit Alg13 was found in the depleted fractions of the pluripotency and the differentiation screen, pointing to a possible role as a pluripotency-destabilizing factor.

6.1. Dusp9 as a mediator of sex differences in mESCs

The series of pooled CRISPR knockout screens generated in female mESCs identified two top candidates as modulators of the observed sex differences in mESCs: Dusp9 and Klhl13.

Dusp9 is a known Erk phosphatase and inhibitor of the MAPK signaling pathway (Caunt and Keyse, 2013). Dusp9 overexpression in male mESCs leads to higher levels of pluripotency factors, significantly slower differentiation kinetics and a partial loss of global CpG methylation. Additionally, these cells express lower levels of MAPK target genes and display higher levels of Mek phosphorylation and lower levels of Erk phosphorylation, in accordance to its role as an Erk phosphatase.

Curiously, female mESCs with an heterozygous Dusp9 mutation exhibit a very marginal and non-significant downregulation of pluripotency factors and differentiate only slightly faster compared to their wildtype counterparts. However, Mek phosphorylation levels in these mutants are significantly lower than the ones observed in female cells, almost reaching the levels displayed by XO cells, pointing to a strong effect of Dusp9 on the phosphorylation of this MAPK pathway component. MAPK target genes are additionally upregulated in these mutants, in accordance to the role of Dusp9 as a MAPK inhibitor.

Female wildtype mESCs exhibit higher Mek phosphorylation levels compared to their male counterparts. Additionally, differences in MAPK target gene expression are consistently observed, with female cells displaying lower levels than XO cells. Given these variations concerning the MAPK signaling pathway in XX vs XO cells, its is probable that differences in Erk activity are also present between these cell lines. However, we observed similar pErk levels between XX wildtype cells, their XO subclones and the Dusp9 female mutants (both heterozygous and homozygous, data not shown), which is curious given the previously confirmed role of Dusp9 as an Erk phosphatase through its overexpression in male cells. It is nevertheless possible, that the various negative feedback loops that ensure homeostasis of the MAPK signaling pathway are able to guarantee stable pErk levels in the long-term, even in Dusp9 homozygous mutants. Stable pErk levels could then be observed in cell lines with a constitutive Dusp9 mutation, and less in the Dusp9 overexpression scenario, where expression is induced for only few days.

Our results concerning the upregulation of pluripotency factors and a loss of global CpG methylation through Dusp9 overexpression in male mESCs are in accordance to a previous study (Choi et al. 2017). However, the latter study also reports an increase in Mek and Erk phosphorylation upon Dusp9 overexpression, which they state is due to Dusp9 acting downstream of Erk and to the accompanying decrease in feedback regulation of the MAPK pathway (Fig. 49) (Choi et al., 2017). This is in contrast to our results, where we observe a clear decrease in Erk phosphorylation upon Dusp9 overexpression, which would be in accordance with the role of Dusp9 as an Erk phosphatase (Fig. 49). These discrepancies could be due to the different cell harvesting conditions used for Immunoblotting, as requirement of trypsinization in feeder-dependent cell lines leads to drastic alterations in phosphorylation levels of MAPK pathway components.

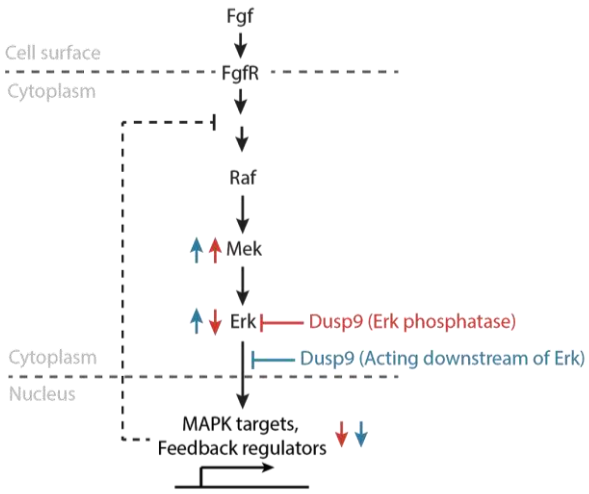

Figure 49. Possible mechanisms of Dusp9 mediated inhibition of the MAPK pathway. Schematic representation of the two proposed mechanisms by which Dusp9 might inhibit the MAPK pathway. A study conducted by Choi et al., 2017 reports an increase in both Erk and Mek phosphoryation upon Dusp9 overexpression, stating that the MAPK inhibitor could act downstream of Erk. The present work observes a strong increase in Mek phosphorylation together with a decrease in pErk levels, in accordance with the role of Dusp9 as an Erk phosphatase. Discrepancies between the two studies could be due to different protein harvesting conditions, as trypsinization previous to cell lysis of Dusp9 overexpressing cell lines leads to strong increases in pErk levels.

The Choi et al. study also generated female heterozygous mutants for Dusp9, assessing only global CpG methylation levels and showing that these mutants could almost recapitulate male global CpG levels (Choi et al. 2017). Our study confirms a rise in global CpG methylation levels in Dusp9 HET mutants compared to wildtype female cells, however, the increases are not as strong as the ones observed in this previous study, probably due to differences in the implemented cell lines, culture conditions and/or methylation assay.

A previous study showed that female mESCs carrying a Dusp9 mutation in one of their two alleles do not display significantly lower levels of pluripotency factor expression or faster differentiation kinetics (Song et al., 2019), which is in contrast to other studies showing significant decreases in pluripotency factors upon Dusp9 knockdown in male cells (Li et al., 2012). Our work confirms that female heterozygous Dusp9 mutants show marginal decreases in pluripotency factor expression and slightly faster differentiation kinetics compared to female wildtype mESCs, even though these small differences lead to considerable stronger effects in Dusp9/Klhl13 double heterozygous mutants.

In summary, Dusp9 represents an important mediator of sex differences in mESCs by acting as an inhibitor of the MAPK pathway. Whether Dusp9 acts as an Erk phosphatase or downstream of the pathway seems to be a subject of debate, however, our results suggest that it indeed dephosphorylates the key MAPK pathway component Erk. The weak shift towards the primed pluripotency phenotype displayed by Dusp9 HET mutants is in accordance with a previous study (Song et al. 2019), hinting that additional genes are involved in mediating the reported sex differences in mESCs. However, the stronger shift towards the naive pluripotency phenotype upon Dusp9 overexpression in male cells observed in our study also reproduces previous results (Choi et al. 2017). The strong differences observed between the gain- and loss of function experiments could be due to adaptation to the constitutive mutation in female mESCs over several passages, in contrast to the induction of Dusp9 overexpression over a few days. Additionally, Dusp9 loss could be compensated by other MAPK regulators that act in a redundant manner.

6.2. Klhl13 as a key and novel mediator of sex differences in mESCs

Among the two top hits identified in the series of generated CRISPR screens is a novel and key modulator of the observed sex differences in mESCs: Klhl13. A deeper study of Klhl13 and the molecular mechanisms behind its function could be relevant for several clinical contexts. For once, mutations in Klhl13 diagnosed in patients with Inherited peripheral neuropathies (IPN) via whole exome sequencing (WES) identify this gene as a novel disease-related candidate (Schabhüttl et al., 2014). Additionally, Klhl13 has been found to be differentially expressed in patients with Stage I-II laryngopharyngeal squamous cell carcinoma, linking this dysregulation in expresion to low survival prediction (Reddy et al., 2019).

In this work, we find that heterozygous mutation of Klhl13 in female mESCs, and to an even larger extent its homozygous mutation, leads to a shift towards the primed pluripotency state. These cells express lower levels of pluripotency factors, significantly faster differentiation kinetics, higher global CpG methylation levels and higher levels of MAPK target genes than their female wildtype counterparts. Klhl13 also appears to contribute more strongly than Dusp9 to the global transcriptome differences observed between XX and their XO cell lines. Interestingly, Klhl13 does not affect phosphorylation of MAPK pathway intermediates, meaning that repression of MAPK target genes could be mediated at the chromatin level. This work thus represents the first study that links Klhl13 to the modulation of the pluripotent state.

Klhl13 overexpression in male mESCs leads to a weaker shift towards the naive pluripotency state. Only slightly higher levels of pluripotency factors and lower levels of MAPK target genes are observed in Klhl13 male overexpressing cells. Significantly slower differentiation kinetics are, however, detected in these cell lines. This smaller shift towards the naive pluripotent state could be attributed to the fact that Klhl13 overexpression levels are quite low in these cell lines, which is of great importance since these differences seem to be strongly dose dependent. Furthermore, unlike Dusp9, Klhl13 mediates its function as part of a complex, which might lead to its stoichiometric imbalance upon overexpression of only one of its members, leading to less pronounced overexpression phenotypes. The fact that small but significant differences are observed in Klhl13 overexpressing male cells points to its role in mediating sex differences in mESCs.

Klhl13 is a substrate adaptor protein of the E3 ubiquitin ligase complex (Sumara et al., 2007). A previous study has conferred a role to Klhl13 in the regulation of proper mitotic progression, together with other components of the E3 ubiquitin ligase complex such as Cul3 and Klhl9 (Sumara et al., 2007). The latter study reports that the Cul3-Klhl19-Klhl13 complex is needed to remove the passenger Aurora B kinase from mitotic chromosomes in order to complete cytokinesis. However, Klhl13 homozygous clones with a normal karyotype could be generated without major difficulties in this study, pointing to another role of Klhl13 in mESCs.

Another former study has generated three large-fragment (LF1-3) heterozygous deletions on the X chromosome in female wildtype mESCs in order to corroborate a model in which several, and not single, X-linked genes mediate the observed sex differences in mESCs (Song et al. 2019). Faster differentiation kinetics compared to female wildtype mESCs were more strongly observed in the LF1, followed by the LF2 mutants. LF3 mutants showed marginal effects. The LF1 deletion encompases all genes between the Tfe3 and Zic3 locus, the LF2 deletion encloses all genes between the Zic3 and the Dusp9 locus, and lastly, the LF3 deletion, all genes between the Dusp9 and Nr0b1 locus. Interestingly, both Klhl13 and the Fthl17 cluster, which includes two strong candidate genes found in the generated screens (Fthl17e and Fthl17f), are found in the LF1 deleted region. This may support the faster differentiation kinetics observed in Klhl13 heterozygous mutants compared to Dusp9 heterozygous mutants, and at the same time, it reinforces the hypothesis that several genes are responsible for mediating the sex differences observed in mESCs.

Overall, this work shows that Klhl13 is a key mediator of sex differences in mESCs and that heterozygous Klhl13 and Dusp9 female mESCs mutants qualitatively recapitulate all aspects of the male pluripotency phenotype. Furthermore, we demonstrate that effects on pluripotency factor expression and differentiation kinetics are mainly mediated by Klhl13. Surprisingly, a double dosage of Klhl13 in female mESCs leads to lower levels of MAPK target gene expression, even though it does not affect Mek phosphorylation. The elucidation of the molecular mechanism behind the role of Klhl13 in mediating the female pluripotency phenotype could shed further light into the nature of the observed phenotypes.

6.3. Identification of putative Klhl13 target proteins

Since the molecular mechanisms behind Klhl13´s modulation of the pluripotency phenotype remain elusive, a strategy was implemented to find Klhl13 target genes that were upregulated in K13-HOM mutants and that interacted with the full Klhl13 protein and its substrate-binding Kelch domain. Using this approach, five putative target proteins were identified: Alg13, Scml2, Peg10, Larp1 and lastly, Cct3.

In order to confirm and validate the interaction of Klhl13 with the identified targets, their tagged proteins could be overexpressed in Hek293T cells together with a tagged Klhl13 protein. The latter could then be immunoprecipitated and the target pull-down determined via Immunoblotting. Additionally, the endogenous Klhl13 locus could be tagged in order to confirm interaction with endogenous target proteins. Ubiquitination of target proteins could be further confirmed by overexpressing the tagged target proteins in either female

wildtype cells or K13-HOM mutants followed by protein pull-down and quantification of the fraction of ubiquitinated protein via immunoblotting. The later experiments would further confirm the nature of Alg13, Scml2, Peg10, Larp1 and Cct3 as Klhl13 target proteins.

Alg13 represents a subunit of a bipartite UDP-N-acetylglucosamine transferase complex (Gao et al., 2005). However, a second isoform could also function as a deubiquitinase enzyme (Mevissen et al. 2013). This X-linked gene was targeted in both the GeCKOx as well as the GeCKOxs library, being found among the 50 most depleted genes genes in the primary screen. It was also depleted in the pluripotency and differentiation screen, pointing to a role as a pro-differentiation factor. It would be of interest to see whether overexpression of this gene in female wildtype mESCs or knockdown in K13-HOM mutants leads to a male-like pluripotency phenotype in the first or phenotypic rescue in the latter.

Scml2 is a member of the Polycomb group proteins and is therefore associated with transcriptional repression (Montini et al. 1999; Shao et al. 1999; Wang et al. 2010). Since no changes are detected in the phosphorylation levels of MAPK pathway components in Klhl13 mutant female mESCs cells, Scml2 could mediate the observed differences in MAPK target gene expression at the chromatin level. Indeed, even though Scml2 has been shown to lead to the deposition of repressive histone marks such as H3K27me3 and H2AK119ub, it has also been implicated in the removal of the latter through the recruitment of the deubiquitinase enzyme Usp7 (Bonasio et al., 2014; Hasegawa et al., 2015; Maezawa et al., 2018). This points to a possible role of Scml2 in both transcriptional activation as well as transcriptional repression. It would be of interest to determine whether Scml2 overexpression in female wildtype cells leads to changes in MAPK target gene and pluripotency factor expression, and therefore a general shift towards a more primed state of pluripotency. If this is indeed the case, chromatin immunoprecipitation (ChIP) experiments could help to verify whether Scml2 overexpressing cells indeed display different levels of polycomb-mediated repressive histone marks at MAPK target genes or pluripotency genes compared to wildtype cells and whether Scml2 binds directly to these genes.

If the degradation of Scml2 via a double dosage of Klhl13 indeed leads to the more naïve state of pluripotency observed in female mESCs, its knockdown in K13-HOM mutants should rescue their phenotype. Scml2 was among the genes targeted in the primary CRISPR screen, being encoded on the X chromosome, but was neither in the depleted or enriched gene fraction. However, Scml2 could still mediate the phenotypic changes observed in Klhl13 mutants, since the chromatin regulatory elements that could be subject to deubiquitination by Scml2 are not present in the surroundings of the randomly integrated SRE-Elk reporter used in the screen. Additionally, the levels of Scml2 in K13-HOM mutants are significantly higher than the ones displayed by wildtype female mESCs, the cell line in which the SRE-Elk screen was performed. It could therefore be possible that a shift back towards a more naïve state of pluripotency is only possible to detect upon Scml2 knockdown in K13-HOM cells.

A third interesting candidate worth investigating is the maternally imprinted/paternally expressed Peg10 (Ono et al., 2001). This gene is retrotransposon-derived and its mutation leads to embryonic lethality around 10.5 dpc due to severe placental defects (Ono et al., 2006). The inhibition of the MAPK pathway through culture with an inhibitor of Mek leads to its downregulation in mESCs, representing a MAPK target gene. This, however, could explain why it is significantly upregulated in K13-HOM mutants, which show an increase in MAPK target gene levels, raising therefore the possibility that Peg10 might not represent a direct Klhl13 target gene.

Peg10 is a known oncogene and its knockdown has been shown to lead to lower Erk phosphorylation levels, even though the present work does not detect changes in the phosphorylation of MAPK pathway components caused by Klhl13 (Peng et al., 2017; Xie et al., 2018). Additionally, it has been found to interact with Nanog and Oct4 in human cancer cells (Oliviero et al., 2015). It would be therefore nevertheless interesting to determine whether Peg10 overexpression in female wildtype mESCs leads to changes in MAPK targets or pluripotency factor expression, even though its mechanisms of action are still incompletely understood.

Protein ubiquitylation is a mechanism implicated in a variety of cellular processes that not only include the proteasomal degradation pathway. Proteins can be tagged with just one ubiquitin (Ub) molecule (monoubiquitylation), which has been linked, among others, to the regulation of endocytosis and DNA repair (Haglund and Dikic 2005). A protein can also be ubiquitylated at various lysine residues (multiubiquitinylation), and since ubiquitin itself harbors seven of these residues (Lys6, Lys11, Lys27, Lys29, Lys33, Lys48 and Lys63), a single ubiquitin molecule can be ubiquitylated to form ubiquitin chains (polyubiquitylation). It has been shown that while Lys48-linked poly-Ub (Ub^{Lys48}) leads to proteasomal degradation of target substrates (Hershko and Ciechanover 1998), mono-Ub and Ub^{Lys63} chains have been associated to cellular signaling (Silverman and Maniatis 2001; Newton et al. 2008; Parvatiyar et al. 2010; Haglund and Dikic 2005). It is therefore possible that some of the Klhl13 interacting proteins found in both pull-down experiments might not be upregulated in K13-HOM mutants, but could nevertheless be involved in the activation of signaling pathways that lead to a more primed state of pluripotency.

In conclusion, we have identified, through the implementation of Klhl13 Immunoprecipitation experiments together with proteomics profiling of the K13-HOM mutants compared to wildtype female mESCs, five putative Klhl13 target proteins: Alg13, Scml2, Peg10, Cct3 and Larp1. The most promising candidate seem to be, however, Alg13, which could represent a pluripotency-destabilizing factor as it was found in the depleted fractions of both the pluripotency as well as the differentiation screen.

6.4. Multiple genes underlie the observed the sex differences in mESCs

The series of CRISPR knockout screens generated in this work revealed four candidates genes mediating the sex differences observed in mESCs that scored in at least two of the four screens and are expressed at least two fold higher in female mESCs compared to male cells: Klhl13, Dusp9, Fthl17e and Fthl17f. Additionally, Zic3 and Stag2 were also significantly enriched in at least two screens, however, their expression levels in female and male mESCs were similar.

By generating heterozygous and homozygous female mESC mutants for Klhl13 and Dusp9 we showed that effects on pluripotency factor expression and differentiation kinetics are mainly mediated by Klhl13. However, Klhl13 does not affect Mek phosphorylation, whereas Dusp9 heterozygous mutants display pMek levels almost reaching the ones observed in XO subclones. Interestingly, both genes seem to affect MAPK target gene expression similarly. By overexpressing Dusp9 in male mESCs we see a clear decrease in Erk phosphorylation and an accompanying rise in pMek levels due to reduced feedback regulation, pointing to the role of Dusp9 as an Erk phosphatase and MAPK inhibitor. The mechanism by which Klhl13 affects MAPK target genes remains, however, slightly more unclear. We find one putative Klhl13 target protein, Alg13, as a possible pluripotency-destabilizing factor, since it was depleted in both the pluripotency as well as the differentiation screen. The role of the other identified putative target proteins in mediating the effects observed in Klhl13 mutants is subject of future study.

Klhl13 and Dusp9 double heterozygous mutants (D9K13-HET) display lower levels of pluripotency factors, higher levels of MAPK target genes and faster differentiation kinetics than their single heterozygous mutants, which clearly shows that both genes are implicated in mediating sex differences in mESCs. However, for most of the phenotypes assessed in this work, D9K13-HET mutants can account for approx. half of the differences observed between female and male mESCs, pointing to the fact that there must be additional mediators of the female pluripotency phenotype. These most probably include some of the additional genes identified in the generated CRISPR screens: Fthl17e, Fthl17f, Zic3 and Stag2.

Zic3 is known to enhance iPSC generation and regulate Nanog expression, as its knockdown leads to a downregulation of the latter (Declercq et al., 2013; Lim et al., 2007, 2010). Because of this, Zic3 could contribute to the increase in pluripotency factor expression and slower differentiation kinetics observed in female mESCs,

as also shown in the secondary screens. The fact that it is significantly enriched in the primary SRE-Elk screen but not in the pMek screen shows similarities to Klhl13´s phenotype, hinting that it could also mediate the increases in MAPK target gene expression at the chromatin level or otherwise through indirect regulation. Analysis of RNA-seq data in 1.8 XX vs XO cell lines showed that female cells expressed Zic3 at slightly lower levels than XO cells, however, a higher expression of this gene in female compared to male cells has been reported in other cell lines (Song et al., 2019).

Studies have shown that female cells harboring an heterozygous mutation for Zic3 display no significant decreases in pluripotency factor expression or faster differentiation kinetics (Song et al., 2019). However, this report drew the same conclusion about the heterozygous mutation of Dusp9 in female cells, which, as we show in the present work, leads to considerable additive effects in cells with a Klhl13 heterozygous mutant background. It is therefore possible that a further shift towards a male-like pluripotency phenotype could be observed in Dusp9, Klhl13 and Zic3 triple heterozygous female mESCs.

Stag2, on the other hand, is a member of the cohesin complex, which has been shown to modulate pluripotency factor expression through the establishment of long-range interactions between gene regulatory elements (Kagey et al., 2010). Recent studies, however, show that the dysregulation of pluripotency factor expression could be due to DNA damage caused by the absence of cohesin during DNA replication (Gupta et al., 2016). It would therefore be of interest to determine whether the effects of Stag2 on MAPK target gene and pluripotency factor expression are due to a global transcriptional dysregulation that could lead to confounding results.

A particularly interesting candidate is the Fthl17 gene cluster, which encodes seven ferritin-like proteins that lack ferroxidase activity and are partially located in the nucleus (Ruzzenenti et al., 2015). It is maternally imprinted and only expressed from the paternal X chromosome in female blastocysts, which is also observed in the higher expression patterns of Fthl17f and Fthl17e, the only two genes expressed from this cluster, in female mESCs (Kobayashi et al., 2010). Previous studies have reported that XmO blastocysts with a maternally inherited X chromosome develop in a similar rate compared to male blastocyst, whereas XpO blastocyst, whose X chromosome is paternally derived, develop much slower (Thornhill and Burgoyne, 1993). This points to a “retardation factor” expressed from the paternal X chromosome, which could be represented by the maternally imprinted Fthl17 cluster.

In summary, we have identified and validated two genes implicated in mediating sex differences in mESCs. However, given that female mESCs carrying a double heterozygous mutation for Klhl13 and Dusp9 do not fully recapitulate the male pluripotency phenotype, additional genes might be involved, the most promising candidate being the Fthl17 gene cluster.

6.5. Identified modulators of sex differences in mESCs and their potential roles in sex-specific stem cell therapies

This work uncovered several X-linked genes that, when present in a double dosage in female cells, lead to differences in their signaling and pluripotency state. These results could therefore possibly contribute to the development of future sex-specific stem cell therapies. Since a double dosage of the identified X-linked genes influences pluripotency factor expression in the undifferentiated state together with differentiation kinetics, it is likely that it also affects the efficiency of iPSC generation. Due to the fact that these genes also modulate the signaling strength of several pathways, it is likely that in vitro differentiation protocols for specific lineages would lead to different outcomes regarding cell fate determination in a sex-specific manner.

Human female-derived iPSCs and hPSCs retain their inactive X chromosome in culture, since they are thought to be found in a more primed state of pluripotency (Kim et al., 2014a; Silva et al., 2008). However, a phenomenon

called X chromosome erosion is often observed after several passages in vitro, where the lncRNA Xist becomes gradually silenced and the inactive X chromosome partially reactivated (Silva et al., 2008; Vallot et al., 2015). The eroded state of the inactive X chromosome is irreversible and is maintained throughout differentiation, potentially leading to sex differences in differentiation propensity (D'Antonio-Chronowska et al., 2019b, 2019a; Patel et al., 2017). Recently, culture conditions have been developed that lead to the reactivation of the inactive X chromosome by shifting hPSCs to a more naive state of pluripotency, as observed in pre-implantation blastocysts (Takashima et al., 2014; Theunissen et al., 2014). However, there are still marked differences between the in vivo and in vitro situation. For once, in vivo preimplantation blastocysts express Xist from both X chromosomes, even though this phenomenon does not lead to XCI (Okamoto et al., 2011; Petropoulos et al., 2016; Vallot et al., 2017). In contrast, the majority of hPSCs maintained in the so called "5iLAF" or "t2iL+Gö" medium express Xist from only one X chromosome, even though a small fraction of cells expresses Xist biallelically (Sahakyan et al., 2017; Vallot et al., 2017). Additionally, when induced to differentiate, the X chromosome that was previously silenced before reprogramming to the naive state will become inactivated anew during differentiation, making the process of XCI in this scenario non-random (Sahakyan et al., 2017). This absence of random X chromosome inactivation together with the inability to fully recapitulate the in vivo pre-implantation state in vitro points to the need of further optimization of the defined culture conditions for hPSCs.

The aforementioned phenomenon of X chromosome erosion in hPSCs induces, either fully or partially, the expression of X-linked genes in a double dosage in female cells, which could lead to sex differences concerning signaling and pluripotency states. This would also be the case if culture conditions are developed where full X chromosome reaction is achieved in female hPSCs. Thus, these sex-differences could, as mentioned previously, affect lineage-specific differentiation protocols in a sex-specific manner.

In conclusion, the current study has uncovered several X-linked genes that mediate sex differences in mESCs and that could play a role in sex-specific stem cell therapies. In general, sex differences between female and male individuals in the generation of human PSCs is an understudied phenomenon that deserves further investigation.

6.6. Identified MAPK pathway modulators in female mESCs and their potential roles in sex-specific cancer therapies

In this work, a primary CRISPR knockout screen was implemented for the identification of X-linked MAPK regulators by using a MAPK sensitive fluorescent reporter. The purpose of this screen was aimed at identifying MAPK inhibitors that would mediate the sex differences observed in mESCs. However, the MAPK pathway has been shown to be implicated in a myriad of cellular processes such as cell survival and its dysregulation has been linked to many diseases such as cancer (Roberts and Der, 2007). The results of the aforementioned primary screen could be therefore relevant for more clinical fields, such as sex-differences in cancer, a field that is gaining more attention in the past years. Indeed, it has been recently shown that X-linked escape genes might be involved in the protection of females against certain cancer types, such as Atrx, Cnksr2, Ddx3x, Kdm5c, Kdm6a and Magec3 (Dunford et al., 2017).

The primary screen implemented for the identification of X-linked genes modulating the MAPK signaling pathway revealed 9 putative MAPK inhibitors together with 18 activators. Among the identified MAPK inhibitors, only Dusp9 has been previously linked to the modulation of the pathway by dephosphorylating and subsequently inactivating Erk (Choi et al., 2017; Li et al., 2012; Song et al., 2019). The present study additionally validates the role of Klhl13 as a MAPK inhibitor acting primarily on target gene expression. It would be nevertheless of interest to study the involvement of the other identified genes in the inhibition of the MAPK signaling pathway and the molecular mechanisms leading to it.

On the other hand, several of the identified MAPK activators have been linked to the modulation of MAPK signaling, including Klf8, Eras, Pgk1 and Kdm6a. Klf8 has been known to activate Egfr in breast cancer, confirming its involvement as pathway activator (Li et al., 2015a). Eras knockdown, on the other hand, has been shown to lead to decreased levels of Erk phosphorylation and target gene expression in mESCs (Zhao et al., 2015), and a similar decrease of Erk phosphorylation has been observed upon Pgk1 knockdown in cancer cells (Zhou et al., 2019). Finally, the Erk pathway has been shown to be dysregulated in Kdm6a Knockout female mice (Kaneko and Li, 2018). Curiously, Kdm6a seems to play a role as a tumor suppressor and is frequently mutated in human cancers (Wang and Shilatifard, 2019). It would be therefore interesting to validate whether indeed the remaining putative MAPK activators represent novel modulators of the MAPK signaling pathway.

Dysregulation of XCI in cancer cells is a known albeit understudied phenomenon. Indeed, investigations from several decades ago identified the loss of the Barr body in breast cancer cells (Barr and Moore, 1957; Borah et al., 1980). An increase in X-chromosomal dosage in cancer cells has been reported since then due to loss of the inactive X, followed by duplication of the active X chromosome, as well as epigenetic instability and loss of silencing of the inactive X chromosome (Chaligné et al., 2015; Kawakami et al., 2004; Richardson et al., 2006; Sirchia et al., 2005). This rise in X-chromosomal dosage in female cancer cells could therefore lead to the dysregulation of the MAPK signaling pathway.

Indeed, several of the identified MAPK activators have been reported to play a role in cancer progression including Klf8, Eras, Nr0b1, Dkc1, Pgk1 and Rpl10 (He et al., 2019; Hou et al., 2019; Lahiri and Zhao, 2012; Oda et al., 2009; Shi et al., 2018; Sieron et al., 2009; Suárez-Cabrera et al., 2018). A contribution of the novel putative MAPK activators in cancer progression through the modulation of the MAPK signaling pathway could therefore be a subject of future study.

On the other hand, a tumor suppressor function has been attributed to the known Erk phosphatase Dusp9 (Liu et al., 2007). Additionally, dysregulation of Klhl13 expression has been linked with lower survival prediction in patients with Stage I-II laryngopharyngeal squamous cell carcinoma (Reddy et al., 2019). However, whether any of the remaining identified MAPK inhibitors might play a role in tumor suppression remains to be resolved in future works.

Overall, this work has uncovered several X-linked MAPK modulators, whose role in sex-specific cancer progression still remains largely unclear. These results might therefore help to better understand the sex biases observed in certain cancer types and contribute to future sex-specific cancer therapies.

6.7. Limitations of the study

The present work has uncovered several X-linked genes that could act collectively to modulate the female specific pluripotency phenotype. Female mESCs that carry heterozygous mutations for the two strongest hits, Klhl13 and Dusp9, display significant decreases in pluripotency factor expression together with higher levels of MAPK pathway activity, global CpG methylation and faster differentiation kinetics. However, these cells do not fully recapitulate the male pluripotency phenotype. Heterozygous mutation of other candidate genes in female D9K13-HET cells, such as the Fthl17 cluster, could induce a further shift towards the primed state of pluripotency. Still, other genes that were not identified in this study could be additionally involved in the observed sex differences.

First, pooled CRISPR Knockout screens are not able to target lncRNAs due to the fact that their effectiveness depends on the induction of frameshift mutations in protein-coding genes, which in the case of lncRNAs is not applicable, as they do not undergo translation. The X chromosome harbors around 100 annotated lncRNAs, whose contribution to the reported sex differences in mESCs cannot be excluded in the present work.

Additionally, combinatorial or synergistic effects of several genes cannot be identified by using CRISPR screens, where only one gene is perturbed individually in each cell. Therefore, in order to find genes that might work synergistically together with Dusp9 or Klhl13, the primary screen could be repeated by making use of the Dusp9/Klhl13 double heterozygous cell line instead of wildtype female mESCs. This would allow screening for additional X-linked genes that lead to small but additive effects in female mESCs.

This work made use of a primary CRISPR knockout screen in order to identify X-linked MAPK inhibitors, and a series of secondary CRISPR screens on the hits from the primary screen in order to find genes that would additionally modulate pluripotency factor expression and differentiation kinetics. However, some X-linked genes could affect pluripotency factor expression or differentiation kinetics without modulating the MAPK signaling pathway. For this, an additional knockout screen could be carried out using the 1.8 Nanog-mCherry cell line or the 1.8 Esrrb-mCherry cell line targeting all X-linked genes, where their effects on pluripotency factor expression and differentiation kinetics would be assessed.

Other signaling pathways, such as the Gsk3 or Akt signaling pathway, are known to modulate the pluripotency state. Gsk3 signaling leads to higher expression of primed pluripotency markers such as Fgf5 and Otx2, whereas Akt signaling positively affects the expression of naive pluripotency markers such as Nanog, Prdm14 and Tcl1 (Popkie et al. 2010; Storm et al. 2009; Watanabe et al. 2006). It is therefore possible that one or several X-linked genes could modulate either of these two signaling pathways, subsequently affecting pluripotency factor expression, yet without inducing strong effects on MAPK signaling. Since no changes in Gsk3 phosphorylation can be observed between female and male mESCs (Schulz et al. 2014), a Gsk3 reporter would have to be generated in order to implement a CRISPR screen targeting all X-linked genes for modulators of the Gsk3 signaling pathway. On the other hand, Akt phosphorylation is significantly higher in female mESCs, making the implementation of a pAkt staining readout feasible for the identification of X-linked Akt pathway activators (Schulz et al. 2014).

Regarding the identification of Klhl13 targets, the transient nature of its interacting partners makes their pull-down through protein tags quite challenging. This work made use of the proteasomal inhibitor MG132 in order to increase their stabilization and prevent their proteasomal degradation, however, the use of biotinylating enzymes for the identification of transient interactions is a popular alternative (Branon et al., 2018). Here, fusing the protein of interest with a promiscuous biotin ligase allows for the labeling of interacting proteins, which can be subsequently enriched through streptavidin-mediated pull-down (Branon et al., 2018). The later strategy was unsuccessful in the current work due to inefficient pull-down of biotinylated proteins, however, further optimization could help to identify target proteins that were not detected in the generated GFP Immunoprecipitation experiments due to transient interactions.

6.8. Outlook

During early embryonic development, female mammalian blastocysts develop more slowly compared to their male counterparts, which is reflected in the later exhibiting higher weights and reaching sooner more advanced developmental stages. It remains to be proven whether these sex specific differences arise from faster proliferation rates or faster differentiation kinetics (or both) exhibited by male/XO blastocysts. Indeed, it has recently been shown that XO mouse iPSCs display higher proliferation rates compared to female iPSCs (Song et al., 2019). It would be therefore important to determine, whether female blastocysts express higher levels of pluripotency factors specifically in the pre-implantation epiblast before the process of XCI has taken place, which would hint towards faster differentiation kinetics in males. This could be addressed by analysing single-cell RNA-seq data from female and male blastocysts during early development, which would allow for the identification of an epiblast population through specific markers genes, followed by analysis of pluripotency factor expression. However, ideally embryos from both sexes would be compared in the same litter. If it is proven that the epiblast

of female pre-implantation embryos indeed expresses higher levels of pluripotency factors, it would be of interest to see whether female embryos carrying heterozygous mutations for Dusp9 and Klhl13 display significantly reduced levels of the latter. In addition, one could assess whether these embryos reach certain developmental stages at faster rates, as observed for male blastocysts (Seller and Perkins-Cole, 1987; Tsunoda et al., 1985).

Differences in proliferation rates between 1.8 XX and XO mESCs were not assessed in this work. However, it would indeed be interesting to determine whether the observations reported in previous studies also apply for the cell lines used in this work, and additionally, whether D9K13-HET cells proliferate at faster rates compared to female wildtype mESCs. Nevertheless, the later might be unlikely due to the fact that none of the identified X-linked hits from the primary and secondary screens lead to slower proliferation rates in female mESCs (Fig. 27, see section 5.1.5). Additionally, differences in proliferation rates between XX and XO mESCs were routinetely observed during the generated experiments in this work, even though they were never quantified, with XO cells proliferating at faster rates. However, no differences were observed between XX wildtype cells and D9K13-HET mutants, further confirming the hypothesis that neither of these genes affects proliferation dynamics.

Our results from the primary CRISPR screen uncovered genes that affected mESC proliferation by comparing the sgRNA composition of the cloned plasmid library to the one from the input samples after seven days of expansion. sgRNAs targeting X-linked genes present in a double dosage in female mESCs that lead to decreased proliferation rates would accumulate after expansion, given the faster proliferation dynamics of the cells carrying these sgRNAs upon gene knockout. In this work, only one X-linked gene was identified that was significantly enriched in the input population after expansion: Olfr1321 (Fig. 27, see section 5.1.5). This gene encodes an olfactory receptor protein, which are members of a family of G-protein-coupled receptors (GPCR). It would be of interest to see whether Olfr1321 heterozygous female mESC mutants indeed display faster proliferation rates compared to their wildtype counterparts.

Having generated female cells that have the ability to downregulate pluripotency factors significantly faster during differentiation, such as the D9K13-HET mutants, it will now be possible to study in detail how the process of X chromosome inactivation is coupled to developmental progression. It has been previously hypothesized that the slow differentiation kinetics displayed by female cells are necessary for proper silencing of one of the two active x chromosomes, so that only cells that have effectively undergone the process of XCI will contribute to the adult organism (Schulz et al., 2014).

It has been proposed that Xist upregulation at the initiation of XCI should be a slow and stochastic process, which would allow the expression of Xist from only one of the two X chromosomes in female cells (Mutzel and Schulz 2020). This could be guaranteed by a tight regulation of the levels of Xist repressors such as Tsix or pluripotency factors (Oct4, Nanog, Rex1, etc). This process would be followed by the fast silencing of a trans-acting Xist activator, such as Rnf12, in order to prevent upregulation of Xist from the second X chromosome, which would lead to biallelic Xist expression in female cells (see section 1.4.2) (Mutzel and Schulz 2020). It has been indeed shown that reducing the amount of Xist repressors, either due to full Tsix loss or knockdown of the pluripotency factor Oct4, leads to a higher fraction of female mESCs expressing Xist biallelically (Donohoe et al., 2009; Lee, 2005). This is in accordance with other studies that have proven that the timing of Xist expression is crucial for proper XCI to occur, and that over early Xist upregulation through the lack of a cis acting Xist repressor leads to biallelic Xist upregulation (Mutzel et al., 2019).

Since D9K13-HET cells downregulate pluripotency factors significantly faster compared to female cells, it is likely that this reduction of Xist repressor levels could also lead to a higher fraction of cells expressing Xist biallelically. However, it has been shown that this state can be resolved by cells into monoallelic Xist expression through the silencing of a trans-acting Xist activator such as Rnf12 (Mutzel et al., 2019). Therefore, the consequences of this dysregulation remain obscure. A higher apoptosis rate in Tsix knockout cells has been reported in vitro, however,

in vivo studies in Tsix knockout embryos remain challenging due to their early embryonic lethality (Lee, 2005). If D9K13-HET mutants indeed display a higher portion of biallelically Xist expressing cells, it would be of interest to assess whether this would lead to a higher rate of apoptosis in the pre- or postimplantation epiblast.

Another interesting aspect for further study is whether the sex differences observed in mESCs and early mouse embryonic development are displayed by human PSCs and human embryos. The fact that both the primed state as well as the naïve state of hPSCs is maintained in culture through the use of MAPK modulators (Fgf2 and a Raf inhibitor, respectively), makes the assessment of sex differences in the undifferentiated state quite challenging. However, differences in differentiation kinetics starting from naïve culture conditions, where both X chromosomes are active, are now possible (Sahakyan et al., 2017; Vallot et al., 2017). If it is indeed the case that female hPSCs downregulate pluripotency factors slower compared to their male counterparts, it would be interesting to see whether these differences are also mediated through Klhl13 and Dusp9, among the other identified regulators.

7. Summary

Double X-chromosomal dosage leads to substantial sex differences during early development, before the process of X chromosome inactivation has occurred. Since these observations occur before fetal hormones are produced, they have been attributed to variations in X-chromosomal dosage. Sex differences can be also observed by using mESCs as an *in vitro* model, where female cells display lower levels of the differentiation-inducing MAPK signaling pathway leading to higher expression of pluripotency factors and slower differentiation kinetics and are therefore found in a more naïve state of pluripotency compared to their male counterparts. These effects are underlied by X-linked MAPK inhibitors present in a double dosage in female mESCs, whose identity, until now, has remained obscured.

We have therefore carried out a series of CRISPR knockout screens to identify the genes behind the female pluripotency phenotype, finding in an unbiased and high-throughput manner several genes that act together to shift female mESCs to a more naive state of pluripotency. Among these genes, we find the E3 ubiquitin ligase adaptor protein Klhl13, which induces higher pluripotency factor expression, slower differentiation kinetics and lower MAPK target gene expression (Fig. 50). Klhl13 acts together with Dusp9, a known Erk phosphatase and MAPK inhibitor, to mediate the sex differences observed in mESC, as double Klhl13 and Dusp9 heterozygous mutants qualitatively recapitulate the male pluripotency phenotype. Dusp9, however, seems to act primarily on the MAPK signaling pathway as an Erk phosphatase, as its effects on pluripotency factor expression and differentiation kinetics are considerably weaker compared to the effects mediated by Klhl13 (Fig. 50).

We have additionally determined, through Klhl13 pull-down experiments and proteomics profiling of Klhl13 homozygous mutants, several putative Klhl13 target proteins: Alg13, Scml2, Peg10, Larp1 and Cct3. Alg13 might represent a pluripotency-destabilizing factor, as it was found depleted in screens implemented for the identification of X-linked genes that increase pluripotency factor expression and lead to slower differentiation kinetics (Fig. 50). The role of the other putative candidates in mediating the effects observed in Klhl13 mutants remains, however, subject of further study.

We have thus identified several genes behind the sex differences observed in mESCs in an unbiased manner, and we have validated the top two candidates: Klhl13 and Dusp9 (Fig. 50). This work is the first to link Klhl13 to the modulation of pluripotency and to the sex differences observed in mESCs. Additionally, it has begun to shed some light into possible mechanisms through which Klhl13 might mediate the reported female pluripotency phenotype.

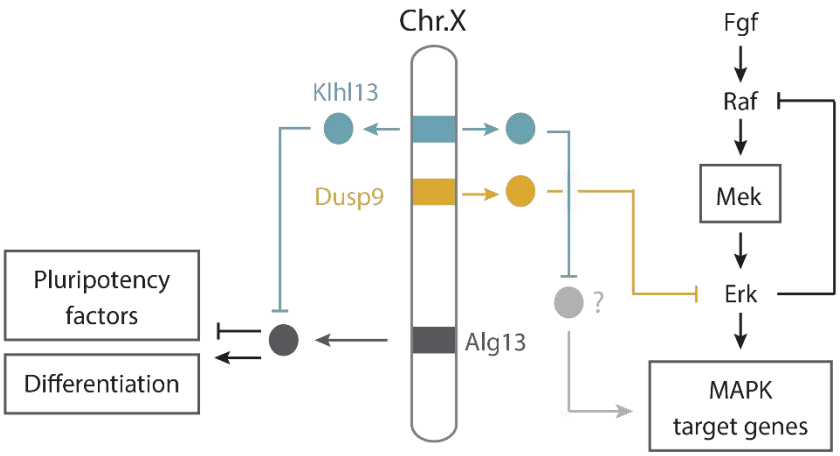

Figure 50. The female pluripotency phenotype is mediated through an additive effect of two key regulators: Klhl13 and Dusp9. Schematic representation of X-chromosomal dosage effects mediated by Klhl13 and Dusp9, leading to lower MAPK signaling levels, higher pluripotency factor expression and slower differentiation kinetics in female mESCs.

8. Zusammenfassung

Eine doppelte Dosis X-chromosomaler Genprodukte in weiblichen im Vergleich zu männlichen Zellen führt zu erheblichen Geschlechtsunterschieden in der frühen embryonalen Entwicklung, bevor der Prozess der X Chromosomen-Inaktivierung stattgefunden hat. Da dieses Phänomen vor der Produktion von fetalen Hormonen auftritt, resultiert es aus Variationen in der Dosierung des X Chromosomes. Geschlechtsunterschiede können auch bei der Verwendung von embryonalen Stammzellen der Maus (mES-Zellen) als In-vitro-Modell beobachtet werden, wobei weibliche Zellen ein niedrigeres Niveau des differenzierungsinduzierenden MAPK-Signalweges aufweisen, was zu einer höheren Expression von Pluripotenzfaktoren und einer langsameren Differenzierungskinetik führt. Sie befinden sich daher im Vergleich zu männlichen Zellen in einem naiveren Zustand der Pluripotenz. Diese Effekte werden durch X-chromosomal codierte MAPK-Inhibitoren untermauert, die in weiblichen mES-Zellen in doppelter Dosierung vorhanden sind und deren Identität bisher unbekannt war.

Wir haben daher eine Reihe von CRISPR Knockout Screens durchgeführt, um die Gene zu identifizieren, die hinter dem Phänotyp der weiblichen Pluripotenz stehen. Wir haben auf dieser Art unvoreingenommen und im Hochdurchsatz mehrere Gene identifiziert, die zusammenwirken, um weibliche mES-Zellen in einen naiveren Zustand der Pluripotenz zu versetzen. Eines dieser Gene codiert das E3-Ubiquitin-Ligase-Adaptor-Protein Klhl13, das eine höhere Expression von Pluripotenzfaktoren, eine langsamere Differenzierungskinetik und eine geringere Expression von MAPK-Zielgenen induziert. Klhl13 wirkt zusammen mit Dusp9, einem bekannten Erk-Phosphatase- und MAPK-Inhibitor, um die in mES-Zellen beobachteten Geschlechtsunterschiede zu vermitteln. Doppelte heterozygote Mutanten für Klhl13 und Dusp9 rekapitulieren also qualitativ den männlichen Pluripotenz-Phänotyp. Dusp9 scheint jedoch in erster Linie auf den MAPK-Signalweg zu wirken, da seine Auswirkungen auf die Expression von Pluripotenzfaktoren und die Differenzierungskinetik im Vergleich zu den durch Klhl13 vermittelten Effekten erheblich schwächer sind.

Zusätzlich haben wir durch Klhl13-Pulldown-Experimente und quantitative Massenspektrometrie von Klhl13-homozygoten Mutanten mehrere mutmaßliche Klhl13-Zielproteine bestimmt: Alg13, Scml2, Peg10, Larp1 und Cct3. Alg13 könnte einen Pluripotenz-destabilisierenden Faktor darstellen, da es in den hier durchgeführten Screens zur Identifizierung X-chromosomaler Gene, die die Expression von Pluripotenzfaktoren erhöhen und die Differenzierungskinetik verlangsamen, dezimiert war. Die Rolle der anderen mutmaßlichen Kandidaten bei der Vermittlung der in Klhl13-Mutanten beobachteten Effekte bleibt jedoch Gegenstand weiterer Untersuchungen.

Auf diese Weise haben wir unvoreingenommen mehrere Gene identifiziert, die die in mES-Zellen beobachteten Geschlechtsunterschieden vermitteln, und wir haben die beiden stärksten Kandidaten validiert: Klhl13 und Dusp9. Diese Arbeit ist die erste, die Klhl13 mit der Modulation der Pluripotenz und mit den in mES-Zellen beobachteten Geschlechtsunterschieden in Verbindung bringt. Darüber hinaus hat sie begonnen, die Mechanismen zu entschlüsseln, durch die Klhl13 den berichteten weiblichen Pluripotenz-Phänotyp vermitteln könnte.

9. References

Acampora, D., Di Giovannantonio, L.G., and Simeone, A. (2013). Otx2 is an intrinsic determinant of the embryonic stem cell state and is required for transition to a stable epiblast stem cell condition. Development *140*, 43–55.

Adan, A., Alizada, G., Kiraz, Y., Baran, Y., and Nalbant, A. (2017). Flow cytometry: basic principles and applications. Crit. Rev. Biotechnol. *37*, 163–176.

Afgan, E., Baker, D., van den Beek, M., Blankenberg, D., Bouvier, D., Čech, M., Chilton, J., Clements, D., Coraor, N., Eberhard, C., et al. (2016). The Galaxy platform for accessible, reproducible and collaborative biomedical analyses: 2016 update. Nucleic Acids Res. *44*, W3–W10.

Albritton, S.E., and Ercan, S. (2018). Caenorhabditis elegans Dosage Compensation: Insights into Condensin-Mediated Gene Regulation. Trends Genet. *34*, 41–53.

Alfarawati, S., Fragouli, E., Colls, P., Stevens, J., Gutiérrez-Mateo, C., Schoolcraft, W.B., Katz-Jaffe, M.G., and Wells, D. (2011). The relationship between blastocyst morphology, chromosomal abnormality, and embryo gender. Fertil. Steril. *95*, 520–524.

Arman, E., Haffner-Krausz, R., Chen, Y., Heath, J.K., and Lonai, P. (1998). Targeted disruption of fibroblast growth factor (FGF) receptor 2 suggests a role for FGF signaling in pregastrulation mammalian development. Proc Natl Acad Sci USA *95*, 5082–5087.

Augui, S., Nora, E.P., and Heard, E. (2011). Regulation of X-chromosome inactivation by the X-inactivation centre. Nat. Rev. Genet. *12*, 429–442.

Avery, B., Bak, A., and Schmidt, M. (1989). Differential cleavage rates and sex determination in bovine embryos. Theriogenology *32*, 139–147.

Avery, B., Madison, V., and Greve, T. (1991). Sex and development in bovine in-vitro fertilized embryos. Theriogenology *35*, 953–963.

Avilion, A.A., Nicolis, S.K., Pevny, L.H., Perez, L., Vivian, N., and Lovell-Badge, R. (2003). Multipotent cell lineages in early mouse development depend on SOX2 function. Genes Dev. *17*, 126–140.

Azami, T., Matsumoto, K., Jeon, H., Waku, T., Muratani, M., Niwa, H., Takahashi, S., and Ema, M. (2018). Klf5 suppresses ERK signaling in mouse pluripotent stem cells. PLoS ONE *13*, e0207321.

Baba, M., Furihata, M., Hong, S.-B., Tessarollo, L., Haines, D.C., Southon, E., Patel, V., Igarashi, P., Alvord, W.G., Leighty, R., et al. (2008). Kidney-targeted Birt-Hogg-Dube gene inactivation in a mouse model: Erk1/2 and Akt-mTOR activation, cell hyperproliferation, and polycystic kidneys. J Natl Cancer Inst *100*, 140–154.

Bao, S., Tang, F., Li, X., Hayashi, K., Gillich, A., Lao, K., and Surani, M.A. (2009). Epigenetic reversion of post-implantation epiblast to pluripotent embryonic stem cells. Nature *461*, 1292–1295.

Barakat, T.S., Gunhanlar, N., Pardo, C.G., Achame, E.M., Ghazvini, M., Boers, R., Kenter, A., Rentmeester, E., Grootegoed, J.A., and Gribnau, J. (2011). RNF12 activates Xist and is essential for X chromosome inactivation. PLoS Genet. *7*, e1002001.

Barakat, T.S., Loos, F., van Staveren, S., Myronova, E., Ghazvini, M., Grootegoed, J.A., and Gribnau, J. (2014). The trans-activator RNF12 and cis-acting elements effectuate X chromosome inactivation independent of X-pairing. Mol. Cell *53*, 965–978.

Barlow, P., Owen, D.A., and Graham, C. (1972). DNA synthesis in the preimplantation mouse embryo. J. Embryol. Exp. Morphol. *27*, 431–445.

Barr, M.L., and Bertram, E.G. (1949). A morphological distinction between neurones of the male and female, and the behaviour of the nucleolar satellite during accelerated nucleoprotein synthesis. Nature *163*, 676.

Barr, M.L., and Moore, K.L. (1957). Chromosomes, sex chromatin, and cancer. Proc. Can. Cancer Conf. *2*, 3–16.

Bedzhov, I., and Zernicka-Goetz, M. (2014). Self-organizing properties of mouse pluripotent cells initiate morphogenesis upon implantation. Cell *156*, 1032–1044.

Bélanger, L.-F., Roy, S., Tremblay, M., Brott, B., Steff, A.-M., Mourad, W., Hugo, P., Erikson, R., and Charron, J. (2003). Mek2 is dispensable for mouse growth and development. Mol. Cell. Biol. *23*, 4778–4787.

Berletch, J.B., Yang, F., and Disteche, C.M. (2010). Escape from X inactivation in mice and humans. Genome Biol. *11*, 213.

Betschinger, J., Nichols, J., Dietmann, S., Corrin, P.D., Paddison, P.J., and Smith, A. (2013). Exit from pluripotency is gated by intracellular redistribution of the bHLH transcription factor Tfe3. Cell *153*, 335–347.

Bissonauth, V., Roy, S., Gravel, M., Guillemette, S., and Charron, J. (2006). Requirement for Map2k1 (Mek1) in extra-embryonic ectoderm during placentogenesis. Development *133*, 3429–3440.

Bonasio, R., Lecona, E., Narendra, V., Voigt, P., Parisi, F., Kluger, Y., and Reinberg, D. (2014). Interactions with RNA direct the Polycomb group protein SCML2 to chromatin where it represses target genes. Elife *3*, e02637.

Borah, V., Shah, P.N., Ghosh, S.N., Sampat, M.B., and Jussawalla, D.J. (1980). Further studies on the prognostic importance of Barr body frequency in human breast cancer: with discussion on its probable mechanism. J. Surg. Oncol. *13*, 1–7.

Borensztein, M., Syx, L., Ancelin, K., Diabangouaya, P., Picard, C., Liu, T., Liang, J.-B., Vassilev, I., Galupa, R., Servant, N., et al. (2017a). Xist-dependent imprinted X inactivation and the early developmental consequences of its failure. Nat. Struct. Mol. Biol. *24*, 226–233.

Borensztein, M., Okamoto, I., Syx, L., Guilbaud, G., Picard, C., Ancelin, K., Galupa, R., Diabangouaya, P., Servant, N., Barillot, E., et al. (2017b). Contribution of epigenetic landscapes and transcription factors to X-chromosome reactivation in the inner cell mass. Nat. Commun. *8*, 1297.

Boroviak, T., Loos, R., Lombard, P., Okahara, J., Behr, R., Sasaki, E., Nichols, J., Smith, A., and Bertone, P. (2015). Lineage-Specific Profiling Delineates the Emergence and Progression of Naive Pluripotency in Mammalian Embryogenesis. Dev. Cell *35*, 366–382.

Borsani, G., Tonlorenzi, R., Simmler, M.C., Dandolo, L., Arnaud, D., Capra, V., Grompe, M., Pizzuti, A., Muzny, D., Lawrence, C., et al. (1991). Characterization of a murine gene expressed from the inactive X chromosome. Nature *351*, 325–329.

Bousard, A., Raposo, A.C., Zylicz, J.J., Picard, C., Pires, V.B., Qi, Y., Syx, L., Chang, H.Y., Heard, E., and da Rocha, S.T. (2018). Exploring the role of Polycomb recruitment in Xist-mediated silencing of the X chromosome in ES cells. BioRxiv.

Boyer, L.A., Lee, T.I., Cole, M.F., Johnstone, S.E., Levine, S.S., Zucker, J.P., Guenther, M.G., Kumar, R.M., Murray, H.L., Jenner, R.G., et al. (2005). Core transcriptional regulatory circuitry in human embryonic stem cells. Cell *122*, 947–956.

Branon, T.C., Bosch, J.A., Sanchez, A.D., Udeshi, N.D., Svinkina, T., Carr, S.A., Feldman, J.L., Perrimon, N., and Ting, A.Y. (2018). Efficient proximity labeling in living cells and organisms with TurboID. Nat. Biotechnol. *36*, 880–887.

Brockdorff, N. (2017). Polycomb complexes in X chromosome inactivation. Philos. Trans. R. Soc. Lond. B. Biol. Sci *372*.

Brockdorff, N., Ashworth, A., Kay, G.F., Cooper, P., Smith, S., McCabe, V.M., Norris, D.P., Penny, G.D., Patel, D., and Rastan, S. (1991). Conservation of position and exclusive expression of mouse Xist from the inactive X chromosome. Nature *351*, 329–331.

Brockdorff, N., Ashworth, A., Kay, G.F., McCabe, V.M., Norris, D.P., Cooper, P.J., Swift, S., and Rastan, S. (1992). The product of the mouse Xist gene is a 15 kb inactive X-specific transcript containing no conserved ORF and located in the nucleus. Cell *71*, 515–526.

Brons, I.G.M., Smithers, L.E., Trotter, M.W.B., Rugg-Gunn, P., Sun, B., Chuva de Sousa Lopes, S.M., Howlett, S.K., Clarkson, A., Ahrlund-Richter, L., Pedersen, R.A., et al. (2007). Derivation of pluripotent epiblast stem cells from mammalian embryos. Nature *448*, 191–195.

Brown, S.D. (1991). XIST and the mapping of the X chromosome inactivation centre. Bioessays *13*, 607–612.

Brown, C.J., Hendrich, B.D., Rupert, J.L., Lafrenière, R.G., Xing, Y., Lawrence, J., and Willard, H.F. (1992). The human XIST gene: analysis of a 17 kb inactive X-specific RNA that contains conserved repeats and is highly localized within the nucleus. Cell *71*, 527–542.

Brummer, T., Naegele, H., Reth, M., and Misawa, Y. (2003). Identification of novel ERK-mediated feedback phosphorylation sites at the C-terminus of B-Raf. Oncogene *22*, 8823–8834.

Buecker, C., Srinivasan, R., Wu, Z., Calo, E., Acampora, D., Faial, T., Simeone, A., Tan, M., Swigut, T., and Wysocka, J. (2014). Reorganization of enhancer patterns in transition from naive to primed pluripotency. Cell Stem Cell *14*, 838–853.

Burdon, T., Stracey, C., Chambers, I., Nichols, J., and Smith, A. (1999). Suppression of SHP-2 and ERK signalling promotes self-renewal of mouse embryonic stem cells. Dev. Biol. *210*, 30–43.

Burgar, H.R., Burns, H.D., Elsden, J.L., Lalioti, M.D., and Heath, J.K. (2002). Association of the signaling adaptor FRS2 with fibroblast growth factor receptor 1 (Fgfr1) is mediated by alternative splicing of the juxtamembrane domain. J. Biol. Chem. *277*, 4018–4023.

Burgoyne, P.S., Thornhill, A.R., Boudrean, S.K., Darling, S.M., Bishop, C.E., and Evans, E.P. (1995). The genetic basis of XX-XY differences present before gonadal sex differentiation in the mouse. Philos. Trans. R. Soc. Lond. B. Biol. Sci *350*, 253-60 discussion 260.

Cacalano, N.A., Sanden, D., and Johnston, J.A. (2001). Tyrosine-phosphorylated SOCS-3 inhibits STAT activation but binds to p120 RasGAP and activates Ras. Nat. Cell Biol. *3*, 460–465.

Campeau, E., Ruhl, V.E., Rodier, F., Smith, C.L., Rahmberg, B.L., Fuss, J.O., Campisi, J., Yaswen, P., Cooper, P.K., and Kaufman, P.D. (2009). A versatile viral system for expression and depletion of proteins in mammalian cells. PLoS ONE *4*, e6529.

Carmona, S., Lin, B., Chou, T., Arroyo, K., and Sun, S. (2018). LncRNA Jpx induces Xist expression in mice using both trans and cis mechanisms. PLoS Genet. *14*, e1007378.

Carrel, L., and Willard, H.F. (2005). X-inactivation profile reveals extensive variability in X-linked gene expression in females. Nature *434*, 400–404.

Carroll, D. (2017). Genome editing: past, present, and future. Yale J. Biol. Med. *90*, 653–659.

Casci, T., Vinós, J., and Freeman, M. (1999). Sprouty, an intracellular inhibitor of Ras signaling. Cell *96*, 655–665.

Cash, T.P., Gruber, J.J., Hartman, T.R., Henske, E.P., and Simon, M.C. (2011). Loss of the Birt-Hogg-Dubé tumor suppressor results in apoptotic resistance due to aberrant TGFβ-mediated transcription. Oncogene *30*, 2534–2546.

Caunt, C.J., and Keyse, S.M. (2013). Dual-specificity MAP kinase phosphatases (MKPs): shaping the outcome of MAP kinase signalling. FEBS J. *280*, 489–504.

Chaligné, R., Popova, T., Mendoza-Parra, M.-A., Saleem, M.-A.M., Gentien, D., Ban, K., Piolot, T., Leroy, O., Mariani, O., Gronemeyer, H., et al. (2015). The inactive X chromosome is epigenetically unstable and transcriptionally labile in breast cancer. Genome Res. *25*, 488–503.

Chambers, I., Colby, D., Robertson, M., Nichols, J., Lee, S., Tweedie, S., and Smith, A. (2003). Functional expression cloning of Nanog, a pluripotency sustaining factor in embryonic stem cells. Cell *113*, 643–655.

Chambers, I., Silva, J., Colby, D., Nichols, J., Nijmeijer, B., Robertson, M., Vrana, J., Jones, K., Grotewold, L., and Smith, A. (2007). Nanog safeguards pluripotency and mediates germline development. Nature *450*, 1230–1234.

Chaumeil, J., Le Baccon, P., Wutz, A., and Heard, E. (2006). A novel role for Xist RNA in the formation of a repressive nuclear compartment into which genes are recruited when silenced. Genes Dev. *20*, 2223–2237.

Chaumeil, J., Augui, S., Chow, J.C., and Heard, E. (2008). Combined immunofluorescence, RNA fluorescent in situ hybridization, and DNA fluorescent in situ hybridization to study chromatin changes, transcriptional activity, nuclear organization, and X-chromosome inactivation. Methods Mol. Biol. *463*, 297–308.

Chazaud, C., Yamanaka, Y., Pawson, T., and Rossant, J. (2006). Early lineage segregation between epiblast and primitive endoderm in mouse blastocysts through the Grb2-MAPK pathway. Dev. Cell *10*, 615–624.

Cheng, A.M., Saxton, T.M., Sakai, R., Kulkarni, S., Mbamalu, G., Vogel, W., Tortorice, C.G., Cardiff, R.D., Cross, J.C., Muller, W.J., et al. (1998). Mammalian Grb2 regulates multiple steps in embryonic development and malignant transformation. Cell *95*, 793–803.

Cheng, S., Pei, Y., He, L., Peng, G., Reinius, B., Tam, P.P.L., Jing, N., and Deng, Q. (2019). Single-Cell RNA-Seq Reveals Cellular Heterogeneity of Pluripotency Transition and X Chromosome Dynamics during Early Mouse Development. Cell Rep. *26*, 2593-2607.e3.

Cheng, Y., Chen, G., Martinka, M., Ho, V., and Li, G. (2013). Prognostic significance of Fbw7 in human melanoma and its role in cell migration. J. Invest. Dermatol. *133*, 1794–1802.

Chen, B., Gilbert, L.A., Cimini, B.A., Schnitzbauer, J., Zhang, W., Li, G.-W., Park, J., Blackburn, E.H., Weissman, J.S., Qi, L.S., et al. (2013). Dynamic imaging of genomic loci in living human cells by an optimized CRISPR/Cas system. Cell *155*, 1479–1491.

Chen, T., Ueda, Y., Dodge, J.E., Wang, Z., and Li, E. (2003). Establishment and maintenance of genomic methylation patterns in mouse embryonic stem cells by Dnmt3a and Dnmt3b. Mol. Cell. Biol. *23*, 5594–5605.

Chen, X., Xu, H., Yuan, P., Fang, F., Huss, M., Vega, V.B., Wong, E., Orlov, Y.L., Zhang, W., Jiang, J., et al. (2008). Integration of external signaling pathways with the core transcriptional network in embryonic stem cells. Cell *133*, 1106–1117.

Choi, J., Clement, K., Huebner, A.J., Webster, J., Rose, C.M., Brumbaugh, J., Walsh, R.M., Lee, S., Savol, A., Etchegaray, J.-P., et al. (2017). DUSP9 modulates DNA hypomethylation in female mouse pluripotent stem cells. Cell Stem Cell *20*, 706-719.e7.

Chow, J.C., Hall, L.L., Baldry, S.E.L., Thorogood, N.P., Lawrence, J.B., and Brown, C.J. (2007). Inducible XIST-dependent X-chromosome inactivation in human somatic cells is reversible. Proc Natl Acad Sci USA *104*, 10104–10109.

Cho, S.W., Kim, S., Kim, J.M., and Kim, J.-S. (2013). Targeted genome engineering in human cells with the Cas9 RNA-guided endonuclease. Nat. Biotechnol. *31*, 230–232.

Chureau, C., Chantalat, S., Romito, A., Galvani, A., Duret, L., Avner, P., and Rougeulle, C. (2011). Ftx is a non-coding RNA which affects Xist expression and chromatin structure within the X-inactivation center region. Hum. Mol. Genet. *20*, 705–718.

Chu, C., Zhang, Q.C., da Rocha, S.T., Flynn, R.A., Bharadwaj, M., Calabrese, J.M., Magnuson, T., Heard, E., and Chang, H.Y. (2015). Systematic discovery of Xist RNA binding proteins. Cell *161*, 404–416.

Clemson, C.M., McNeil, J.A., Willard, H.F., and Lawrence, J.B. (1996). XIST RNA paints the inactive X chromosome at interphase: evidence for a novel RNA involved in nuclear/chromosome structure. J. Cell Biol. *132*, 259–275.

Colognori, D., Sunwoo, H., Kriz, A.J., Wang, C.-Y., and Lee, J.T. (2019). Xist Deletional Analysis Reveals an Interdependency between Xist RNA and Polycomb Complexes for Spreading along the Inactive X. Mol. Cell *74*, 101-117.e10.

Cong, L., Ran, F.A., Cox, D., Lin, S., Barretto, R., Habib, N., Hsu, P.D., Wu, X., Jiang, W., Marraffini, L.A., et al. (2013). Multiplex genome engineering using CRISPR/Cas systems. Science *339*, 819–823.

Costanzi, C., and Pehrson, J.R. (1998). Histone macroH2A1 is concentrated in the inactive X chromosome of female mammals. Nature *393*, 599–601.

D'Antonio-Chronowska, A., Donovan, M.K.R., Benaglio, P., Greenwald, W.W., Ward, M.C., Matsui, H., Fujita, K., Hashem, S., Soncin, F., Parast, M., et al. (2019a). Human iPSC gene signatures and X chromosome dosage impact response to WNT inhibition and cardiac differentiation fate. BioRxiv.

D'Antonio-Chronowska, A., Donovan, M.K.R., Young Greenwald, W.W., Nguyen, J.P., Fujita, K., Hashem, S., Matsui, H., Soncin, F., Parast, M., Ward, M.C., et al. (2019b). Association of Human iPSC Gene Signatures and X Chromosome Dosage with Two Distinct Cardiac Differentiation Trajectories. Stem Cell Reports *13*, 924–938.

Declercq, J., Sheshadri, P., Verfaillie, C.M., and Kumar, A. (2013). Zic3 enhances the generation of mouse induced pluripotent stem cells. Stem Cells Dev. *22*, 2017–2025.

Deng, X., Berletch, J.B., Nguyen, D.K., and Disteche, C.M. (2014). X chromosome regulation: diverse patterns in development, tissues and disease. Nat. Rev. Genet. *15*, 367–378.

DeWitt, M.A., Corn, J.E., and Carroll, D. (2017). Genome editing via delivery of Cas9 ribonucleoprotein. Methods *121–122*, 9–15.

Dhaliwal, N.K., Miri, K., Davidson, S., Tamim El Jarkass, H., and Mitchell, J.A. (2018). KLF4 Nuclear Export Requires ERK Activation and Initiates Exit from Naive Pluripotency. Stem Cell Reports *10*, 1308–1323.

Dhanoa, B.S., Cogliati, T., Satish, A.G., Bruford, E.A., and Friedman, J.S. (2013). Update on the Kelch-like (KLHL) gene family. Hum Genomics *7*, 13.

Diaz, A.A., Qin, H., Ramalho-Santos, M., and Song, J.S. (2015). HiTSelect: a comprehensive tool for high-complexity-pooled screen analysis. Nucleic Acids Res. *43*, e16.

Dickinson, R.J., and Keyse, S.M. (2006). Diverse physiological functions for dual-specificity MAP kinase phosphatases. J. Cell Sci. *119*, 4607–4615.

Dickinson, R.J., Williams, D.J., Slack, D.N., Williamson, J., Seternes, O.-M., and Keyse, S.M. (2002). Characterization of a murine gene encoding a developmentally regulated cytoplasmic dual-specificity mitogen-activated protein kinase phosphatase. Biochem. J. *364*, 145–155.

Disteche, C.M. (2012). Dosage compensation of the sex chromosomes. Annu. Rev. Genet. *46*, 537–560.

Disteche, C.M. (2016). Dosage compensation of the sex chromosomes and autosomes. Semin. Cell Dev. Biol. *56*, 9–18.

Disteche, C.M., and Berletch, J.B. (2015). X-chromosome inactivation and escape. J. Genet. *94*, 591–599.

Dixon-McDougall, T., and Brown, C. (2016). The making of a Barr body: the mosaic of factors that eXIST on the mammalian inactive X chromosome. Biochem. Cell Biol. *94*, 56–70.

Dobin, A., Davis, C.A., Schlesinger, F., Drenkow, J., Zaleski, C., Jha, S., Batut, P., Chaisson, M., and Gingeras, T.R. (2013). STAR: ultrafast universal RNA-seq aligner. Bioinformatics *29*, 15–21.

Donohoe, M.E., Silva, S.S., Pinter, S.F., Xu, N., and Lee, J.T. (2009). The pluripotency factor Oct4 interacts with Ctcf and also controls X-chromosome pairing and counting. Nature *460*, 128–132.

Dossin, F., Pinheiro, I., Żylicz, J.J., Roensch, J., Collombet, S., Le Saux, A., Chelmicki, T., Attia, M., Kapoor, V., Zhan, Y., et al. (2020). SPEN integrates transcriptional and epigenetic control of X-inactivation. Nature *578*, 455–460.

Dull, T., Zufferey, R., Kelly, M., Mandel, R.J., Nguyen, M., Trono, D., and Naldini, L. (1998). A third-generation lentivirus vector with a conditional packaging system. J. Virol. *72*, 8463–8471.

Dunford, A., Weinstock, D.M., Savova, V., Schumacher, S.E., Cleary, J.P., Yoda, A., Sullivan, T.J., Hess, J.M., Gimelbrant, A.A., Beroukhim, R., et al. (2017). Tumor-suppressor genes that escape from X-inactivation contribute to cancer sex bias. Nat. Genet. *49*, 10–16.

Dunn, S.J., Martello, G., Yordanov, B., Emmott, S., and Smith, A.G. (2014). Defining an essential transcription factor program for naïve pluripotency. Science *344*, 1156–1160.

Eblen, S.T., Slack-Davis, J.K., Tarcsafalvi, A., Parsons, J.T., Weber, M.J., and Catling, A.D. (2004). Mitogen-activated protein kinase feedback phosphorylation regulates MEK1 complex formation and activation during cellular adhesion. Mol. Cell. Biol. *24*, 2308–2317.

Eferl, R., and Wagner, E.F. (2003). AP-1: a double-edged sword in tumorigenesis. Nat. Rev. Cancer *3*, 859–868.

El-Brolosy, M.A., and Stainier, D.Y.R. (2017). Genetic compensation: A phenomenon in search of mechanisms. PLoS Genet. *13*, e1006780.

Elshire, R.J., Glaubitz, J.C., Sun, Q., Poland, J.A., Kawamoto, K., Buckler, E.S., and Mitchell, S.E. (2011). A robust, simple genotyping-by-sequencing (GBS) approach for high diversity species. PLoS ONE *6*, e19379.

Evans, M.J., and Kaufman, M.H. (1981). Establishment in culture of pluripotential cells from mouse embryos. Nature *292*, 154–156.

Evers, B., Jastrzebski, K., Heijmans, J.P.M., Grernrum, W., Beijersbergen, R.L., and Bernards, R. (2016). CRISPR knockout screening outperforms shRNA and CRISPRi in identifying essential genes. Nat. Biotechnol. *34*, 631–633.

Fang, L., Zhang, L., Wei, W., Jin, X., Wang, P., Tong, Y., Li, J., Du, J.X., and Wong, J. (2014). A methylation-phosphorylation switch determines Sox2 stability and function in ESC maintenance or differentiation. Mol. Cell *55*, 537–551.

Feldman, B., Poueymirou, W., Papaioannou, V.E., DeChiara, T.M., and Goldfarb, M. (1995). Requirement of FGF-4 for postimplantation mouse development. Science *267*, 246–249.

Ferguson-Smith, A.C. (2011). Genomic imprinting: the emergence of an epigenetic paradigm. Nat. Rev. Genet. *12*, 565–575.

Ficz, G., Hore, T.A., Santos, F., Lee, H.J., Dean, W., Arand, J., Krueger, F., Oxley, D., Paul, Y.-L., Walter, J., et al. (2013). FGF signaling inhibition in ESCs drives rapid genome-wide demethylation to the epigenetic ground state of pluripotency. Cell Stem Cell *13*, 351–359.

Fiddler, M., Abdel-Rahman, B., Rappolee, D.A., and Pergament, E. (1995). Expression of SRY transcripts in preimplantation human embryos. Am. J. Med. Genet. *55*, 80–84.

Fritsche-Guenther, R., Witzel, F., Sieber, A., Herr, R., Schmidt, N., Braun, S., Brummer, T., Sers, C., and Blüthgen, N. (2011). Strong negative feedback from Erk to Raf confers robustness to MAPK signalling. Mol. Syst. Biol. *7*, 489.

Fujii, S., Nishikawa-Torikai, S., Futatsugi, Y., Toyooka, Y., Yamane, M., Ohtsuka, S., and Niwa, H. (2015). Nr0b1 is a negative regulator of Zscan4c in mouse embryonic stem cells. Sci. Rep. *5*, 9146.

Fukada, T., Hibi, M., Yamanaka, Y., Takahashi-Tezuka, M., Fujitani, Y., Yamaguchi, T., Nakajima, K., and Hirano, T. (1996). Two signals are necessary for cell proliferation induced by a cytokine receptor gp130: involvement of STAT3 in anti-apoptosis. Immunity *5*, 449–460.

Furlan, G., Gutierrez Hernandez, N., Huret, C., Galupa, R., van Bemmel, J.G., Romito, A., Heard, E., Morey, C., and Rougeulle, C. (2018). The ftx noncoding locus controls X chromosome inactivation independently of its RNA products. Mol. Cell *70*, 462-472.e8.

Galan-Caridad, J.M., Harel, S., Arenzana, T.L., Hou, Z.E., Doetsch, F.K., Mirny, L.A., and Reizis, B. (2007). Zfx controls the self-renewal of embryonic and hematopoietic stem cells. Cell *129*, 345–357.

Galupa, R., and Heard, E. (2018). X-Chromosome Inactivation: A Crossroads Between Chromosome Architecture and Gene Regulation. Annu. Rev. Genet. *52*, 535–566.

Gao, X.-D., Tachikawa, H., Sato, T., Jigami, Y., and Dean, N. (2005). Alg14 recruits Alg13 to the cytoplasmic face of the endoplasmic reticulum to form a novel bipartite UDP-N-acetylglucosamine transferase required for the second step of N-linked glycosylation. J. Biol. Chem. *280*, 36254–36262.

Gendrel, A.-V., and Heard, E. (2014). Noncoding RNAs and epigenetic mechanisms during X-chromosome inactivation. Annu. Rev. Cell Dev. Biol. *30*, 561–580.

Gendrel, A.-V., Apedaile, A., Coker, H., Termanis, A., Zvetkova, I., Godwin, J., Tang, Y.A., Huntley, D., Montana, G., Taylor, S., et al. (2012). Smchd1-dependent and -independent pathways determine developmental dynamics of CpG island methylation on the inactive X chromosome. Dev. Cell *23*, 265–279.

Gilbert, S.F. (2000). Developmental Biology.

Gilbert, L.A., Horlbeck, M.A., Adamson, B., Villalta, J.E., Chen, Y., Whitehead, E.H., Guimaraes, C., Panning, B., Ploegh, H.L., Bassik, M.C., et al. (2014). Genome-scale CRISPR-mediated control of gene repression and activation. Cell *159*, 647–661.

Gille, H., Kortenjann, M., Thomae, O., Moomaw, C., Slaughter, C., Cobb, M.H., and Shaw, P.E. (1995). ERK phosphorylation potentiates Elk-1-mediated ternary complex formation and transactivation. EMBO J. *14*, 951–962.

Girardot, C., Scholtalbers, J., Sauer, S., Su, S.-Y., and Furlong, E.E.M. (2016). Je, a versatile suite to handle multiplexed NGS libraries with unique molecular identifiers. BMC Bioinformatics *17*, 419.

Goldin, S.N., and Papaioannou, V.E. (2003). Paracrine action of FGF4 during periimplantation development maintains trophectoderm and primitive endoderm. Genesis *36*, 40–47.

Gontan, C., Achame, E.M., Demmers, J., Barakat, T.S., Rentmeester, E., van IJcken, W., Grootegoed, J.A., and Gribnau, J. (2012). RNF12 initiates X-chromosome inactivation by targeting REX1 for degradation. Nature *485*, 386–390.

Gontan, C., Mira-Bontenbal, H., Magaraki, A., Dupont, C., Barakat, T.S., Rentmeester, E., Demmers, J., and Gribnau, J. (2018). REX1 is the critical target of RNF12 in imprinted X chromosome inactivation in mice. Nat. Commun. *9*, 4752.

Gotoh, N. (2008). Regulation of growth factor signaling by FRS2 family docking/scaffold adaptor proteins. Cancer Sci. *99*, 1319–1325.

Grabole, N., Tischler, J., Hackett, J.A., Kim, S., Tang, F., Leitch, H.G., Magnúsdóttir, E., and Surani, M.A. (2013). Prdm14 promotes germline fate and naive pluripotency by repressing FGF signalling and DNA methylation. EMBO Rep. *14*, 629–637.

Grant, J., Mahadevaiah, S.K., Khil, P., Sangrithi, M.N., Royo, H., Duckworth, J., McCarrey, J.R., VandeBerg, J.L., Renfree, M.B., Taylor, W., et al. (2012). Rsx is a metatherian RNA with Xist-like properties in X-chromosome inactivation. Nature *487*, 254–258.

Guo, G., Yang, J., Nichols, J., Hall, J.S., Eyres, I., Mansfield, W., and Smith, A. (2009). Klf4 reverts developmentally programmed restriction of ground state pluripotency. Development *136*, 1063–1069.

Guo, G., Huss, M., Tong, G.Q., Wang, C., Li Sun, L., Clarke, N.D., and Robson, P. (2010). Resolution of cell fate decisions revealed by single-cell gene expression analysis from zygote to blastocyst. Dev. Cell *18*, 675–685.

Gupta, P., Lavagnolli, T., Mira-Bontenbal, H., Fisher, A.G., and Merkenschlager, M. (2016). Cohesin's role in pluripotency and reprogramming. Cell Cycle *15*, 324–330.

Habibi, E., Brinkman, A.B., Arand, J., Kroeze, L.I., Kerstens, H.H.D., Matarese, F., Lepikhov, K., Gut, M., Brun-Heath, I., Hubner, N.C., et al. (2013). Whole-genome bisulfite sequencing of two distinct interconvertible DNA methylomes of mouse embryonic stem cells. Cell Stem Cell *13*, 360–369.

Hackett, J.A., Dietmann, S., Murakami, K., Down, T.A., Leitch, H.G., and Surani, M.A. (2013). Synergistic mechanisms of DNA demethylation during transition to ground-state pluripotency. Stem Cell Reports *1*, 518–531.

Haglund, K., and Dikic, I. (2005). Ubiquitylation and cell signaling. EMBO J. *24*, 3353–3359.

Hanafusa, H., Torii, S., Yasunaga, T., and Nishida, E. (2002). Sprouty1 and Sprouty2 provide a control mechanism for the Ras/MAPK signalling pathway. Nat. Cell Biol. *4*, 850–858.

Hasegawa, K., Sin, H.-S., Maezawa, S., Broering, T.J., Kartashov, A.V., Alavattam, K.G., Ichijima, Y., Zhang, F., Bacon, W.C., Greis, K.D., et al. (2015). SCML2 establishes the male germline epigenome through regulation of histone H2A ubiquitination. Dev. Cell *32*, 574–588.

Hasegawa, Y., Brockdorff, N., Kawano, S., Tsutui, K., Tsutui, K., and Nakagawa, S. (2010). The matrix protein hnRNP U is required for chromosomal localization of Xist RNA. Dev. Cell *19*, 469–476.

Hatano, N., Mori, Y., Oh-hora, M., Kosugi, A., Fujikawa, T., Nakai, N., Niwa, H., Miyazaki, J., Hamaoka, T., and Ogata, M. (2003). Essential role for ERK2 mitogen-activated protein kinase in placental development. Genes Cells *8*, 847–856.

Heigwer, F., Zhan, T., Breinig, M., Winter, J., Brügemann, D., Leible, S., and Boutros, M. (2016). CRISPR library designer (CLD): software for multispecies design of single guide RNA libraries. Genome Biol. *17*, 55.

Hein, M.Y., Hubner, N.C., Poser, I., Cox, J., Nagaraj, N., Toyoda, Y., Gak, I.A., Weisswange, I., Mansfeld, J., Buchholz, F., et al. (2015). A human interactome in three quantitative dimensions organized by stoichiometries and abundances. Cell *163*, 712–723.

Hermann, A., Goyal, R., and Jeltsch, A. (2004). The Dnmt1 DNA-(cytosine-C5)-methyltransferase methylates DNA processively with high preference for hemimethylated target sites. J. Biol. Chem. *279*, 48350–48359.

Hershko, A., and Ciechanover, A. (1998). The ubiquitin system. Annu. Rev. Biochem. *67*, 425–479.

Heurtier, V., Owens, N., Gonzalez, I., Mueller, F., Proux, C., Mornico, D., Clerc, P., Dubois, A., and Navarro, P. (2019). The molecular logic of Nanog-induced self-renewal in mouse embryonic stem cells. Nat. Commun. *10*, 1109.

He, Y., Luo, Y., Zhang, D., Wang, X., Zhang, P., Li, H., Ejaz, S., and Liang, S. (2019). PGK1-mediated cancer progression and drug resistance. Am. J. Cancer Res. *9*, 2280–2302.

Hodge, C., Liao, J., Stofega, M., Guan, K., Carter-Su, C., and Schwartz, J. (1998). Growth hormone stimulates phosphorylation and activation of elk-1 and expression of c-fos, egr-1, and junB through activation of extracellular signal-regulated kinases 1 and 2. J. Biol. Chem. *273*, 31327–31336.

Horlbeck, M.A., Gilbert, L.A., Villalta, J.E., Adamson, B., Pak, R.A., Chen, Y., Fields, A.P., Park, C.Y., Corn, J.E., Kampmann, M., et al. (2016). Compact and highly active next-generation libraries for CRISPR-mediated gene repression and activation. Elife *5*.

Horvath, P., and Barrangou, R. (2010). CRISPR/Cas, the immune system of bacteria and archaea. Science *327*, 167–170.

Hosoi, Y., Soma, M., Shiura, H., Sado, T., Hasuwa, H., Abe, K., Kohda, T., Ishino, F., and Kobayashi, S. (2018). Female mice lacking Ftx lncRNA exhibit impaired X-chromosome inactivation and a microphthalmia-like phenotype. Nat. Commun. *9*, 3829.

Hou, P., Shi, P., Jiang, T., Yin, H., Chu, S., Shi, M., Bai, J., and Song, J. (2019). DKC1 enhances angiogenesis by promoting HIF-1α transcription and facilitates metastasis in colorectal cancer. Br. J. Cancer.

Hsu, P.D., Scott, D.A., Weinstein, J.A., Ran, F.A., Konermann, S., Agarwala, V., Li, Y., Fine, E.J., Wu, X., Shalem, O., et al. (2013). DNA targeting specificity of RNA-guided Cas9 nucleases. Nat. Biotechnol. *31*, 827–832.

Huang, Y., Osorno, R., Tsakiridis, A., and Wilson, V. (2012). In Vivo differentiation potential of epiblast stem cells revealed by chimeric embryo formation. Cell Rep. *2*, 1571–1578.

Hubner, N.C., Bird, A.W., Cox, J., Splettstoesser, B., Bandilla, P., Poser, I., Hyman, A., and Mann, M. (2010). Quantitative proteomics combined with BAC TransgeneOmics reveals in vivo protein interactions. J. Cell Biol. *189*, 739–754.

Imkeller, K., Ambrosi, G., Boutros, M., and Huber, W. (2020). gscreend: modelling asymmetric count ratios in CRISPR screens to decrease experiment size and improve phenotype detection. Genome Biol. *21*, 53.

Ivanova, N., Dobrin, R., Lu, R., Kotenko, I., Levorse, J., DeCoste, C., Schafer, X., Lun, Y., and Lemischka, I.R. (2006). Dissecting self-renewal in stem cells with RNA interference. Nature *442*, 533–538.

Jackson, M., Krassowska, A., Gilbert, N., Chevassut, T., Forrester, L., Ansell, J., and Ramsahoye, B. (2004). Severe global DNA hypomethylation blocks differentiation and induces histone hyperacetylation in embryonic stem cells. Mol. Cell. Biol. *24*, 8862–8871.

Jeltsch, A. (2006). On the enzymatic properties of Dnmt1: specificity, processivity, mechanism of linear diffusion and allosteric regulation of the enzyme. Epigenetics *1*, 63–66.

Jeong, C.-H., Cho, Y.-Y., Kim, M.-O., Kim, S.-H., Cho, E.-J., Lee, S.-Y., Jeon, Y.-J., Lee, K.Y., Yao, K., Keum, Y.-S., et al. (2010). Phosphorylation of Sox2 cooperates in reprogramming to pluripotent stem cells. Stem Cells *28*, 2141–2150.

Jinek, M., Chylinski, K., Fonfara, I., Hauer, M., Doudna, J.A., and Charpentier, E. (2012). A programmable dual-RNA-guided DNA endonuclease in adaptive bacterial immunity. Science *337*, 816–821.

Johnson, D.E., and Williams, L.T. (1993). Structural and functional diversity in the FGF receptor multigene family. Adv. Cancer Res. *60*, 1–41.

Johnson, G.L., and Lapadat, R. (2002). Mitogen-activated protein kinase pathways mediated by ERK, JNK, and p38 protein kinases. Science *298*, 1911–1912.

Jonkers, I., Barakat, T.S., Achame, E.M., Monkhorst, K., Kenter, A., Rentmeester, E., Grosveld, F., Grootegoed, J.A., and Gribnau, J. (2009). RNF12 is an X-Encoded dose-dependent activator of X chromosome inactivation. Cell *139*, 999–1011.

Kagey, M.H., Newman, J.J., Bilodeau, S., Zhan, Y., Orlando, D.A., van Berkum, N.L., Ebmeier, C.C., Goossens, J., Rahl, P.B., Levine, S.S., et al. (2010). Mediator and cohesin connect gene expression and chromatin architecture. Nature *467*, 430–435.

Kalkan, T., Olova, N., Roode, M., Mulas, C., Lee, H.J., Nett, I., Marks, H., Walker, R., Stunnenberg, H.G., Lilley, K.S., et al. (2017). Tracking the embryonic stem cell transition from ground state pluripotency. Development *144*, 1221–1234.

Kamioka, Y., Yasuda, S., Fujita, Y., Aoki, K., and Matsuda, M. (2010). Multiple decisive phosphorylation sites for the negative feedback regulation of SOS1 via ERK. J. Biol. Chem. *285*, 33540–33548.

Kaneko, S., and Li, X. (2018). X chromosome protects against bladder cancer in females via a KDM6A-dependent epigenetic mechanism. Sci. Adv. *4*, eaar5598.

Kang, M., Piliszek, A., Artus, J., and Hadjantonakis, A.-K. (2013). FGF4 is required for lineage restriction and salt-and-pepper distribution of primitive endoderm factors but not their initial expression in the mouse. Development *140*, 267–279.

Kawakami, T., Zhang, C., Taniguchi, T., Kim, C.J., Okada, Y., Sugihara, H., Hattori, T., Reeve, A.E., Ogawa, O., and Okamoto, K. (2004). Characterization of loss-of-inactive X in Klinefelter syndrome and female-derived cancer cells. Oncogene *23*, 6163–6169.

Keilhauer, E.C., Hein, M.Y., and Mann, M. (2015). Accurate protein complex retrieval by affinity enrichment mass spectrometry (AE-MS) rather than affinity purification mass spectrometry (AP-MS). Mol. Cell. Proteomics *14*, 120–135.

Khalfallah, O., Rouleau, M., Barbry, P., Bardoni, B., and Lalli, E. (2009). Dax-1 knockdown in mouse embryonic stem cells induces loss of pluripotency and multilineage differentiation. Stem Cells *27*, 1529–1537.

Kidger, A.M., Rushworth, L.K., Stellzig, J., Davidson, J., Bryant, C.J., Bayley, C., Caddye, E., Rogers, T., Keyse, S.M., and Caunt, C.J. (2017). Dual-specificity phosphatase 5 controls the localized inhibition, propagation, and transforming potential of ERK signaling. Proc Natl Acad Sci USA *114*, E317–E326.

Kiecker, C., Bates, T., and Bell, E. (2016). Molecular specification of germ layers in vertebrate embryos. Cell. Mol. Life Sci. *73*, 923–947.

Kim, J., Chu, J., Shen, X., Wang, J., and Orkin, S.H. (2008). An extended transcriptional network for pluripotency of embryonic stem cells. Cell *132*, 1049–1061.

Kim, K.-Y., Hysolli, E., Tanaka, Y., Wang, B., Jung, Y.-W., Pan, X., Weissman, S.M., and Park, I.-H. (2014a). X Chromosome of female cells shows dynamic changes in status during human somatic cell reprogramming. Stem Cell Reports *2*, 896–909.

Kim, M.O., Kim, S.-H., Cho, Y.-Y., Nadas, J., Jeong, C.-H., Yao, K., Kim, D.J., Yu, D.-H., Keum, Y.-S., Lee, K.-Y., et al. (2012). ERK1 and ERK2 regulate embryonic stem cell self-renewal through phosphorylation of Klf4. Nat. Struct. Mol. Biol. *19*, 283–290.

Kim, S.-H., Kim, M.O., Cho, Y.-Y., Yao, K., Kim, D.J., Jeong, C.-H., Yu, D.H., Bae, K.B., Cho, E.J., Jung, S.K., et al. (2014b). ERK1 phosphorylates Nanog to regulate protein stability and stem cell self-renewal. Stem Cell Res. *13*, 1–11.

Klein, A.M., Mazutis, L., Akartuna, I., Tallapragada, N., Veres, A., Li, V., Peshkin, L., Weitz, D.A., and Kirschner, M.W. (2015). Droplet barcoding for single-cell transcriptomics applied to embryonic stem cells. Cell *161*, 1187–1201.

Kobayashi, S., Fujihara, Y., Mise, N., Kaseda, K., Abe, K., Ishino, F., and Okabe, M. (2010). The X-linked imprinted gene family Fthl17 shows predominantly female expression following the two-cell stage in mouse embryos. Nucleic Acids Res. *38*, 3672–3681.

Kondoh, H. (2018). Roles of ZIC2 in regulation of pluripotent stem cells. Adv. Exp. Med. Biol. *1046*, 339–351.

Konermann, S., Brigham, M.D., Trevino, A.E., Joung, J., Abudayyeh, O.O., Barcena, C., Hsu, P.D., Habib, N., Gootenberg, J.S., Nishimasu, H., et al. (2015). Genome-scale transcriptional activation by an engineered CRISPR-Cas9 complex. Nature *517*, 583–588.

Kouhara, H., Hadari, Y.R., Spivak-Kroizman, T., Schilling, J., Bar-Sagi, D., Lax, I., and Schlessinger, J. (1997). A lipid-anchored Grb2-binding protein that links FGF-receptor activation to the Ras/MAPK signaling pathway. Cell *89*, 693–702.

Kulak, N.A., Pichler, G., Paron, I., Nagaraj, N., and Mann, M. (2014). Minimal, encapsulated proteomic-sample processing applied to copy-number estimation in eukaryotic cells. Nat. Methods *11*, 319–324.

Kunath, T., Saba-El-Leil, M.K., Almousailleakh, M., Wray, J., Meloche, S., and Smith, A. (2007). FGF stimulation of the Erk1/2 signalling cascade triggers transition of pluripotent embryonic stem cells from self-renewal to lineage commitment. Development *134*, 2895–2902.

Kuroda, M.I., Hilfiker, A., and Lucchesi, J.C. (2016). Dosage Compensation in Drosophila-a Model for the Coordinate Regulation of Transcription. Genetics *204*, 435–450.

Lahiri, S.K., and Zhao, J. (2012). Krüppel-like factor 8 emerges as an important regulator of cancer. Am. J. Transl. Res. *4*, 357–363.

Lake, D., Corrêa, S.A.L., and Müller, J. (2016). Negative feedback regulation of the ERK1/2 MAPK pathway. Cell. Mol. Life Sci. *73*, 4397–4413.

Langmead, B., and Salzberg, S.L. (2012). Fast gapped-read alignment with Bowtie 2. Nat. Methods *9*, 357–359.

Lanner, F., and Rossant, J. (2010). The role of FGF/Erk signaling in pluripotent cells. Development *137*, 3351–3360.

Lax, I., Wong, A., Lamothe, B., Lee, A., Frost, A., Hawes, J., and Schlessinger, J. (2002). The Docking Protein FRS2α Controls a MAP Kinase-Mediated Negative Feedback Mechanism for Signaling by FGF Receptors. Molecular Cell *10*, 709–719.

Lee, J.T. (2005). Regulation of X-chromosome counting by Tsix and Xite sequences. Science *309*, 768–771.

Lee, J.T., and Lu, N. (1999). Targeted mutagenesis of Tsix leads to nonrandom X inactivation. Cell *99*, 47–57.

Lee, J.T., Davidow, L.S., and Warshawsky, D. (1999). Tsix, a gene antisense to Xist at the X-inactivation centre. Nat. Genet. *21*, 400–404.

Leitch, H.G., McEwen, K.R., Turp, A., Encheva, V., Carroll, T., Grabole, N., Mansfield, W., Nashun, B., Knezovich, J.G., Smith, A., et al. (2013). Naive pluripotency is associated with global DNA hypomethylation. Nat. Struct. Mol. Biol. *20*, 311–316.

Lei, H., Oh, S.P., Okano, M., Jüttermann, R., Goss, K.A., Jaenisch, R., and Li, E. (1996). De novo DNA cytosine methyltransferase activities in mouse embryonic stem cells. Development *122*, 3195–3205.

Lim, L.S., Loh, Y.-H., Zhang, W., Li, Y., Chen, X., Wang, Y., Bakre, M., Ng, H.-H., and Stanton, L.W. (2007). Zic3 is required for maintenance of pluripotency in embryonic stem cells. Mol. Biol. Cell *18*, 1348–1358.

Lim, L.S., Hong, F.H., Kunarso, G., and Stanton, L.W. (2010). The pluripotency regulator Zic3 is a direct activator of the Nanog promoter in ESCs. Stem Cells *28*, 1961–1969.

Lin, H.Y., Kaplow, J., Jaye, M., and Hayman, M.J. (1997). Ligand-binding specificity of human fibroblast growth factor receptor-3 IIIc. FEBS Lett. *411*, 389–392.

Liu, Y., Lagowski, J., Sundholm, A., Sundberg, A., and Kulesz-Martin, M. (2007). Microtubule disruption and tumor suppression by mitogen-activated protein kinase phosphatase 4. Cancer Res. *67*, 10711–10719.

Li, H., and Durbin, R. (2009). Fast and accurate short read alignment with Burrows-Wheeler transform. Bioinformatics *25*, 1754–1760.

Li, H., and Durbin, R. (2010). Fast and accurate long-read alignment with Burrows-Wheeler transform. Bioinformatics *26*, 589–595.

Li, T., Lu, H., Mukherjee, D., Lahiri, S.K., Shen, C., Yu, L., and Zhao, J. (2015a). Identification of epidermal growth factor receptor and its inhibitory microRNA141 as novel targets of Krüppel-like factor 8 in breast cancer. Oncotarget *6*, 21428–21442.

Li, W., Xu, H., Xiao, T., Cong, L., Love, M.I., Zhang, F., Irizarry, R.A., Liu, J.S., Brown, M., and Liu, X.S. (2014). MAGeCK enables robust identification of essential genes from genome-scale CRISPR/Cas9 knockout screens. Genome Biol. *15*, 554.

Li, W., Köster, J., Xu, H., Chen, C.-H., Xiao, T., Liu, J.S., Brown, M., and Liu, X.S. (2015b). Quality control, modeling, and visualization of CRISPR screens with MAGeCK-VISPR. Genome Biol. *16*, 281.

Li, Z., Fei, T., Zhang, J., Zhu, G., Wang, L., Lu, D., Chi, X., Teng, Y., Hou, N., Yang, X., et al. (2012). BMP4 Signaling Acts via dual-specificity phosphatase 9 to control ERK activity in mouse embryonic stem cells. Cell Stem Cell *10*, 171–182.

Loh, Y.-H., Wu, Q., Chew, J.-L., Vega, V.B., Zhang, W., Chen, X., Bourque, G., George, J., Leong, B., Liu, J., et al. (2006). The Oct4 and Nanog transcription network regulates pluripotency in mouse embryonic stem cells. Nat. Genet. *38*, 431–440.

Lowenstein, E.J., Daly, R.J., Batzer, A.G., Li, W., Margolis, B., Lammers, R., Ullrich, A., Skolnik, E.Y., Bar-Sagi, D., and Schlessinger, J. (1992). The SH2 and SH3 domain-containing protein GRB2 links receptor tyrosine kinases to ras signaling. Cell *70*, 431–442.

Luna, M., Duke, M., Copperman, A., Grunfeld, L., Sandler, B., and Barritt, J. (2007). Blastocyst embryo transfer is associated with a sex-ratio imbalance in favor of male offspring. Fertil. Steril. *87*, 519–523.

Lyon, M.F. (1961). Gene action in the X-chromosome of the mouse (Mus musculus L.). Nature *190*, 372–373.

Maezawa, S., Hasegawa, K., Yukawa, M., Kubo, N., Sakashita, A., Alavattam, K.G., Sin, H.-S., Kartashov, A.V., Sasaki, H., Barski, A., et al. (2018). Polycomb protein SCML2 facilitates H3K27me3 to establish bivalent domains in the male germline. Proc Natl Acad Sci USA *115*, 4957–4962.

Makarova, K.S., Haft, D.H., Barrangou, R., Brouns, S.J.J., Charpentier, E., Horvath, P., Moineau, S., Mojica, F.J.M., Wolf, Y.I., Yakunin, A.F., et al. (2011). Evolution and classification of the CRISPR-Cas systems. Nat. Rev. Microbiol. *9*, 467–477.

Mak, W., Nesterova, T.B., de Napoles, M., Appanah, R., Yamanaka, S., Otte, A.P., and Brockdorff, N. (2004). Reactivation of the paternal X chromosome in early mouse embryos. Science *303*, 666–669.

Mank, J.E. (2013). Sex chromosome dosage compensation: definitely not for everyone. Trends Genet. *29*, 677–683.

Marahrens, Y., Panning, B., Dausman, J., Strauss, W., and Jaenisch, R. (1997). Xist-deficient mice are defective in dosage compensation but not spermatogenesis. Genes Dev. *11*, 156–166.

Marais, R., Wynne, J., and Treisman, R. (1993). The SRF accessory protein Elk-1 contains a growth factor-regulated transcriptional activation domain. Cell *73*, 381–393.

Margarit, S.M., Sondermann, H., Hall, B.E., Nagar, B., Hoelz, A., Pirruccello, M., Bar-Sagi, D., and Kuriyan, J. (2003). Structural evidence for feedback activation by Ras.GTP of the Ras-specific nucleotide exchange factor SOS. Cell *112*, 685–695.

Marks, H., Kalkan, T., Menafra, R., Denissov, S., Jones, K., Hofemeister, H., Nichols, J., Kranz, A., Stewart, A.F., Smith, A., et al. (2012). The transcriptional and epigenomic foundations of ground state pluripotency. Cell *149*, 590–604.

Martello, G., Sugimoto, T., Diamanti, E., Joshi, A., Hannah, R., Ohtsuka, S., Göttgens, B., Niwa, H., and Smith, A. (2012). Esrrb is a pivotal target of the Gsk3/Tcf3 axis regulating embryonic stem cell self-renewal. Cell Stem Cell *11*, 491–504.

Martello, G., Bertone, P., and Smith, A. (2013). Identification of the missing pluripotency mediator downstream of leukaemia inhibitory factor. EMBO J. *32*, 2561–2574.

Martin, G.R. (1981). Isolation of a pluripotent cell line from early mouse embryos cultured in medium conditioned by teratocarcinoma stem cells. Proc Natl Acad Sci USA *78*, 7634–7638.

Masui, S., Nakatake, Y., Toyooka, Y., Shimosato, D., Yagi, R., Takahashi, K., Okochi, H., Okuda, A., Matoba, R., Sharov, A.A., et al. (2007). Pluripotency governed by Sox2 via regulation of Oct3/4 expression in mouse embryonic stem cells. Nat. Cell Biol. *9*, 625–635.

Matsuda, T., and Cepko, C.L. (2007). Controlled expression of transgenes introduced by in vivo electroporation. Proc Natl Acad Sci USA *104*, 1027–1032.

Matsuda, K., Mikami, T., Oki, S., Iida, H., Andrabi, M., Boss, J.M., Yamaguchi, K., Shigenobu, S., and Kondoh, H. (2017). ChIP-seq analysis of genomic binding regions of five major transcription factors highlights a central role for ZIC2 in the mouse epiblast stem cell gene regulatory network. Development *144*, 1948–1958.

Matsuda, T., Nakamura, T., Nakao, K., Arai, T., Katsuki, M., Heike, T., and Yokota, T. (1999). STAT3 activation is sufficient to maintain an undifferentiated state of mouse embryonic stem cells. EMBO J. *18*, 4261–4269.

Mattila, E., Pellinen, T., Nevo, J., Vuoriluoto, K., Arjonen, A., and Ivaska, J. (2005). Negative regulation of EGFR signalling through integrin-alpha1beta1-mediated activation of protein tyrosine phosphatase TCPTP. Nat. Cell Biol. *7*, 78–85.

McHugh, C.A., Chen, C.-K., Chow, A., Surka, C.F., Tran, C., McDonel, P., Pandya-Jones, A., Blanco, M., Burghard, C., Moradian, A., et al. (2015). The Xist lncRNA interacts directly with SHARP to silence transcription through HDAC3. Nature *521*, 232–236.

Ménézo, Y.J.., Chouteau, J., Torelló, M.J., Girard, A., and Veiga, A. (1999). Birth weight and sex ratio after transfer at the blastocyst stage in humans. Fertility and Sterility *72*, 221–224.

Mevissen, T.E.T., Hospenthal, M.K., Geurink, P.P., Elliott, P.R., Akutsu, M., Arnaudo, N., Ekkebus, R., Kulathu, Y., Wauer, T., El Oualid, F., et al. (2013). OTU deubiquitinases reveal mechanisms of linkage specificity and enable ubiquitin chain restriction analysis. Cell *154*, 169–184.

von Meyenn, F., Iurlaro, M., Habibi, E., Liu, N.Q., Salehzadeh-Yazdi, A., Santos, F., Petrini, E., Milagre, I., Yu, M., Xie, Z., et al. (2016). Impairment of DNA methylation maintenance is the main cause of global demethylation in naive embryonic stem cells. Mol. Cell *62*, 848–861.

Milagre, I., Stubbs, T.M., King, M.R., Spindel, J., Santos, F., Krueger, F., Bachman, M., Segonds-Pichon, A., Balasubramanian, S., Andrews, S.R., et al. (2017). Gender Differences in Global but Not Targeted Demethylation in iPSC Reprogramming. Cell Rep. *18*, 1079–1089.

Minajigi, A., Froberg, J., Wei, C., Sunwoo, H., Kesner, B., Colognori, D., Lessing, D., Payer, B., Boukhali, M., Haas, W., et al. (2015). Chromosomes. A comprehensive Xist interactome reveals cohesin repulsion and an RNA-directed chromosome conformation. Science *349*.

Mitalipov, S., and Wolf, D. (2009). Totipotency, pluripotency and nuclear reprogramming. Adv. Biochem. Eng. Biotechnol. *114*, 185–199.

Mitsui, K., Tokuzawa, Y., Itoh, H., Segawa, K., Murakami, M., Takahashi, K., Maruyama, M., Maeda, M., and Yamanaka, S. (2003). The homeoprotein Nanog is required for maintenance of pluripotency in mouse epiblast and ES cells. Cell *113*, 631–642.

Mittwoch, U. (1993). Blastocysts prepare for the race to be male. Hum. Reprod. *8*, 1550–1555.

Mohammed, H., Hernando-Herraez, I., Savino, A., Scialdone, A., Macaulay, I., Mulas, C., Chandra, T., Voet, T., Dean, W., Nichols, J., et al. (2017). Single-Cell Landscape of Transcriptional Heterogeneity and Cell Fate Decisions during Mouse Early Gastrulation. Cell Rep. *20*, 1215–1228.

Moindrot, B., Cerase, A., Coker, H., Masui, O., Grijzenhout, A., Pintacuda, G., Schermelleh, L., Nesterova, T.B., and Brockdorff, N. (2015). A Pooled shRNA Screen Identifies Rbm15, Spen, and Wtap as Factors Required for Xist RNA-Mediated Silencing. Cell Rep. *12*, 562–572.

Monfort, A., Di Minin, G., Postlmayr, A., Freimann, R., Arieti, F., Thore, S., and Wutz, A. (2015). Identification of Spen as a Crucial Factor for Xist Function through Forward Genetic Screening in Haploid Embryonic Stem Cells. Cell Rep. *12*, 554–561.

Montini, E., Buchner, G., Spalluto, C., Andolfi, G., Caruso, A., den Dunnen, J.T., Trump, D., Rocchi, M., Ballabio, A., and Franco, B. (1999). Identification of SCML2, a second human gene homologous to the Drosophila sex comb on midleg (Scm): A new gene cluster on Xp22. Genomics *58*, 65–72.

Moreira de Mello, J.C., de Araújo, E.S.S., Stabellini, R., Fraga, A.M., de Souza, J.E.S., Sumita, D.R., Camargo, A.A., and Pereira, L.V. (2010). Random X inactivation and extensive mosaicism in human placenta revealed by analysis of allele-specific gene expression along the X chromosome. PLoS ONE *5*, e10947.

Morris, S.A., Teo, R.T.Y., Li, H., Robson, P., Glover, D.M., and Zernicka-Goetz, M. (2010). Origin and formation of the first two distinct cell types of the inner cell mass in the mouse embryo. Proc Natl Acad Sci USA *107*, 6364–6369.

Motosugi, N., Bauer, T., Polanski, Z., Solter, D., and Hiiragi, T. (2005). Polarity of the mouse embryo is established at blastocyst and is not prepatterned. Genes Dev. *19*, 1081–1092.

Mutzel, V., and Schulz, E.G. (2020). Dosage Sensing, Threshold Responses, and Epigenetic Memory: A Systems Biology Perspective on Random X-Chromosome Inactivation. Bioessays *42*, e1900163.

Mutzel, V., Okamoto, I., Dunkel, I., Saitou, M., Giorgetti, L., Heard, E., and Schulz, E.G. (2019). A symmetric toggle switch explains the onset of random X inactivation in different mammals. Nat. Struct. Mol. Biol. *26*, 350–360.

Mzoughi, S., Zhang, J., Hequet, D., Teo, S.X., Fang, H., Xing, Q.R., Bezzi, M., Seah, M.K.Y., Ong, S.L.M., Shin, E.M., et al. (2017). PRDM15 safeguards naive pluripotency by transcriptionally regulating WNT and MAPK-ERK signaling. Nat. Genet. *49*, 1354–1363.

Nabet, B., Roberts, J.M., Buckley, D.L., Paulk, J., Dastjerdi, S., Yang, A., Leggett, A.L., Erb, M.A., Lawlor, M.A., Souza, A., et al. (2018). The dTAG system for immediate and target-specific protein degradation. Nat. Chem. Biol. *14*, 431–441.

Navarro, P., Pichard, S., Ciaudo, C., Avner, P., and Rougeulle, C. (2005). Tsix transcription across the Xist gene alters chromatin conformation without affecting Xist transcription: implications for X-chromosome inactivation. Genes Dev. *19*, 1474–1484.

Navarro, P., Page, D.R., Avner, P., and Rougeulle, C. (2006). Tsix-mediated epigenetic switch of a CTCF-flanked region of the Xist promoter determines the Xist transcription program. Genes Dev. *20*, 2787–2792.

Navarro, P., Chambers, I., Karwacki-Neisius, V., Chureau, C., Morey, C., Rougeulle, C., and Avner, P. (2008). Molecular coupling of Xist regulation and pluripotency. Science *321*, 1693–1695.

Navarro, P., Chantalat, S., Foglio, M., Chureau, C., Vigneau, S., Clerc, P., Avner, P., and Rougeulle, C. (2009). A role for non-coding Tsix transcription in partitioning chromatin domains within the mouse X-inactivation centre. Epigenetics Chromatin *2*, 8.

Navarro, P., Oldfield, A., Legoupi, J., Festuccia, N., Dubois, A., Attia, M., Schoorlemmer, J., Rougeulle, C., Chambers, I., and Avner, P. (2010). Molecular coupling of Tsix regulation and pluripotency. Nature *468*, 457–460.

Nekrasova, T., Shive, C., Gao, Y., Kawamura, K., Guardia, R., Landreth, G., and Forsthuber, T.G. (2005). ERK1-deficient mice show normal T cell effector function and are highly susceptible to experimental autoimmune encephalomyelitis. J. Immunol. *175*, 2374–2380.

Nesterova, T.B., Wei, G., Coker, H., Pintacuda, G., Bowness, J.S., Zhang, T., Almeida, M., Bloechl, B., Moindrot, B., Carter, E.J., et al. (2019). Systematic allelic analysis defines the interplay of key pathways in X chromosome inactivation. Nat. Commun. *10*, 3129.

Newton, K., Matsumoto, M.L., Wertz, I.E., Kirkpatrick, D.S., Lill, J.R., Tan, J., Dugger, D., Gordon, N., Sidhu, S.S., Fellouse, F.A., et al. (2008). Ubiquitin chain editing revealed by polyubiquitin linkage-specific antibodies. Cell *134*, 668–678.

Nichols, J., and Smith, A. (2009). Naive and primed pluripotent states. Cell Stem Cell *4*, 487–492.

Nichols, J., Zevnik, B., Anastassiadis, K., Niwa, H., Klewe-Nebenius, D., Chambers, I., Schöler, H., and Smith, A. (1998). Formation of pluripotent stem cells in the mammalian embryo depends on the POU transcription factor Oct4. Cell *95*, 379–391.

Nishioka, N., Inoue, K., Adachi, K., Kiyonari, H., Ota, M., Ralston, A., Yabuta, N., Hirahara, S., Stephenson, R.O., Ogonuki, N., et al. (2009). The Hippo signaling pathway components Lats and Yap pattern Tead4 activity to distinguish mouse trophectoderm from inner cell mass. Dev. Cell *16*, 398–410.

Niwa, H., Burdon, T., Chambers, I., and Smith, A. (1998). Self-renewal of pluripotent embryonic stem cells is mediated via activation of STAT3. Genes Dev. *12*, 2048–2060.

Niwa, H., Ogawa, K., Shimosato, D., and Adachi, K. (2009). A parallel circuit of LIF signalling pathways maintains pluripotency of mouse ES cells. Nature *460*, 118–122.

Oda, T., Tian, T., Inoue, M., Ikeda, J.-I., Qiu, Y., Okumura, M., Aozasa, K., and Morii, E. (2009). Tumorigenic role of orphan nuclear receptor NR0B1 in lung adenocarcinoma. Am. J. Pathol. *175*, 1235–1245.

Ohhata, T., Hoki, Y., Sasaki, H., and Sado, T. (2008). Crucial role of antisense transcription across the Xist promoter in Tsix-mediated Xist chromatin modification. Development *135*, 227–235.

Okada, M. (2012). Regulation of the SRC family kinases by Csk. Int. J. Biol. Sci. *8*, 1385–1397.

Okamoto, I., Otte, A.P., Allis, C.D., Reinberg, D., and Heard, E. (2004). Epigenetic dynamics of imprinted X inactivation during early mouse development. Science *303*, 644–649.

Okamoto, I., Patrat, C., Thépot, D., Peynot, N., Fauque, P., Daniel, N., Diabangouaya, P., Wolf, J.-P., Renard, J.-P., Duranthon, V., et al. (2011). Eutherian mammals use diverse strategies to initiate X-chromosome inactivation during development. Nature *472*, 370–374.

Okano, M., Bell, D.W., Haber, D.A., and Li, E. (1999). DNA methyltransferases Dnmt3a and Dnmt3b are essential for de novo methylation and mammalian development. Cell *99*, 247–257.

Oliviero, G., Munawar, N., Watson, A., Streubel, G., Manning, G., Bardwell, V., Bracken, A.P., and Cagney, G. (2015). The variant Polycomb Repressor Complex 1 component PCGF1 interacts with a pluripotency sub-network that includes DPPA4, a regulator of embryogenesis. Sci. Rep. *5*, 18388.

Ong, S.H., Guy, G.R., Hadari, Y.R., Laks, S., Gotoh, N., Schlessinger, J., and Lax, I. (2000). FRS2 proteins recruit intracellular signaling pathways by binding to diverse targets on fibroblast growth factor and nerve growth factor receptors. Mol. Cell. Biol. *20*, 979–989.

Ono, R., Kobayashi, S., Wagatsuma, H., Aisaka, K., Kohda, T., Kaneko-Ishino, T., and Ishino, F. (2001). A retrotransposon-derived gene, PEG10, is a novel imprinted gene located on human chromosome 7q21. Genomics *73*, 232–237.

Ono, R., Nakamura, K., Inoue, K., Naruse, M., Usami, T., Wakisaka-Saito, N., Hino, T., Suzuki-Migishima, R., Ogonuki, N., Miki, H., et al. (2006). Deletion of Peg10, an imprinted gene acquired from a retrotransposon, causes early embryonic lethality. Nat. Genet. *38*, 101–106.

Ooi, S.K.T., Qiu, C., Bernstein, E., Li, K., Jia, D., Yang, Z., Erdjument-Bromage, H., Tempst, P., Lin, S.-P., Allis, C.D., et al. (2007). DNMT3L connects unmethylated lysine 4 of histone H3 to de novo methylation of DNA. Nature *448*, 714–717.

Ooi, S.K., Wolf, D., Hartung, O., Agarwal, S., Daley, G.Q., Goff, S.P., and Bestor, T.H. (2010). Dynamic instability of genomic methylation patterns in pluripotent stem cells. Epigenetics Chromatin *3*, 17.

Ornitz, D.M., and Itoh, N. (2001). Fibroblast growth factors. Genome Biol. *2*, REVIEWS3005.

Owens, D.M., and Keyse, S.M. (2007). Differential regulation of MAP kinase signalling by dual-specificity protein phosphatases. Oncogene *26*, 3203–3213.

Paling, N.R.D., Wheadon, H., Bone, H.K., and Welham, M.J. (2004). Regulation of embryonic stem cell self-renewal by phosphoinositide 3-kinase-dependent signaling. J. Biol. Chem. *279*, 48063–48070.

Parvatiyar, K., Barber, G.N., and Harhaj, E.W. (2010). TAX1BP1 and A20 inhibit antiviral signaling by targeting TBK1-IKKi kinases. J. Biol. Chem. *285*, 14999–15009.

Pasque, V., Karnik, R., Chronis, C., Petrella, P., Langerman, J., Bonora, G., Song, J., Vanheer, L., Sadhu Dimashkie, A., Meissner, A., et al. (2018). X Chromosome Dosage Influences DNA Methylation Dynamics during Reprogramming to Mouse iPSCs. Stem Cell Reports *10*, 1537–1550.

Patel, S., Bonora, G., Sahakyan, A., Kim, R., Chronis, C., Langerman, J., Fitz-Gibbon, S., Rubbi, L., Skelton, R.J.P., Ardehali, R., et al. (2017). Human Embryonic Stem Cells Do Not Change Their X Inactivation Status during Differentiation. Cell Rep. *18*, 54–67.

Patil, D.P., Chen, C.-K., Pickering, B.F., Chow, A., Jackson, C., Guttman, M., and Jaffrey, S.R. (2016). m(6)A RNA methylation promotes XIST-mediated transcriptional repression. Nature *537*, 369–373.

Pearson, G., Robinson, F., Beers Gibson, T., Xu, B.E., Karandikar, M., Berman, K., and Cobb, M.H. (2001). Mitogen-activated protein (MAP) kinase pathways: regulation and physiological functions. Endocr. Rev. *22*, 153–183.

Peng, Y.-P., Zhu, Y., Yin, L.-D., Zhang, J.-J., Wei, J.-S., Liu, X., Liu, X.-C., Gao, W.-T., Jiang, K.-R., and Miao, Y. (2017). PEG10 overexpression induced by E2F-1 promotes cell proliferation, migration, and invasion in pancreatic cancer. J. Exp. Clin. Cancer Res. *36*, 30.

Penny, G.D., Kay, G.F., Sheardown, S.A., Rastan, S., and Brockdorff, N. (1996). Requirement for Xist in X chromosome inactivation. Nature *379*, 131–137.

Petropoulos, S., Edsgärd, D., Reinius, B., Deng, Q., Panula, S.P., Codeluppi, S., Reyes, A.P., Linnarsson, S., Sandberg, R., and Lanner, F. (2016). Single-Cell RNA-Seq Reveals Lineage and X Chromosome Dynamics in Human Preimplantation Embryos. Cell *167*, 285.

Philippe, L., Vasseur, J.-J., Debart, F., and Thoreen, C.C. (2018). La-related protein 1 (LARP1) repression of TOP mRNA translation is mediated through its cap-binding domain and controlled by an adjacent regulatory region. Nucleic Acids Res. *46*, 1457–1469.

Pilsner, J.R., Lazarus, A.L., Nam, D.-H., Letcher, R.J., Sonne, C., Dietz, R., and Basu, N. (2010). Mercury-associated DNA hypomethylation in polar bear brains via the LUminometric Methylation Assay: a sensitive method to study epigenetics in wildlife. Mol. Ecol. *19*, 307–314.

Pintacuda, G., Wei, G., Roustan, C., Kirmizitas, B.A., Solcan, N., Cerase, A., Castello, A., Mohammed, S., Moindrot, B., Nesterova, T.B., et al. (2017). hnRNPK Recruits PCGF3/5-PRC1 to the Xist RNA B-Repeat to Establish Polycomb-Mediated Chromosomal Silencing. Mol. Cell *68*, 955-969.e10.

Pintard, L., Willems, A., and Peter, M. (2004). Cullin-based ubiquitin ligases: Cul3-BTB complexes join the family. EMBO J. *23*, 1681–1687.

Plusa, B., Piliszek, A., Frankenberg, S., Artus, J., and Hadjantonakis, A.-K. (2008). Distinct sequential cell behaviours direct primitive endoderm formation in the mouse blastocyst. Development *135*, 3081–3091.

Popkie, A.P., Zeidner, L.C., Albrecht, A.M., D'Ippolito, A., Eckardt, S., Newsom, D.E., Groden, J., Doble, B.W., Aronow, B., McLaughlin, K.J., et al. (2010). Phosphatidylinositol 3-kinase (PI3K) signaling via glycogen synthase kinase-3 (Gsk-3) regulates DNA methylation of imprinted loci. J. Biol. Chem. *285*, 41337–41347.

Pruitt, K.D., Tatusova, T., and Maglott, D.R. (2005). NCBI Reference Sequence (RefSeq): a curated non-redundant sequence database of genomes, transcripts and proteins. Nucleic Acids Res. *33*, D501-4.

Pruitt, K.D., Brown, G.R., Hiatt, S.M., Thibaud-Nissen, F., Astashyn, A., Ermolaeva, O., Farrell, C.M., Hart, J., Landrum, M.J., McGarvey, K.M., et al. (2014). RefSeq: an update on mammalian reference sequences. Nucleic Acids Res. *42*, D756-63.

Rajalingam, K., Schreck, R., Rapp, U.R., and Albert, S. (2007). Ras oncogenes and their downstream targets. Biochim. Biophys. Acta *1773*, 1177–1195.

Ramesh, S., Qi, X.-J., Wildey, G.M., Robinson, J., Molkentin, J., Letterio, J., and Howe, P.H. (2008). TGF beta-mediated BIM expression and apoptosis are regulated through SMAD3-dependent expression of the MAPK phosphatase MKP2. EMBO Rep. *9*, 990–997.

Ramírez, F., Ryan, D.P., Grüning, B., Bhardwaj, V., Kilpert, F., Richter, A.S., Heyne, S., Dündar, F., and Manke, T. (2016). deepTools2: a next generation web server for deep-sequencing data analysis. Nucleic Acids Res. *44*, W160-5.

Ran, F.A., Hsu, P.D., Wright, J., Agarwala, V., Scott, D.A., and Zhang, F. (2013). Genome engineering using the CRISPR-Cas9 system. Nat. Protoc. *8*, 2281–2308.

Rappolee, D.A., Basilico, C., Patel, Y., and Werb, Z. (1994). Expression and function of FGF-4 in peri-implantation development in mouse embryos. Development *120*, 2259–2269.

Rastan, S., and Robertson, E.J. (1985). X-chromosome deletions in embryo-derived (EK) cell lines associated with lack of X-chromosome inactivation. J. Embryol. Exp. Morphol. *90*, 379–388.

Ratnu, V.S., Emami, M.R., and Bredy, T.W. (2017). Genetic and epigenetic factors underlying sex differences in the regulation of gene expression in the brain. J. Neurosci. Res. *95*, 301–310.

Rayon, T., Menchero, S., Nieto, A., Xenopoulos, P., Crespo, M., Cockburn, K., Cañon, S., Sasaki, H., Hadjantonakis, A.-K., de la Pompa, J.L., et al. (2014). Notch and hippo converge on Cdx2 to specify the trophectoderm lineage in the mouse blastocyst. Dev. Cell *30*, 410–422.

Ray, P.F., Conaghan, J., Winston, R.M., and Handyside, A.H. (1995). Increased number of cells and metabolic activity in male human preimplantation embryos following in vitro fertilization. J. Reprod. Fertil. *104*, 165–171.

Reddy, R.B., Khora, S.S., and Suresh, A. (2019). Molecular prognosticators in clinically and pathologically distinct cohorts of head and neck squamous cell carcinoma-A meta-analysis approach. PLoS ONE *14*, e0218989.

Richardson, A.L., Wang, Z.C., De Nicolo, A., Lu, X., Brown, M., Miron, A., Liao, X., Iglehart, J.D., Livingston, D.M., and Ganesan, S. (2006). X chromosomal abnormalities in basal-like human breast cancer. Cancer Cell *9*, 121–132.

Ridings-Figueroa, R., Stewart, E.R., Nesterova, T.B., Coker, H., Pintacuda, G., Godwin, J., Wilson, R., Haslam, A., Lilley, F., Ruigrok, R., et al. (2017). The nuclear matrix protein CIZ1 facilitates localization of Xist RNA to the inactive X-chromosome territory. Genes Dev. *31*, 876–888.

Ritt, D.A., Monson, D.M., Specht, S.I., and Morrison, D.K. (2010). Impact of feedback phosphorylation and Raf heterodimerization on normal and mutant B-Raf signaling. Mol. Cell. Biol. *30*, 806–819.

Roberts, P.J., and Der, C.J. (2007). Targeting the Raf-MEK-ERK mitogen-activated protein kinase cascade for the treatment of cancer. Oncogene *26*, 3291–3310.

Robert Finestra, T., and Gribnau, J. (2017). X chromosome inactivation: silencing, topology and reactivation. Curr. Opin. Cell Biol. *46*, 54–61.

Robinson, M.D., McCarthy, D.J., and Smyth, G.K. (2010). edgeR: a Bioconductor package for differential expression analysis of digital gene expression data. Bioinformatics *26*, 139–140.

Roskoski, R. (2012). ERK1/2 MAP kinases: structure, function, and regulation. Pharmacol. Res. *66*, 105–143.

Ruzzenenti, P., Asperti, M., Mitola, S., Crescini, E., Maccarinelli, F., Gryzik, M., Regoni, M., Finazzi, D., Arosio, P., and Poli, M. (2015). The Ferritin-Heavy-Polypeptide-Like-17 (FTHL17) gene encodes a ferritin with low stability and no ferroxidase activity and with a partial nuclear localization. Biochim. Biophys. Acta *1850*, 1267–1273.

Saba-El-Leil, M.K., Vella, F.D.J., Vernay, B., Voisin, L., Chen, L., Labrecque, N., Ang, S.-L., and Meloche, S. (2003). An essential function of the mitogen-activated protein kinase Erk2 in mouse trophoblast development. EMBO Rep. *4*, 964–968.

Sado, T., Hoki, Y., and Sasaki, H. (2005). Tsix silences Xist through modification of chromatin structure. Dev. Cell *9*, 159–165.

Sahakyan, A., Kim, R., Chronis, C., Sabri, S., Bonora, G., Theunissen, T.W., Kuoy, E., Langerman, J., Clark, A.T., Jaenisch, R., et al. (2017). Human naive pluripotent stem cells model X chromosome dampening and X inactivation. Cell Stem Cell *20*, 87–101.

Sanjana, N.E., Shalem, O., and Zhang, F. (2014). Improved vectors and genome-wide libraries for CRISPR screening. Nat. Methods *11*, 783–784.

Sarabipour, S., and Hristova, K. (2016). Mechanism of FGF receptor dimerization and activation. Nat. Commun. *7*, 10262.

Sasaki, A., Taketomi, T., Kato, R., Saeki, K., Nonami, A., Sasaki, M., Kuriyama, M., Saito, N., Shibuya, M., and Yoshimura, A. (2003). Mammalian Sprouty4 suppresses Ras-independent ERK activation by binding to Raf1. Nat. Cell Biol. *5*, 427–432.

Sato, N., Meijer, L., Skaltsounis, L., Greengard, P., and Brivanlou, A.H. (2004). Maintenance of pluripotency in human and mouse embryonic stem cells through activation of Wnt signaling by a pharmacological GSK-3-specific inhibitor. Nat. Med. *10*, 55–63.

Savarese, F., Flahndorfer, K., Jaenisch, R., Busslinger, M., and Wutz, A. (2006). Hematopoietic precursor cells transiently reestablish permissiveness for X inactivation. Mol. Cell. Biol. *26*, 7167–7177.

Schabhüttl, M., Wieland, T., Senderek, J., Baets, J., Timmerman, V., De Jonghe, P., Reilly, M.M., Stieglbauer, K., Laich, E., Windhager, R., et al. (2014). Whole-exome sequencing in patients with inherited neuropathies: outcome and challenges. J. Neurol. *261*, 970–982.

Schlessinger, J., Plotnikov, A.N., Ibrahimi, O.A., Eliseenkova, A.V., Yeh, B.K., Yayon, A., Linhardt, R.J., and Mohammadi, M. (2000). Crystal structure of a ternary FGF-FGFR-heparin complex reveals a dual role for heparin in FGFR binding and dimerization. Mol. Cell *6*, 743–750.

Schulz, E.G. (2017). X-chromosome dosage as a modulator of pluripotency, signalling and differentiation? Philos. Trans. R. Soc. Lond. B. Biol. Sci *372*.

Schulz, E.G., Meisig, J., Nakamura, T., Okamoto, I., Sieber, A., Picard, C., Borensztein, M., Saitou, M., Blüthgen, N., and Heard, E. (2014). The two active X chromosomes in female ESCs block exit from the pluripotent state by modulating the ESC signaling network. Cell Stem Cell *14*, 203–216.

Schurz, H., Salie, M., Tromp, G., Hoal, E.G., Kinnear, C.J., and Möller, M. (2019). The X chromosome and sex-specific effects in infectious disease susceptibility. Hum Genomics *13*, 2.

Scott, W.J., and Holson, J.F. (1977). Weight differences in rat embryos prior to sexual differentiation. J. Embryol. Exp. Morphol. *40*, 259–263.

Seller, M.J., and Perkins-Cole, K.J. (1987). Sex difference in mouse embryonic development at neurulation. J. Reprod. Fertil. *79*, 159–161.

Shalem, O., Sanjana, N.E., Hartenian, E., Shi, X., Scott, D.A., Mikkelson, T., Heckl, D., Ebert, B.L., Root, D.E., Doench, J.G., et al. (2014). Genome-scale CRISPR-Cas9 knockout screening in human cells. Science *343*, 84–87.

Shao, Z., Raible, F., Mollaaghababa, R., Guyon, J.R., Wu, C.T., Bender, W., and Kingston, R.E. (1999). Stabilization of chromatin structure by PRC1, a Polycomb complex. Cell *98*, 37–46.

Shibata, S., Yokota, T., and Wutz, A. (2008). Synergy of Eed and Tsix in the repression of Xist gene and X-chromosome inactivation. EMBO J. *27*, 1816–1826.

Shi, J., Zhang, L., Zhou, D., Zhang, J., Lin, Q., Guan, W., Zhang, J., Ren, W., and Xu, G. (2018). Biological function of ribosomal protein L10 on cell behavior in human epithelial ovarian cancer. J. Cancer *9*, 745–756.

Shi, X., Luo, X., Yan, Q., Zhang, W., Wu, Y., Zhang, M., Zhao, J., Peng, Y., Chen, Y., Zhang, Y., et al. (2015). Suppression of KLF8 induces cell differentiation and sensitizes colorectal cancer to 5-fluorouracil. Oncol. Rep. *34*, 1221–1230.

Shi, Y., Downes, M., Xie, W., Kao, H.Y., Ordentlich, P., Tsai, C.C., Hon, M., and Evans, R.M. (2001). Sharp, an inducible cofactor that integrates nuclear receptor repression and activation. Genes Dev. *15*, 1140–1151.

Sieron, P., Hader, C., Hatina, J., Engers, R., Wlazlinski, A., Müller, M., and Schulz, W.A. (2009). DKC1 overexpression associated with prostate cancer progression. Br. J. Cancer *101*, 1410–1416.

Silva, J., Nichols, J., Theunissen, T.W., Guo, G., van Oosten, A.L., Barrandon, O., Wray, J., Yamanaka, S., Chambers, I., and Smith, A. (2009). Nanog is the gateway to the pluripotent ground state. Cell *138*, 722–737.

Silva, S.S., Rowntree, R.K., Mekhoubad, S., and Lee, J.T. (2008). X-chromosome inactivation and epigenetic fluidity in human embryonic stem cells. Proc Natl Acad Sci USA *105*, 4820–4825.

Silverman, N., and Maniatis, T. (2001). NF-kappaB signaling pathways in mammalian and insect innate immunity. Genes Dev. *15*, 2321–2342.

Simon, J.A., and Schreiber, S.L. (1995). Grb2 SH3 binding to peptides from Sos: evaluation of a general model for SH3-ligand interactions. Chem. Biol. *2*, 53–60.

Singh, P., Schimenti, J.C., and Bolcun-Filas, E. (2015). A mouse geneticist's practical guide to CRISPR applications. Genetics *199*, 1–15.

Sirchia, S.M., Ramoscelli, L., Grati, F.R., Barbera, F., Coradini, D., Rossella, F., Porta, G., Lesma, E., Ruggeri, A., Radice, P., et al. (2005). Loss of the inactive X chromosome and replication of the active X in BRCA1-defective and wild-type breast cancer cells. Cancer Res. *65*, 2139–2146.

Smirnov, A., Fishman, V., Yunusova, A., Korablev, A., Serova, I., Skryabin, B.V., Rozhdestvensky, T.S., and Battulin, N. (2020). DNA barcoding reveals that injected transgenes are predominantly processed by homologous recombination in mouse zygote. Nucleic Acids Res. *48*, 719–735.

Smith, A.G., and Hooper, M.L. (1987). Buffalo rat liver cells produce a diffusible activity which inhibits the differentiation of murine embryonal carcinoma and embryonic stem cells. Dev. Biol. *121*, 1–9.

Smith, Z.D., and Meissner, A. (2013). DNA methylation: roles in mammalian development. Nat. Rev. Genet. *14*, 204–220.

Smith, A.G., Heath, J.K., Donaldson, D.D., Wong, G.G., Moreau, J., Stahl, M., and Rogers, D. (1988). Inhibition of pluripotential embryonic stem cell differentiation by purified polypeptides. Nature *336*, 688–690.

Smith, Z.D., Chan, M.M., Mikkelsen, T.S., Gu, H., Gnirke, A., Regev, A., and Meissner, A. (2012). A unique regulatory phase of DNA methylation in the early mammalian embryo. Nature *484*, 339–344.

Snell, D.M., and Turner, J.M.A. (2018). Sex Chromosome Effects on Male-Female Differences in Mammals. Curr. Biol. *28*, R1313–R1324.

Song, J., Janiszewski, A., De Geest, N., Vanheer, L., Talon, I., El Bakkali, M., Oh, T., and Pasque, V. (2019). X-Chromosome Dosage Modulates Multiple Molecular and Cellular Properties of Mouse Pluripotent Stem Cells Independently of Global DNA Methylation Levels. Stem Cell Reports *12*, 333–350.

Sowa, M.E., Bennett, E.J., Gygi, S.P., and Harper, J.W. (2009). Defining the human deubiquitinating enzyme interaction landscape. Cell *138*, 389–403.

Stavridis, M.P., Lunn, J.S., Collins, B.J., and Storey, K.G. (2007). A discrete period of FGF-induced Erk1/2 signalling is required for vertebrate neural specification. Development *134*, 2889–2894.

Storm, M.P., Kumpfmueller, B., Thompson, B., Kolde, R., Vilo, J., Hummel, O., Schulz, H., and Welham, M.J. (2009). Characterization of the phosphoinositide 3-kinase-dependent transcriptome in murine embryonic stem cells: identification of novel regulators of pluripotency. Stem Cells *27*, 764–775.

Sturm, O.E., Orton, R., Grindlay, J., Birtwistle, M., Vyshemirsky, V., Gilbert, D., Calder, M., Pitt, A., Kholodenko, B., and Kolch, W. (2010). The mammalian MAPK/ERK pathway exhibits properties of a negative feedback amplifier. Sci. Signal. *3*, ra90.

Suárez-Cabrera, C., de la Peña, B., González, L.L., Page, A., Martínez-Fernández, M., Casanova, M.L., Paramio, J.M., Rojo-Sebastián, A., Moreno-Bueno, G., Maroto, A., et al. (2018). The Ras-related gene ERAS is involved in human and murine breast cancer. Sci. Rep. *8*, 13038.

Sumara, I., Quadroni, M., Frei, C., Olma, M.H., Sumara, G., Ricci, R., and Peter, M. (2007). A Cul3-based E3 ligase removes Aurora B from mitotic chromosomes, regulating mitotic progression and completion of cytokinesis in human cells. Dev. Cell *12*, 887–900.

Sunwoo, H., Colognori, D., Froberg, J.E., Jeon, Y., and Lee, J.T. (2017). Repeat E anchors Xist RNA to the inactive X chromosomal compartment through CDKN1A-interacting protein (CIZ1). Proc Natl Acad Sci USA *114*, 10654–10659.

Sun, B.K., Deaton, A.M., and Lee, J.T. (2006). A transient heterochromatic state in Xist preempts X inactivation choice without RNA stabilization. Mol. Cell *21*, 617–628.

Sun, S., Del Rosario, B.C., Szanto, A., Ogawa, Y., Jeon, Y., and Lee, J.T. (2013). Jpx RNA activates Xist by evicting CTCF. Cell *153*, 1537–1551.

Tai, C.-I., and Ying, Q.-L. (2013). Gbx2, a LIF/Stat3 target, promotes reprogramming to and retention of the pluripotent ground state. J. Cell Sci. *126*, 1093–1098.

Takagi, N. (2003). Imprinted X-chromosome inactivation: enlightenment from embryos in vivo. Seminars in Cell & Developmental Biology *14*, 319–329.

Takahashi, K., and Yamanaka, S. (2006). Induction of pluripotent stem cells from mouse embryonic and adult fibroblast cultures by defined factors. Cell *126*, 663–676.

Takahashi, K., Mitsui, K., and Yamanaka, S. (2003). Role of ERas in promoting tumour-like properties in mouse embryonic stem cells. Nature *423*, 541–545.

Takashima, Y., Guo, G., Loos, R., Nichols, J., Ficz, G., Krueger, F., Oxley, D., Santos, F., Clarke, J., Mansfield, W., et al. (2014). Resetting transcription factor control circuitry toward ground-state pluripotency in human. Cell *158*, 1254–1269.

Tam, P.P., Williams, E.A., and Chan, W.Y. (1993). Gastrulation in the mouse embryo: ultrastructural and molecular aspects of germ layer morphogenesis. Microsc. Res. Tech. *26*, 301–328.

Tanenbaum, M.E., Gilbert, L.A., Qi, L.S., Weissman, J.S., and Vale, R.D. (2014). A protein-tagging system for signal amplification in gene expression and fluorescence imaging. Cell *159*, 635–646.

Tang, Y.A., Huntley, D., Montana, G., Cerase, A., Nesterova, T.B., and Brockdorff, N. (2010). Efficiency of Xist-mediated silencing on autosomes is linked to chromosomal domain organisation. Epigenetics Chromatin *3*, 10.

Tcherkezian, J., Cargnello, M., Romeo, Y., Huttlin, E.L., Lavoie, G., Gygi, S.P., and Roux, P.P. (2014). Proteomic analysis of cap-dependent translation identifies LARP1 as a key regulator of 5'TOP mRNA translation. Genes Dev. *28*, 357–371.

Tesar, P.J., Chenoweth, J.G., Brook, F.A., Davies, T.J., Evans, E.P., Mack, D.L., Gardner, R.L., and McKay, R.D.G. (2007). New cell lines from mouse epiblast share defining features with human embryonic stem cells. Nature *448*, 196–199.

Theunissen, T.W., Powell, B.E., Wang, H., Mitalipova, M., Faddah, D.A., Reddy, J., Fan, Z.P., Maetzel, D., Ganz, K., Shi, L., et al. (2014). Systematic identification of culture conditions for induction and maintenance of naive human pluripotency. Cell Stem Cell *15*, 471–487.

Thomson, J.A., Itskovitz-Eldor, J., Shapiro, S.S., Waknitz, M.A., Swiergiel, J.J., Marshall, V.S., and Jones, J.M. (1998). Embryonic stem cell lines derived from human blastocysts. Science *282*, 1145–1147.

Thornhill, A.R., and Burgoyne, P.S. (1993). A paternally imprinted X chromosome retards the development of the early mouse embryo. Development *118*, 171–174.

Tian, D., Sun, S., and Lee, J.T. (2010). The long noncoding RNA, Jpx, is a molecular switch for X chromosome inactivation. Cell *143*, 390–403.

Tsumura, A., Hayakawa, T., Kumaki, Y., Takebayashi, S., Sakaue, M., Matsuoka, C., Shimotohno, K., Ishikawa, F., Li, E., Ueda, H.R., et al. (2006). Maintenance of self-renewal ability of mouse embryonic stem cells in the absence of DNA methyltransferases Dnmt1, Dnmt3a and Dnmt3b. Genes Cells *11*, 805–814.

Tsunoda, Y., Tokunaga, T., and Sugie, T. (1985). Altered sex ratio of live young after transfer of fast- and slow-developing mouse embryos. Gamete Res. *12*, 301–304.

Vallier, L., Alexander, M., and Pedersen, R.A. (2005). Activin/Nodal and FGF pathways cooperate to maintain pluripotency of human embryonic stem cells. J. Cell Sci. *118*, 4495–4509.

Vallot, C., Ouimette, J.-F., Makhlouf, M., Féraud, O., Pontis, J., Côme, J., Martinat, C., Bennaceur-Griscelli, A., Lalande, M., and Rougeulle, C. (2015). Erosion of X Chromosome Inactivation in Human Pluripotent Cells Initiates with XACT Coating and Depends on a Specific Heterochromatin Landscape. Cell Stem Cell *16*, 533–546.

Vallot, C., Patrat, C., Collier, A.J., Huret, C., Casanova, M., Liyakat Ali, T.M., Tosolini, M., Frydman, N., Heard, E., Rugg-Gunn, P.J., et al. (2017). XACT Noncoding RNA Competes with XIST in the Control of X Chromosome Activity during Human Early Development. Cell Stem Cell *20*, 102–111.

Vicoso, B., and Bachtrog, D. (2009). Progress and prospects toward our understanding of the evolution of dosage compensation. Chromosome Res. *17*, 585–602.

van Vliet, C., Bukczynska, P.E., Puryer, M.A., Sadek, C.M., Shields, B.J., Tremblay, M.L., and Tiganis, T. (2005). Selective regulation of tumor necrosis factor-induced Erk signaling by Src family kinases and the T cell protein tyrosine phosphatase. Nat. Immunol. *6*, 253–260.

Walkley, N.A., Demaine, A.G., and Malik, A.N. (1996). Cloning, structure and mRNA expression of human Cctg, which encodes the chaperonin subunit CCT gamma. Biochem. J. *313 (Pt 2)*, 381–389.

Wang, L., and Shilatifard, A. (2019). UTX mutations in human cancer. Cancer Cell *35*, 168–176.

Wang, L., Jahren, N., Miller, E.L., Ketel, C.S., Mallin, D.R., and Simon, J.A. (2010). Comparative analysis of chromatin binding by Sex Comb on Midleg (SCM) and other polycomb group repressors at a Drosophila Hox gene. Mol. Cell. Biol. *30*, 2584–2593.

Wang, Z., Oron, E., Nelson, B., Razis, S., and Ivanova, N. (2012). Distinct lineage specification roles for NANOG, OCT4, and SOX2 in human embryonic stem cells. Cell Stem Cell *10*, 440–454.

Watanabe, S., Umehara, H., Murayama, K., Okabe, M., Kimura, T., and Nakano, T. (2006). Activation of Akt signaling is sufficient to maintain pluripotency in mouse and primate embryonic stem cells. Oncogene *25*, 2697–2707.

Whitmarsh, A.J., Shore, P., Sharrocks, A.D., and Davis, R.J. (1995). Integration of MAP kinase signal transduction pathways at the serum response element. Science *269*, 403–407.

Wicklow, E., Blij, S., Frum, T., Hirate, Y., Lang, R.A., Sasaki, H., and Ralston, A. (2014). HIPPO pathway members restrict SOX2 to the inner cell mass where it promotes ICM fates in the mouse blastocyst. PLoS Genet. *10*, e1004618.

Williams, R.L., Hilton, D.J., Pease, S., Willson, T.A., Stewart, C.L., Gearing, D.P., Wagner, E.F., Metcalf, D., Nicola, N.A., and Gough, N.M. (1988). Myeloid leukaemia inhibitory factor maintains the developmental potential of embryonic stem cells. Nature *336*, 684–687.

Wong, J.W.H., and Cagney, G. (2010). An overview of label-free quantitation methods in proteomics by mass spectrometry. Methods Mol. Biol. *604*, 273–283.

Wray, J., Kalkan, T., and Smith, A.G. (2010). The ground state of pluripotency. Biochem. Soc. Trans. *38*, 1027–1032.

Wray, J., Kalkan, T., Gomez-Lopez, S., Eckardt, D., Cook, A., Kemler, R., and Smith, A. (2011). Inhibition of glycogen synthase kinase-3 alleviates Tcf3 repression of the pluripotency network and increases embryonic stem cell resistance to differentiation. Nat. Cell Biol. *13*, 838–845.

Wutz, A., and Jaenisch, R. (2000). A shift from reversible to irreversible X inactivation is triggered during ES cell differentiation. Mol. Cell *5*, 695–705.

Wutz, A., Rasmussen, T.P., and Jaenisch, R. (2002). Chromosomal silencing and localization are mediated by different domains of Xist RNA. Nat. Genet. *30*, 167–174.

Wu, Y., Chen, Z., and Ullrich, A. (2003). EGFR and FGFR signaling through FRS2 is subject to negative feedback control by ERK1/2. Biol. Chem. *384*, 1215–1226.

Xie, T., Pan, S., Zheng, H., Luo, Z., Tembo, K.M., Jamal, M., Yu, Z., Yu, Y., Xia, J., Yin, Q., et al. (2018). PEG10 as an oncogene: expression regulatory mechanisms and role in tumor progression. Cancer Cell Int. *18*, 112.

Yadav, B.R., King, W.A., and Betteridge, K.J. (1993). Relationships between the completion of first cleavage and the chromosomal complement, sex, and developmental rates of bovine embryos generated in vitro. Mol. Reprod. Dev. *36*, 434–439.

Yamaji, M., Ueda, J., Hayashi, K., Ohta, H., Yabuta, Y., Kurimoto, K., Nakato, R., Yamada, Y., Shirahige, K., and Saitou, M. (2013). PRDM14 ensures naive pluripotency through dual regulation of signaling and epigenetic pathways in mouse embryonic stem cells. Cell Stem Cell *12*, 368–382.

Yamamoto, T., Sekine, Y., Kashima, K., Kubota, A., Sato, N., Aoki, N., and Matsuda, T. (2002). The nuclear isoform of protein-tyrosine phosphatase TC-PTP regulates interleukin-6-mediated signaling pathway through STAT3 dephosphorylation. Biochem. Biophys. Res. Commun. *297*, 811–817.

Yamanaka, Y., Lanner, F., and Rossant, J. (2010). FGF signal-dependent segregation of primitive endoderm and epiblast in the mouse blastocyst. Development *137*, 715–724.

Yang, F., Babak, T., Shendure, J., and Disteche, C.M. (2010). Global survey of escape from X inactivation by RNA-sequencing in mouse. Genome Res. *20*, 614–622.

Yan, K.S., Kuti, M., Yan, S., Mujtaba, S., Farooq, A., Goldfarb, M.P., and Zhou, M.-M. (2002). FRS2 PTB domain conformation regulates interactions with divergent neurotrophic receptors. J. Biol. Chem. *277*, 17088–17094.

Yeo, J.-C., Jiang, J., Tan, Z.-Y., Yim, G.-R., Ng, J.-H., Göke, J., Kraus, P., Liang, H., Gonzales, K.A.U., Chong, H.-C., et al. (2014). Klf2 is an essential factor that sustains ground state pluripotency. Cell Stem Cell *14*, 864–872.

Ye, S., Li, P., Tong, C., and Ying, Q.-L. (2013). Embryonic stem cell self-renewal pathways converge on the transcription factor Tfcp2l1. EMBO J. *32*, 2548–2560.

Ying, Q.-L., and Smith, A. (2017). The art of capturing pluripotency: creating the right culture. Stem Cell Reports *8*, 1457–1464.

Ying, Q.-L., Wray, J., Nichols, J., Batlle-Morera, L., Doble, B., Woodgett, J., Cohen, P., and Smith, A. (2008). The ground state of embryonic stem cell self-renewal. Nature *453*, 519–523.

Ying, Q.L., Nichols, J., Chambers, I., and Smith, A. (2003). BMP induction of Id proteins suppresses differentiation and sustains embryonic stem cell self-renewal in collaboration with STAT3. Cell *115*, 281–292.

Yuan, H., Corbi, N., Basilico, C., and Dailey, L. (1995). Developmental-specific activity of the FGF-4 enhancer requires the synergistic action of Sox2 and Oct-3. Genes Dev. *9*, 2635–2645.

Yusoff, P., Lao, D.-H., Ong, S.H., Wong, E.S.M., Lim, J., Lo, T.L., Leong, H.F., Fong, C.W., and Guy, G.R. (2002). Sprouty2 inhibits the Ras/MAP kinase pathway by inhibiting the activation of Raf. J. Biol. Chem. *277*, 3195–3201.

Zakrzewska, M., Haugsten, E.M., Nadratowska-Wesolowska, B., Oppelt, A., Hausott, B., Jin, Y., Otlewski, J., Wesche, J., and Wiedlocha, A. (2013). ERK-mediated phosphorylation of fibroblast growth factor receptor 1 on Ser777 inhibits signaling. Sci. Signal. *6*, ra11.

Zhang, J., Liu, G., Ruan, Y., Wang, J., Zhao, K., Wan, Y., Liu, B., Zheng, H., Peng, T., Wu, W., et al. (2014). Dax1 and Nanog act in parallel to stabilize mouse embryonic stem cells and induced pluripotency. Nat. Commun. *5*, 5042.

Zhao, Z.-A., Yu, Y., Ma, H.-X., Wang, X.-X., Lu, X., Zhai, Y., Zhang, X., Wang, H., and Li, L. (2015). The roles of ERAS during cell lineage specification of mouse early embryonic development. Open Biol. *5*.

Zhou, J.-W., Tang, J.-J., Sun, W., and Wang, H. (2019). PGK1 facilities cisplatin chemoresistance by triggering HSP90/ERK pathway mediated DNA repair and methylation in endometrial endometrioid adenocarcinoma. Mol. Med. *25*, 11.

Zuris, J.A., Thompson, D.B., Shu, Y., Guilinger, J.P., Bessen, J.L., Hu, J.H., Maeder, M.L., Joung, J.K., Chen, Z.-Y., and Liu, D.R. (2015). Cationic lipid-mediated delivery of proteins enables efficient protein-based genome editing in vitro and in vivo. Nat. Biotechnol. *33*, 73–80.

Zvetkova, I., Apedaile, A., Ramsahoye, B., Mermoud, J.E., Crompton, L.A., John, R., Feil, R., and Brockdorff, N. (2005). Global hypomethylation of the genome in XX embryonic stem cells. Nat. Genet. *37*, 1274–1279.

Zwingman, T., Erickson, R.P., Boyer, T., and Ao, A. (1993). Transcription of the sex-determining region genes Sry and Zfy in the mouse preimplantation embryo. Proc Natl Acad Sci USA *90*, 814–817.

Żylicz, J.J., Bousard, A., Žumer, K., Dossin, F., Mohammad, E., da Rocha, S.T., Schwalb, B., Syx, L., Dingli, F., Loew, D., et al. (2019). The implication of early chromatin changes in X chromosome inactivation. Cell *176*, 182-197.e23.

(2010). Handbook of cell signaling (Elsevier).

10. Appendix

10.1. Supplemental tables

10.1.1 Instruments

Table S1. Instruments used in this study

Instrument	Source
Accuspin Micro 17 Centrifuge	Thermo Fisher Scientific
Centrifuge 5424 R	Eppendorf
Centrifuge 5810 R	Eppendorf
Heraeus Megafuge 8	Thermo Fisher Scientific
Mastercycler Pro	Eppendorf
Precision GP 02 water bath	Thermo Fisher Scientific
Hybrigene Incubator	Techne
Herasafe Hood for Cell Culture	Thermo Fisher Scientific
Heracell 150i CO2 incubator for Cell Culture	Thermo Fisher Scientific
Aqualine Water bath AL 12	Lauda
Axio Vert.A1 Microscope	Zeiss
4D Nucleofector	Lonza
EVE™ Automated Cell Counter	NanoEnTek
Pyromark Q24	Qiagen
BD FACSAria II	BD Biosciences
BD FACSAria Fusion	BD Biosciences
ABI 7900HT Real-time PCR machine	Thermo Fisher Scientific
QuantStudio™ 7 Flex Real-Time PCR machine	Thermo Fisher Scientific
Gel Doc™ XR+ Gel Documentation System	Bio-Rad

10.1.2 Enzymes

Table S2. Enzymes used in this study

Enzyme	Supplier	Number

Restriction enzymes		
ApaI	New England Biolabs	R0114S
BsmBI	New England Biolabs	R0580S
BlpI	New England Biolabs	FD0094
BstXI	New England Biolabs	FD1024
HpaII	New England Biolabs	R0171S
MspI	New England Biolabs	R0106S
EcoRI	New England Biolabs	R3101S
KpnI	New England Biolabs	R3142S
NlaIII	New England Biolabs	R0125S
PstI	New England Biolabs	R3140S
NheI	New England Biolabs	R3131S
BsrGI	New England Biolabs	R3575 S
NcoI	New England Biolabs	R3193S
NaeI	New England Biolabs	R0190S
BsaAI	New England Biolabs	R0531S
Polymerases		
Phusion Hotstart Flex DNA Polymerase	New England Biolabs	M0535S
KAPA HiFi HS RM	Roche	7958935001
HotStart Taq Polymerase	Qiagen	203203
Phusion High-Fidelity DNA Polymerase	New England Biolabs	M0530L
CloneAmp HiFi PCR Premix	Takara Bio	639298
Other		
RNAse A	Thermo Fisher Scientific	AM2269
Proteinase K	Thermo Fisher Scientific	25530049
Recombinant Cas9 from Alt-R® CRISPR-Cas9 System	IDT	1081060
Superscript III Reverse Transcriptase	Thermo Fisher Scientific	18080093

T4 DNAse ligase	New England Biolabs	M0202S
Trypsin	Thermo Fisher Scientific	25300054
Benzonase	Merck	70746-3
Gibson Assembly MasterMix	New England Biolabs	E2611S

10.1.3 Kits

Table S3. Kits used in this study

Kit	Function	Supplier	Number
DNeasy Blood and Tissue kit	gDNA isolation	Qiagen	69504
Direct-Zol RNA Miniprep Kit	RNA purification	Zymo Research	R2070
QuantSeq 3‘ mRNA-Seq Library Prep Kit	RNA sequencing	Lexogen	Quote LexGmbH-24-06-2019-001189
Peqgold Plasmid Miniprep Kit I	Plasmid DNA purification	VWR	732-2780
NucleoBond Xtra Midi Plus	Plasmid DNA purification	Macherey-Nagel	740412.50
NucleoBond BAC	BAC DNA purification	Macherey-Nagel	740579
NucleoSpin Gel and PCR Clean-up	PCR Clean-up	Macherey-Nagel	740609.50
Nick translation kit	FISH probe labeling	Abbot	07J00-001

10.1.4 Bacterial strains

Table S4. Bacterial strains used in this study

Bacterial strain	Function	Supplier	Number
MegaX DH10B T1R Electrocompetent cells	sgRNA library transformation	Thermo Fisher Scientific	C640003
One Shot Stbl3 Chemically competent cells	Lentiviral plasmid transformation	Thermo Fisher Scientific	C737303
Stellar chemically competent cells	Non-lentiviral and lentiviral plasmid transformation	Takara Bio	636762

One Shot TOP10 chemically competent cells	Non-lentiviral plasmid transformation	Thermo Fisher Scientific	C404003

10.1.5 SRE-Elk promoter sequence

Table S5. SRE-Elk promoter sequence

Name	Sequence
SRE-Elk (MAPK-sensitive promoter)	CAGGATGTCCATATTAGGACACAGGATGTCCATATTAGGACACAGGA TGTCCATATTAGGACACAGGATGTCCATATTAGGACACAGGATGTCCA TATTAGGACACAGGATGTCCATATTAGGACAAAGCTTAATTAAGTTCC GCCCAGTGACGTAGGAAGTCCATCCATTCACAGCGCTTCTATAAAGGC GCCAGCTGAGGCGCCTACTACTCCAACCGCGACTGCAGCGAGCAACT GAGAAGACTGGATAGAGCCGGCGGTTCCGCGAACGAGCAGTGACCG CGCTCCCACCCAGCTCTGCTCTGCAGCTCCCACCAGTGCCA

10.1.6 Illumina barcodes

Table S6. Illumina barcodes used in this study

Barcode number	Barcode sequence	Primer number	Sample
27	ATTCCT	OG126	SRE-Elk screen: Unsorted D7 R1 Nanog screen: Unsorted D7 R1 pMek screen: Unsorted unfixed R1
33	CAGGCG	OG127	SRE-Elk screen: Sorted 25% D7 R1 Nanog screen: Sorted 25% Top D7 R1 pMek screen: Unsorted fixed R1
34	CATGGC	OG128	SRE-Elk screen: Unsorted D7 R2 Nanog screen: Sorted Bottom D7 R1 pMek screen: Sorted Top 25% R1
35	CATTTT	OG129	SRE-Elk screen: Sorted D7 R2 Nanog screen: Unsorted Top D9 R1 pMek screen: Sorted Bottom 25% R1
36	CCAACA	OG130	SRE-Elk screen: Unsorted D7 R3 Nanog screen: Sorted Top D9 R1 pMek screen: Unsorted unfixed R2
37	CGGAAT	OG131	SRE-Elk screen: Sorted D7 R3 Nanog screen: Unsorted Bottom D9 R1 pMek screen: Unsorted fixed R2

38	CTAGCT	OG132	SRE-Elk screen: Unsorted D9 R1 Nanog screen: Sorted Bottom D9 R1 pMek screen: Sorted Top 25% R2
39	CTATAC	OG133	SRE-Elk screen: Sorted D9 R1 Nanog: Unsorted D7 R2 pMek screen: Sorted Bottom 25% R2
40	CTCAGA	OG134	SRE-Elk screen: Unsorted D9 R2 Nanog screen: Sorted Top D7 R2 pMek screen: Unsorted unfixed R3
41	GACGAC	OG135	SRE-Elk screen: Sorted D9 R2 Nanog screen: Sorted Bottom D7 R2 pMek screen: Unsorted fixed R3
42	TAATCG	OG136	SRE-Elk screen: Unsorted D9 R3 Nanog screen: Unsorted Top D9 R2 pMek screen: Sorted Bottom 25% R3
43	TACAGC	OG137	SRE-Elk screen: Sorted D9 R3 Nanog screen: Sorted Top D9 R2 pMek screen: Sorted Bottom 25% R3
1	ATCACG	OG170	Nanog screen: Unsorted Bottom D9 R2
2	CGATGT	OG171	Nanog screen: Sorted Bottom D9 R2
3	TTAGGC	OG172	Esrrb screen: Unsorted undifferentiated R1
4	TGACCA	OG173	Esrrb screen: Unsorted differentiated R1
5	ACAGTG	OG174	Esrrb screen: Sorted Top 20% undifferentiated R1
6	GCCAAT	OG175	Esrrb screen: Sorted Bottom 20% undifferentiated R1
7	CAGATC	OG176	Esrrb screen: Sorted Top 10% undifferentiated R1
8	ACTTGA	OG177	Esrrb screen: Sorted Bottom 10% undifferentiated R1
9	GATCAG	OG178	Esrrb screen: Unsorted undifferentiated R2
10	TAGCTT	OG179	Esrrb screen: Unsorted differentiated R2
11	GGCTAC	OG180	Esrrb screen: Sorted Top 20% undifferentiated R2
12	CTTGTA	OG181	Esrrb screen: Sorted Bottom 20% undifferentiated R2
13	AGTCAA	OG182	Esrrb screen: Sorted Top 10% undifferentiated R2
14	AGTTCC	OG183	Esrrb screen: Sorted Bottom 10% undifferentiated R2
15	ATGTCA	OG184	Esrrb screen: Unsorted undifferentiated R3
16	CCGTCC	OG185	Esrrb screen: Unsorted differentiated R3

17	GTAGAG	OG186	Esrrb screen: Sorted Top 20% undifferentiated R3
18	GTCCGC	OG187	Esrrb screen: Sorted Bottom 20% undifferentiated R3
19	GTGAAA	OG188	Esrrb screen: Sorted Top 10% undifferentiated R3
20	GTGGCC	OG189	Esrrb screen: Sorted Bottom 10% undifferentiated R3

10.1.7 Software

Table S7. Software used in this study

Name	**Source**	**Application**
R Studio	(Robinson et al., 2010)	Data analysis and visualization
Geneious	https://www.geneious.com/	Sequence database for plasmids, primers, gDNA, etc, and molecular cloning design tool
FlowJo V10 Software	BD Biosciences	FCS file gating and analysis
Image Lab Software	https://www.bio-rad.com/de-de/product/image-lab-software?ID=KRE6P5E8Z	Gel visualization and analysis
Galaxy	https://usegalaxy.eu/ (Afgan et al., 2016)	CRISPR KO screen analysis and Karyotyping analysis
Pyromark Q24 2.0.8	https://www.qiagen.com/us/resources/resourcedetail?id=273a81ee-f6fb-4dcf-8fb4-ae56dd947706&lang=en	Pyrosequencing analysis
Image Studio Lite Ver 5.2	LI-COR	Immunoblotting quantification and analysis
SDS 2.1	https://www.thermofisher.com/de/de/home/technical-resources/software-downloads/applied-biosystems-7900ht-fast-real-timespcr-system.html	qPCR analysis
QuantStudio 7	https://www.thermofisher.com/de/de/home/global/forms/life-science/quantstudio-6-7-flex-software.html	qPCR analysis
Zen lite 2012	Zeiss	Microscopy Image analysis
BlueBee NGS data analysis platform	https://www.bluebee.com/	RNA-seq analysis

MaxQuant v1.6.0.1	https://www.maxquant.org/	LFQ intensity calculation
Perseus v1.6.1.3	http://www.perseus.tufts.edu	Proteomics data analysis
NCBI primer blast	https://www.ncbi.nlm.nih.gov/tools/primer-blast/	qPCR primer design
CRISPR EDU MIT	http://crispr.mit.edu:8079/	sgRNA design
Adobe Illustrator CC (64 Bit)	https://adobe.com/products/illustrator/	Figure generation

10.2. Vector maps

10.2.1 302 (SP35)

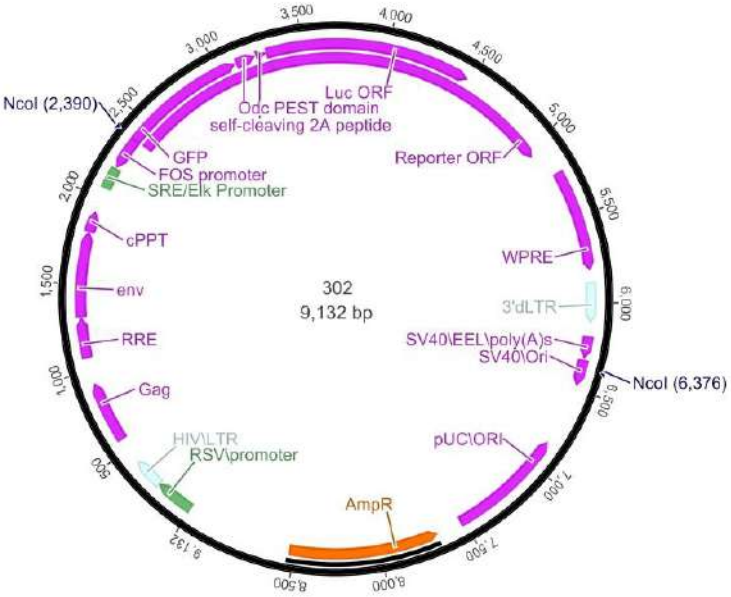

10.2.2 lenti-MS2-P65-HSF1-Hygro (SP63)

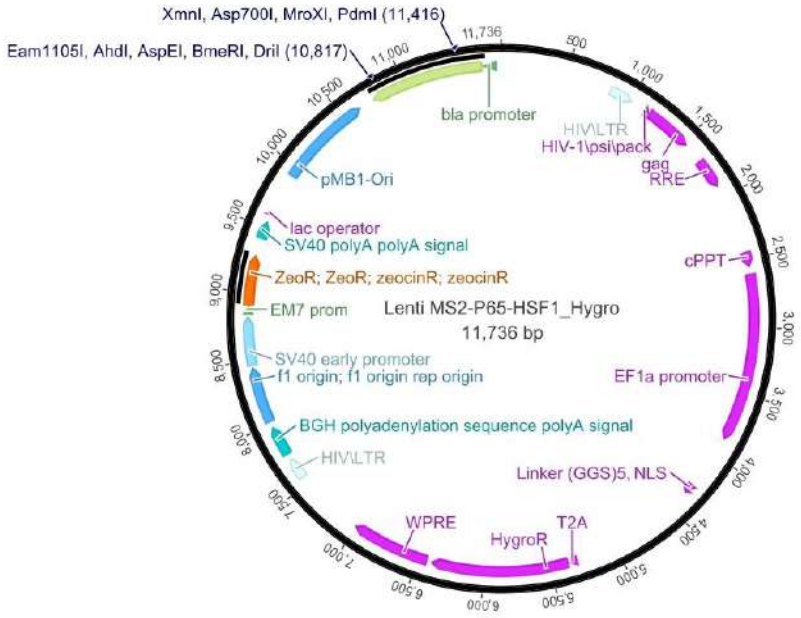

10.2.3 lenti-SRE-Elk-GFP-PEST-Hygro (SP300)

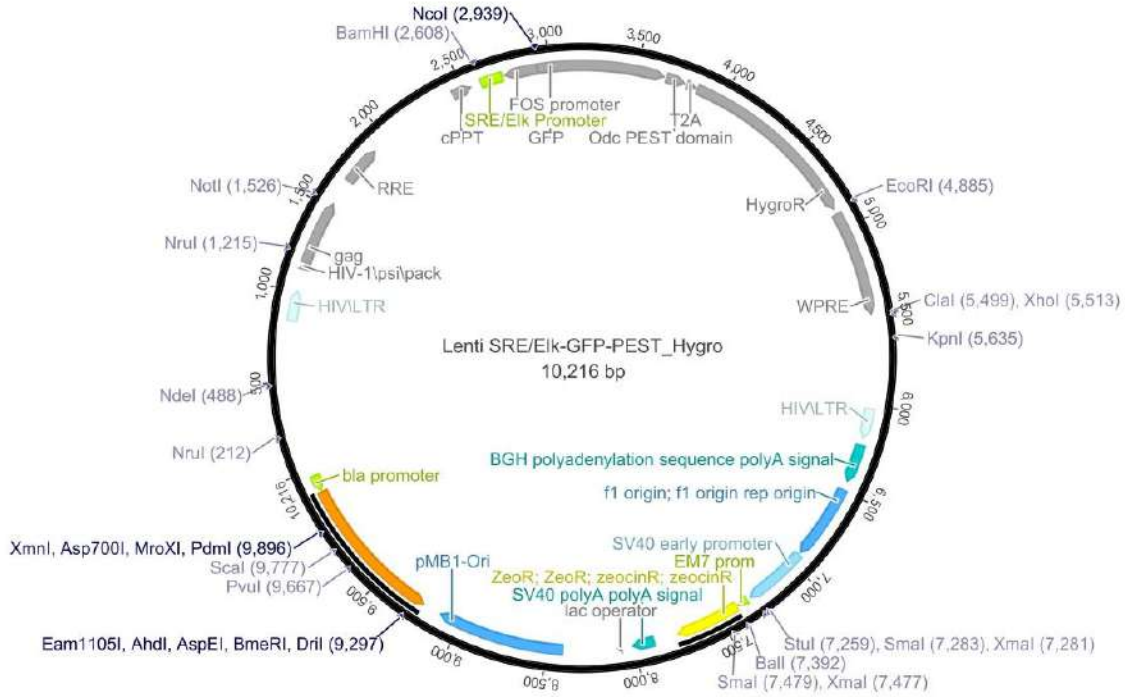

10.2.4 lentiGuide-Puro (SP32)

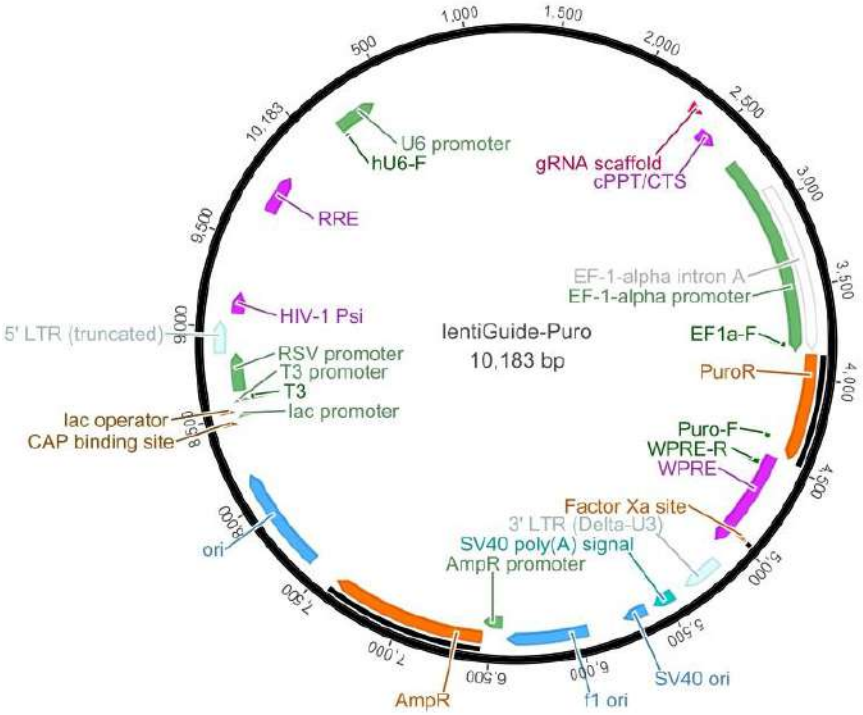

10.2.5 pBROAD3-hyBASE-IRES-Zeocin (SP99)

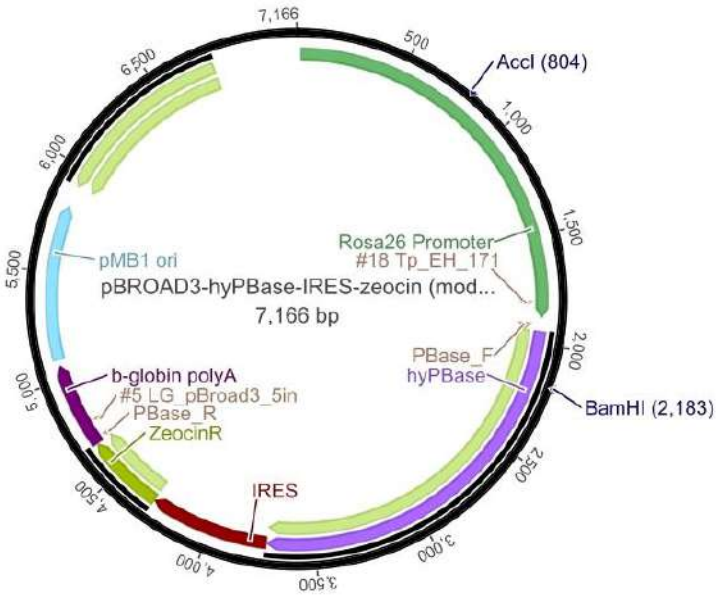

10.2.6 pLenti-PGK-Degron-GFP-Blast (SP234)

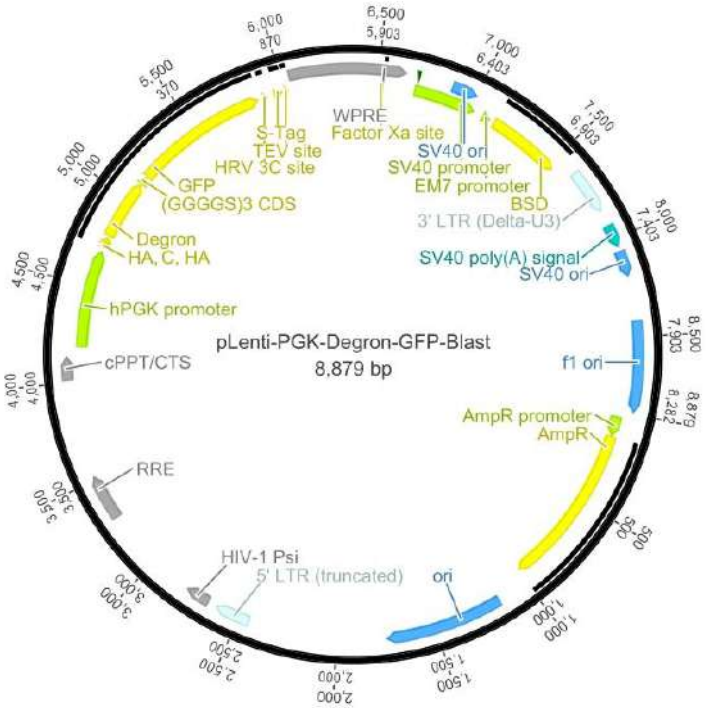

10.2.7 pLenti-PGK-Degron-GFP-Klhl13-Blast (SP235)

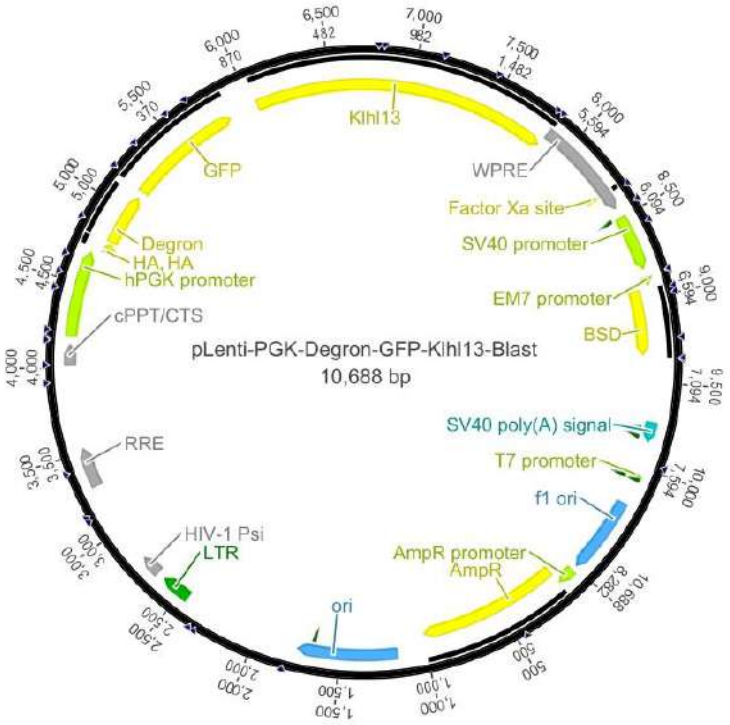

10.2.8 pLenti-PGK-GFP-Blast (SP51, Original plasmid)

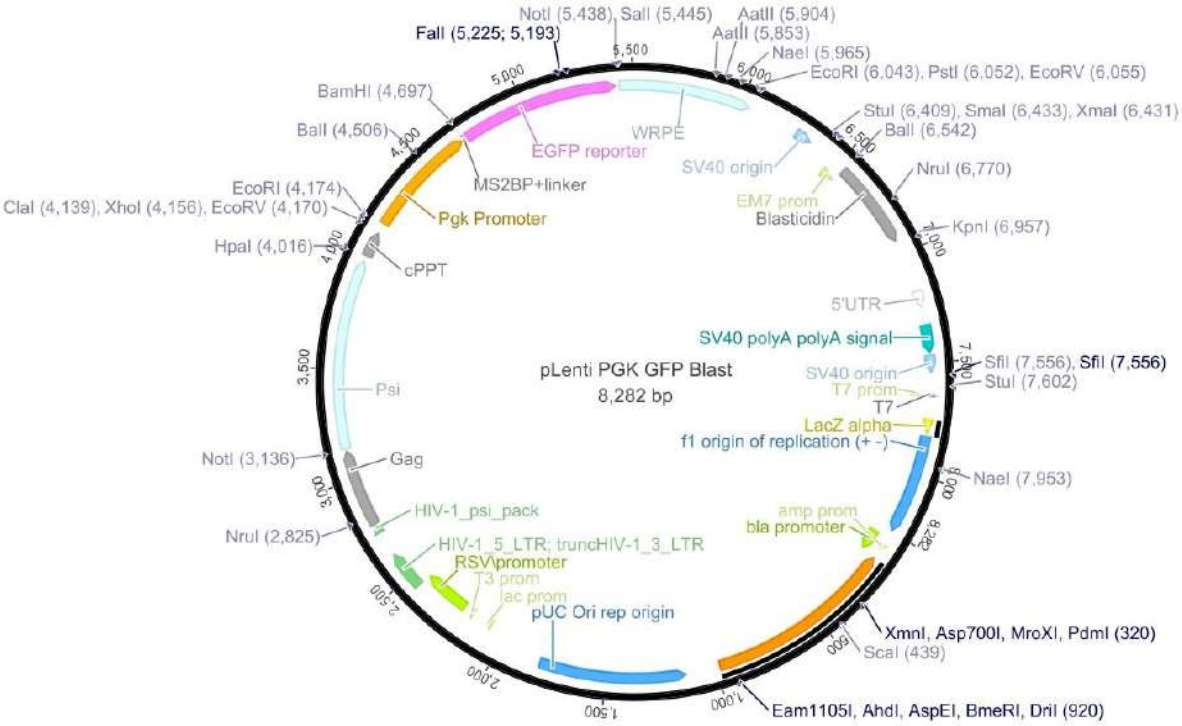

10.2.9 pLenti-PGK-GFP-Blast (SP233, Modified GFP)

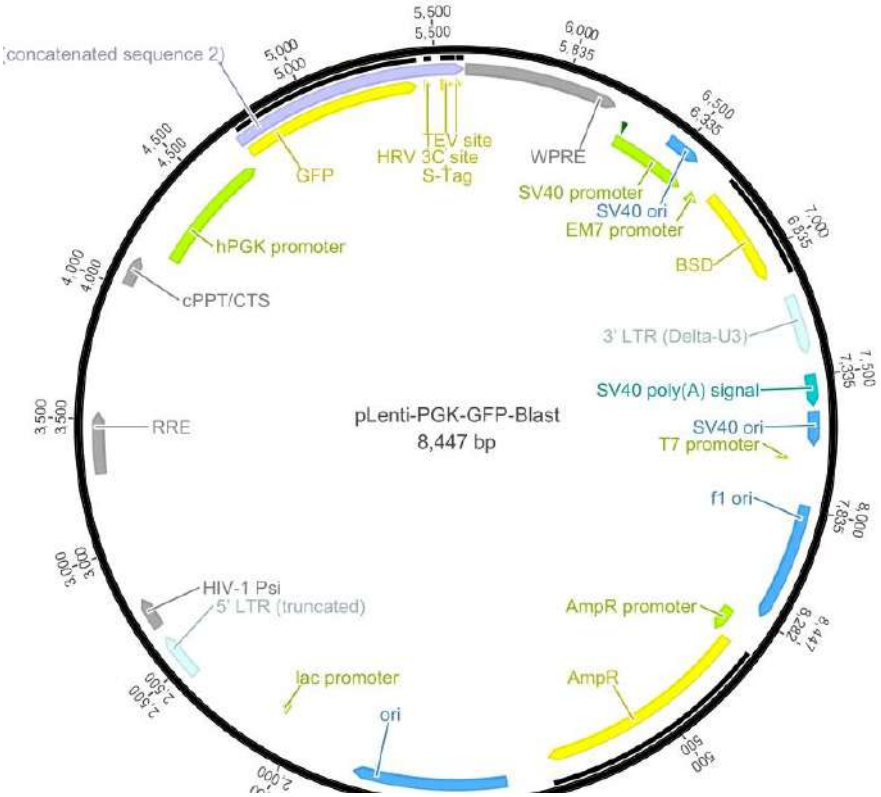

10.2.10 pLenti-PGK-GFP-Kelch-Blast (SP238)

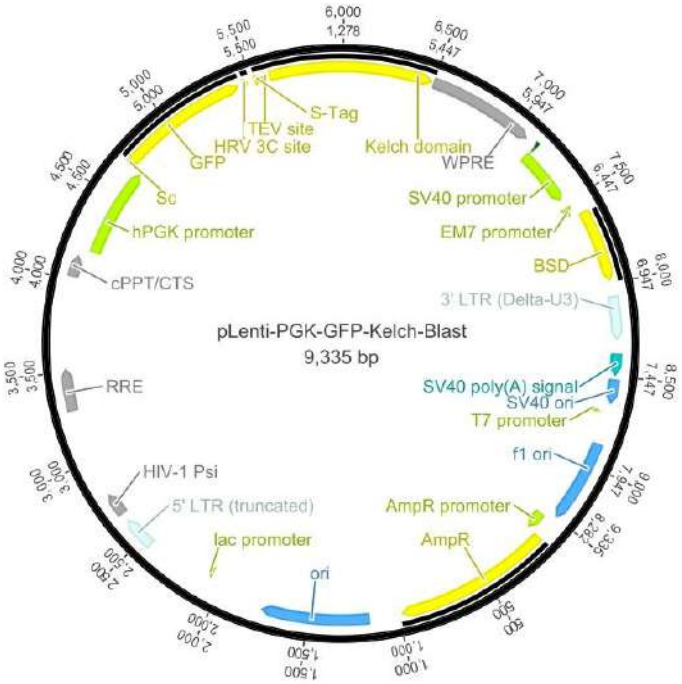

10.2.11 pU6-sgRNA-EF1a-Puro-T2A-BFP (SP65)

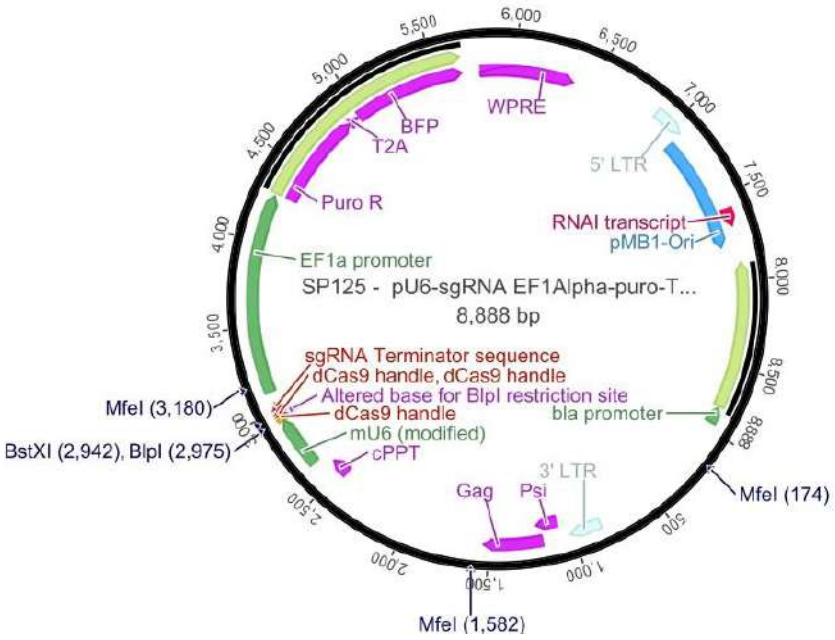

10.2.12 pUC19 (SP194)

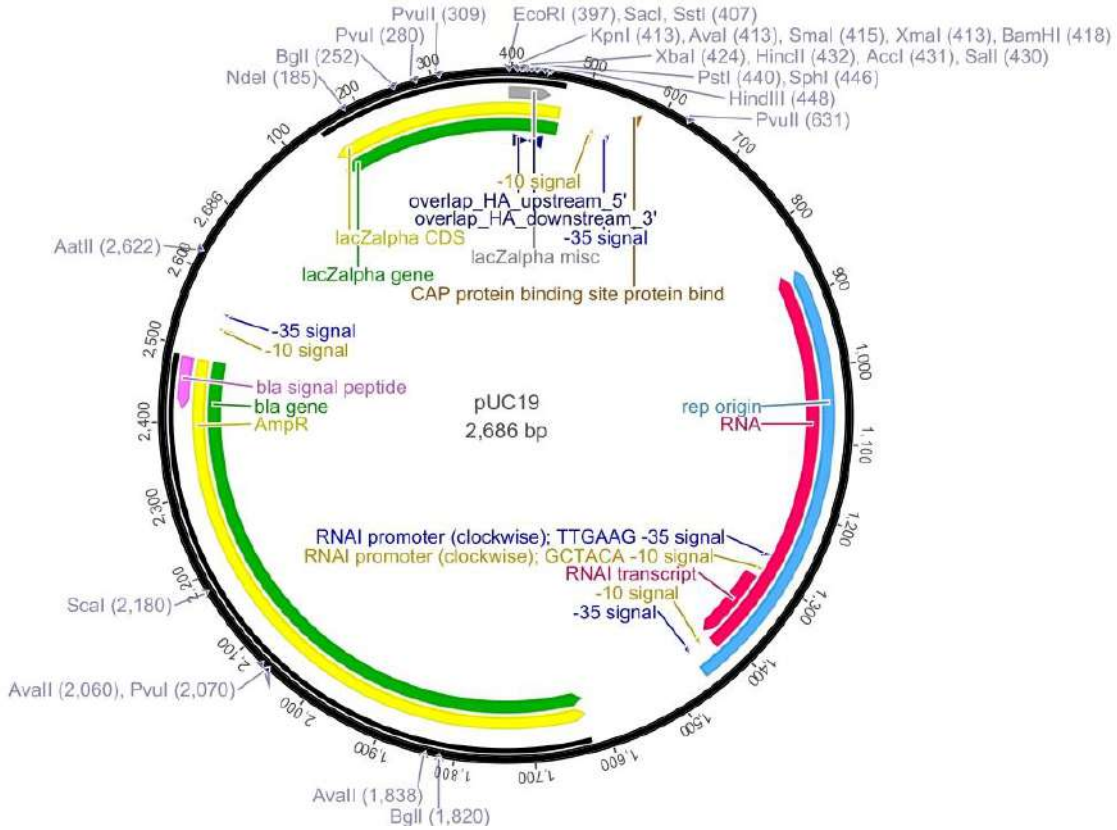

10.2.13 pUC19-Esrrb-P2A-mCherry-T2A-Puro

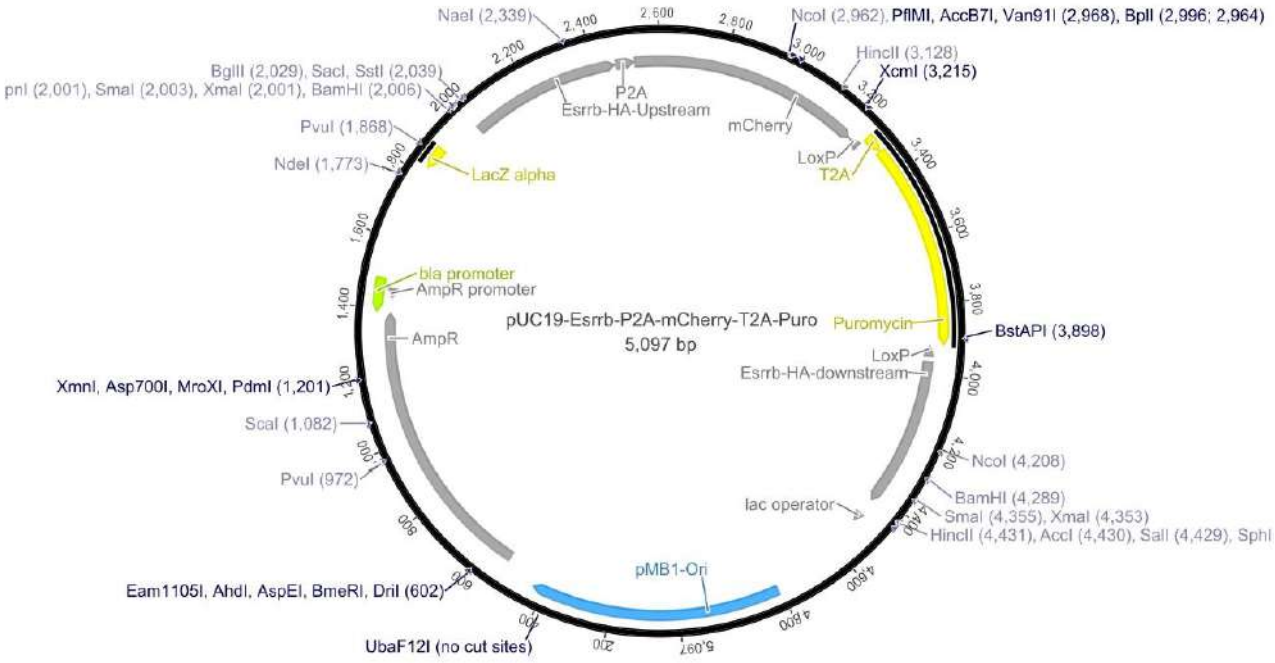

10.2.14 pUC19-Nanog-P2A-mCherry-T2A-Puro

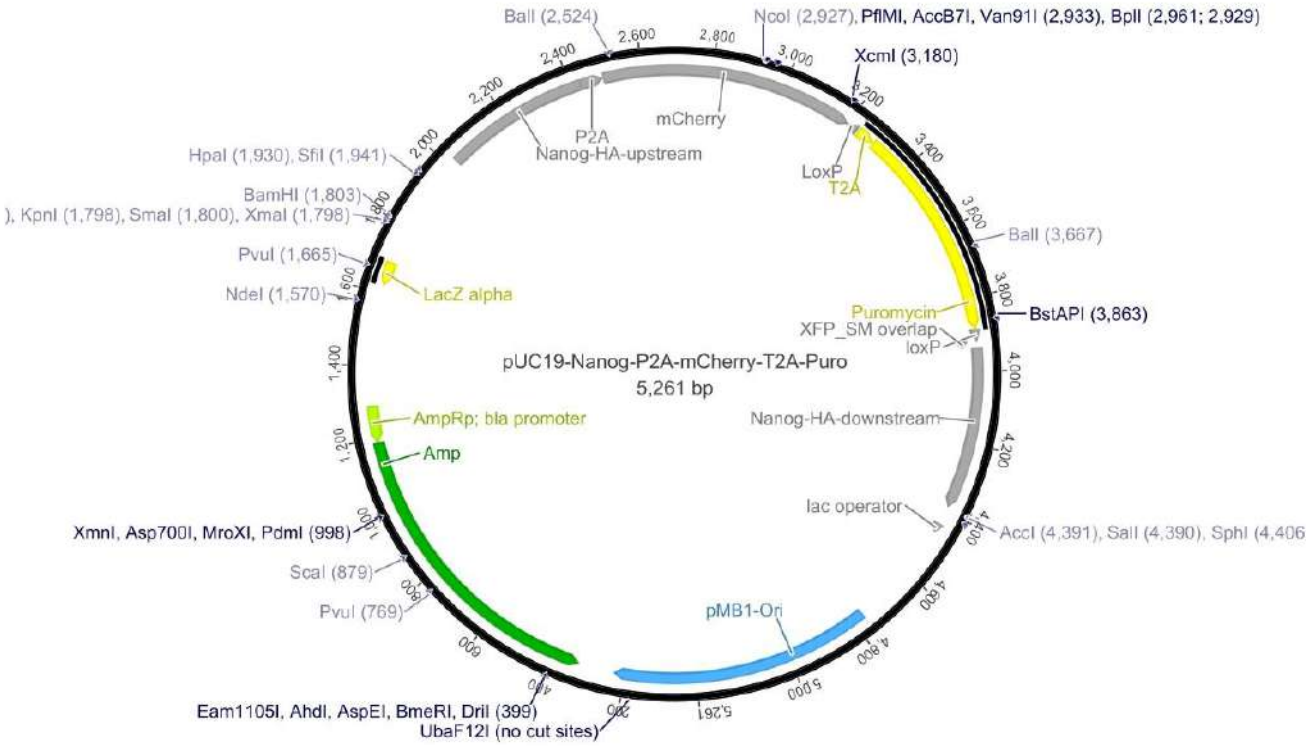

10.2.15 PX330 (SP301)

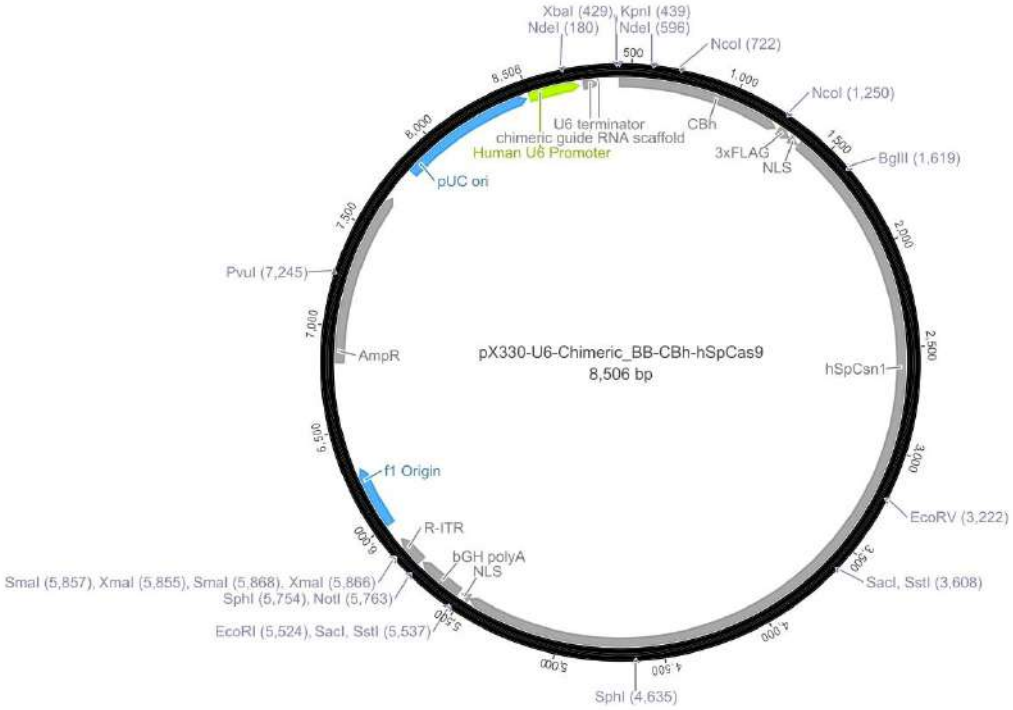

10.2.16 PX458 (SP177)

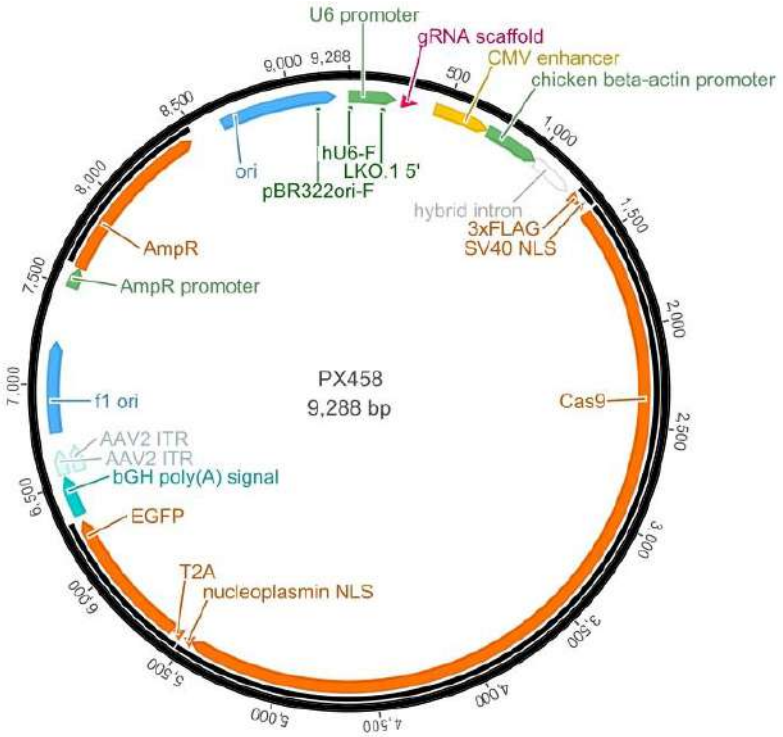

10.2.17 pCAG-Cre (SP44)

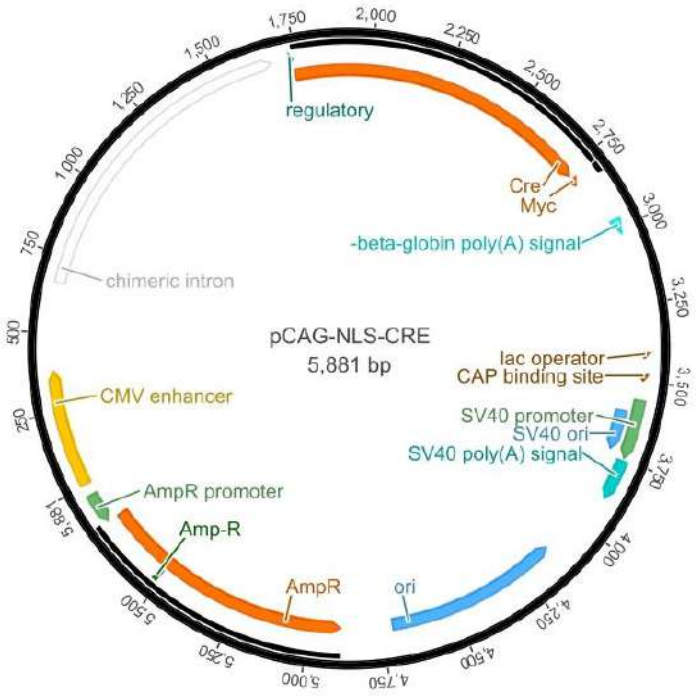

10.2.18 lentiCas9-Blast (SP54)

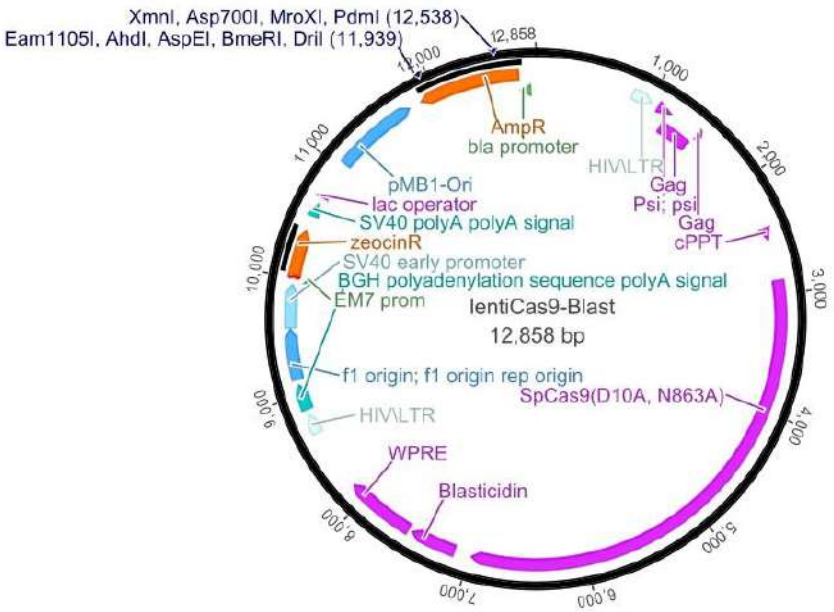

10.2.19 pSuper-Puro (SP10)

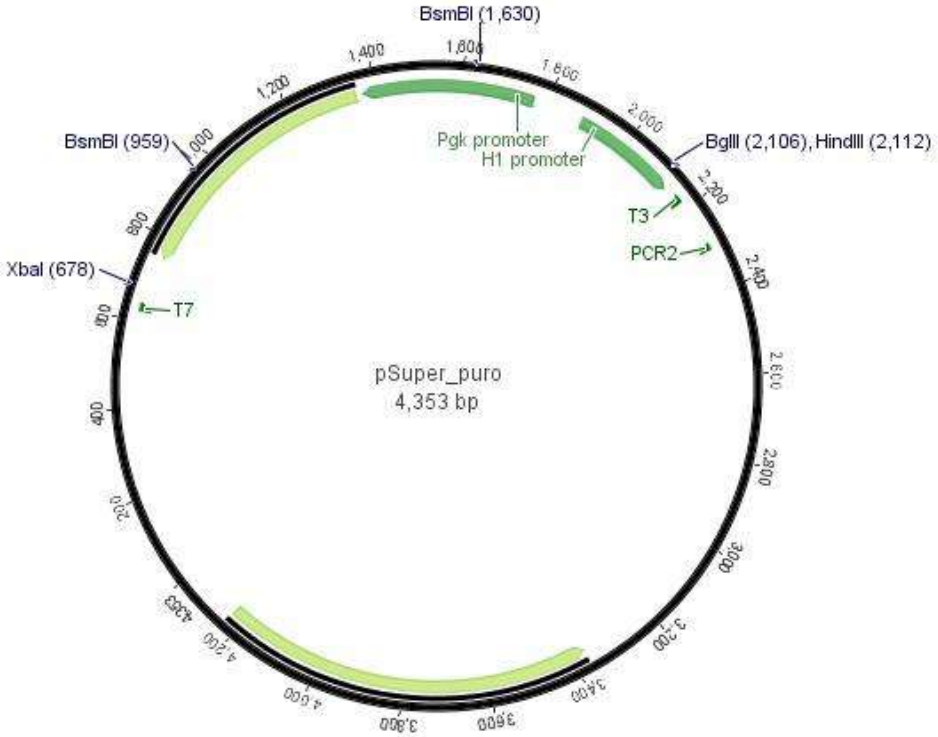

10.2.20 pSuper-Puro-MCS-PolyA (SP27)

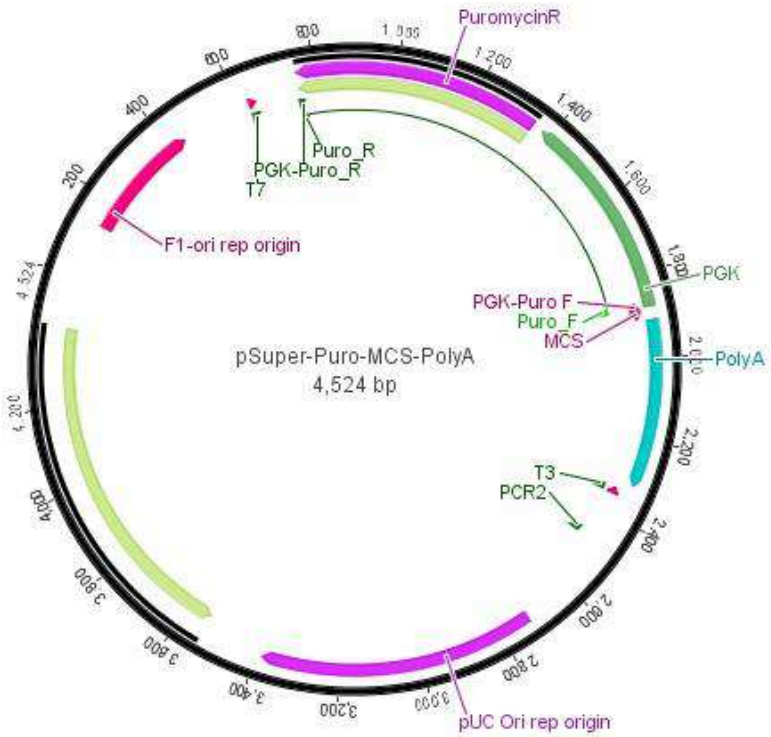

10.2.21 pSuper-Puro-SRE/Elk-GFP-PEST-PolyA (SP25)

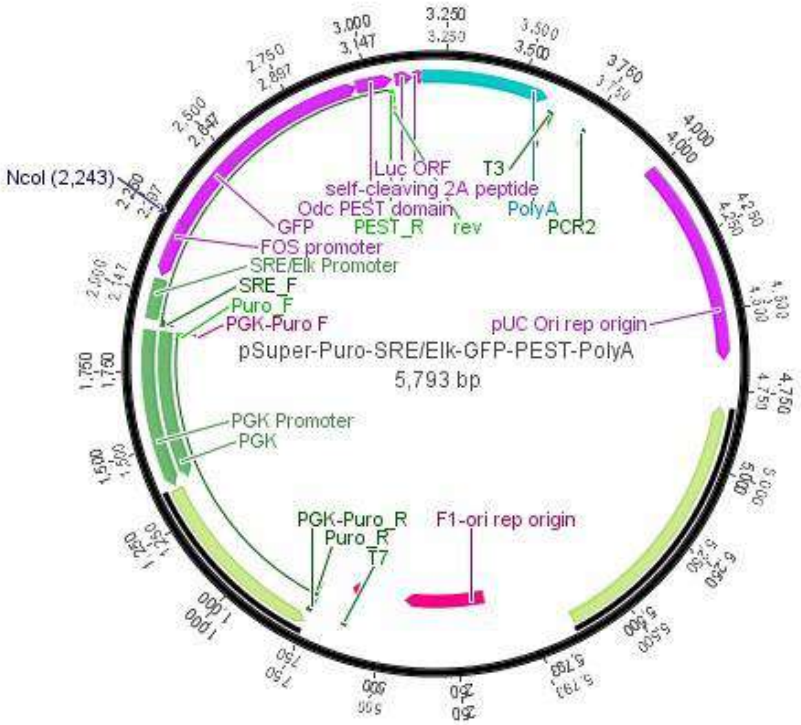

10.2.22 pCAGG-L-GFP (SP9)

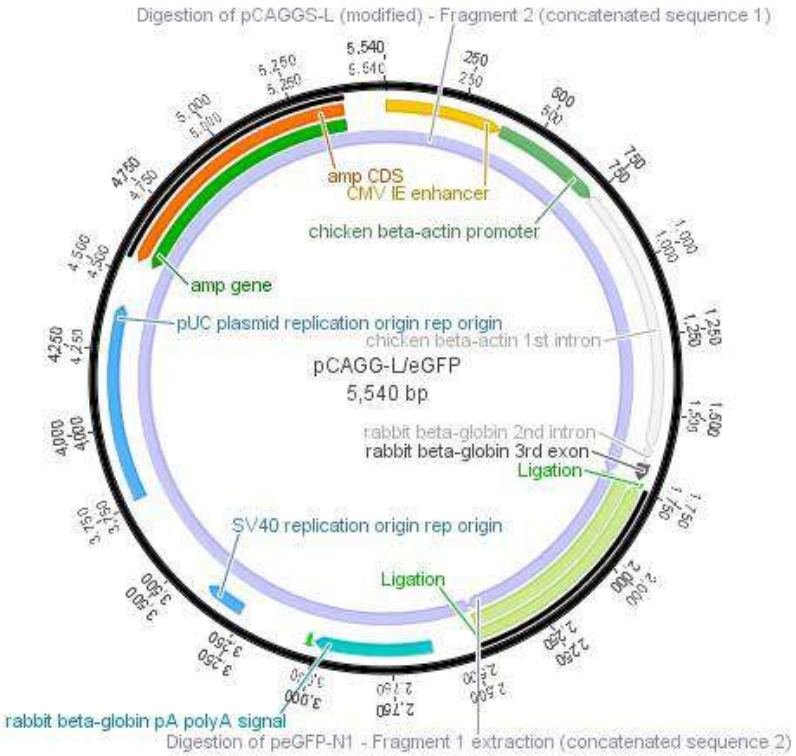

10.3. List of Figures

10.4. List of Tables

10.5. List of abbreviations

°C	Degrees Celsius
µ	Micro (prefix)
n	Nano (prefix)
bp	Base pair
CRISPR	Clustered regularly interspaced short palindromic repeats

DNA	Deoxyribonucleic acid
E. coli	Escherichia coli
g	Gram
h	Hour
kb	Kilo bases
mESCs	Mouse embryonic stem cells
m	Mili (prefix)
min	Minutes
mol	Moles
mRNA	Messenger RNA
PBS	Phosphate-buffered saline
PCR	Polymerase chain reaction
PFA	Paraformaldehyde
qRT-PCR	Quantitative real time PCR
RNA	Ribonucleic acid
RPM	Rounds per minute
RT	Room temperature
sec	Seconds
SSC	Saline sodium citrate buffer
Tm	Melting Temperature
TSS	Transcriptional start site
x g	Times gravity

10.6. Scientific publications

In submission

Genolet, O., Monaco, AA., Dunkel, I., Boettcher, M., Schulz, EG. (2020). Identification of X-chromosomal genes that drive global X-dosage effects in mammals. BioRxiv**.**

Genolet, O., Ravid, L., Dunkel, I., Schmiedel, V., Schulz, EG. (2020). Transgene-free enrichment strategies based on protein and RNA abundance accelerate pooled CRISPR screens.

Peer reviewed

Cheedipudi, S., **Genolet, O.** & Dobreva, G. (2014). Epigenetic inheritance of cell fates during embryonic development. Front. Genet. 5.

Cervelló, I., Gil-Sanchis, C., Santamaria, X., Faus, A., Vallve-Juanico, J., Diaz-Gimeno, P., **Genolet, O**., Pellicer, A., Simon, C. (2017). Leucine-rich repeat-containing G- protein-coupled receptor 5-positive cells in the endometrial stem cell niche. Fertil. Steril. 107, 510–519.e3.

10.7. Declaration of independent work

I hereby declare the present work has been independently conceived and written, and that no technical aid has been used. I assure that this work or any part of it has not been submitted to, approved, or rejected by any other academic institution.

Berlin, 21.12.2020……..

Oriana Genolet